Technische Universität München
TUM School of Medicine and Health

Endoplasmic Reticulum Stress Signaling Actively Contributes to Therapy Resistance in Colorectal Cancer

Daisuke Sasaki

Vollständiger Abdruck der von der TUM School of Medicine and Health der Technischen Universität München zur Erlangung eines

Doctor of Philosophy (Ph.D.)

genehmigten Dissertation.

Vorsitz: Priv.-Doz. Dr. Maike Buchner-Mayr

Betreuer: Prof. Dr. Klaus-Peter Janßen

Prüfende der Dissertation:

1. Prof. Dr. Markus Gerhard
2. Priv.-Doz. Raquel Mejías-Luque, Ph.D.

Die Dissertation wurde am 27.06.2024 bei der TUM School of Medicine and Health der Technischen Universität München eingereicht und durch die TUM School of Medicine and Health am 20.09.2024 angenommen.

「細胞は、刺激があればそれにユニフォームに反応するといった単純な機械ではないのだ。
それは、条件によって異なった行動の選択をする。」

"A cell is not just a machine that responds uniformly to stimuli.
Instead, it adopts different behaviors depending on the context."

Tomio Tada (1934–2010)

Tada, T. (1997). *Seimei no Imiron* [Theory of the meaning of life].
Tokyo, Japan: Shincho-sha

ZUSAMMENFASSUNG

Das kolorektale Karzinom (CRC) stellt ein globales medizinisches Problem dar. Chemo- und Radiotherapie stellen eine der wichtigsten Optionen bei fortgeschrittenem CRC dar, obwohl viele Patienten entweder kein primäres Ansprechen zeigen oder Resistenz gegen die Behandlung entwickeln. Daher stellt die Entschlüsselung der Mechanismen, die der Behandlungsresistenz zugrunde liegen, sowie die Entwicklung neuer Therapie-Optionen ein wichtiges Forschungsfeld dar. Eine zelluläre Stressantwort, die bei Chemotherapie mutmaßlich aktiviert wird, stellt die „unfolded protein response“ im Endoplasmatischen Retikulum (ER) dar, die durch Akkumulation ungefalteter Proteine ausgelöst wird. Der genaue Beitrag dieser ER-Stress-Antwort zur Therapieresistenz ist allerdings noch unklar.

In der vorliegenden Arbeit wurde mit Hilfe des TCGA Datensatzes zunächst gezeigt, dass wichtige Mediatoren der ER-Stressantwort, darunter vor allem das Gen ATF6, in vielen soliden Tumorarten häufig amplifiziert waren, mit negativer prognostischer Assoziation. Weiterhin wurden humane Darmkrebszelllinien, sowie primäre Colon-Organoide aus operativ reseziertem Gewebe *in vitro* einer Chemo-/Radiotherapie unterzogen und anschließend auf die Ausprägung von ER-Stress-Markern untersucht. Es zeigte sich, dass das basale Expressionsniveau von ATF4, XBP1 und ATF6 mit dem Ansprechen (IC_{50}-Wert) auf das Chemotherapeutikum Oxaliplatin (OxaPt) korreliert war.

Um die Aktivierung der ER-Stressantwort in lebenden Zellen untersuchen zu können, wurden „Reporter-Zelllinien“ generiert, welche die ER-Stress-Mediatoren ATF4, XBP1 und ATF6, sowie als Kontrolle Histon H2A, stabil ausprägen, jeweils als Fusionsprotein mit einem Fluorophor. Diese Reporter-Zelllinien wurden eingesetzt, um die Expression und die Kinetik der intrazellulären Aktivierung der ER-Stress-Signalwege nach Bestrahlung oder Behandlung mit OxaPt zu untersuchen. Hier zeigte sich, dass ATF6 nach OxaPt-Behandlung sehr rasch aktiviert wird, im Vergleich zur kanonischen Aktivierung durch Thapsigargin. Weiterhin zeigte sich, dass die XBP1-Reporterlinie eine signifikant erhöhte Resistenz gegenüber OxaPt aufwies, während ATF6-Reporterzellen im Vergleich zu Kontrollen eine signifikant gesteigerte Resistenz gegenüber Bestrahlung aufwiesen. Diese Effekte sind mutmaßlich auf die in den Reporterlinien erhöhte Expression des jeweiligen ER-Stress Mediators zurückzuführen. Im Gegenzug führte die pharmakologische Hemmung des ATF6-Signalwegs zu einem verbesserten Ansprechen auf

eine Behandlung mit OxaPt, dies wurde bei der Darmkrebs-Zelllinie HCT116 beobachtet, sowie als vorläufiger Befund bei primären Colon-Organoiden. Des Weiteren wurden Frischgewebe und Formalin-fixierte Proben von Patienten mit CRC mittels Durchflußzytometrie auf die Expression von ATF6 überprüft. Hier zeigte sich an einer kleinen Kohorte, dass bei Vorliegen von DNA-Mikrosatelliten-Instabilität signifikant mehr ATF6 im Zellkern vorhanden war. Schließlich wurden Proteom-Analysen durchgeführt, die deutliche Hinweise darauf ergaben, dass sich die jeweiligen Antworten auf OxaPt zwischen den verschiedenen Armen der ER-Stress-Signaltransduktion deutlich unterscheiden. Die ATF6-abhängigen zellulären Programme führen vor allem zur Aktivierung der DNA-Schadensreparatur, während die XBP1-abhängigen Antworten multifunktionell sind, mit einem Schwerpunkt auf der ribosomalen Biogenese.

Zusammenfassend lässt sich festhalten, dass die Aktivierung der ER-Stress-Antwort die Resistenz gegenüber Chemo- und Strahlentherapie deutlich erhöhen kann, auch wenn weitere Untersuchungen zur Aufklärung der molekularen Mechanismen nötig sind. Darüber hinaus könnte sich ATF6, aufgrund der beobachteten zytoprotektiven Rolle, als prädiktiver Biomarker oder mögliches therapeutisches Ziel eignen.

ABSTRACT

Colorectal cancer (CRC) is a major health problem worldwide. While chemotherapy and radiotherapy remain a main approach for treating late-stage CRC, many patients fail to respond initially or develop therapy resistance and eventually die of uncontrollable disease progression. Therefore, the identification of mechanisms of drug resistance and the development of strategies to overcome therapy failure hold great significance. The unfolded protein response in the endoplasmic reticulum (ER), a mechanism to protect cells from intracellular stress, was proposed to be involved in chemotherapy response. However, the specific contribution of the ER stress response to therapy resistance in CRC is still not fully understood.

In the present thesis, the functional contribution of the main ER stress mediators ATF4, XBP1 and ATF6 in carcinogenesis and therapy response was analyzed. In the public TCGA dataset, mainly ATF6 was found to be frequently amplified on the genome level and negatively associated with prognosis in the most frequent solid cancer types. Next, a panel of human CRC cell lines and primary patient-derived organoids were characterized under chemo-/radiotherapy *in vitro* for expression and activation of ER stress proteins. Basal expression levels of ATF4, XBP1 and ATF6 were positively correlated with the respective IC_{50} values for treatment with oxaliplatin (OxaPt).

To monitor ER stress activation in live cells, reporter cell lines expressing fluorophore-coupled ATF4, XBP1, ATF6 or histone H2A as control were established. These ER stress reporter cell lines were utilized to monitor the expression and intracellular activation kinetics of the fluorescent reporter proteins after chemotherapy treatment or X-ray irradiation. OxaPt induced ER stress with rapid activation of ATF6, compared to canonical ER stress induction by thapsigargin. Of note, XBP1-reporter cells showed significantly enhanced resistance to OxaPt and ATF6-reporter cells to irradiation, compared to parental and control cells, likely due to increased expression of the respective ER stress mediator. In contrast, pharmacological inhibition of the ATF6 pathway sensitized human HCT116 cells to OxaPt treatment and was tested in a preliminary fashion in patient-derived colon organoids. Furthermore, formalin-fixed and fresh tissue samples from a small cohort of CRC patients were tested for ATF6 expression by flow cytometry, and nuclear ATF6 was significantly associated with DNA microsatellite instability. Finally, proteome analysis showed that the cellular response to OxaPt differs

between the branches of the ER stress response. ATF6-dependent responses appeared to be involved in DNA damage repair, while XBP1 drives a rather multifunctional response and is involved in ribosomal biogenesis stress.

In conclusion, activation of the ER stress signaling may promote primary and acquired chemo- and radioresistance, even though further mechanistic insights are required. Based on the observed cytoprotective role of ATF6 in multimodal cancer therapy, it holds potential as a predictive biomarker and putative therapeutic target.

TABLE OF CONTENTS

1. INTRODUCTION

1.1. Therapy Resistance in Colorectal Cancer

1.1.1. Colorectal cancer: general introduction and challenges in its treatment

Colorectal cancer (CRC) is the third most prevalent malignancy, representing the second most lethal cancer worldwide. In 2020, over 1.9 million new cases and 0.9 million deaths were estimated for CRC around the world, which accounts for nearly 10% of all cancer cases and deaths (Sung et al., 2021). The incidence rate of CRC is positively correlated with the Human Development Index (HDI), which is widely used as a measure of countries' living standards in terms of income, health and education (UNDP, 2019) — the age-standardized incidence rates in countries with very high HDI (≥0.80) are approximately four folds of those in countries with low HDI (<0.55) (Xi & Xu, 2021). The CRC incidence rates are rapidly increasing, particularly in middle-to-high HDI countries of Eastern Europe, Southeast Asia and South America, where mortality rates are also rising (Arnold et al., 2017). It is primarily attributed to the population shift toward lifestyles with a Western diet and less physical activity (Arnold et al., 2020). In contrast, the incidence and mortality appear to be stabilizing or declining, albeit remaining high, in some high HDI countries, including the United States, Australia, New Zealand, Japan, Israel and several Western European countries (Arnold et al., 2017), which in turn may reflect the growing trend toward healthier lifestyles, improved treatments and implementation of nationwide screening programs for early CRC detection over the past decade (Arnold et al., 2020; Edwards et al., 2010). According to demographic projections based on HDI, the global burden of CRC is predicted to reach annually 3.2 million new cases and 1.6 million deaths by 2040 (Morgan et al., 2023).

While hereditary genetic aberrations such as Lynch or familial adenomatosis polyposis (FAP) syndrome and further low-penetrance genetic variations present a strongly increased risk for developing CRC (Jiao et al., 2014; Kastrinos et al., 2020; Song et al., 2020), the majority of CRC arises sporadically, accounting for 60–65% of all CRC cases, with no family history nor inherited genetic predisposition (Keum & Giovannucci, 2019; Tian et al., 2019). Therefore, the

development of CRC is largely attributable to acquired somatic genetic mutations or epigenetic modifications. Most sporadic CRC cases are considered to follow the “adenoma-carcinoma pathway” (**Figure 1A**), where aberrant crypt foci evolve into adenomas and then invasive carcinomas by progressive accumulation of mutations, activating oncogenes and inactivating tumor suppressor genes (Grady & Carethers, 2008; Li et al., 2021; Parmar & Easwaran, 2022; Vogelstein et al., 1988). It is usually initiated by loss of function in adenomatous polyposis coli (APC), leading to aberrant activation of WNT/β-catenin signaling and promoting cellular proliferation and survival. Subsequently, the mutation in Kirsten rat sarcoma proto-oncogene (KRAS) causes persistent activation of the mitogen-activated protein kinase (MAPK) and phosphoinositide-3-kinase (PI3K) signaling, which further enhances the cell viability (Janssen et al., 2006; Janssen et al., 2002). In the later phase, the loss of tumor protein p53 (TP53) function coincides with chromosomal instability (CIN), driving further mutation and tumor progression. In a parallel mechanism, termed the “serrated pathway” (**Figure 1B**), initial hyperplastic polyps advance to carcinomas via sessile serrated adenomas, which are characterized by mutation in B-raf proto-oncogene (BRAF), hypermethylation in CpG islands and microsatellite instability (MSI) (Leggett & Whitehall, 2010; Parmar & Easwaran, 2022). MSI is a condition where insertion/deletion errors accumulate at short nucleotide repeats within the genome, termed microsatellites, due to the mismatch-repair deficiency, and it is also observed in hereditary CRC syndromes such as Lynch syndrome (Cherri et al., 2022). In contrast, chronic inflammatory bowel diseases, like ulcerative colitis and Crohn’s disease, can lead to carcinogenesis through dysplasia (known as the “dysplasia-carcinoma pathway” (**Figure 1C**)), which is typically more aggressive than sporadic adenoma (Baker et al., 2019; Porter et al., 2021; Warren & Sommers, 1949). Collectively, these mechanistic understandings form the basis of current clinical recommendations and research priorities for CRC. Furthermore, there are additional pathways involved in the CRC development, such as those mediated by deregulation of a tumor suppressor SAM and SH3 domain containing 1 (SASH1) and its adaptor protein v-crk avian sarcoma virus CT10 oncogene homolog-like (CRKL) that our group has investigated (Franke et al., 2019; Franke et al., 2020; Jaufmann et al., 2021), emerging as promising prognostic factors and drug targets.

Therapeutic strategies for CRC are determined on the basis of pathologic staging, which represents the most established prognostic factor. The most commonly used staging system is

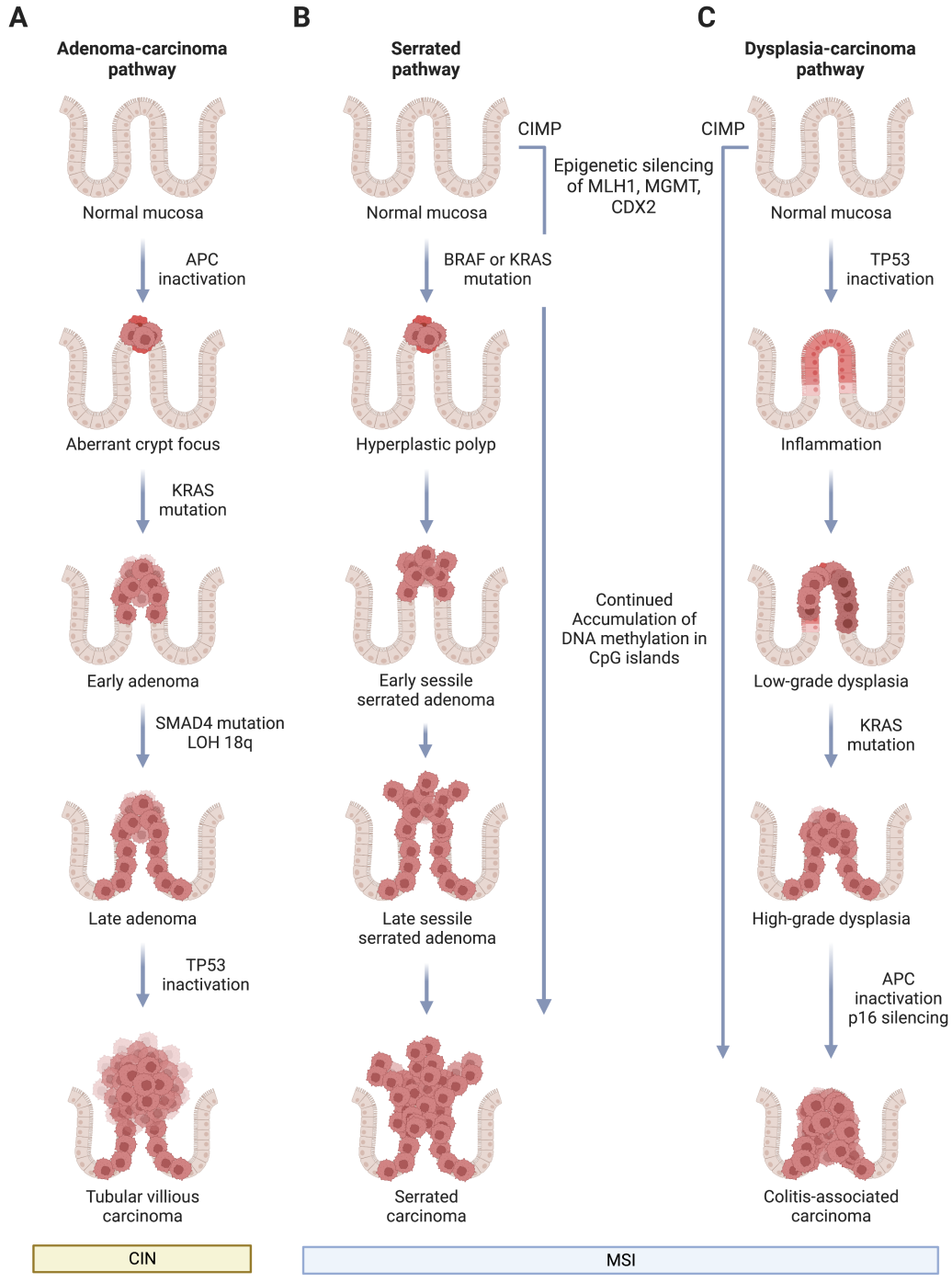

Figure 1: Current models for the molecular pathogenesis of different forms of colorectal cancer. The adenoma-carcinoma pathway **(A)**, serrated pathway **(B)** and the dysplasia-carcinoma pathway **(C)**, annotated with typical molecular features such as mutations in tumor suppressor genes and oncogenes as well as histological features. LOH 18q, loss of heterozygosity at chromosome 18q; CIN, chromosomal instability; CIMP, CpG island methylator phenotype; MLH1, MutL homolog 1; MGMT, O^6-methylguanine-DNA methyltransferase; CDX2, caudal-related homeobox transcription factor 2, MSI, DNA microsatellite instability. The graphics were created with BioRender.com, based on review articles (Parmar & Easwaran, 2022; Porter et al., 2021).

the pathological Tumor-Node-Metastasis (pTNM) classification that was defined by the American Joint Committee on Cancer/Union Internationale Contre le Cancer (AJCC/UICC), stratifying patients into stages I–IV and substages based on the depth of tumor invasion, extent of regional lymph node involvement and presence of distant metastasis (O'Sullivan et al., 2017). For more indication of the risk for poor therapy outcomes, several additional markers have also been identified, including clinicopathologic features (*e.g.*, poorly differentiated histology, lymphovascular and perineural invasion, bowel obstruction or perforation and an elevated preoperative level of carcinoembryonic antigen (Compton et al., 2000; Krasna et al., 1988; Moertel et al., 1995; Wanebo et al., 1978; Wolmark et al., 1984)) as well as gene expression signatures and other molecular features (*e.g.*, BRAF or KRAS mutations, MSI and loss of heterozygosity at chromosome 18q (Maak et al., 2013; Nitsche et al., 2012; Nitsche et al., 2013; Popat & Houlston, 2005; Shibata et al., 1996)). For example, high levels of MSI (MSI-H) are detected in 10–15% of stage II CRC cases and accepted as a predictive factor for poor therapy responses (Cherri et al., 2022).

The first-line treatment option for CRC is surgical resection of the primary tumor and metastatic lesions. In early stages with localized tumors (UICC stages I/II), CRC can often be treated by endoscopic resection or radical surgery alone and cured with a high survival rate (Nishizawa & Yahagi, 2017). However, nearly 25% of all patients already present with advanced CRC spread to nearby lymph nodes (stage III) and another 15–25% with metastases in distant organs as well (stage IV) at the time of initial diagnosis, and they need to be managed by a series of systematic therapy combined with surgery (Chou et al., 2010; Hayashi et al., 2010; Manfredi et al., 2006). The delayed diagnosis is probably because the symptoms, such as bowel obstruction, rectal bleeding and abdominal pains, only appear in advanced disease stages (John et al., 2011). Of note, as mentioned earlier, the uptake of screening by non-invasive stool tests and colonoscopy has proven effective in detecting CRC at an early, asymptomatic stage, and new screening modalities are becoming available (Schreuders et al., 2015). Nevertheless, CRC screening is still largely opportunistic and is currently offered to only a limited proportion of the target population in many affected countries (Hilmi et al., 2010; Koo et al., 2012; Schreuders et al., 2015). Therefore, optimal therapeutic management remains a central issue for controlling CRC, especially in late stages.

For advanced and metastatic CRC, post- or preoperative adjuvant chemotherapy with

genotoxic agents (chemo- and radiotherapy for stage II/III rectal cancer and stage III colon cancer), in addition to surgery, is the leading strategy to control diseases by shrinking the tumor and metastases and suppressing further cancer progression and spread (Argilés et al., 2020; Martini et al., 2017; Van Cutsem et al., 2016; Xie et al., 2020). Stage IV patients who present CRC with lymph node metastasis and solitary liver and peritoneal metastasis are usually treated by surgery and subsequent chemotherapy with curative intent (Ismaili, 2011; Jagad et al., 2008). Chemotherapy is also combined with palliative surgery or even recommended without surgery for CRC patients with extensive local invasion and/or multiple unresectable metastases (Ismaili, 2011; Jagad et al., 2008; Rossi et al., 2012). Multiple chemotherapeutic regimes containing one or several drugs have been developed, and clinical trials performed in recent decades demonstrated that the use of chemotherapy in combination with surgery prolonged the overall survival time by over two years compared to surgery alone (Cassidy et al., 2004; Colucci et al., 2005; Goldberg et al., 2004).

Although the benefit of adjuvant chemotherapy for late-stage CRC has been well established, it is often accompanied by limitations, such as unspecific toxicity, unsatisfying and unpredictable response and acquired resistance, which make it difficult to achieve sufficient therapeutic effects with minimal adverse events (Cassidy et al., 2004; Colucci et al., 2005; Goldberg et al., 2004). That is also why chemotherapy for stage II CRC with high-risk features is still controversial (Lin et al., 2014). Similarly, the effect of preoperative radiotherapy on the clinical response of rectal cancer is highly heterogeneous across studies (Gérard et al., 1988; Goldberg et al., 1994; Lin et al., 2014; Marks et al., 1985; Minsky et al., 1995; Wong et al., 2007). As a consequence, around 30% of stage I–III CRC patients succumb to disease recurrence and/or metastasis after initial treatment (Pita-Fernández et al., 2015; Rose et al., 2014), and up to 65% of stage IV CRC patients who undergone curative-intent treatment also develop relapsed diseases later on (de Jong et al., 2009; Glehen et al., 2004; Jones et al., 2012; Pfannschmidt et al., 2007; Verwaal et al., 2003; Warwick & Page, 2007).

For a more selective approach, molecularly targeted therapy is also being explored, and several drugs are approved by the Food and Drug Administration (FDA) for treating metastatic CRC. For example, the vascular endothelial growth factor (VEGF) inhibitor bevacizumab is a first- and second-line targeted agent that could slow tumor progression by suppressing excessive angiogenesis (Hurwitz et al., 2004). The epidermal growth factor receptor (EGFR)

inhibitors cetuximab and panitumumab are used for first-line treatment of KRAS wild-type metastatic CRCs (10–20% of all cases), targeting to compete with EGF and the transforming growth factor α (TGFα) to inactivate the downstream signaling pathways including the MAPK and PI3K pathways (Cunningham et al., 2004; Douillard et al., 2014; Karapetis et al., 2008). Furthermore, several immunotherapeutic agents that block the ability of tumor cells to escape surveillance by T-cells, termed immune checkpoint inhibitors, have gained approval for treating MSI-H metastatic CRCs, *e.g.,* the programmed cell death 1 (PD1) inhibitors pembrolizumab and nivolumab (Ganesh et al., 2019). However, the success of immune checkpoint therapy seems limited to the minority of DNA microsatellite unstable cases. Collectively, the targeted therapies play a complementary role to chemo- and radiotherapy, allowing more personalized approaches for treating CRC. However, this also means that therapy outcome is susceptible to the genetic variation between patients and may only apply to limited subgroups. In general, directly blocking specific pathways that contribute to tumor progression can easily develop resistance because of existing cross-over and multiple bypass mechanisms, which decreases the potential of targeted drugs or hinders their clinical application. Therefore, most targeted agents need adjuvant settings with chemo- or radiotherapy, and many other agents remain in preclinical or phase I/II trials (Xie et al., 2020).

In summary, CRC is a growing burden with rising incidence and mortality worldwide, and the therapeutic management balancing risks and benefits is a major concern. Adjuvant chemo- and radiotherapy combined with surgery is currently the mainstay for treating late-stage CRC. However, there is an unmet need to better predict and improve the therapeutic outcomes.

1.1.2. Oxaliplatin: mechanisms of action and resistance

In systemic chemotherapy regimens for CRC, the DNA intercalating agents 5-fluorouracil, oxaliplatin and the topoisomerase type I inhibitor irinotecan are currently the most frequently used drugs. The following will focus on oxaliplatin because of its crucial contribution to the chemotherapy resistance of CRC.

Oxaliplatin (OxaPt), *cis*-oxalato(*trans*-L-1,2-diaminocyclohexane)platinum(II), is a third-generation platinum-based anti-tumor drug developed in the late 1970s as an attempt to overcome resistance associated with the parent drug cisplatin and second-generation drug carboplatin (Kidani et al., 1980). Indeed, OxaPt shows increased cytotoxicity against several

types of cancer cell lines and murine tumor models that are resistant to other platinum agents (Dunn et al., 1997; Fukuda et al., 1995; Mathé et al., 1989; Rixe et al., 1996; Tashiro et al., 1989). The clinical properties of OxaPt have been intensively studied in the treatment of advanced stages of metastatic CRC and other gastrointestinal cancers, where cisplatin and carboplatin have only minimal efficacy (Culy et al., 2000; Zaniboni & Meriggi, 2005).

The benefit of OxaPt-based adjuvant chemotherapy for stage II/III colon cancer was extensively evaluated in two phase III clinical studies, known as the MOSAIC and NSABP trials, which demonstrated that OxaPt combined with 5-fluorouracil (5-FU)/folinic acid significantly improved the response rate and disease-free survival with a trend toward increased overall survival in stage III patients, compared with 5-FU/folinic acid alone (Lévi et al., 1997; Lévi et al., 1994). Notably, although it was not statistically significant, additional analysis performed in the subset of the MOSAIC trial also showed an absolute reduction of tumor recurrence in high-risk stage II patients, defined by some clinicopathologic features (Hickish et al., 2004), which was supported by a recent cohort study (Kumar et al., 2015). In the current practice setting, the combination of 5-FU/folinic acid/OxaPt (FOLFOX) is widely accepted as the standard OxaPt-based chemotherapy regimen for metastatic CRC, while the other combinations Xeloda/OxaPt (XELOX) and irinotecan/OxaPt (IROX) are also used for first- or second-line therapy (Lee & Sun, 2016).

The dominant mechanisms of OxaPt action are, somewhat surprisingly, still largely unclear. As stated above, OxaPt displays an increased cytotoxicity against several cancers compared to cisplatin. However, OxaPt is less reactive toward DNA (Raymond et al., 2002; Riddell, 2018; Wong & Giandomenico, 1999) and interacts more strongly with proteins than cisplatin does (Pendyala et al., 1995), forming fewer DNA-protein or DNA-DNA cross-links that potentially disturb DNA replication and transcription. One explanation for the high efficacy of OxaPt is the formation of specific DNA lesions that are hardly targeted by DNA damage recognition and repair pathways because of its bulky hydrophobic diaminocyclohexane (DACH) carrier ligand (Chaney & Vaisman, 1999; Raymond et al., 1998). Another possible explanation is the interaction of OxaPt with ribosomal RNA (rRNA) and the resulting ribosomal biogenesis stresses, which has also been emphasized as an essential factor for its unique cytotoxicity in a recent study (Bruno et al., 2017). Moreover, OxaPt-protein interactions may affect the activity of enzymes, receptors and other functional proteins, which likely induce proteotoxic stresses

and apoptosis. In particular, the hydrophobic DACH moiety in OxaPt could facilitate the interaction with hydrophobic binding pockets in proteins (Woynarowski et al., 2000).

Albeit effective early on, most patients who undergo an OxaPt-based therapy will eventually develop resistance (Douillard et al., 2013). Even worse, once cancer cells acquire the OxaPt resistance, they can also exhibit cross-resistance to many other chemically and functionally related agents (Hsu et al., 2018), probably because OxaPt affects a broad spectrum of cellular functions. It potentially decreases the options for curative and palliative treatment. Therefore, the ability to accurately predict the response to OxaPt and modulate mechanisms responsible for resistance to OxaPt will be beneficial for selecting better treatment options for individual patients. Drug resistance can generally be represented by various intrinsic or acquired characteristics (**Figure 2**), *e.g.*, decreased drug uptake, enhanced detoxification and damage-repair capacity, and insensitivity to drug-induced apoptosis (Gottesman, 2002; Holohan et al., 2013). However, similar to its mode of action, the mechanisms of the resistance against OxaPt are still not fully characterized.

To summarize, OxaPt is a key component of the standard combination chemotherapy regimens for metastatic CRC that has demonstrated improved efficacy with a significant reduction in recurrence and mortality. However, intrinsic or acquired resistance to OxaPt is still a major challenge in CRC treatment, and the underlying mechanisms remain to be elucidated.

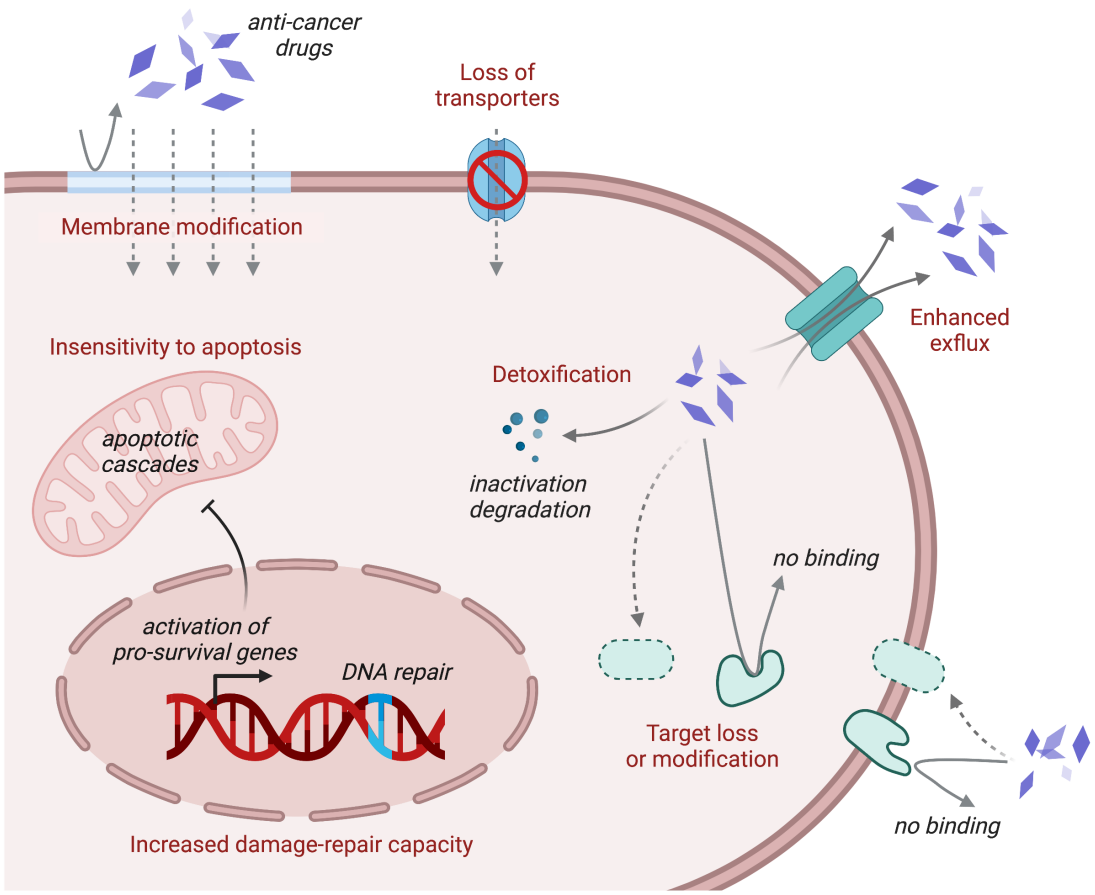

Figure 2: General mechanisms involved in drug resistance. Cells limit drug accumulation by modifying their membrane composition, downregulating or losing drug transporters and enhancing drug efflux activity. Induction of detoxifying mechanisms may also lead to drug inactivation or degradation. Moreover, loss or modification of the drug targets can contribute to therapy resistance. Finally, cells upregulate pro-survival genes to increase their damage-repair capacity and to prevent activation of apoptotic pathways. The graphics were created with BioRender.com, based on a review article (Avril et al., 2017).

1.2. Endoplasmic Reticulum (ER) Stress Response

One proposed mechanism by which cancer cells can resist chemo- and radiotherapy is through an intrinsic stress adaptation program, commonly known as the "endoplasmic reticulum (ER) stress response" or unfolded protein response.

1.2.1. ER stress signaling pathways

The endoplasmic reticulum (ER) is a multifunctional organelle present in all eukaryotic cells that is responsible for the synthesis, maturation and trafficking of proteins as well as for calcium storage and lipid metabolism (Schwarz & Blower, 2016). Ribosomally synthesized proteins are translocated to the ER lumen, where they are folded and assembled into their native three-dimensional structures and undergo post-translational modifications such as glycosylation, carbohydrate addition, lipidation and disulfide formation. Properly matured proteins are then exported through the secretory pathways (Vitale & Denecke, 1999), whereas irreparably malformed proteins are retro-translocated and degraded by cytosolic proteasomes in a process termed ER-associated degradation (ERAD) (Meusser et al., 2005). The ER is also the site for the biosynthesis of membrane lipids, such as steroids and phospholipids, playing essential roles in controlling membrane lipid composition (Fagone & Jackowski, 2009). All these functions are orchestrated by ER-resident molecular chaperones and enzymes, many of which depend on a tightly controlled calcium concentration (maintained 10^3–10^4-fold higher than in cytosol (Clapham, 2007; Samtleben et al., 2013)) and oxidizing potential in the ER lumen (Braakman & Bulleid, 2011). Therefore, homeostasis in the ER environment is crucial for proper protein and lipid production.

However, ER homeostasis is perturbed by various stress factors in physiological or pathological settings, collectively referred to as ER stress. For example, ER stress is activated in normal physiological processes that require high protein turnover, such as cell differentiation and hormone secretion (Moenner et al., 2007). In addition, various disorders, including cancer, autoimmunity, diabetes, heart disease, stroke and neurodegeneration, are associated with defective protein synthesis (Moenner et al., 2007). The sources of ER stress range from a point mutation in the protein to dynamic changes in the intracellular environment, in which accumulation of unfolded or misfolded proteins is the typical stress

indicator (Braakman & Bulleid, 2011). Overload of misfolded proteins in the ER lumen induces an evolutionally conserved mechanism termed the ER stress response, where multiple signal transduction events occur in parallel to restore the ER homeostasis or eliminate irreversibly damaged cells by apoptotic pathways (**Figure 3**) (Kaufman, 2002; Mori, 2000). In mammalian cells, the ER stress response is initiated by three major receptors localized at the ER membrane — protein kinase RNA-like ER kinase (PERK), inositol-requiring gene 1 (IRE1) and activating transcription factor 6 (ATF6) (Harding et al., 1999; Haze et al., 1999; Shamu & Walter, 1996). These receptors are kept inactive in a homeostatic state where their intralumenal domains are bound with a molecular chaperone, glucose-regulated protein 78 (GRP78, also known as BiP). When a large number of misfolded proteins accumulate in the ER, GRP78 is attracted toward their exposed stretches of hydrophobic residues and dissociated from the intralumenal domains of these receptors, which allows activation of three parallel signaling branches that regulate unique transcriptional and translational programs.

PERK is a serine/threonine kinase that is activated through autophosphorylation and subsequent dimerization upon release from GRP78. The activated PERK then phosphorylates the eukaryotic translation initiation factor 2α (eIF2α) at serine 51 to induce global translational repression, thereby decreasing the load of newly synthesized proteins (Wortham & Proud, 2015). However, the phosphorylated eIF2α also allows the selective translation of some proteins, such as the activating transcription factor 4 (ATF4), due to a specific mechanism involving their upstream open reading frames (Palam et al., 2011; Vattem & Wek, 2004). ATF4 has a basic leucine zipper (b-ZIP) domain in the C-terminus that induces the expression of a gene cluster responsible for amino acid metabolism, redox control and autophagy, as well as protein folding (Harding et al., 2003). ATF4 is also involved in apoptotic pathways by regulating the expression of the CCAAT-enhancer-binding protein homologous protein (CHOP), a transcription factor that upregulates pro-apoptotic target genes such as members of the B cell lymphoma 2 (BCL2) protein family (Palam et al., 2011). In turn, ATF4 mediates negative feedback to the over-induction of these responses by activating the expression of growth arrest and DNA damage-inducible protein 34 (GADD34), a co-factor of eIF2α phosphatase, which downregulates eIF2α when recovered from proteotoxic stress (Vattem & Wek, 2004). In addition to the ER-resident PERK receptor, three other cytosolic kinases have been identified to converge on the phosphorylation of eIF2α, namely the general control nonderepressible 2

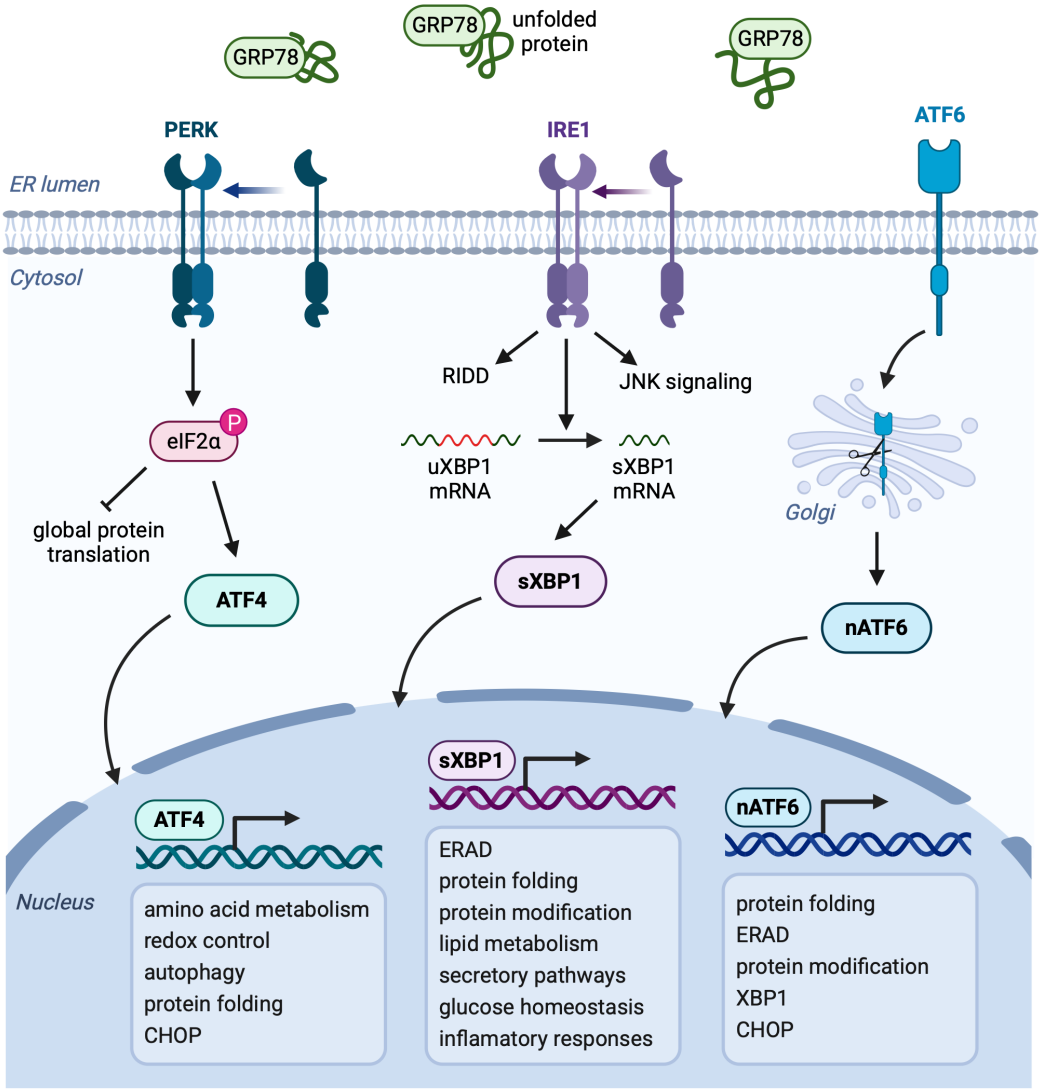

Figure 3: Endoplasmic reticulum (ER) stress signaling pathways. Upon ER stress by an accumulation of misfolded proteins, the glucose-regulated protein 78 (GRP78) binds to unfolded proteins, activating three ER-resident signal transducers, the protein kinase RNA-like ER kinase (PERK), inositol-requiring gene 1 (IRE1) and activating transcription factor 6 (ATF6). PERK is activated by dimerization to phosphorylate the eukaryotic translation initiation factor 2α (eIF2α). The activated eIF2α inhibits global translation with the exception of some proteins, including the activating transcription factor 4 (ATF4). In turn, ATF4 induces the transcription of downstream genes involved in amino acid metabolism, redox control, autophagy, protein folding and the CCAAT-enhancer-binding protein homologous protein (CHOP). IRE1 dimerizes to activate its endoRNase activity, producing a spliced form of the X-box binding protein 1 (sXBP1) as an active transcription factor. sXBP1 induces the expression of genes responsible for multiple responses such as the ER-associated protein degradation (ERAD), folding and modification of proteins. Moreover, IRE1 induces the regulated IRE1-dependent RNA decay (RIDD) and the c-Jun N-terminal kinase (JNK) signaling for further translational regulation and inflammatory responses. ATF6 translocates from the ER to the Golgi apparatus, where it is cleaved by proteases to release the N-terminal fragment of ATF6 (nATF6). nATF6 regulates the transcription of genes for protein folding, ERAD and protein modification as well as XBP1 and CHOP. The graphics were created with BioRender.com.

(GCN2), dsRNA-dependent protein kinase (PKR) and heme regulated inhibitor (HRI). They are activated through a lack of amino acids, viral infection and iron depletion, respectively. Thus, together with PERK, they sense a variety of intracellular stresses and funnel the eIF2α-mediated signaling pathways, collectively termed the integrated stress response (ISR) (Harding et al., 2003).

IRE1(α), a serine/threonine kinase-regulated endoribonuclease, is the most evolutionarily conserved signal transducer in the ER stress response (Cox et al., 1993). It is dimerized/oligomerized and autophosphorylated upon ER stress, leading to its endoRNase activity. Active IRE1 catalyzes unconventional splicing of a 26-nucleotide intron within the X-box binding protein 1 (XBP1) mRNA, which usually encodes an unstable protein uXBP1 (unspliced isoform of XBP1). The spliced mRNA is then translated into a stable protein sXBP1 (spliced isoform of XBP1) as a result of the reading frame shift (Calfon et al., 2002; Lee et al., 2002). sXBP1 is an active transcription factor with a b-ZIP domain in the C-terminus that modulates the expression of genes involved in a wide range of proteostatic processes, including ERAD, folding and maturation of proteins (Lee et al., 2003; Yoshida et al., 2003). sXBP1 is also responsible for transcriptional regulation in lipid metabolism, secretory pathways, glucose homeostasis and inflammatory responses depending on the specific stimuli and cell types (Acosta-Alvear et al., 2007; Byrd & Brewer, 2012; Wu et al., 2015). On the other hand, under severe ER stress, IRE1 recruits an adapter protein, the tumor necrosis factor receptor-associated factor (TRAF), to activate the c-Jun N-terminal kinase (JNK)-mediated apoptotic pathway, and sXBP1 also induces calcium release from ER and cell death (Fink et al., 2018; Yang et al., 2006). Moreover, IRE1 can also degrade other mRNAs and microRNAs through a mechanism named regulated IRE1-dependent decay (RIDD), which is considered important for further translational regulation and additional inflammatory responses (Hollien et al., 2009).

ATF6(α) is an ER transmembrane protein bearing a cytoplasmic N-terminal b-ZIP domain (Haze et al., 1999). The dissociation from GRP78 triggers ATF6 translocation to the Golgi apparatus, where it undergoes intramembrane proteolysis via the site-1 and site-2 proteases (S1P and S2P) to release the cytoplasmic domain (Haze et al., 1999). Consequently, the N-terminal fragment, nATF6, migrates to the nucleus and functions as an active transcription factor. nATF6 binds to ER stress elements (ERSE and ERSE-II) in the promoter of target genes, including ER chaperones, ERAD components, protein disulfide isomerases (PDIs) (Kokame et

al., 2001; Roy & Lee, 1999; Wang et al., 2000; Yoshida et al., 1998; Yoshida et al., 2000). nATF6 also upregulates XBP1 and CHOP via these elements to affect the other ER signaling branches (Yoshida et al., 2000). The target genes of nATF6 largely overlap with those of sXBP1, which also binds to ESREs as well as the unfolded protein response element (UPRE). Of interest, while sXBP1 binds to ESREs independently, nATF6 binds in the presence of the CCAAT-binding factor (CBF, also known as NF-Y), which likely accounts for certain differences in their translational regulation (Yoshida et al., 2000, 2001). On top of that, nATF6 can bind to the cyclic AMP response element (CRE), which is also targeted by ATF4, and possibly involves in the regulation of lipid homeostasis, albeit shown in relation to certain metabolic burdens and dysfunctions (X. Chen et al., 2016; Howarth et al., 2014; Wang et al., 2010; Zeng et al., 2004). Although the feedback regulation of the IRE1 and ATF6 pathways largely remains unknown, it is suggested that the excessive IRE1 activity can be restrained by ERAD and the binding of some PDIs (Sun et al., 2015; Yu et al., 2020). uXBP1 is also a negative regulator that targets nATF6 for degradation by the proteasome via direct association (Yoshida et al., 2006). Once ER stress is relieved with a reduced load of malformed proteins, redundant GRP78 and co-chaperones are directed toward re-association with the PERK, IRE1 and ATF6 receptors, thereby attenuating the global ER stress signaling pathways.

The initiation mechanisms of the ER stress response described above are known as canonical pathways that are passively induced by an overload of unfolded and misfolded proteins in the ER lumen. However, increasing evidence supports the existence of so-called “anticipatory” mechanisms, which are triggered independently of or preceding the proteotoxic stress within the ER (Shapiro et al., 2016). The anticipatory mode of the ER stress response was first observed in differentiating adaptive immune cells, which produce massive amounts of immunoglobulins upon maturation (Hu et al., 2009; van Anken et al., 2003). It was also confirmed that rapid induction of mitogenic steroid/peptide hormones such as estrogen, VGEF and EGF occurs in the absence of ER stress, indicating anticipatory activation (Shapiro et al., 2016). Mechanistically, it is induced by the efflux of calcium ions from the ER lumen through the ER inositol triphosphate (IP3) receptor calcium channels (Shapiro et al., 2016). IP3 is produced by the phosphorylated form of phospholipase Cγ (PLCγ), which can, in turn, be activated by those hormones (Andruska et al., 2015; Karali et al., 2014; Yu et al., 2016). PLCγ is also activated through the signaling from B cell antigen receptor (BCR), initiating the

anticipatory ER stress response (Kurosaki et al., 2000). For another example of non-canonical pathways, ATF6 can also be activated by lipotoxic stress of specific sphingolipids to induce ER lipid biosynthetic genes via transmembrane domains distinct from that targeted by proteotoxic stress (Tam et al., 2018).

Furthermore, ER stress signaling can interplay with other essential physiological processes such as DNA damage response (DDR) and epigenetic regulation (Dicks et al., 2015; González-Quiroz et al., 2020). For example, several studies performed in various mouse and human cells revealed that sXBP1 regulates a cluster of DDR genes encoding damage sensing/repair proteins, such as breast cancer 1 (BRCA1), Rad51 recombinase (RAD51) and X-ray repair cross-complementing protein 1 (XRCC1) (Acosta-Alvear et al., 2007). Moreover, in mouse embryonic fibroblasts where RIDD is exclusively induced without XBP1 mRNA splicing by genotoxic drugs, IRE1 deficiency caused cell-cycle deregulation by disrupting the phosphorylation of checkpoint kinases and the histone H2AX (Dufey et al., 2020). The phosphorylated H2AX (γH2AX) is a reporter protein required for DNA double-strand break (DSB) repair and the activation of cell-cycle arrest (Dufey et al., 2020). Therefore, these reports suggest a direct connection between ER stress signaling and the maintenance of genomic stability. Of note, oxidative stress leads to the generation of reactive oxygen species (ROS), which cause various types of DNA legions (Bolland et al., 2021). Therefore, the antioxidative role of ER stress signaling can indirectly influence the DNA damage repair processes. ER stress can also affect chromatin remodeling through the regulation of post-translational modifications on histones, such as methylation and acetylation, which modulate gene expression patterns (Dicks et al., 2015).

To sum up, the ER stress response is a conserved self-regulatory system that allow cells to cope with perturbed ER homeostasis, in which the three main signaling branches initiated by PERK, IRE1 and ATF6 cooperate through a unique transcriptional and translational regulation program to restore ER homeostasis or to provoke apoptosis depending on the stress and cell types. Importantly, the gene expression programs are individually fine-tuned by transcription factors ATF4, sXBP1 and nATF6, orchestrating a wide range of compensatory processes. Of note, emerging mechanisms for ER stress regulation and cross-talks between these branches and other signaling pathways challenge the simplistic view that ER stress signaling is induced just by unfolded proteins and regulated through separately defined

pathways.

1.2.2. Tumor-specific mechanisms for the induction of ER stress

Tumor cells are exposed to a variety of environmental and cell-intrinsic stress factors that exert selective pressure to favor malignant transformation and promote the acquisition of cancer hallmarks necessary for adaptation and further progression. For example, cancer cells confront external hostile conditions such as hypoxia, nutrient deprivation, acidosis and inflammatory responses. Poor blood perfusion due to abnormal vasculature causes hypoxia and a lack of glucose and amino acids, perturbing redox and metabolic balances within the ER (Gutiérrez & Simmen, 2014; Koritzinsky et al., 2013). Hypoxia upregulates glucose transporters and multiple enzymes of the glycolytic pathway, which renders cancer cells more reliant on aerobic glycolytic energy production (known as the Warburg effect), leading to acidosis with excessive production of lactates (Hanahan & Weinberg, 2011). The hypoxic cells also induce angiogenic and apoptotic/necrotic signaling cascades, which promote inflammatory responses resulting in the release of cellular contents in a cytotoxic manner and further tissue damage (Leyland-Jones & O'Shaughnessy J, 2003). Furthermore, cancer cells also need to overcome intracellular stress factors such as genomic instability, genotoxic stress induced by oncogene activation/loss of tumor suppressors and increased energy consumption, which can cause defective protein production and perturbation in other ER functions (Tameire et al., 2015).

Activation of the ER stress signaling has been observed in many types of human tumors, including glioma, lymphoma, myeloma and carcinoma (Wang et al., 2014). It is associated with the loss of tumor suppressor genes such as the tuberous sclerosis complex (TSC1 and TSC2), as well as the activation of oncogenes such as cellular myelocytomatosis (c-MYC), Rat sarcoma (RAS), BRAF and human epidermal growth factor receptor 2 (HER2) (Bobrovnikova-Marjon et al., 2010; Croft et al., 2014; Denoyelle et al., 2006; Iritani & Eisenman, 1999; Ozcan et al., 2008). Of note, according to genome-wide sequencing studies in human cancers, somatic mutations have also been found in the genes encoding the three ER stress sensors PERK, IRE1 and ATF6 with distinct patterns (Chevet et al., 2015; Greenman et al., 2007): in the PERK gene, missense mutations are mainly observed; in the IRE1 gene, silent mutations as well as in-frame deletions and insertions are predominant, while in the ATF6 gene, nonsense mutations are enriched in cancer. Moreover, the incidence of mutations found in these genes also exhibited tissue

specificity. For example, bone cancers predominantly present with PERK mutations, whereas urologic and lung cancers show higher mutation rates in PERK and ATF6. While IRE1 mutations are pronounced in nervous system cancers, ATF6 mutations are most frequently found in genital cancers. Interestingly, gastrointestinal cancers exhibit the highest rates of mutations in the IRE1 and ATF6 genes among all cancers analyzed. Although these genetic aberrations indicate an intricate involvement of ER stress signaling in cancer beyond its physiological roles, the biological and clinical relevance remains largely unelucidated.

The roles of ER stress signaling have been functionally studied in multiple cellular and animal models. The involvement of the ER stress response in very early phases of cell transformation is considered to be rather tumor-suppressive, preventing oncogene-induced malignant progression. For example, a study performed in a cellular model of RAS-transformed melanoma suggested that the cells undergo ER stress-mediated premature senescence, which could restrict further oncogenic transformation such as $BRAF^{V600E}$ mutation (Denoyelle et al., 2006). On the other hand, in advanced phases of transformation acquiring highly proliferative and invasive phenotypes, the ER stress signaling can also operate as a tumor-promoting mechanism that allows cells to adapt to adverse environmental and intrinsic changes associated with the malignant progression. For example, ablation of the PERK gene in mammalian cells delayed HER2-dependent carcinogenesis, suggesting a pro-tumorigenic role of the PERK signaling (Bobrovnikova-Marjon et al., 2010). Another study in multiple mouse models showed that activation of the PERK-eIF2α-ATF4 arm promotes c-MYC-driven cell transformation and increases cell survival through autophagy (Nagy et al., 2013). The IRE1-XBP1 signaling axis has also been linked to tumor promotion or suppression, depending on the context. For example, high expression of XBP1 was associated with human multiple myeloma and transgenic mice engineered to overexpress sXBP1 in B-cells showed features that resemble those observed in multiple myeloma transformation (Carrasco et al., 2007). Importantly, analysis of human multiple myeloma tumor lines that are resistant to proteasome inhibitors identified loss-of-function mutations in either IRE1 or XBP1, indicating a tumor-promoting role of IRE1 and XBP1 mediated by ERAD (Leung-Hagesteijn et al., 2013). However, a suppressive role of XBP1 in tumor formation was reported in mouse models of intestinal cancer (Niederreiter et al., 2013). ATF6 has been reported to promote hepatocellular carcinogenesis through the activation of the target genes, including GRP78 (Arai et al., 2006).

Moreover, a missense variation in ATF6 that increases its mRNA expression was associated with the risk of hepatocarcinoma (Wu et al., 2014). Overexpressed nATF6 has also been shown to promote prostate cancer progression by forming a reciprocal feedback loop with the phosphatase and tensin homolog (PTEN) to activate the PI3K signaling pathway (Feng et al., 2023).

The ER stress signaling pathways are also involved in mediating the inflammatory environment and immune responses conducive to tumorigenesis and progression. It has been observed that ER stress can be transmitted from cancer cells to surrounding myeloid cells, promoting, for example, macrophage activation through GRP78, GADD34, CHOP and sXBP1 upregulation and releasing pro-inflammatory cytokines, chemokines and metalloproteases (Mahadevan et al., 2011). These factors interfere with antitumor inflammatory responses through antigen processing and presentation and diminish T-cell proliferation (Mahadevan et al., 2012). Moreover, a recent study indicates that tumor-infiltrating dendritic cells display high levels of sXBP1 and not only release pro-tumorigenic cytokines but also arginases, which suppress the activity of T-cells (Mahadevan et al., 2012). Mechanistically, ER stress in these dendritic cells may result from increased generation of ROS and lipid peroxidation products (Garris & Pittet, 2015). Furthermore, a recent study using a transgenic mouse model that expresses nATF6 in the intestinal epithelium showed that activation of ATF6 induces microbial dysbiosis and innate immune signaling to promote spontaneous tumor development (Coleman et al., 2018). It is essentially mediated by favorable changes in the mucosal lipid composition for tumor-relevant bacteria through ATF6 signaling (Coleman et al., 2023).

In addition to the roles in tumorigenic transformation and immune modulation, the activation of ER stress response is associated with several other hallmarks during cancer progression (**Figure 4**). For example, chronically activated angiogenesis is one of the cancer hallmarks, which is promoted by hypoxic ER stress through the upregulation of several pro-angiogenic factors, such as VEGF. The expression of VEGF is modulated by direct binding of ATF4 and ATF6 to its promoter (Ghosh et al., 2010; Pereira et al., 2010). In endothelial cells, angiogenesis is also controlled by sXBP1 and the hypoxia-inducible factor 1α (HIF1α), a central regulator of VEGF (Chen et al., 2014). As described above, the ER stress signaling can also be induced through an anticipatory mechanism involving VEGF and PLCγ, operating as a positive feedback loop of angiogenesis in tumor and endothelial cells.

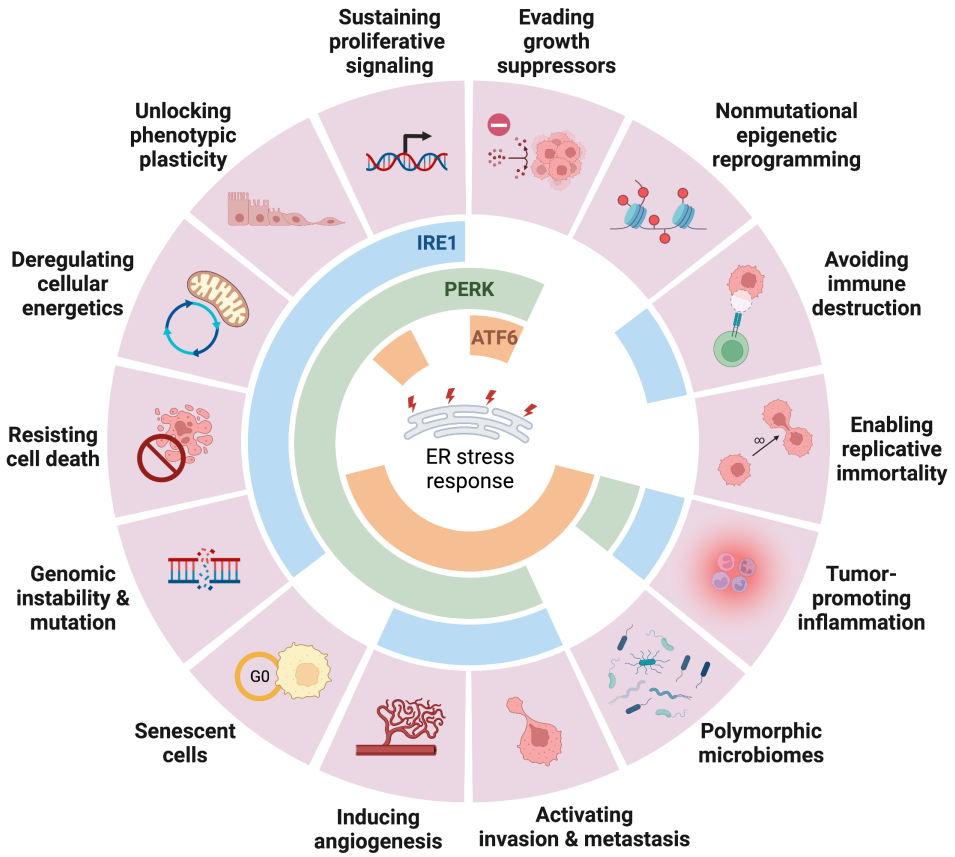

Figure 4: Overview: connections between the ER stress signaling and cancer hallmarks. Tumor cells acquire multiple hallmark capabilities that allow cancer initiation and progression (Hanahan, 2022). The available data suggest that most of these hallmarks are associated with the ER stress signaling pathways initiated from the protein kinase RNA-like ER kinase (PERK), inositol-requiring enzyme 1 (IRE1) and activation factor 6 (ATF6). The assignment of their roles to the cancer hallmarks was adapted from a review article (Urra et al., 2016) and revised based on updates of recent studies (Benedetti et al., 2022; Coleman et al., 2018; Parmar & Easwaran, 2022; Wang & Mi, 2023). The graphics were created with BioRender.com.

The ER stress signaling is also involved in metabolic reprogramming and thus impacts the deregulation of energetics during cancer progression. Indeed, pharmacological inhibition of PERK reduced human tumor xenograft growth in mice by a concerted impairment of amino acid metabolism and angiogenesis (Atkins et al., 2013). Moreover, sXBP1 has been reported to regulate glycolysis by forming a heterodimer with HIF1α and to control the expression of key proteins, including glucose transporter 1 (GLUT1) and lactate dehydrogenase A (LDHA) in triple-negative breast cancer (TNBC) (Chen et al., 2014; Jiang et al., 2017; Romero-Ramirez et al., 2004). sXBP1 is also involved in lipid metabolism by inducing the expression of enzymes

such as stearoyl-CoA-desaturase 1 (SCD1), fatty acid synthase (FASN), as well as the regulation of the hexosamine biosynthetic pathway (HBP), which is necessary for the synthesis of precursors for protein glycosylation (Wang et al., 2014).

Genomic instability is yet another hallmark of cancer progression that can trigger ER stress. For example, aneuploidy and gene copy number variations disrupt the stoichiometry of gene products, leading to an unbalanced global proteome (Oromendia & Amon, 2014). Moreover, several studies suggest that activation of the ER stress signaling may support the genomic integrity. Genetic suppression of PERK promoted the onset of genomic instability, which coincided with oxidative DNA damage in mammary carcinoma (Bobrovnikova-Marjon et al., 2010). Similarly, IRE1-deficient yeast cells showed increased loss of chromosomes (Henry et al., 2010). Furthermore, genetic or pharmacological inhibition of ATF6 in colon cancer cells decreased the stability of DNA repair proteins such as BRCA1 through downregulating the mammalian target of rapamycin (mTOR) signaling (Benedetti et al., 2022).

The ER stress is also an emerging driver of tumor invasion and metastasis, actively remodeling the environment and reprogramming cellular properties. Along that line, the genetic and cellular process termed the epithelial-to-mesenchymal transition (EMT) that is thought to underlie metastasis formation is a hallmark of metastatic cancer progression (Gupta et al., 2019; Lamouille et al., 2014). During EMT, epithelial-derived carcinoma cells lose apical-basal polarity and adhesion to the basement membrane, gaining invasive and migratory traits of mesenchymal stem cells (Lamouille et al., 2014). EMT is triggered by various micro-environmental factors such as hypoxia, cytokines and growth factors (*e.g.*, TGFβ, EGF and WNT) and regulated by transcriptional factors including zinc finger E-box binding homeobox 1 (ZEB1), Twist-related protein 1 (TWIST1), Snail homolog 1 (SNAIL) and 2 (SLUG) and corresponding intracellular signaling pathways that involve adapter proteins like SASH1 (De Craene & Berx, 2013; Gupta et al., 2019). Cancer cells undergoing EMT acquire a highly secretory phenotype that activates several cellular stress responses, including ER stress signaling (Feng et al., 2014; Sheshadri et al., 2014). For example, ATF4 regulates the expression of lysosome-associated membrane protein 3 (LAMP3), a mediator of hypoxia-induced metastasis, and matrix metalloproteinases to promote cell invasion and metastasis (Mujcic et al., 2013; Nagelkerke et al., 2013; Zhu et al., 2014). Moreover, the IRE1-XBP1 activity has been associated with the adhesive and migratory properties depending on the tumor context: while

sXBP1 promotes the lung metastasis of TNBC through HIF1α-mediated hypoxic responses, the IRE1 signaling negatively regulates adhesion and migration through the RIDD-mediated attenuation of several key signaling pathways in glioblastoma cells (Auf et al., 2010; Chen et al., 2014; Dejeans et al., 2012). Furthermore, the activity of PERK and ATF6 are modulated by human squamous cell carcinoma antigen 1 (SCCA1), a pro-metastatic factor during EMT (Sheshadri et al., 2014).

In summary, the ER stress response is essential for cancer cell survival and adaptation to adverse environmental challenges and intrinsic stresses associated with tumor progression. Cooperating with many other cellular regulatory processes, it actively promotes cancer hallmark capabilities, including modulation of angiogenesis and inflammatory/immune responses, metabolic reprogramming, driving genomic instability, invasion and metastasis.

1.2.3. Role(s) of the ER stress response in cancer therapy resistance

Recent studies have suggested that the activation of ER stress signaling in cancer cells affects the effectiveness of traditional treatments, including chemotherapy, radiotherapy, hormone therapy and targeted therapies, which were mainly demonstrated in cellular models in many types of cancer (Avril et al., 2017; Bahar et al., 2019; Kim et al., 2019). Thus, ER stress response may be involved in several non-mutually exclusive cellular pathways associated with cancer therapy. Taking examples of CRC models, adaptation to pharmacological ER stress led to enhanced resistance against several genotoxic agents, including 5-FU, OxaPt and doxorubicin, as a consequence of the constitutive activation of the nuclear factor erythroid 2-related factor 2 (NRF2) mediated by PERK (Salaroglio et al., 2017). In contrast, genetic or pharmacological inhibition of the PERK-eIF2α-ATF4 pathway sensitized several human colon cancer cells to 5-FU treatment (Shi et al., 2019). These findings suggest that the ER stress signaling pathways promote cell survival under chemotherapy. However, some studies performed in CRC cells emphasized that the apoptotic and autophagic cell death induced by ER stress is important for the antitumor effect (Dilly et al., 2020; Tung et al., 2015; Zhang et al., 2021). To date, the connection between ER stress and CRC chemoresistance has been mainly reported on 5-FU treatment. For example, SNUC5 colon cancer cells and its 5-FU-resistant clone (SNUC5/FUR) have been used to explore the relationship with ER stress. Indeed, SNUC5/FUR cells showed higher basal expression of GRP78, sXBP1, ATF6, activated PERK and

eIF2α, and small interfering RNA (siRNA)-mediated knockdown of GRP78 and ATF6 rescued the sensitivity toward 5-FU (Kim et al., 2016). As a similar approach, radiation-resistant CRC cell lines were established by sequential radiation exposure and exhibited decreased ROS production, which attenuated apoptosis through the IRE1-induced JNK signaling pathway (Park et al., 2019). Collectively, these studies suggest the critical role(s) of the ER stress signaling in chemo- and radiotherapy resistance of CRC cells.

As described before, ER stress signaling drives various aspects of cancer biology (**Figure 4**). Those cancer hallmark capabilities are closely related to the potential for cancer cell survival in cytotoxic conditions of cancer therapy. For example, adaptation to a hypoxic environment confers cancer cells with more ability to remove ROS generated by chemo- or radiotherapeutic agents and decrease their genotoxic effect (Akman et al., 2021). Poor vasculature and decreased blood supply could also limit drug delivery to the tumor sites (Dewhirst & Secomb, 2017). Moreover, insensitivity to DNA damage and genomic instability are essential characteristics that drive chemo- and radiotherapy resistance (Beksac et al., 2020; Replogle et al., 2020). Furthermore, emerging evidence has suggested the existence of a process termed dormancy, where cancer cells transitorily exit proliferation to resist chemo- and radiotherapy (De Angelis et al., 2019). Cancer cell dormancy is characterized by non-dividing cancer cells arrested in the G0/G1 phase of the cell cycle and is thought to be involved in minimal residual disease. Dormant cancer cells may resume proliferation, potentially leading to cancer recurrence after therapy (Páez et al., 2012). Of interest, several studies suggest a functional link between the ATF6 signaling and cancer cell dormancy. For example, in a human squamous carcinoma cell model, ATF6 was shown to be constitutively activated in dormant tumor cells, inducing survival signaling by the mTOR pathway (Schewe & Aguirre-Ghiso, 2008). In line with this observation, recurrent tumors showed high expression levels of ATF6 (Ginos et al., 2004). ATF6 levels were also correlated with a poor prognosis of CRC (Lin et al., 2007). Furthermore, a recent study in glioblastoma cells highlighted the role of ATF6 in the development of radiotherapy resistance, where ATF6 upregulates the expression of adaptive proteins such as GRP78 and the neurogenic locus notch homolog protein 1 (NOTCH1) (Dadey et al., 2016). Moreover, the drug resistance of dormant carcinoma cells is also modulated by PERK activation and eIF2α phosphorylation (Ranganathan et al., 2006).

Owing to the potential involvement of the ER stress response in cancer progression and

therapy resistance, pharmacologic intervention in ER stress signaling has been proposed as a strategy for cancer therapy. Many compounds that selectively target three arms of the ER stress signaling have been discovered from natural products in plants and various protozoan parasites and their derivatives. Although very few ER stress-targeting drug candidates have reached clinical trials, they have been extensively used for biological research to probe the roles of individual ER stress signaling branches (Almanza et al., 2019). In the following, a brief introduction is given to the drugs used in this study. Thapsigargin (Tg) is a plant-derived compound that specifically inhibits the ER calcium-dependent ATPase, which decreases ER calcium levels and, thus, its protein folding capacity (Thastrup et al., 1990). The small molecule GSK-2606414 (GSK'414) and its derivative GSK-2656157 (GSK'157) were both identified as selective PERK inhibitors that block the autophosphorylation of PERK (Axten et al., 2012; Axten et al., 2013). STF-083010 (STF'010) is an IRE1α endonuclease inhibitor that block the splicing of XBP1 mRNA without affecting its kinase activity (Papandreou et al., 2011). Ceapins are a class of pyrazole amides that inhibit the activation of ATF6α by blocking its ER-to-Golgi transport (Gallagher et al., 2016).

In summary, emerging evidence suggests that the ER stress response has critical role(s) in the adaptive survival signaling that promotes therapy resistance. It could become a potential biomarker for predicting cancer therapy response and a target for the new development of therapeutics. However, the detailed molecular mechanisms of how individual ER stress signaling branches are linked and regulated in therapy resistance remain poorly understood.

1.3. Objective of the Present Thesis

Tumor resistance to chemo- and radiotherapy obviously is a major challenge in CRC treatment, and thus, identification of the underlying mechanisms and developing strategies to overcome resistance hold great importance in the disease management of CRC. Activation of the ER stress response, with three main signaling branches regulated by the transcription factors ATF4, sXBP1 and nATF6, has been suggested as a key driver of cancer hallmarks associated with therapy resistance. However, it is poorly understood how the individual branches contribute to the adaptive cellular responses during cancer therapy. Therefore, further experimental evidence is needed to explore their potential as predictive biomarkers and therapeutic targets.

The present work aimed to better understand the role of the ER stress response in chemo- and radiotherapy resistance of CRC, focusing on the nuclear activity of ATF4, sXBP1 and nATF6. First, to address their roles in the clinical context, genomic alterations of ATF4, XBP1 and/or ATF6 in human solid tumors were assessed with respect to prognosis and genomic instability based on the publicly available datasets. Moreover, surgically resected CRC patient tumor samples were tested for expression of the ER stress markers by flow cytometry and associated with clinical characteristics, such as tumor stage, grading or microsatellite status. Second, a panel of human cell lines (CRC and controls), as well as patient-derived colon organoids, were characterized under therapeutic conditions for expression and activation of ER stress proteins, and the resulting cytotoxicity was determined. To monitor and modulate ER stress activation in live cells with subcellular resolution, stable reporter cell lines expressing ATF4, sXBP1 or ATF6 proteins fused with a fluorophore were established. These lines were tested for gene or protein expression and cytotoxicity assays to analyze how activation or inhibition of ER stress proteins affects the cellular responses to oxaliplatin (OxaPt) treatment or X-ray irradiation. Finally, to obtain an unbiased readout on the cellular responses to chemotherapy driven by the activation of the ER stress proteins, mass spectrometric proteome analysis was performed.

Taken together, the aim was to characterize cellular stress-adaptation pathways that can confer resistance to cancer therapy, providing insights into the individual role of the transcription factor ATF4, sXBP1 and nATF6.

2. MATERIALS AND METHODS

2.1. Patient Samples and Clinical Data

Human CRC tumor and adjacent healthy colon tissue samples were obtained from CRC patients enrolled in the Department of Surgery, Klinikum Rechts der Isar, TUM (Munich, Germany). Written informed consent was obtained from all patients for the use of tissue (330/18S; 2022-169-S-KH). All experiments were approved by the ethics committee at the Faculty of Medicine of TUM and performed in line with relevant guidelines and regulations proposed in the Declaration of Helsinki. The surgically resected samples were immediately used for experiments or processed into formalin-fixed paraffin-embedded (FFPE) specimens by fixation in 3.5–3.7% (w/v) formaldehyde neutral solution (Otto Fischar, Saarbrücken, Germany) at RT overnight or at 4 °C for 1–3 days, followed by dehydration and paraffin embedding. Genomic DNA of the tumor was analyzed for MSI at the Department of Pathology, Klinikum Rechts der Isar, using the Type-it Microsatellite PCR Kit (Qiagen, Hilden, Germany) and following procedures for routine diagnostics. Two mononucleotide and three dinucleotide Bethesda markers (BAT25, BAT26, D2S123, D5S346 and D17S250) were investigated. The diagnosis of CRC in each case (*e.g.,* staging, grading, tumor location and MSI) and clinical follow-up data were confirmed by the original histopathological report. Commercial FFPE samples, purchased from ProteoGenex (Inglewood, USA) by Nitto Boseki Co., Ltd. (Tokyo, Japan), were also analyzed in combination with the TUM cohort, with appropriate Institutional Review Board/Independent Ethics Committee (IRB/IEC) approval (PG-ONC 2003/1).

Genomic datasets of human cancer from The Cancer Genome Atlas (TCGA), consisting of 10,967 samples from 10,953 patients included in TCGA PanCancer Atlas Studies, were analyzed using the cBioPortal platform (https://www.cbioportal.org/) for low or high levels of amplification (GAIN or AMP, respectively) of ATF4, XBP1 and ATF6, and used for prognostic association. Furthermore, the 10,953 patients and a subset of 594 CRC patients were analyzed for the ATF6 genomic amplification and the TP53 mutation/homozygous deletion (MUT or HOMDEL, respectively) in association with the aneuploidy score and prognosis.

2.2. Molecular Biological Methods

2.2.1. Amplification and isolation of plasmid DNA

All the plasmid DNAs used in this study were obtained from the Addgene plasmid repository (Cambridge, USA). The plasmids pLHCX-ATF4 mScarlet NLS (Addgene plasmid #115970) and pLHCX-XBP1 mNeonGreen NLS (Addgene plasmid #115971) were gifts from David Andrews (Nougarède et al., 2018). The plasmid pEGFP-ATF6 (Addgene plasmid #32955) was a gift from Ron Prywes (Chen et al., 2002). The control plasmid pmScarlet H2A C1 (Addgene plasmid #85051) was a gift from Dorus Gadella (Bindels et al., 2017). These plasmids were shipped as transformed bacteria in agar stabs.

The information for amplification of the respective plasmids in bacteria is provided below. Bacteria were streaked onto LB agar plates containing 100 µg/ml ampicillin or 50 µg/ml kanamycin, respectively, and incubated at 37 °C. The next day, single colonies were transferred to 5 ml of LB medium supplemented with 100 µg/ml ampicillin or 50 µg/ml kanamycin and shaken at 37 °C for 8 h. The culture was then diluted 1:1000 (v/v) into 500 ml (for low-copy plasmids) or 100 ml (for high-copy plasmids) LB medium containing the selective antibiotic and shaken overnight under the same condition. The subsequent plasmid isolation was carried out using the Plasmid Maxi Kit (Qiagen) according to the manufacturer's protocol. The DNA was dissolved in ddH_2O, and the concentration was spectroscopically estimated with NanoDrop 1000 (Thermo Fisher Scientific, Waltham, USA). The DNA solution was stored at −20 °C. The remaining bacterial suspension was mixed together with the same volume of 95% glycerol, aliquoted and stored at −80 °C until further use.

	Amplification in bacteria	
Plasmid	Selective antibiotic	Final culture volume [ml]
pLHCX-ATF4 mScarlet NLS	Ampicillin	500
pLHCX-XBP1 mNeonGreen NLS	Ampicillin	500
pEGFP-ATF6	Kanamycin	100
pmScarlet H2A C1	Kanamycin	100

2.2.2. Restriction with endonucleases

The plasmids were digested with specific bacterial restriction endonucleases to quickly check the identity of plasmids by agarose gel electrophoresis. The restriction enzymes used for each plasmid are shown below. A total amount of 1 µg DNA was digested with the appropriate restriction enzymes at 37 °C for 5 min using the FastDigest system (Thermo Fisher Scientific). The digests were then subjected to 1% (w/v) agarose gel electrophoresis (described in section 2.2.6) to analyze the specific banding patterns (**Appendix Figure S4**).

Plasmids	Restriction enzymes	Expected band sizes [bp]
pLHCX-ATF4 mScarlet NLS	HindIII, ClaI	1173, 6800
pLHCX-XBP1 mNeonGreen NLS	HindIII, ClaI	1068, 6800
pEGFP-ATF6	HindIII, SalI	2020, 4709

2.2.3. RNA isolation and reverse transcription

Isolation of RNA was performed with the RNeasy Mini Kit (Qiagen) according to the manufacturer's protocol. The RNA was dissolved in ddH_2O, and the concentration was spectroscopically estimated with NanoDrop 1000 (Thermo Fisher Scientific). The RNA was reverse transcribed to complementary DNA (cDNA), which was used as a template for PCR, using the RevertAid H Minus Reverse Transcriptase system (Thermo Fisher Scientific). A total amount of 1 µg RNA was mixed with random hexamer primer and $Oligo(dT)_{18}$ primer as follows:

Component	Amount
RNA	1 µg
Random hexamer primer	0.2 µg
$Oligo(dT)_{18}$ primer	0.5 µg
ddH_2O	to 12.5 µl

The mixture was then incubated at 70 °C for 10 min and cooled down on ice to let the primers anneal to the RNA. Afterwards, the following components were added to the mixture:

Component	Amount
5 × Reaction buffer	4 µl
RNase inhibitor	20 U
dNTP mix	1 mM each
RevertAid H Minus RT	200 U
ddH_2O	to 20 µl

The reaction mixture was incubated at RT for 10 min, subsequently at 42 °C for 60 min, and then at 95 °C for 5 min. The cDNA was diluted 1:10 or 1:100 with ddH_2O for use in real-time qPCR or directly used for semi-qPCR after the concentration was determined by NanoDrop 1000. The RNA and cDNA solutions were stored at −20 °C until use.

2.2.4. Real-time qPCR

Gene expression was determined by real-time qPCR on the cDNA template using the LightCycler 480 II system (Roche Diagnostics, Basel, Switzerland) with the corresponding primers (listed below). Depending on the primer design, the PCR amplification was monitored either by the Universal ProbeLibrary (UPL) method, which is based on hybridization of short hydrolysis probes specifically to the amplicons, or by the SYBR Green method, which is based on intercalation of the SYBR Green dye into double-stranded PCR products. Primers and probes for the UPL method (#1–8) were designed using the ProbeFinder software (v.2.53, Roche Diagnostics). The design for the specific primers of sXBP1 and uXBP1 (#9a–b, 10) was adapted from a previous study (Yoon et al., 2019). All primers were purchased from the custom oligonucleotide synthesis service, Metabion (Planegg, Germany), and stored as 100 µM solutions at −20 °C. For both methods, the expression of human hypoxanthine-guanine phosphoribosyltransferase (HPRT) was used as an internal housekeeping control. cDNA obtained from HEK293/HCT116 cells was used for normalization.

Oligo ID	Target gene	Direction	Oligonucleotide sequence	Method
#1	ATF4	Forward	TCTCCAGCGACAAGGCTAA	UPL (probe #2)/
#2		Reverse	CCAATCTGTCCCGGAGAA	SYBR Green
#3	ATF6	Forward	AATACTGAACTATGGACCTATGAGCA	UPL (probe #62)/
#4		Reverse	TTGCAGGGCTCACACTAGG	SYBR Green
#5	HPRT	Forward	GACCAGTCAACAGGGGACAT	UPL (probe #22)/
#6		Reverse	GTGTCAATTATATCTTCCACAATCAAG	SYBR Green
#7	XBP1	Forward	CCCTGGTTGCTGAAGAGG	SYBR Green
#8		Reverse	TGGAGGGGTGACAACTGG	
#9a	sXBP1	Forward	GCTGAGTCCGCAGCAGGT	SYBR Green
#10		Reverse	CAGACTACGTGCACCTCTGC	
#9b	uXBP1	Forward	CTGGGTCCAAGTTGTCCAGAAT	SYBR Green
#10		Reverse	CAGACTACGTGCACCTCTGC	

The qPCR by the UPL method was performed using the LightCycler 480 Probes Master mix (Roche Diagnostics). The reaction mixtures were set up in a 96-well plate as follows:

Component	Amount per well
2 × Master mix	10 µl
Forward and reverse primers	4 pmol each
UPL probe	0.2 µl
Diluted cDNA	5 µl
ddH_2O	to 20 µl

The qPCR by the SYBR Green method was performed using the LightCycler 480 SYBR Green I Master mix (Roche Diagnostics). The reaction mixtures were set up in a 96-well plate as follows:

Component	Amount per well
2 × Master mix	10 µl
Forward and reverse primers	8 pmol each
Diluted cDNA	4 µl
ddH_2O	to 20 µl

Each reaction was prepared in duplicate. The qPCR programs “Mono Color Hydrolysis

Probe/UPL Probe" and "SYBR Green I/HRM Dye" from the manufacturer were used for the UPL and SYBR Green methods, respectively. The data was analyzed using the LightCycler 480 software (v.1.5, Roche Diagnostics) to calculate the threshold cycle (C_t) values. The relative gene expression was determined using the $2^{-\Delta\Delta Ct}$ method.

2.2.5. XBP1 mRNA splicing assay

The presence of the spliced form of XBP1 mRNA was analyzed by PCR followed by agarose gel electrophoresis. cDNA was amplified by PCR using the XBP1-specific primers (#7, 8) and the Taq DNA Polymerase Kit (Thermo Fisher Scientific) with the following setup:

Component	Amount
10 × Taq Buffer with KCl	2 µl
$MgCl_2$	1.5 mM
dNTP mix	0.1 mM each
Forward and reverse primers	20 pmol each
cDNA	1 µg
Taq DNA polymerase	100 U
ddH_2O	to 20 µl

Step	Temperature [°C]	Time [s]	Cycles
1	94	180	1
2	94	30	40
3	60	60	
4	72	30	
5	72	120	1
6	4	-	-

The DNAs were resolved on a 2.5% (w/v) agarose gel, and the signals were quantified (described in section 2.2.6). The splicing ratio of XBP1 mRNA was estimated from the signals representing an sXBP1 fragment (104 bp) and a uXBP1 fragment (130 bp).

2.2.6. Agarose gel electrophoresis

Agarose gel electrophoresis was performed using the Agagel Mini system (Biometra, Göttingen, Germany). Agarose powder was boiled with 1 × TAE buffer to 1% or 2.5% (w/v) agarose solution, and 0.4 µg/ml ethidium bromide was added before solidification of the gel. DNA samples were spiked with 6 × TriTrack DNA Loading Dye (Thermo Fisher Scientific) and separated on the gel alongside GeneRuler DNA Ladder (Thermo Fisher Scientific) in 1 × TAE buffer at 100 V. The DNA bands were visualized by UV transillumination using the UVP GelSolo imaging system (Analytik Jena, Jena, Germany). The band intensities were quantified using the Fiji/ImageJ software (v.2.3.0, NIH, Bethesda, USA, https://imagej.nih.gov/ij/).

2.3. Cell Biological Methods

2.3.1. Cell culture

Human cell lines were obtained from the American Type Culture Collection, ATCC (Manassas, USA) and maintained at 37 °C in a humidified 7% (v/v) CO_2 atmosphere unless otherwise noted. DLD1, HCT116, HEK293, HT29, SW480 and SW620 cells were cultured in Dulbecco's Modified Eagle Medium, DMEM (Thermo Fisher Scientific) supplemented with 10% (v/v) fetal calf serum, FCS (Biochrom, Cambridge, UK), 2 mM L-glutamine (Thermo Fisher Scientific), 50 U/ml penicillin (Biochrom) and 50 µg/ml streptomycin (Biochrom) unless otherwise noted. Human cell line HepaRG (Sigma-Aldrich, St. Louis, USA) was cultured in William's E Medium, WEM (Thermo Fisher Scientific) supplemented with 10% (v/v) FCS, 2 mM L-alanyl-L-glutamine (GlutaMAX, Thermo Fisher Scientific), 5 ng/ml human insulin (Sanofi, Paris, France), 50 µM hydrocortisone hemisuccinate (Sigma-Aldrich), 10 U/ml penicillin and 10 µg/ml streptomycin. For glucose deprivation experiments, the culture medium was replaced by glucose-free DMEM (Thermo Fisher) with the supplements above. For passaging, cells were washed with PBS, incubated with Trypsin-EDTA solution (Sigma-Aldrich) at 37 °C for 5–10 min and continuously resuspended in the medium. Cells were screened for mycoplasma contamination by PCR and agarose gel electrophoresis (the primer sequences are presented in the Appendix). Infected cell lines were treated with Mycoplasma Removal Reagent (Bio-Rad, Hercules, USA) for 1 week and then cultured for another week before the PCR test to ensure complete elimination. Cells were frozen in 10% (v/v) DMSO in FCS and kept in liquid nitrogen for long-term storage.

2.3.2. Plasmid DNA transfection to generate stable cell clones

Transfection of plasmids into cells was performed either by calcium phosphate precipitation or a liposome-mediated transfection method. Cells were grown in 6-well plates until 60–70% confluence. One day before transfection, the culture medium was replaced by an antibiotics-free medium (2 ml per well). HEK293 cells were transfected by calcium phosphate precipitation. Briefly, plasmid DNA (4 µg per well) was diluted in 250 mM $CaCl_2$ (100 µl per well) before 2 × BES buffer (100 µl per well) was added dropwise during vortexing.

The mixture was incubated for 10 min at RT and subsequently added dropwise to the cells. DLD1 and HCT116 cells were transfected by a lipid-mediated method using FuGENE HD (Promega, Madison, USA). Briefly, plasmid DNA (2 µg per well) was mixed with Opti-MEM (Thermo Fisher Scientific) (100 µl per well) and FuGENE HD (Promega, 8 µl per well). After vortexing, the mixture was incubated at RT for 10 min and subsequently added dropwise to the cells. The medium was refreshed 24 h after transfection. Two days post-transfection, the cells were subjected to antibiotic selection to acquire stably transfected cells. The cells were selected with Hygromycin B (Invitrogen, Carlsbad, USA) or G418 (Thermo Fisher Scientific) for at least 3 weeks, according to the following conditions:

		Concentrations for selection [µg/ml]		
Plasmid	Antibiotic	DLD1	HCT116	HEK293
pLHCX-ATF4 mScarlet NLS	Hygromycin	500	200	200
pLHCX-XBP1 mNeonGreen NLS	Hygromycin	500	200	200
pEGFP-ATF6	G418	2000	800	400
pmScarlet H2A C1	G418	2000	800	400

Single colonies were isolated, expanded and further subcloned by limiting dilution. Positive cells were further enriched by fluorescence-activated cell sorting, FACS (Aria III, BD Biosciences, San Jose, USA). The cells were tested for the expression of the fluorescent markers by flow cytometry (described in section 2.3.6) to select positive cells for further use.

2.3.3. Isolation and culture of patient-derived organoids

Human organoids, colonoids and tumoroids, were initiated from surgically resected healthy colon tissue or CRC tumor, respectively, after sterilizing treatment with 2 × Antibiotic-Antimycotic (Thermo Fisher Scientific) and 200 µg/ml normocin (Invitrogen) in PBS at RT for 20 min. For colonoids, crypts were isolated from minced mucosa by shaking with 5 mM EDTA in PBS at 4 °C for 10 and 30 min and mechanically disrupting by pipetting in ice-cold PBS with subsequent gravity sedimentation. For tumoroids, minced CRC tumor was dissociated into 5–10 cell-sized fragments by digestion with 100 U/ml collagenase type IV (Merck, Darmstadt, Germany) and 5 U/ml dispase II (Sigma-Aldrich) at 37 °C for 20–40 min under vigorous shaking, followed by filtration through a 40–70 µm cell strainer. The crypts or tumor cells were washed

with the Advanced DMEM/F-12 (Thermo Fisher Scientific) containing 10 mM HEPES, 2 mM GlutaMAX (ADF^{3+}), resuspended in Matrigel (Corning, Corning, USA) and solidified in a 24-well plate. The gels were overlaid with ADF^{3+} containing the following supplements (ADF^{4+}): 10 mM nicotinamide, 1 mM N-acetylcysteine, 1 × B-27 supplement (Thermo Fisher Scientific), 10 µM Y-27632 ROCK inhibitor (Sigma-Aldrich), 50 ng/ml EGF (PeproTech, Rocky Hill, USA), 50 nM A83-01 ALK5 inhibitor (Tocris Bioscience, Bristol, UK), 10 nM prostaglandin E2, PGE2 (Sigma-Aldrich), 7.5 µM SB-202190 p38 pathway inhibitor (Sigma-Aldrich), 50% (v/v) L-WRN conditioned medium (only for colonoids from crypts), 1 × Antibiotic-Antimycotic and 100 µg/ml normocin. The culture was maintained at 37 °C in a humidified 7% (v/v) CO_2 atmosphere with the medium being refreshed every 2–3 days. Y-27632 was omitted after the first 2 days. Organoids were passaged once in 1–2 weeks by Trypsin-EDTA incubation combined with pipetting (3 cycles of 3 min at 37 °C) to remove Matrigel and dissociate organoids into smaller fragments, and splitting into 1:2–1:4 ratio in a new Matrigel. For long-term storage, organoids were frozen in 10% (v/v) DMSO, 20% (v/v) FCS in the Advanced DMEM/F-12 and kept in liquid nitrogen.

2.3.4. Chemotherapeutical/radiation treatment

Thapsigargin, Tg (Sigma-Aldrich) was dissolved in DMSO at 10 mM concentration and stored at –20 °C. Oxaliplatin, OxaPt was supplied as a 5 mg/ml solution by the Hospital Pharmacy of Klinikum Rechts der Isar and stored at 4 °C. GSK-2656157 (Merck), STF-083010 and Ceapin-A7 (Sigma-Aldrich) were dissolved in DMSO at 5 mg/ml concentration and stored at –20 °C. Bacillamide C and D were biosynthesized and purified by a cooperation partner (Prof. Dr. Tobias Gulder, Maximilian Hohmann, TU Dresden, Dresden, Germany), dissolved in ethanol at 10 mg/ml concentration and stored at 4 °C. The reagents were diluted in the culture medium to achieve the final concentrations. DMSO (ddH_2O for OxaPt, ethanol for Bacillamides) was used as the corresponding vehicle control for the treatment. Exposure to radiation was performed using an X-ray device at the Dept. of Radiation Oncology, Klinikum rechts der Isar (RS225, Gulmay Medical, Surrey, UK; 200 keV, 15 mA).

2.3.5. Lipotoxic treatment with a saturated fatty acid

10 µl of palmitate stock (100 mM) was added to plain DMEM containing 6 mg/ml fatty acid-free bovine serum albumin (BSA), which was filtrated under a sterile condition and pre-heated at 60 °C. After the solution was then incubated at 60 °C with continuous agitation, and 50 U/ml penicillin and 50 µg/ml streptomycin were added when the solution was cooled down. The BSA-coupled palmitate solution was added to the cell culture for the treatment.

2.3.6. Flow cytometry for analyzing reporter gene expression and apoptosis

Cells were dissociated by trypsinization and collected together with floating cells. The cells were washed with precooled PBS and resuspended in 0.5% (w/v) BSA in PBS. For analysis of cell apoptosis, 2×10^5 cells were resuspended in 200 µl of binding buffer, then added with Annexin V-FITC and PI solutions (2 µl each) at RT in the dark for 15 min using an apoptosis detection kit (Abcam, Cambridge, USA). The fluorescence was detected by a flow cytometer CytoFLEX (Beckmann Coulter, Brea, USA), and data were analyzed using the FlowJo software (v.10.8.1, BD Biosciences). Cut-off levels were set at the upper 95 percentiles of fluorescence from untreated transfected cells to analyze reporter gene expression. For the apoptosis analysis, thresholds were determined by unstained or mono-stained control.

2.3.7. Cell viability and proliferation assays

For the XTT assay, cells were seeded in 96-well plates (1×10^3 cells/well) one day before the start of treatment (in triplicate for each condition). After 24 h of treatment, cell viability was measured with the XTT Cell Proliferation Assay Kit II (Roche Diagnostics) according to the manufacturer's protocol. Reagents were incubated for 4 h, and the increase in absorbance at 450 nm was quantified by subtracting 0 h from 4 h values.

For the MTT assay, cells were seeded in 96-well plates (2×10^3 cells/well) one day before the start of treatment (in triplicate for each condition). After 24 h of treatment, cell viability was measured with the MTT Cell Growth Assay Kit II (Sigma-Aldrich) according to the manufacturer's protocol. Reagents were incubated for 4 h, and the absorbance at 560 nm was quantified. Cell proliferation index was then calculated as the change of absorbance from a measurement of untreated conditions.

2.3.8. Clonogenic assay

One day before treatment, cells were seeded at a density of 400 or 800 cells/well in 12-well plates precoated with 0.1% (w/v) gelatin (in triplicate for each condition). After irradiation, the cells were cultured for 1–2 weeks until visible sizes of colonies formed. The colonies were fixed with 3% (w/v) PFA in PBS containing 100 µM $CaCl_2$ and 100 µM $MgCl_2$ at RT for 5 min and visualized by staining with 0.1% (w/v) crystal violet (Sigma-Aldrich) in ddH_2O at RT for 30 min. Colonization was then measured as a ratio of areas occupied by colonies to the total surface areas using the Fiji/ImageJ software. Cell survival rate was calculated as the decrease in colony formation compared to the measurement of untreated conditions.

2.3.9. Glycolysis assay

Cells were seeded at a density of 6×10^3 cells/well in 96-well plates (in triplicate for each condition). The next day, the cells were incubated in a CO_2-free incubator at 37 °C for 3 h, and the media were replaced with pH-sensitive reagent in a respiration buffer (Abcam, ab197244). As a positive control, 60 µg/ml glucose oxidase in the respiration buffer was included. The fluorometric kinetics were evaluated using the Fluoroskan Ascent FL (Thermo Fisher Scientific): excitation wavelength: 355 nm; emission wavelength: 620 nm; interval: 1 min 30 s; temperature: 37 °C. The extracellular acidification index was then calculated by subtracting blank control with no cells from signals at each time point.

2.3.10. Immunofluorescence imaging

Two days before the start of treatment, cells were seeded on coverslips precoated with 0.1% (w/v) gelatin. At the time points after 0, 0.5, 1, 3, 6 and 24 h of treatment, the cells were fixed with 3% (w/v) PFA in PBS containing 100 µM $CaCl_2$ and 100 µM $MgCl_2$ at RT for 20 min. The PFA was quenched by treatment with 50 mM NH_4Cl in PBS at RT for 20 min, followed by permeabilization with 0.1% (v/v) Triton X-100 in PBS for 3 min, blocking with 2% (w/v) BSA in PBS for 20 min. Then cells were incubated with anti-Golgin-97 antibody (1:100, A-21270, Thermo Fisher Scientific) in 2% (w/v) BSA at 4 °C overnight, subsequently incubated with Cy3-conjugated anti-mouse or Alexa488-conjugated anti-mouse antibody (1:300, Thermo Fisher Scientific) and DAPI (2 µg/ml) in 2% (w/v) BSA at RT for 2 h. The coverslips were mounted on

glass slides with glycerol gelatin (Sigma-Aldrich). Optical section images were obtained with a 100 × oil immersion objective using the AxioObserver Z1 microscope equipped with an ApoTome system (Carl Zeiss, Jena, Germany). Deconvolution and further image processing were performed using the ZEN software (v.3.0, Carl Zeiss). The co-localization of different fluorescent probes was analyzed using the Fiji/ImageJ software.

For dead cell staining and detection in organoids, they were washed with TBS and added with SYTOX-Green (1:30,000, Thermo Fisher Scientific) and Hoechst-33342 dyes (1:1000, Thermo Fisher Scientific) in TBS and incubated at 37 °C for 20 min in a humidified 7% (v/v) CO_2 atmosphere. After washing with TBS, organoids were imaged using the AxioObserver Z1 microscope. Fluorescence from each organoid was quantified by the Fiji/ImageJ software.

2.3.11. Time-lapse live cell imaging

Time-lapse imaging was performed to observe organoids' growth behavior or cellular 2D motility assay using the zenCELL owl (innoMe, Espelkamp, Germany). Organoid culture was set up in a 24-well plate and imaged at 20–30 min intervals for 3 days. For the motility assay, trypsinized single cells were seeded in a 24-well plate (3×10^3 cells/well) and kept for 6 h. Then, Bacillamide C or D was added, and time-lapse images were acquired every 15 min. The recorded images were processed to highlight cell positions using the zenCELL owl software (v.2.0, innoMe), and then individual cell tracks were analyzed by using the Fiji/ImageJ software combined with the Manual Tracking plugin (https://github.com/fabricecordelieres/IJ-Manual_Tracking) or the TrackMate plugin (https://github.com/trackmate-sc/TrackMate).

2.4. Immunological and Protein Biochemical Methods

2.4.1. Flow cytometry for analyzing protein expression in human CRC

For flow cytometric analysis, human CRC tumors or adjacent healthy colon tissues were dissociated into single cells by digestion with 5 ml of 150 U/ml collagenase type IV in DMEM containing 25 mM HEPES with vigorous shaking (3 cycles of 10, 10 and 30 min at 37 °C), followed by filtration at 40 µm. All collected cells were fixed with 3% (w/v) PFA in PBS containing 100 µM $CaCl_2$ and 100 µM $MgCl_2$ at RT for 20 min. Subsequently, the cells were treated with 50 mM NH_4Cl in PBS at RT for 20 min to quench the remaining PFA, followed by permeabilization with 0.1% (v/v) Triton X-100 in PBS for 3 min, blocking with 2% (w/v) BSA in PBS for over 20 min.

To collect cell nuclei from FFPE specimens, sections (3 × 20 µm) were deparaffinized and rehydrated in a graded series of xylene-ethanol ending in ddH_2O: xylene (1 ml, 5 min × 3), ethanol (1 ml, 5 min × 3), 50% (v/v) ethanol with ddH_2O (1 ml, 3 min), ddH_2O (1 ml, 3 min) followed by heat-induced antigen retrieval at 95 °C for 40 min using the EnVision FLEX Target Retrieval Solution, Low pH (Agilent, Santa Clara, USA). After cooled down to RT, the tissue sections were washed with TBS and further treated with 100 U/ml thrombin (Sigma-Aldrich) in 50 mM Tris-HCl (pH 8), 150 mM NaCl, 2 mM $CaCl_2$ (300 µl per tube) at 37 °C for 15 min. After washing with TBS, the tissue sections in 0.5 ml TBS were sheared by a rotor-stator homogenizer (Motor handpiece MHX/E, ZENOX, Overijse, Belgium; T10 basic ULTRA TURRAX, IKA Instruments, Staufen, Germany). They were resuspended in ice-cold 1% (v/v) NP-40 detergent with TBS, transferred to a 15 ml tube and ultrasonicated (70% amp., 3 cycles of 10 sec/10 sec interval, SONOPLUS, BANDELIN, Berlin, Germany), followed by filtration at 40 µm. Subsequently, the collected nuclei were subjected to blocking with 6 mg/ml normal goat serum (Invitrogen), 1% (w/v) BSA in TBS for over 20 min, and washed with 0.5% BSA in TBS.

Then, the cells/nuclei were incubated with a primary antibody (1:200 dilution, unless otherwise noted) in 0.5% (w/v) BSA at RT for 20 min. After washing with 0.5% (w/v) BSA, they were incubated with goat anti-rabbit or anti-mouse Alexa488 (1:500, Thermo Fisher Scientific) and DAPI (2 µg/ml) in 0.5% (w/v) BSA at RT for 10 min. The fluorescence was detected by the flow cytometer CytoFLEX, and data were analyzed using the FlowJo software. For the evaluation of the protein marker positivity, cut-off levels were set at the upper 95 percentiles

of fluorescence from the isotype-matched negative stain control.

Primary antibody	Species	Manufacturer, product ID
Anti-ATF6	Rabbit	Abcam, ab203119
Anti-Ki67 (MIB-1)	Mouse	Dako, M7240
Anti-Lamin A/B1/C (EPR4068)	Rabbit	Abcam, ab108922
Anti-XBP1	Rabbit	Abcam, ab37152
Anti-α-Calnexin	Rabbit	Enzo, ADI-SPA-860

2.4.2. Protein extraction

To prepare protein extracts for Immunoblot analysis, cells were washed with PBS and lysed in ice-cold RIPA buffer containing 0.1% (w/v) SDS and protease/phosphatase inhibitors (1 mM Na_3VO_4, 1 mM NaF, 1 mM Pefabloc, 1x Protease Inhibitor Cocktail (Roche Diagnostics), 1 mM β-glycerophosphate, 1 mM benzamidine, 1 mM PMSF, 1 µg/ml Pepstatin A). The mixtures were ultrasonicated for 10 min to ensure the cell lysis and degrade chromosomal DNA into small fragments. After incubation with gentle rotation at 4 °C for 10 min, the lysates were centrifuged at 15,000 rpm, 4 °C for 15 min to obtain the supernatant without cell debris. Total protein concentration was assessed by using the Pierce BCA Protein Assay Kit (Thermo Fisher Scientific) according to the manufacturer's protocol. Based on it, the samples were further diluted with RIPA buffer to normalize the total protein concentration across the samples. 5 × Laemmli buffer was added to the samples to achieve a final 1 × concentration of Laemmli buffer. The samples were then boiled at 95 °C for 5 min to reduce and denature the proteins or stored at −20 °C until use.

2.4.3. Cell fractionation

Cells were fractionated into nuclear and crude cytoplasmic lysates to examine the subcellular localization of proteins by immunoblot analysis. The procedure was as follows: after washing with PBS, cells were refilled with ice-cold PBS and scraped into a reaction tube. The cell suspension was centrifuged at 10,000 rpm, 4 °C for 2 min, and the supernatant was discarded. The cell pellet was thoroughly resuspended by pipetting in ice-cold 0.3% (v/v) NP-40/PBS to lyse cytoplasmic membranes. One-third of the suspension was transferred to a

reaction tube as a “whole cell lysate (W)” fraction. After centrifuging the remaining suspension at 15,000 rpm, 4 °C for 1 min, half the volume of the supernatant was transferred to a new reaction tube as a “cytosolic (C)” fraction. The remaining supernatant was discarded, and the pellet was washed three times with 0.3% (v/v) NP-40/PBS by pipetting and centrifugation at 15,000 rpm, 4 °C for 1 min. The pellet was resuspended in 0.3% (v/v) NP-40/PBS (half the volume of the other fractions) to obtain a “nuclear (N)” fraction. The W and N fractions were ultrasonicated for 10 min and incubated with gentle rotation at 4 °C for 10 min, followed by centrifugation at 15,000 rpm, 4 °C for 15 min to obtain cleared supernatants. 5 × Laemmli buffer were added to the W, N and C fractions to achieve a final 1 × concentration of Laemmli buffer. The samples were then boiled at 95 °C for 5 min to reduce and denature the proteins or stored at −20 °C until use.

2.4.4. SDS-polyacrylamide gel electrophoresis

Protein samples after reduction and denaturation were subjected to denaturing SDS-polyacrylamide gel electrophoresis (SDS-PAGE) using the PerfectBlue gel system (Peqlab, Erlangen, Germany). The gel consisted of a 10% (v/v) resolving gel (pH 8.8) and an overlying 5% (v/v) stacking gel (pH 6.8). The components of these gels are shown below. After loading the samples and PageRuler Prestained Protein Ladder (Thermo Fisher Scientific), the gel was initially run at 80 V in 1 × running buffer to concentrate proteins in the stacking gel and then run at 120 V in the buffer to separate the proteins in the resolving gel.

Component	Volume for 10 ml gel solution	
	10% Resolving gel	5% Stacking gel
ddH_2O	4.0 ml	6.8 ml
30% Acrylamide/0.8% bis-acrylamide solution	3.3 ml	1.7 ml
1.5 M Tris-HCl (pH 8.8)	2.5 ml	-
1.0 M Tris-HCl (pH 6.8)	-	1.25 ml
10% SDS	100 µl	100 µl
10% APS	100 µl	100 µl
TEMED	4 µl	10 µl

2.4.5. Immunoblot analysis

After SDS-PAGE, proteins were transferred from gels to 0.45 µm nitrocellulose membranes (GE Healthcare) using the Fastblot semi-dry blotting system (Analytik Jena, Jena, Germany) at 12 V for 1 h in 1 × transblot buffer. The membrane was blocked with 5% (w/v) blotting grade milk powder (Carl Roth, Karlsruhe, Germany) in PBST at RT for 1 h, washed 3 times with PBST at RT for 5 min, and then incubated with the primary antibody (listed below) in PBST containing 5% (w/v) blotting grade milk powder at 4 °C overnight. After washing 3 times with PBST at RT for 5 min, the membrane was incubated with the appropriate HRP-conjugated secondary antibody (listed below) in PBST containing 5% (w/v) blotting grade milk powder at RT for 1 h. The membrane was washed 3 times with PBST at RT for 5 min. Proteins were then visualized by Pierce ECL Western Blotting Substrate (Thermo Fisher Scientific) and detected with the UVP ChemStudio imaging system (Analytik Jena). The band intensities were quantified using the Fiji/ImageJ software.

Primary antibody	Species	Manufacturer, product ID	Dilution
Anti-ATF4	Rabbit	Abcam, ab270980	1:1000
Anti-ATF6	Rabbit	Abcam, ab203119	1:500
Anti-GRP78	Rabbit	CST, #3177	1:1000
Anti-α-Calnexin	Rabbit	Enzo, ADI-SPA-860	1:1000
Anti-Lamin A/C	Mouse	BD Biosciences, 612163	1:1000
Anti-PARP1	Mouse	SCBT, sc74470	1:1000
Anti-phospho-eIF2α	Rabbit	CST, #3597	1:1000
Anti-α-Tubulin	Mouse	Sigma-Aldrich, CP06	1:2000
Anti-XBP1	Rabbit	Abcam, ab37152	1:500
Anti-β-actin	Mouse	CST, #3700	1:2000

Secondary antibody	Species	Manufacturer, product ID	Dilution
Anti-mouse, HRP-conjugated	Goat	Jackson, 111-035-144	1:4000
Anti-rabbit, HRP-conjugated	Goat	Jackson, 115-035-003	1:4000

2.4.6. Mass spectrometry (MS)-based proteomic analysis

Frozen cell pellets were lysed by incubating at 95°C for 10 min with agitation (1500 rpm) in a previously reported lysis buffer (Kulak et al., 2014). The extracted proteins from each sample were digested overnight (37°C, 1500 rpm) with trypsin and endopeptidase Lys-C at a ratio of 1:100 to the protein amount. The following day, the activity of trypsin was quenched by adding 200 µl 1% (v/v) trifluoroacetic acid (TFA) in isopropanol. Peptides were then desalted using styrene divinylbenzene-reverse phase sulfonate (SDB-RPS) Stage-tips (Kulak et al., 2014). Briefly, after binding to the SDB-RPS, peptides were washed with 100 µl 1% (v/v) TFA in isopropanol and 100 µl 0.2% (v/v) TFA in LC-MS grade H_2O. The peptides were eluted in 60 µl elution buffer (80% (v/v) acetonitrile, 1.25% (v/v) NH_4OH) and dried by a SpeedVac vacuum concentrator (Eppendorf, Hamburg, Germany) at 60°C for 45–60 min. The peptides were resuspended in 20 µl buffer A (2% (v/v) acetonitrile, 0.2% (v/v) TFA) and stored at –80°C until MS measurement. All peptide samples were analyzed in single shots in a trapped ion mobility spectrometry quadrupole time-of-flight mass spectrometer (timsTOF HT, Bruker Daltonics, Billerica, USA) coupled to a Vanquish Neo liquid chromatography system (Thermo Fisher Scientific). In total, 500 ng of each sample was loaded on a 45 cm in-house made HPLC column (packed with 1.9 µM C18 ReproSil Pure-AQ particles) (Müller-Reif et al., 2021) and eluted over a 100 min gradient from 7% to 38% buffer B in 90 min followed by an increase to 98% in 3 min, and a column wash at 98% buffer B for 7 min (buffer A: 0.1% (v/v) formic acid in LC-MS grade H_2O; buffer B: 0.1% (v/v) formic acid, 80% (v/v) acetonitrile, and 19.9% (v/v) LC-MS grade H_2O) with a flow rate of 350 nl/min.

MS data were acquired in a data-independent mode with parallel accumulation followed by serial fragmentation (dia-PASEF) as previously described (Meier et al., 2015). Mass spectra were acquired from 100 to 1700 m/z and 0.7 to 1.45 $1/K_0$ with a 100 ms ramp time at 100% duty cycle at a 1.06 s cycle time. One MS1 scan was followed by 9 dia-PASEF MS2 scans. For raw data analysis, the DIA-NN software (v.1.8.1, https://github.com/vdemichev/DiaNN/) was used to calculate label-free intensities in the library-free mode. Oxidized methionine (OxM) was set as variable modification and carbamidomethyl (C) as fixed modification. The false discovery rate (FDR, also referred to as *q*-value) was set at 0.01 for both peptide and protein levels. The minimal length of the peptides considered for identification was set at seven amino acids, and the option “match between runs” was enabled. Quantification mode was set to

"Robust LC (high precision)," and all other settings were left default. The UniProt database from humans (*Homo sapiens*) was used for peptide and protein identification.

2.5. Statistical Analysis

Pairwise comparison between two groups was performed by Student t-test or Mann-Whitney tests using the Prism software (v.9.5.1, GraphPad, La Jolla, USA), and data are presented as mean (± standard deviation). Comparison of survival rates was performed by Kaplan-Meier analysis with log-rank tests. Differences with $p \leq 0.05$ were considered to be statistically significant. In bioinformatic analyses of the proteome data, a customized Python-based tool was used for statistical analysis and data visualization. Complementarily, the R environment (v.4.2.2, R Foundation for Statistical Computing, Vienna, Austria) was used for data analysis and representation. The Fisher's exact test was used to generate significant enrichment gene ontology (GO) terms with an FDR cut-off level of 0.05.

3. RESULTS

3.1. The Role of ER Stress Signaling in the Clinical Context

3.1.1. ATF6 is amplified in human solid tumors and linked to therapy response

To address the working hypothesis that the ER stress signaling is involved in cancer formation, as well as in cancer therapy responses, a genomic dataset from the publicly available TCGA database was screened for amplification of ATF4, XBP1 and/or ATF6 genes, and associated with prognosis in the form of disease-free survival (**Figure 5**). The frequencies of the amplified genes in major cancer types showed that in several of the most frequent solid cancer types, breast cancer, lung cancer, gastric cancer, CRC and glioblastoma, the ATF6 gene was most frequently amplified among the three ER stress genes (**Figure 5A**). Notably, these ER stress genes were dominantly amplified in the most prevalent human cancer types, and in CRC, the ATF6 gene amplification was the most exclusive to the other genes. Kaplan-Meier analysis revealed that genomic amplification of ATF6 was significantly associated with reduced disease-free survival ($p \leq 0.0001$), while the amplification of ATF4 and XBP1 was not ($p = 0.2232$ and 0.0542, respectively) (**Figure 5B**). For overall survival, in contrast, all three genes showed a significant association with worse survival when upregulated at the genome level (**Figure 5C**, $p \leq 0.0006$).

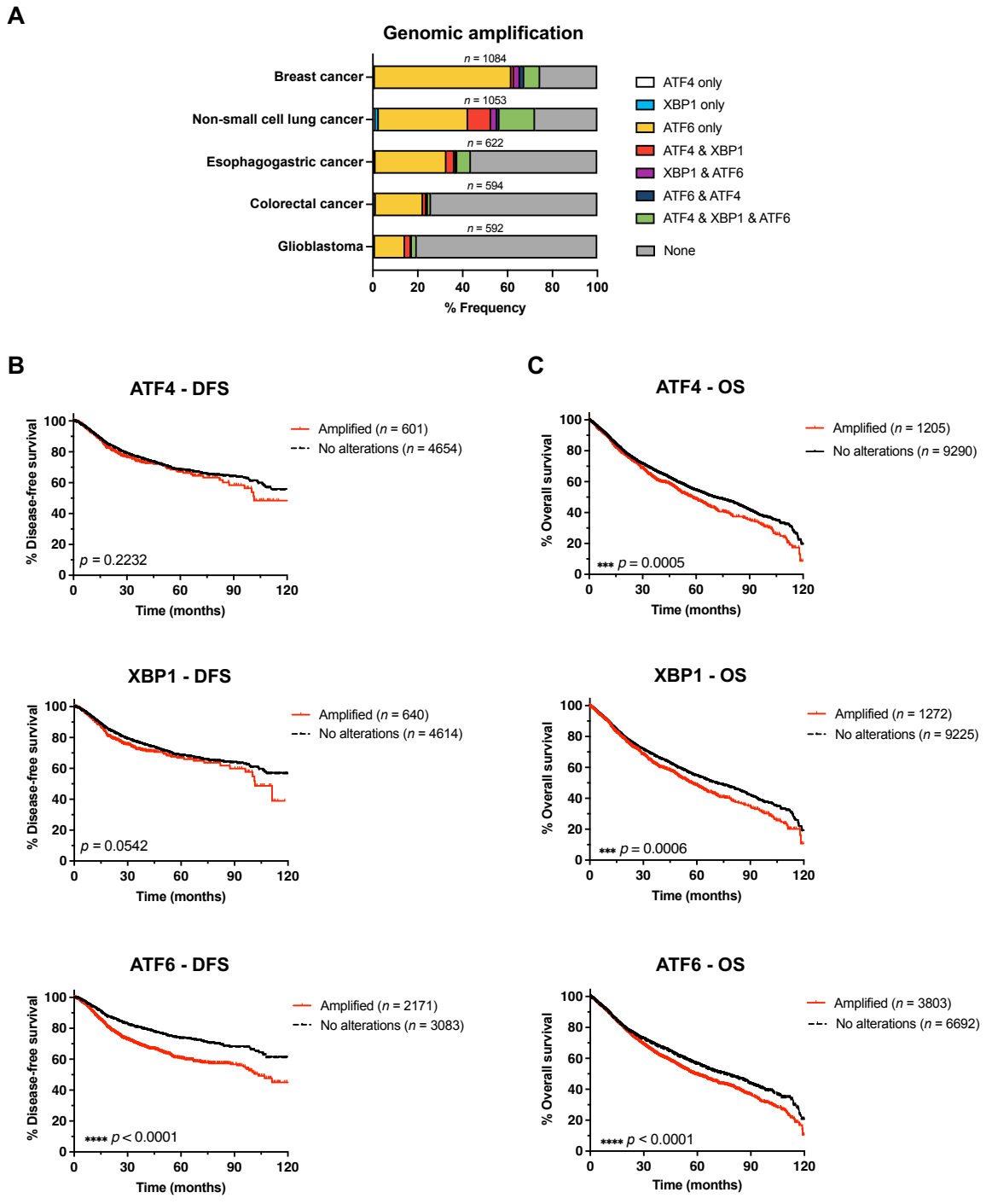

Figure 5: Positive ATF6 specifically associates with disease-free survival in TCGA datasets. (A) Frequencies of ATF4, XBP1 and/or ATF6 genomic amplification in patients with major cancer types. **(B)** Kaplan-Meier analysis of disease-free survival (DFS) among cancer patients with amplified each gene (ATF4, XBP1 or ATF6); **(C)** Kaplan-Meier analysis of overall survival (OS) among cancer patients with amplified each gene (ATF4, XBP1 or ATF6), compared to patients with no alterations from the public TCGA datasets.

3.1.2. ATF6 positively associates with genomic instability in colorectal cancer

Next, the expression of XBP1 and ATF6 was analyzed on protein levels in a small cohort of surgically resected human CRC by flow cytometry (*n* = 7) and compared based on various clinical characteristics. All of the results are summarized in **Table 1**. Three cases were present with MSI, all of which were left-sided. The positivity of ATF6 in the tumor was significantly associated with the presence of MSI, while ATF6 positivity in adjacent normal colon, as well as

Table 1: Correlation between XBP1 or ATF6 positivity and clinical characteristics in cohort 1 (*n* = 7) consisted of human CRC tumors and adjacent normal colon tissues (Mann-Whitney test).

			Comparison between two groups - *p*-values			
			XBP1		**ATF6**	
Clinical characteristics	**All**	**MSI**	**Normal**	**Tumor**	**Normal**	**Tumor**
Gender - no. of patients						
Male	3(2)	1	0.5147	0.8508	0.2137	0.5930
Female	4	2				
Age - years						
Median	73	66	—	—	—	—
Interquartile range	66–80	66–74				
Location - no. of patients						
Right-sided	2(1)	0	0.5232	0.8918	0.7562	0.3726
Left-sided	5	3				
MS status - no. of patients						
MSS	4(3)	–	0.8460	0.5532	0.5211	*0.0195
MSI	3	–				
UICC stages - no. of patients						
I	2(1)	1	—	—	—	—
II	2	0				
III	2	1				
IV	1	1				
pT stages - no. of patients						
T1–2	3(2)	2	0.6104	0.7908	0.1233	*0.0381
T3–4	5	1				
pN stages - no. of patients						
N0	4(3)	1	0.8901	0.8676	0.6230	0.6678
N1–2	3	2				
pM stages - no. of patients						
M0	6(5)	2	0.7066	0.2105	0.7529	0.8952
M1	1	1				

pTNM, pathological tumor-node-metastasis stages; MSI, microsatellite (MS) instable; MSS, microsatellite stable or below the detection limit; () = the sample number for the XBP1 dataset. *$p \leq 0.05$.

XBP1 in tumors, were not. (**Figure 6A**, $p = 0.0195$). Notably, the ATF6 positivity in tumors with MSI tended to be higher than that in matched normal colon upon pairwise comparison, although the difference did not reach significance (**Figure 6B**, $p = 0.1695$). There was also a significant tendency for tumors of earlier pT stages to have higher ATF6 positivity (**Table 1** and

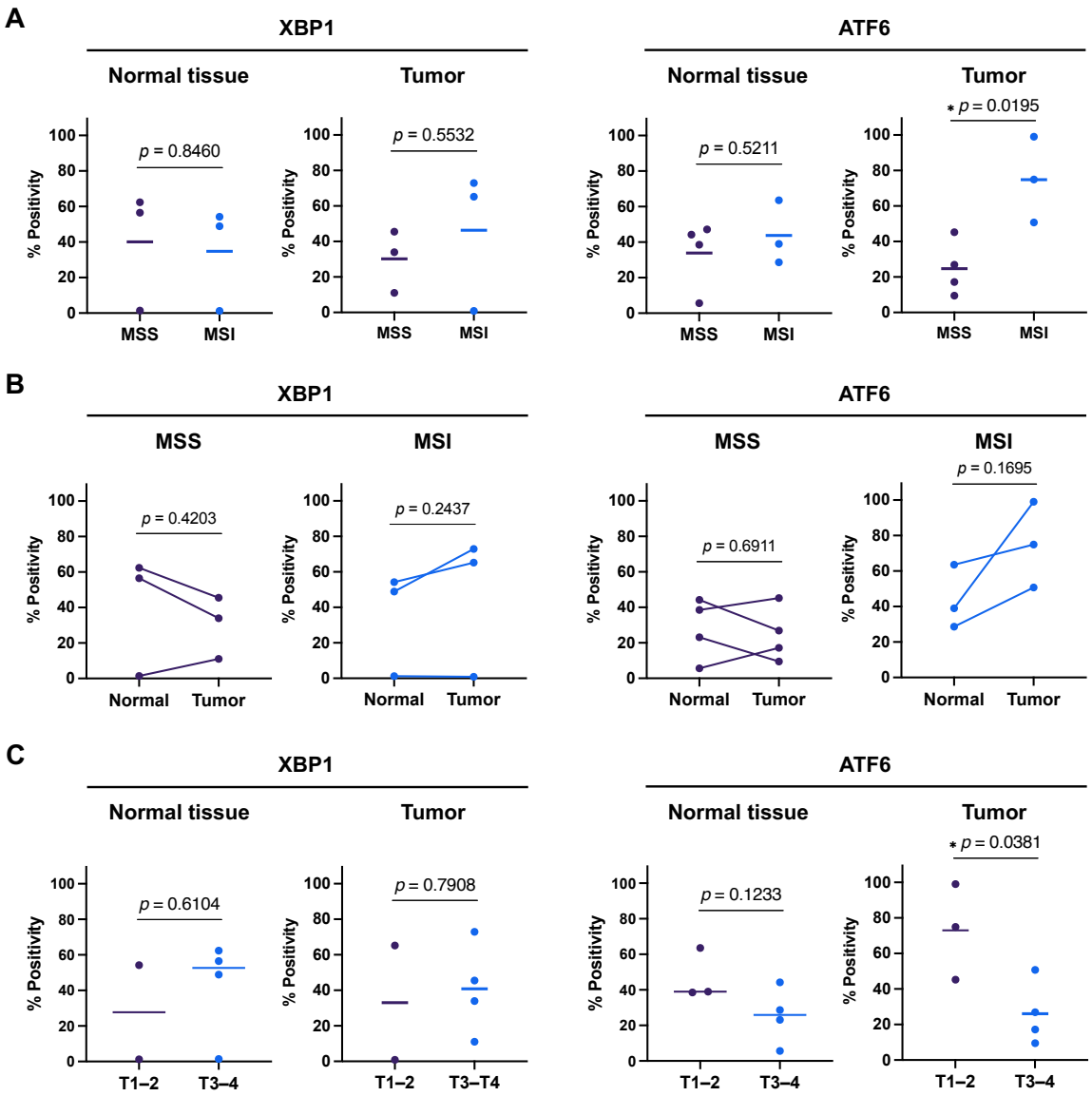

Figure 6: Association of XBP1 and ATF6 staining (FACS) with clinical characteristics derived from surgically resected human CRC. (A) The positivity of XBP1 and ATF6 was assessed by flow cytometry and compared between the MSI group ($n = 3$) and the MSS group ($n = 3–4$). Left, adjacent normal colon tissues; right, colon tumor. **(B)** Comparison between matched pairs of colon tumors and adjacent normal tissues ($n = 3$). Left, MSS group; right, MSI group. **(C)** Comparison between adjacent normal colon tissues or colon tumors at T1–2 and T3–4 stages. MSI, microsatellite instable; MSS, microsatellite stable or below the detection limit.

Figure 6C, $p = 0.0381$). No further significant correlation was observed between the positivity of these markers and any other clinical features such as tumor staging, grading, anatomical location, pN nor pM stages (**Table 1**, $p > 0.05$).

To test the observation that positive ATF6 associates with genomic instability in a larger and independent dataset, we further analyzed TCGA datasets and found that genomic amplification of ATF6 is closely related to DNA aneuploidy and disease-free survival in this context (**Figure 7**). Of note, cancer patient groups were separated into subsets with and without mutation or homozygous deletion in the TP53 gene ($TP53^{MUT}$, $TP53^{WT}$), which has been previously associated with aneuploidy in cancer patients from a TCGA dataset (Taylor et al., 2018). First, patient groups from all cancer types or CRC datasets were compared in terms of the aneuploidy score, defined by the number of chromosome arms with arm-level copy-number alterations (Taylor et al., 2018) (**Figure 7A**). Interestingly, a subgroup with amplified ATF6 gene expression and no TP53 alterations ($ATF6^{AMP}TP53^{WT}$) showed a significant increase in the aneuploidy score ($p \leq 0.0001$) compared to patients with wildtype status for both ATF6 and TP53 ($ATF6^{WT}TP53^{WT}$). In accordance with the well-described role of p53 for genomic stability, TP53 genomic alterations alone were sufficient for a significant association with increased aneuploidy scores ($p \leq 0.0001$, $ATF6^{WT}TP53^{MUT}$ vs. $ATF6^{WT}TP53^{WT}$). However, co-occurrence of ATF6 genomic amplification and TP53 alterations ($ATF6^{AMP}TP53^{MUT}$), which occurred in a substantial fraction of patients, showed the strongest increase in the aneuploidy score ($p \leq 0.0001$), compared to the groups with alterations either in ATF6 or TP53 genes ($ATF6^{AMP}TP53^{WT}$ and $ATF6^{WT}TP53^{MUT}$). Finally, putative prognostic differences between these subgroups were assessed for datasets of all cancer types (PanCancer cohort) or a smaller cohort with CRC by Kaplan-Meier analysis (**Figure 7B**). In the PanCancer dataset, the $ATF6^{WT}TP53^{WT}$ group showed the most favorable survival in comparison to the other groups. Genomic amplification of ATF6, even in a wildtype TP53 background ($ATF6^{AMP}TP53^{WT}$), was significantly associated with reduced overall and disease-free survival ($p \leq 0.01$), and combined alteration of both ATF6 and TP53 ($ATF6^{AMP}TP53^{MUT}$) was associated with even further decreased survival. Notably, the $ATF6^{AMP}TP53^{MUT}$ group in the PanCancer dataset displayed no significant reduction in overall survival compared to the $ATF6^{AMP}TP53^{WT}$ (**Figure 7B**, left). In the dataset of CRC, on the other hand, most likely due to relatively small cohort sizes, no significant difference was observed between the overall survival for these groups. However, the disease-free survival of the $ATF6^{AMP}TP53^{MUT}$ co-occurrence group showed a significant decrease

compared to that of the ATF6^{WT}TP53^{MUT} group, while either ATF6 amplification or TP53 alterations did not show significant association with any changes in the disease-free survival.

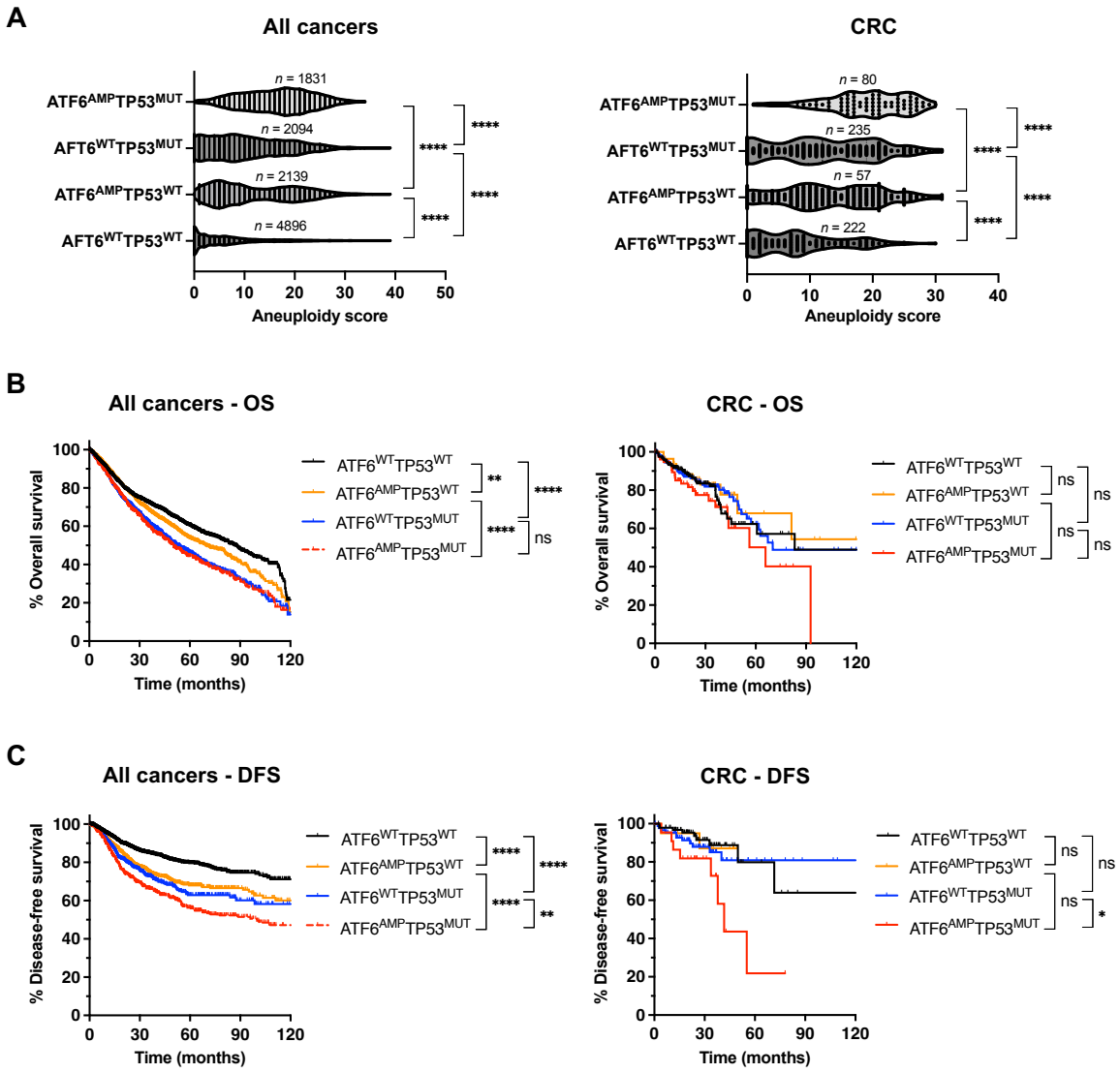

Figure 7: ATF6 genomic amplification concurred with the TP53 mutation closely associates with DNA aneuploidy and poor therapy response in TCGA datasets. (A) Comparison of aneuploidy scores between cancer patients with ATF6 gene amplification (ATF6^{AMP}) plus/minus TP53 mutation or homozygous deletion (TP53^{MUT}) and patients with no alterations (TP53^{WT} and/or ATF6^{WT}). **(B, C)** Kaplan-Meier analysis of overall survival (OS, **B**) and disease-free survival (DFS, **C**) among cancer patients present with TP53^{MUT} and/or ATF6^{AMP} signatures, compared to patients with no alterations (TP53^{WT} and/or ATF6^{WT}) from the public TCGA datasets. Left panels, pooled data from 30 cancer types (PanCancer dataset); right panels, CRC. *$p \leq 0.05$, **$p \leq 0.01$, ****$p \leq 0.0001$.

3.1.3. Application of a new flow cytometric analysis for association of ATF6 positivity with clinical characteristics in a retrospective human CRC cohort

We have been collaborating with Ishihara and Sato group, Nitto Boseki Co., Ltd., in developing a new analytical system based on the isolation of intact cell nuclei from FFPE tissue specimens combined with single-cell assay platforms, including flow cytometry ("Xnuc" system (Sato et al., 2019; Sato & Nakatsuji, 2023)). They established this system on several breast cancer markers for pathological application, such as Ki67, estrogen and progesterone receptors, and validated it in a large trial with retrospective breast cancer patient cohorts in Japan, comparing with a standard pathological evaluation by four trained pathologists on parallel sections (Sato et al., manuscript submitted). Inspired by their approach, a flow cytometric method was established for evaluating the ATF6 positivity in nuclei collected from FFPE tissue specimens (**Figure 8**). Tissue sections (3 × 20 µm) were deparaffinized and

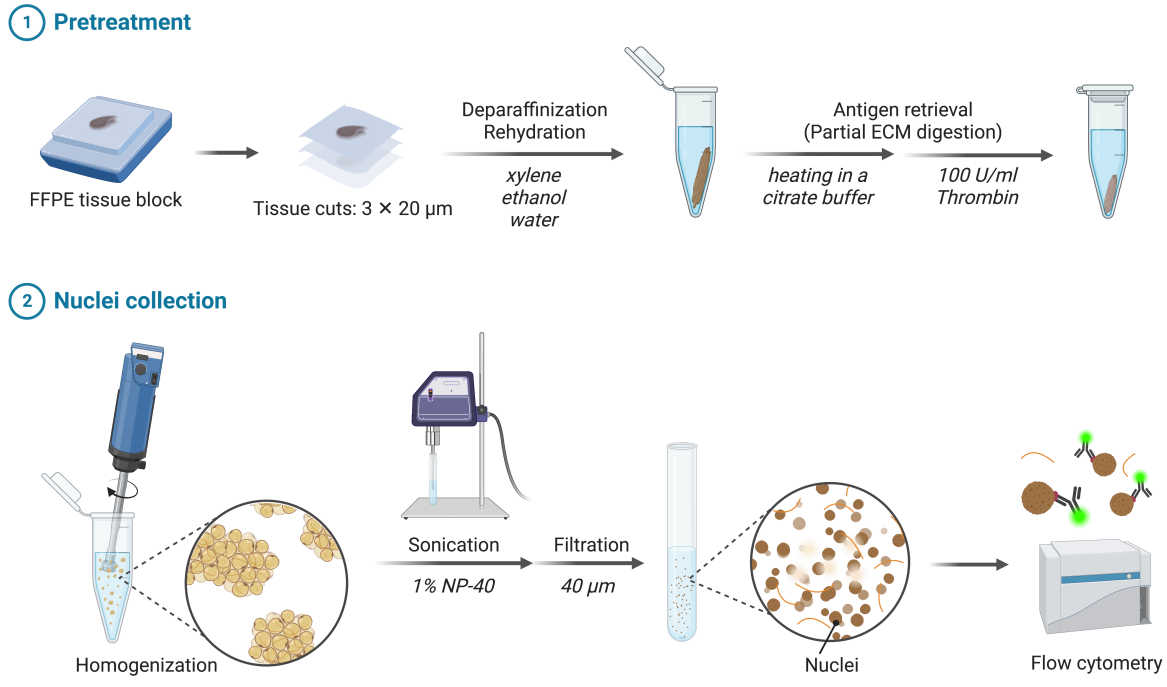

Figure 8: The workflow of nuclei collection from FFPE tissue for flow cytometric analysis. (1) FFPE tissue sections are deparaffinized and rehydrated in xylene-ethanol-water, followed by antigen retrieval by heating in a citrate buffer combined with thrombin digestion for partial degradation of the extracellular matrix (ECM). **(2)** Finally, the tissues are processed by rotor-stator homogenization and sonication in 1% NP-40 and filtration to collect nuclei-rich fraction for flow cytometric characterization. The graphics were created with BioRender.com.

rehydrated in a graded series of xylene-ethanol ending in water, followed by heat-induced antigen retrieval combined with enzymatic digestion that is also intended for partial degradation of the extracellular matrix. For the enzymatic digestion, thrombin was adopted after preliminarily testing several other proteases, including collagenase and dispase, which impaired the stainability of Ki67 below the concentrations benefitting nuclear dissociation (**Appendix Figure S1**). The tissues were further processed with homogenization followed by sonication in buffer containing a nonionic detergent NP-40 and filtration to collect cell nuclei for flow cytometric analysis, where the kind of detergent, its concentration (**Appendix Figure S2**), levels of homogenization and sonication were optimized to achieve sufficient nuclei recovery without much damage in nuclear proteins.

The "Xnuc-based" method was established in order to analyze a retrospective human CRC cohort in the form of FFPE specimens and thus to compensate for the flow cytometric analysis of freshly resected human CRC (**Figure 6**) in a larger sample size and association with clinical follow-up data. Prior to analyzing the cohort samples, these two methods were compared using parallel samples of surgically resected human CRC, part of which were processed into FFPE blocks and used for the flow cytometric analysis of DNA content and several nuclear proteins (**Figure 9**). Cells/nuclei were initially gated on the basis of forward light scatter pulse height and width (FSC-H and -W) to enrich singlet signals (**Figure 9A**, left panels). Compared to the cell population from a fresh tumor, the population from an FFPE sample showed lower FSC-W intensities, indicating a smaller size distribution. Of note, the threshold was arbitrarily set slightly below the level that discriminates singlets from doublets and multiplets of formalin-fixed HCT116 cells. Subsequently, they were further gated on the histograms for DAPI intensities to analyze the DNA content (**Figure 9A**, right panels). Although the particles collected from the FFPE sample contained a large portion of the DAPI-unstained population compared to cells isolated from the fresh tumor, both histograms displayed sharp peaks of DAPI-stained populations ($DAPI^{+}$) at identical intensity. Notably, a subpopulation containing a double amount of DNA (*e.g.,* cells in the G2/M phase, diploid cells) was detected at the twice intensity of the DAPI+ peaks ($DAPI^{++}$) in both histograms, albeit much reduced in the population from the FFPE sample. For simplicity, the positivity of nuclear proteins was determined by focusing on the $DAPI^{+}$ subpopulation (**Figure 9B**). Although the positivity of ATF6 in nuclei collected from FFPE sections was lower than that in cells from the corresponding fresh tumors, the relation between the magnitudes of ATF6 positivity in two different samples

appears to be preserved. However, other nuclear proteins Lamin A/B1/C and Ki67, which reside in the inner nuclear membrane and nucleoplasm, respectively, were much less detectable in the Xnuc-based method. Moreover, optical section images of cell nuclei collected from an FFPE sample showed that ATF6 is inside the nucleus (**Figure 9C**, top). Of note, an ER

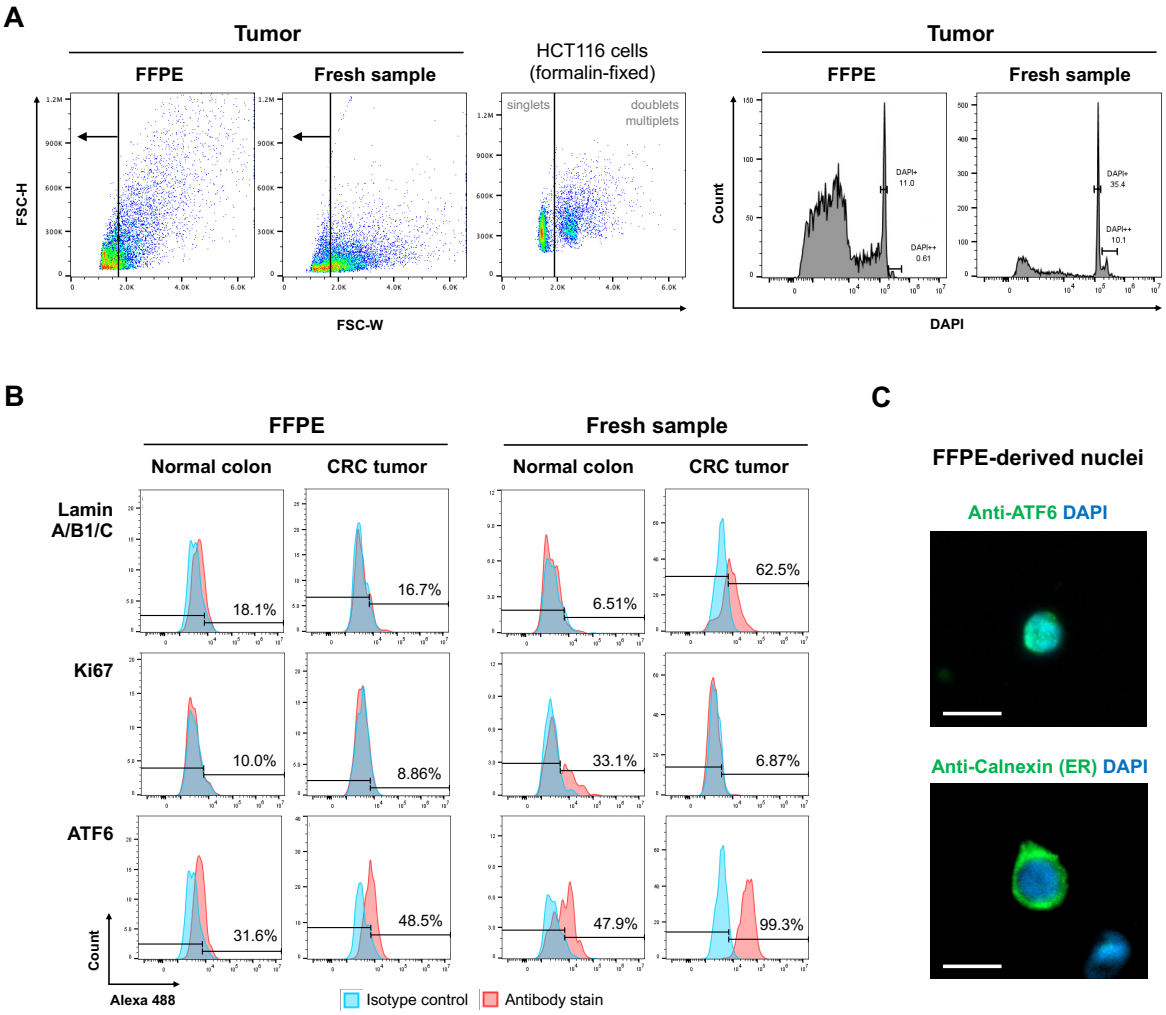

Figure 9: Comparison of two flow cytometric methods for FFPE and fresh tumor using parallel samples of surgically resected human CRC. (A) Scattergrams for forward light scatter pulse height and width (FSC-H/-W) (left) and histograms for DAPI staining (right) of cells/nuclei collected from FFPE/fresh tumor and formalin-fixed HCT116 cells. **(B)** Histograms for isotype control and antibody stain against Lamin A/B1/C, Ki67 and ATF6 (detection: Alexa488-conjugated secondary antibody). Cut-off levels = upper 95 percentile of the isotype control. **(C)** Optical section images of nuclei collected from an FFPE sample co-stained with DAPI and anti-ATF6/anti-calnexin (ER marker) antibodies (detection: Alexa488-conjugated secondary antibody). Scale bar = 20 µm.

protein marker, calnexin, was also clearly detected, suggesting that ER-resident ATF6 remains intact (**Figure 9C**, bottom). Collectively, our protocol for nuclei recovery from FFPE samples was found to be applicable to the flow cytometric analysis of ATF6 positivity in FFPE specimens of human CRC.

Then, ATF6 levels were analyzed in a retrospective human CRC cohort (n = 26) and compared based on their clinical characteristics. Of note, the concentration of antibody and isotype control was optimized by titration on several samples, where the ATF6 positivity was maximized with sufficient differences between median values for the antibody stain and isotype control (**Appendix Figure S3**). The clinical characteristics of all samples and results of comparison between the $ATF6^{low}$ (≤median of ATF6 positivity) and $ATF6^{high}$ (>median of ATF6 positivity) groups are summarized in **Table 2**. Four cases were present with MSI, more than half of which were in the right-sided colon. Comparison between $ATF6^{low}$ and $ATF6^{high}$ groups did not display any significant difference in the clinical characteristics, but the incidence of post-operative disease relapse within one year was associated with high ATF6 levels, albeit failing to achieve significance levels (p = 0.1247). Of note, the $ATF6^{high}$ group tended to be diagnosed at higher ages. On the other hand, the ATF6 positivity was associated (but not significantly) with the presence of MSI and the incidence of disease relapse within 1 year (**Figure 10**, MS status: p = 0.0919; disease relapse, left panel: p = 0.0727). Furthermore, the cumulative risk of disease relapse for the $ATF6^{high}$ group was determined to be significantly higher than that for the $ATF6^{low}$ group (**Figure 10**, p = 0.0206). There was also a weak tendency that tumors of earlier pN stages have higher ATF6 positivity (**Figure 10**, p = 0.1609). No further obvious association between the positivity of ATF6 and any other clinical features such as tumor staging, grading, anatomical location, pT nor pM stages.

Table 2: Correlation between ATF6 positivity and clinical characteristics in cohort 2 (*n* = 26) consisted of human CRC tumors (χ^2-test).

			Comparison between ATF6$^{high/low}$ groups		
Clinical characteristics	**All**	**MSI**	**ATF6^{high} group (%)**	**χ^2**	***p*-value**
Gender - no. of patients					
Male	15	2	8 (53.3)	0.16	0.6914
Female	11	2	5 (45.5)		
Age - years					
Median	70	67	66	—	—
Interquartile range	64–77	63–71	57–70		
Location - no. of patients					
Right-sided	10	3	5 (50.0)	0.00	1.0000
Left-sided	16	1	8 (50.0)		
MS status - no. of patients					
MSS	15	—	7 (46.7)	1.02	0.3133
MSI	4	—	3 (75.0)		
n.a.	7	—	3 (42.9)		
UICC stages - no. of patients					
I	3	1	2 (66.7)	—	—
II	7	1	4 (57.1)		
III	10	2	3 (30.0)		
IV	6	0	4 (66.7)		
pT stages - no. of patients					
T1–2	7	2	4 (57.1)	0.47	0.4951
T3–4	19	2	8 (44.4)		
pN stages - no. of patients					
N0	12	2	7 (58.3)	0.62	0.4314
N1–2	14	2	6 (42.9)		
pM stages - no. of patients					
M0	18	4	8 (44.4)	0.72	0.3954
M1	8	0	5 (62.5)		
Disease relapse - no. of patients					
None (<1 year)	8	2	2 (25.0)	2.36	0.1247
(≥1 year)	7	1	4 (57.1)		
Relapse (<1 year)	4	0	4 (100.0)		
(≥1 year)	0	0	0		
Cancer death	0	0	0		
Non-cancer death	2	0	1 (50.0)		
n.a.	5	1	2 (40.0)		

pTNM, pathological tumor-node-metastasis stages; MSI, microsatellite (MS) instable; MSS, microsatellite stable or below the detection limit; ATF6^{low}, ATF6^{high}, patients who displayed ATF6 positivity above (high) or below (low) the median of all 26 cases. n.a., not available.

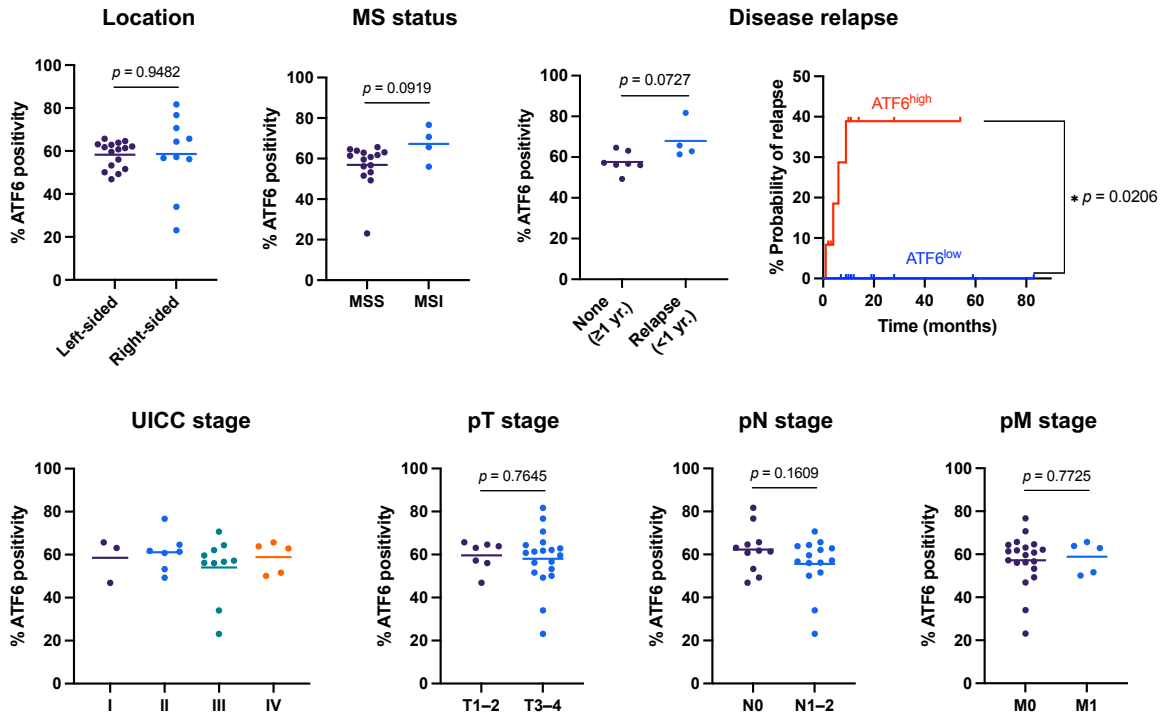

Figure 10: Association of the ATF6 positivity with clinical characteristics derived from a retrospective human CRC cohort. The positivity of ATF6 in FFPE specimens of the human CRC cohort (**Table 2**, *n* = 26) was determined by the collection of cell nuclei and flow cytometric analysis and then compared based on several clinical characteristics: anatomical location, microsatellite (MS) status, disease relapse within 1 year, UICC stage, pT-, pN- and pM-stages. MSI, microsatellite instable; MSS, microsatellite stable or below the detection limit. $ATF6^{high/low}$, patients who displayed ATF6 positivity above (high) or below (low) the median of all 26 cases.

In summary, the genomic analysis of cancer patients showed that ATF6 is predominantly amplified at a genome level in several prevalent types of solid cancer and correlated with an increased risk of postoperative disease relapse. Moreover, in protein levels, high positivity of ATF6 was specifically associated with MSI in surgically resected human CRC. The putative association between high ATF6 levels and genomic instability was supported by further genome-based data showing that amplified ATF6 is closely related to aneuploidy and poor prognosis of CRC in this context. Furthermore, we established a method that is essentially identical to a published one for collecting nuclei from FFPE specimens of human tissue and successfully applied it to the flow cytometric analysis of ATF6 in a retrospective human CRC cohort for the association with clinical characteristics, including follow-up data, indicating positive correlation between high ATF6 levels and MSI or disease relapse, albeit not significant.

3.2. Generation of ER Stress Reporter Cell Lines

3.2.1. Basal ER stress activity and chemoresistance in human cell lines

The observed connection between the ER stress activity and clinical features related to therapy response motivated us to examine the basal activity of ER stress signaling in human cell lines under normal *in vitro* growth conditions, as well as their resistance to oxaliplatin (OxaPt) treatment. A panel of human CRC cell lines, immortalized embryonic kidney cells and hepatocytes were analyzed by qRT-PCR to determine the relative variation in the basal gene expression of ATF4, sXBP1, uXBP1 and ATF6 (**Figure 11A**). Immunoblot analysis of subcellular fractions from HCT116, HT29 and DLD1 cells detected a prominent nuclear localization of sXBP1 (spliced) and nATF6 (cleaved), showing that the ER stress signaling may be constitutively activated in these CRC cell lines (**Figure 11B**). Interestingly, the basal gene expression levels

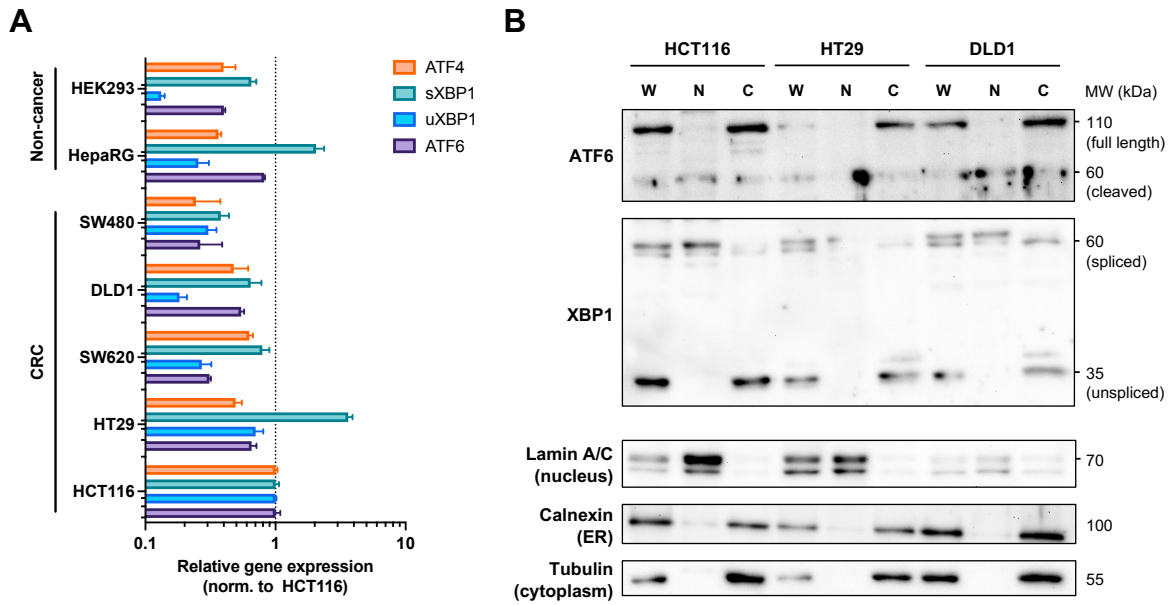

Figure 11: The basal activity of ER stress signaling in human cell lines under standard *in vitro* growth conditions. (A) Comparison of basal gene expression levels of ATF4, (s/u)XBP1 and ATF6 between human cell lines. Individual signals were normalized to those of HCT116 cells (annotated with the dashed line). **(B)** Immunoblot analysis of subcellular fractions from HCT116, HT29 and DLD1 cells against ATF6, XBP1 as well as Lamin A/C (nucleus marker), calnexin (ER marker) and tubulin (cytosolic marker). W, whole cell lysate; N, nucleus fraction; C, cytosolic fraction.

positively correlated with the respective IC_{50} values, determined in MTT assays in response to OxaPt treatment, even though the correlation did not achieve significance (**Figure 12A**, **B**, n = 6, r = 0.3903–0.7362, p = 0.0952–0.4442).

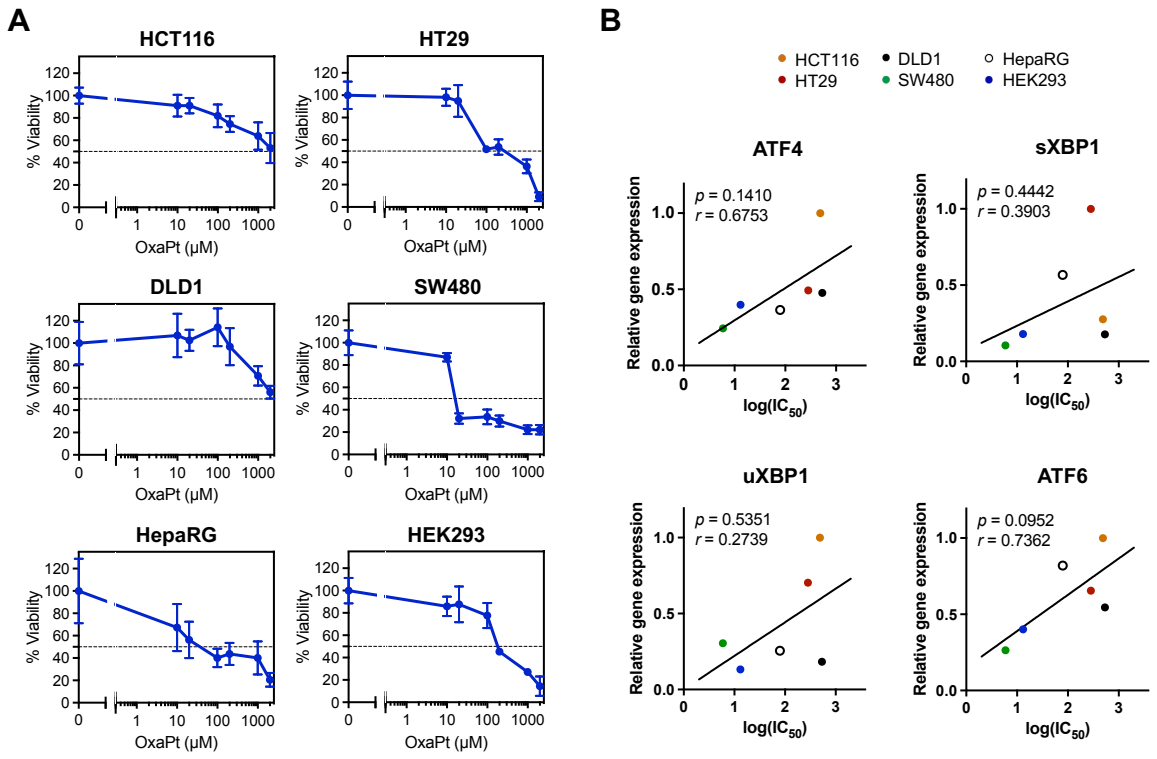

Figure 12: The connection between the basal activity of ER stress signaling and chemoresistance of human cell lines. (A) MTT assays of 6 human cell lines to OxaPt (0–2 mM, 24 h). **(B)** Correlation between the basal gene expression of ATF4, (s/u)XBP1, ATF6 and IC_{50} values determined by MTT assays of 6 human cell lines to OxaPt (0–2 mM, 24 h). *r*, Pearson's correlation coefficient. OxaPt, oxaliplatin.

3.2.2. Generation and characterization of ER stress reporter cell lines

To monitor and modulate the expression and activation of ATF4, XBP1 and ATF6 in detail, HEK293 cells were chosen, which showed relatively low basal ER stress activity. Thus, cells were transfected with plasmid vectors encoding a reporter gene for either ATF4, XBP1 or ATF6 (**Figure 13A**, ATF4-mS, XBP1-mN and ATF6-GFP). Highly similar to the endogenous genes, the ATF4-mS and (s)XBP1-mN are expressed by translational frameshift under ER stresses. Of note, mimicking the nuclear localization sequence (NLS) found in the native systems, a c-MYC NLS

was added to the C-terminus of ATF4-mS and XBP1-mN fusion proteins, which reduced a diffuse of fluorescent signals across the cytosol (Walter et al., 2015). In contrast to the ATF4-mS and XBP1-mN that harbor a fluorophore at the C-terminus, the ATF6-GFP plasmids encode a green fluorescence protein at the N-terminus. ATF6-GFP fusion proteins also undergo the same post-translational processes as native ATF6 under ER stresses, translocating to the Golgi apparatus, followed by cleavage to release (n)ATF6-GFP to the cytosol, which then can enter the nucleus (Chen et al., 2002). As a control for a reporter gene not directly related to the ER stress signaling, a vector encoding with histone H2A and the fluorophore mScarlet (H2A-mS) was used in parallel. The reporter gene expression in stably transfected cells was evaluated under the canonical ER stress induced by pharmacological treatment with Tg. By using flow cytometry (**Figure 13B**), the reporter gene baseline expression was confirmed in the transfected cells, and an upregulation under thapsigargin (Tg) treatment (*i.e.*, bona fide ER stress), while the H2A-mS control failed to respond. Moreover, qRT-PCR confirmed that the transfected cells showed increased expression of total (endogenous and exogenous) ATF4, XBP1 and ATF6, compared to the wildtype cells (**Figure 13C**). Of note, an expression of some exogenous reporter genes was also found to affect the endogenous expression of the others (**Figure 13D**). For example, expression of the reporter XBP1 induced overexpression of the endogenous ATF4 gene under ER stress but not under unstimulated conditions. The reporter ATF6 expression also induced the endogenous ATF4 gene expression on the basal levels without stimulation. Similarly, the ATF4 and ATF6 reporters both increased the expression of the endogenous XBP1 gene, which was comparable to the levels of total XBP1 gene expression induced by the XBP1 reporter. In contrast, the endogenous ATF6 expression levels were not much affected by the ATF4 and XBP1 reporters. Of note, we also attempted to establish reporter cell lines on HCT116 and DLD1 by stable transfection and positive selection for ER stresses. However, reporter gene expression in these cell lines was unstable over several passaging, and even after subcloning, most showed heterogeneous and inconsistent responses to ER stress (**Appendix Figure S5**). Therefore, we used HEK293-based reporter cell lines for further characterization.

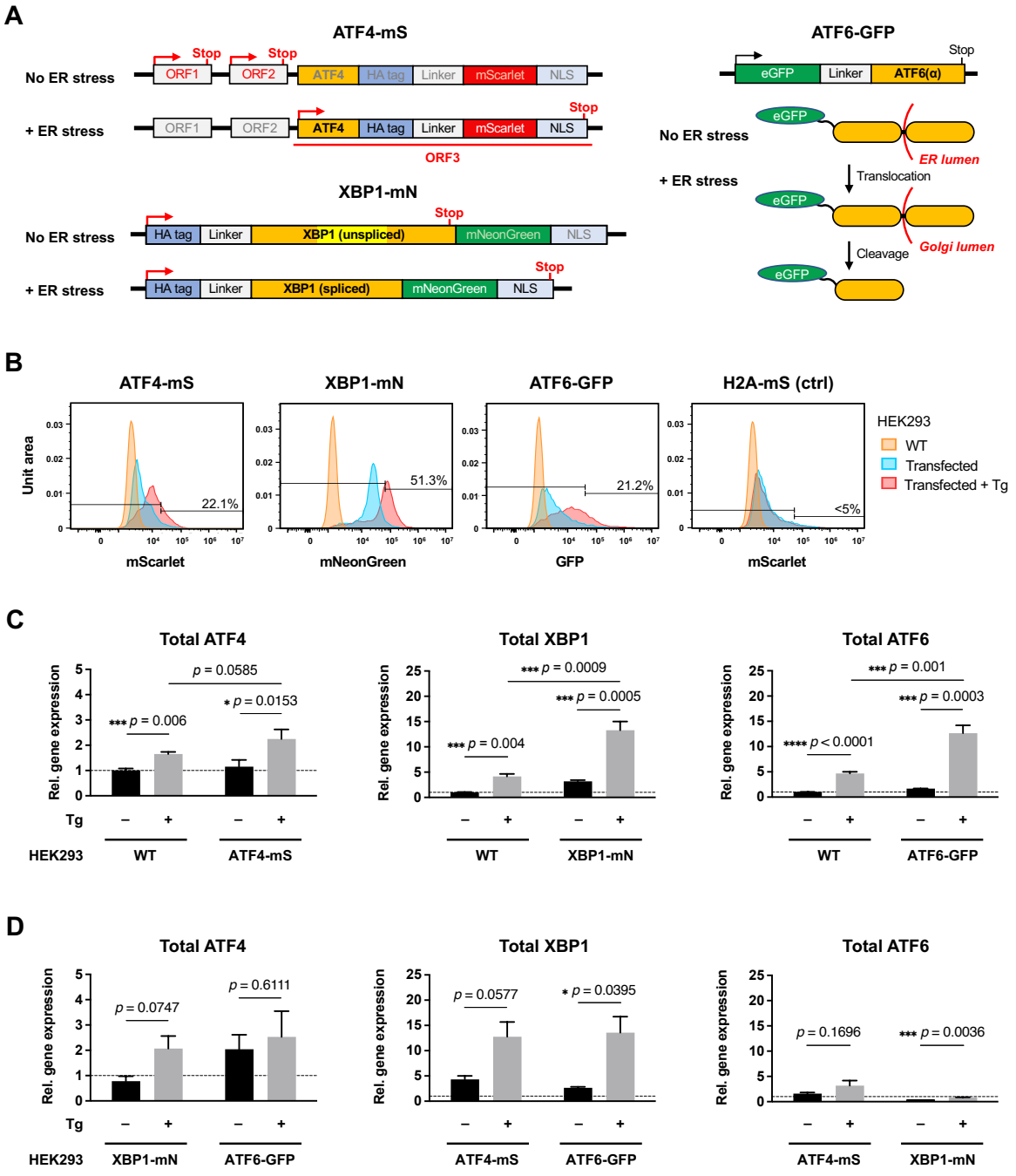

Figure 13: Generation and validation of ER stress reporter cell lines. **(A)** Design of ER stress reporter genes encoded with fluorescently labeled ATF4, XBP1 or ATF6. **(B)** The reporter gene expression in transfected HEK293 cells was validated after treatment with Tg (1 µM, 24 h). Cut-off levels = 95 percentile of transfected cells without Tg treatment. **(C)** Total (endogenous plus exogenous) expression of ATF4, XBP1 and ATF6 in transfected HEK293 cells was analyzed by qRT-PCR after treatment with Tg (1 µM, 24 h). The signals were normalized to that of untreated HEK293 WT cells. **(D)** Cross-effects of the reporter gene expression on endogenous expression of the other ER stress transcription factors. The signals were normalized to that of untreated HEK293 WT cells (annotated with the dashed lines). Tg, thapsigargin.

3.3. The Role of ER Stress Signaling in Chemotherapy Resistance *in Vitro*

3.3.1. Modulation of the ER stress branches positively affects chemoresistance

Next, the reporter cell lines were tested for the response to OxaPt to evaluate their putative functional effects of the modulated ER stress signaling branches. XTT assays were used to derive and compare the IC_{50} values, showing that the reporter gene expression indeed positively affected the resistance against OxaPt (**Figure 14A**). Of note, XBP1-mN expression significantly increased the OxaPt resistance compared to the parental control cells, while the H2A-mS control expression did not show any significant increase. Changes in the total expression of ATF4, XBP1 and ATF6 were evaluated after OxaPt treatment by qRT-PCR analysis (**Figure 14B**). OxaPt induced upregulation of XBP1 significantly in wildtype cells, while the ATF4-mS and XBP1-mN reporter cells did not show any upregulation of ATF4, XBP1 and ATF6. ATF6-GFP reporter cells showed increased expression of all the transcription factors in response to the OxaPt-induced stress. In contrast to the negative controls for the Tg-induced ER stress (**Figure 13C**), these reporter cells showed basally upregulated expression of the respective genes without OxaPt treatment, indicating that the reporter gene expression can be influenced by cell culture artifacts such as confluence. On the other hand, H2A-mS control cells showed a similar pattern to the wildtype cells with lower basal expression levels of all the three factors and significant upregulation of ATF4 and XBP1 in response to OxaPt.

3.3.2. Inhibition of ATF6 sensitizes ER-stressed HCT116 cells to chemotherapy

HCT116 and HEK293 cells were tested with several pharmacological inhibitors targeted to each ER stress signaling branch (GSK-2656157, STF-083010 and Ceapin-A7), to examine their respective effects on the resistance against OxaPt. The compound GSK-2656175 (GSK'157) is known to selectively deactivate PERK phosphorylation, thus interfering with the p-eIF2α/ATF4 pathway (Axten et al., 2013). The compound STF-083010 (STF'010) is an IRE1α endonuclease inhibitor, which blocks the splicing of XBP1 mRNA without affecting its kinase activity (Papandreou et al., 2011). Lastly, Ceapin-A7 was used as an ATF6 inhibitor which specifically blocks ER-to-Golgi transport of ATF6 (Gallagher et al., 2016). The cell viability after the

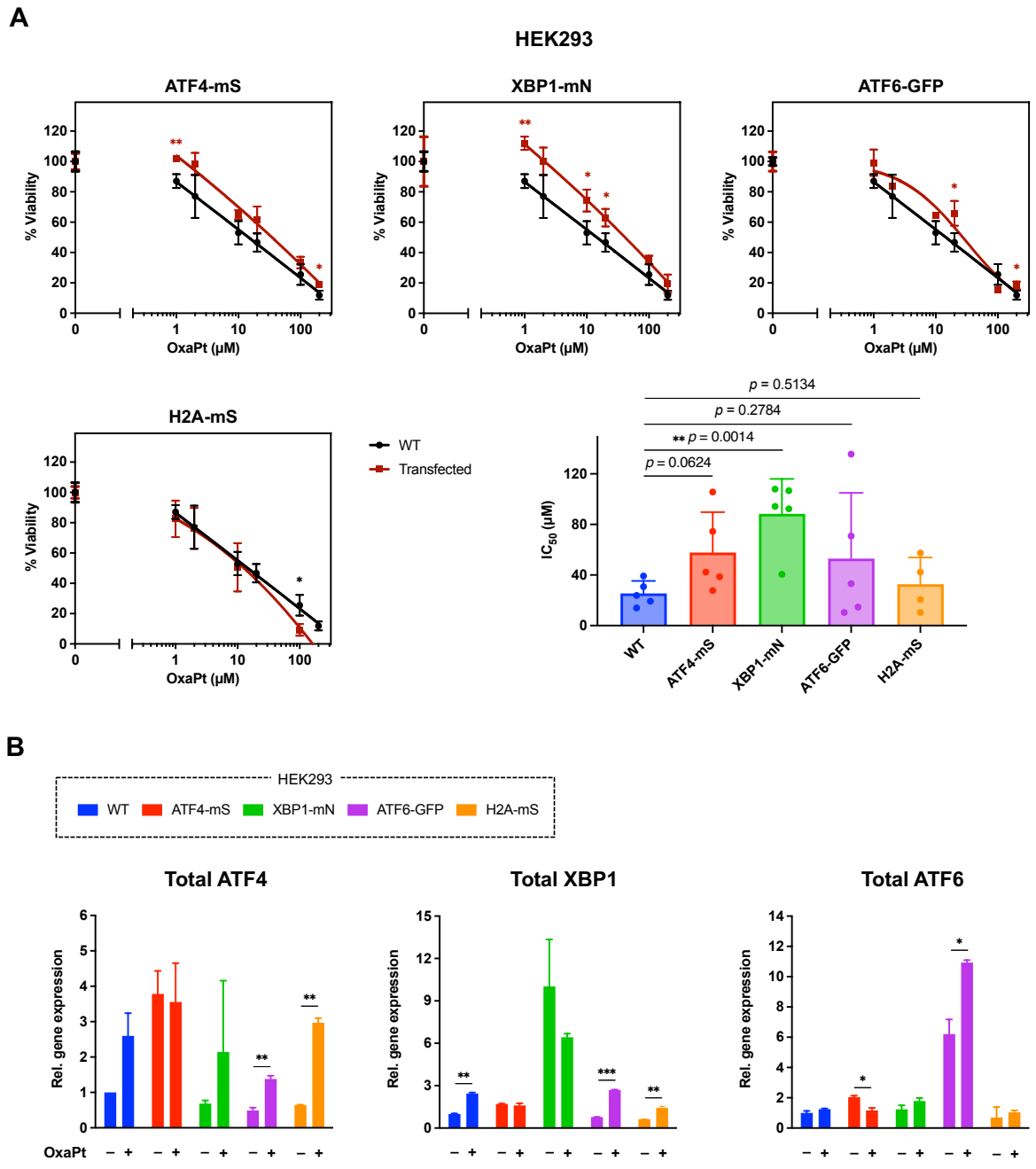

Figure 14: Modulation of the ER stress signaling branches positively affects chemoresistance. (A) XTT assays of ER stress reporter cells to OxaPt (0–200 µM, 24 h). *$p \leq 0.05$, **$p \leq 0.01$, compared to HEK293 WT cells. IC_{50} values determined by the XTT assay (n = 4–5) were compared to HEK293 WT cells. **(B)** Total (endogenous plus exogenous) expression of ATF4, XBP1 and ATF6 in HEK293 reporter cells was analyzed by qRT-PCR after treatment with OxaPt (20 µM, 24 h). *$p \leq 0.05$, ** $p \leq 0.01$, *** $p \leq 0.001$, compared to untreated cells. OxaPt, oxaliplatin.

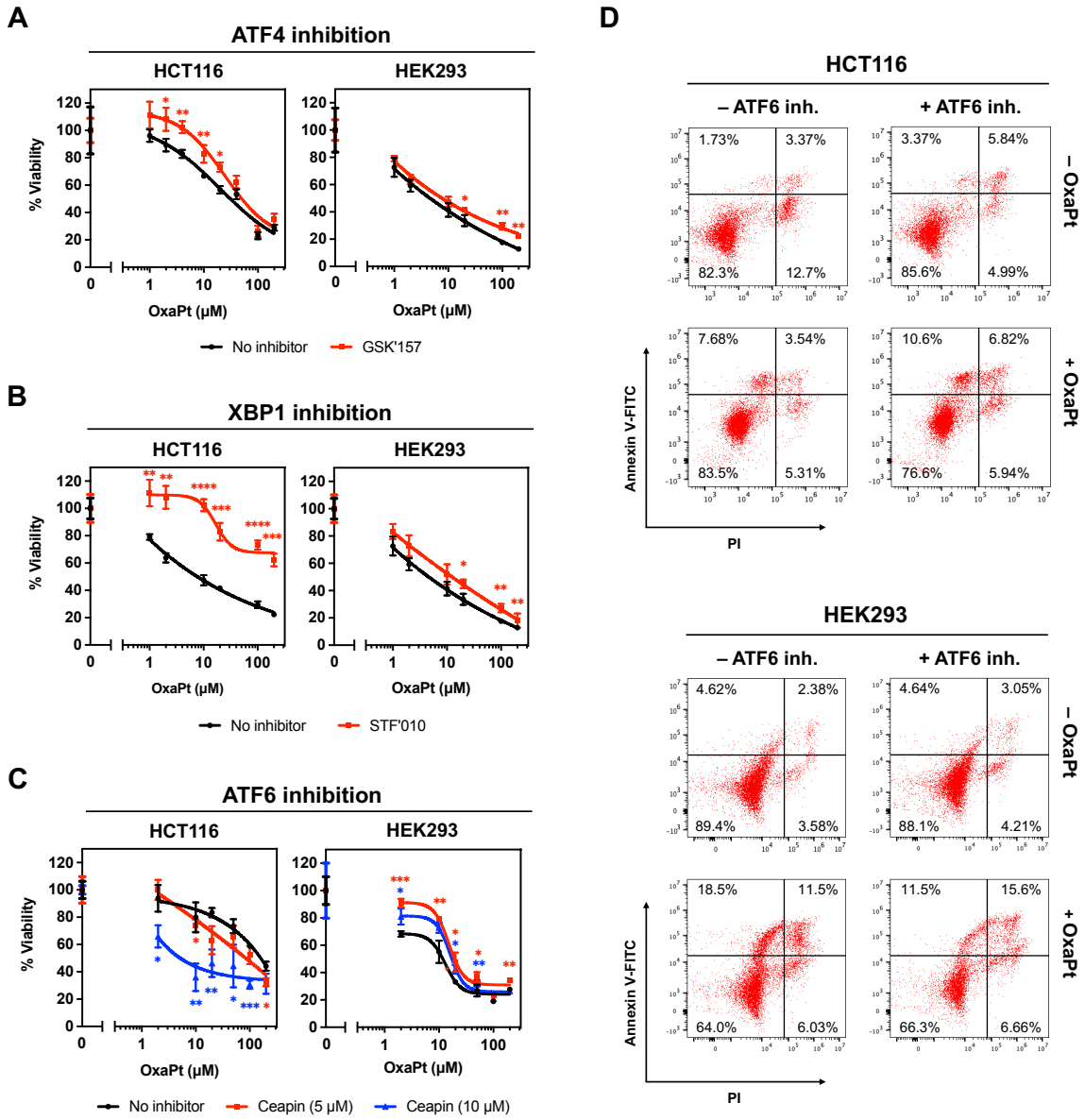

Figure 15: Inhibition of ATF6 sensitizes ER-stressed cells to chemotherapy. (A–C) The XTT assay of HCT116 and HEK293 cells treated with inhibitors for ER-stress receptors and OxaPt. HCT116 and HEK293 cells were treated with GSK2656157 (**A**, GSK'157, 10 μM, 1 h), STF-083010 (**B**, STF'010, 50 μM, 1 h) or Ceapin-A7 (**C**, Ceapin, 5 or 10 μM, 6 h) prior to the treatment with OxaPt (0–200 μM, 24 h). *p ≤ 0.05, **p ≤ 0.01, ***p ≤ 0.001, ****p ≤ 0.0001. **(D)** Flow cytometric analysis of apoptosis in HCT116 and HEK293 cells treated with Ceapin-A7 (ATF6 inh., 5 μM, 1 h) prior to the treatment with OxaPt (20 μM, 24 h). OxaPt, oxaliplatin.

combined treatment with the inhibitors and OxaPt was evaluated by XTT assays (**Figure 15A–C**). ATF6 inhibition in HCT116 cells, which were found in previous assays to have relatively high basal ER stress activity (**Figure 11A, B**), resulted in a clear decrease of the resistance to OxaPt (**Figure 15C**, HCT116), while ATF4 and XBP1 inhibition showed a reverse effect, leading to increased OxaPt resistance (**Figure 15A, B**, HCT116). On the other hand, HEK293 cells, a non-tumor-derived cell line with lower basal ER stress activity (**Figure 11A**) showed increased resistance to OxaPt when treated with these inhibitors (**Figure 15A–C**, HEK293). Moreover, apoptotic cells were preliminarily quantified after the combined treatment with the ATF6 inhibitor and OxaPt by flow cytometric assays based on Annexin V (Annexin) and propidium iodide (PI) staining (**Figure 15D**). HCT116 cells treated with the ATF6 inhibitor showed increased sensitivity to OxaPt, displaying less $Annexin^{-}PI^{-}$ (viable) cells and more $Annexin^{+}PI^{-}$ (early apoptotic) cells and $Annexin^{+}PI^{+}$ (late apoptotic/necrotic) cells, compared to those without ATF6 inhibitory treatment. On the other hand, the ATF6 inhibition in HEK293 cells, which were found to have lower basal ER stress levels than HCT116 cells, was leading to a reduction in early apoptotic cells.

3.3.3. Differential effect of ATF6 inhibition on chemotherapy response between human normal colon organoids and tumor organoids

Organoids, three-dimensional (3D) *in vitro* cellular models from tissue-derived stem cells with the capacity to self-organize into “mini-organs” mimicking the original tissue, represent an advanced experimental tool for the prediction of treatment response, bridging the gaps between traditional 2D culturing techniques and clinical or preclinical setups (Drost & Clevers, 2018). In this study, we established a 3D culture system for organoids derived from patients with CRC or adjacent non-diseased colon mucosa tissue based on previous protocols (Barker et al., 2007; Kondo et al., 2011), and used it to examine the effect of pharmacological ATF6 inhibition on basal viability and the resistance to OxaPt. As depicted in **Figure 16A**, normal colon organoids (colonoids) or tumor organoids (tumoroids) were initiated by isolating colonic crypts or tumor cell clusters, respectively, from surgically resected tissue samples and cultured in a serum-free 3D matrix (Matrigel) along with medium containing stem cell-niche growth factors, which depends on the origin of organoids. Of note, the time-lapse images of the organoids for the first few days (**Figure 16B**) highlighted that normal colonoids grow into well-

organized and more differentiated mono-layered epithelial structures with crypt- and villus-like domains, while tumoroids grow as relatively amorphous structures repeating bubble burst, shrinkage and regrowth, somewhat resembling *in vivo* tumor architectures.

Then, the patient-derived colonoids and tumoroids were subjected to the combined treatment with the ATF6 inhibitor Ceapin-A7 and OxaPt to examine the putative sensitizing

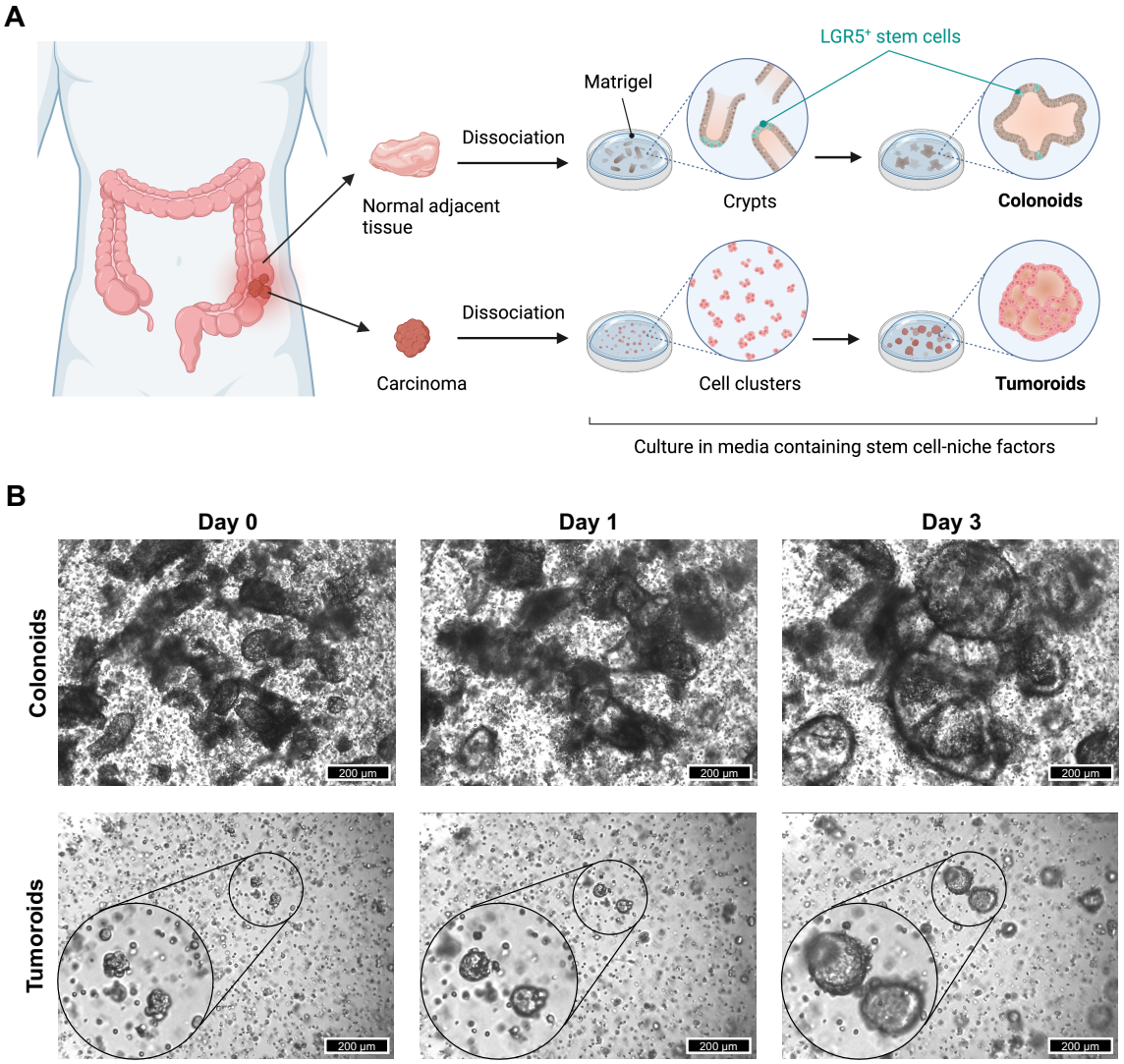

Figure 16: Establishment of a patient-derived colon organoid culture system. (A) Schematic representation of human colonoids or tumoroids culture. Colon crypts (top) or tumor cells (bottom) were isolated from CRC patients, embedded with Matrigel and cultured in media containing stem cell-niche growth factors. **(B)** Time-lapse imaging of colonoids (top) and tumoroids (bottom) growths for 3 days after initiation. The graphics were created with BioRender.com.

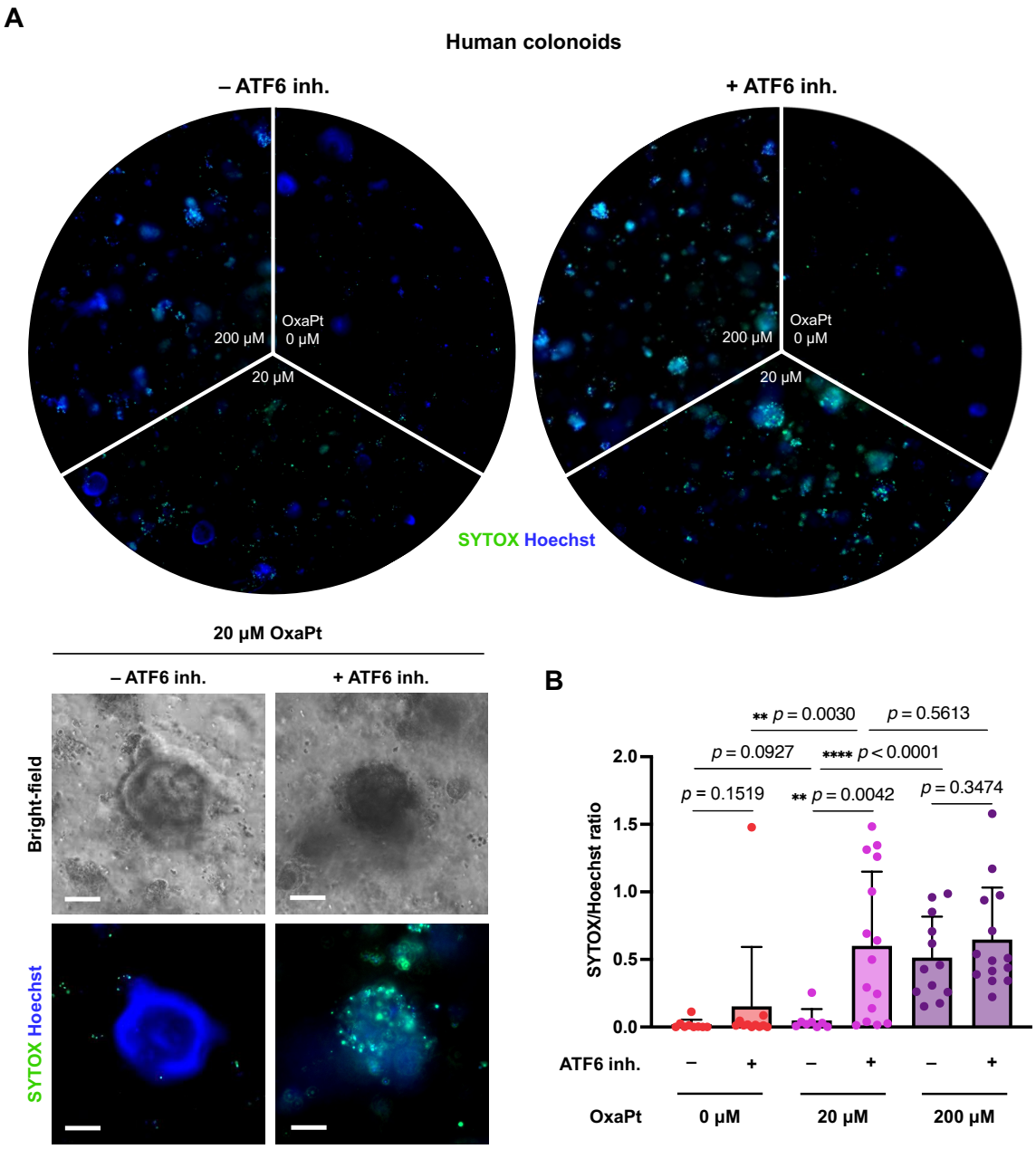

Figure 17: Inhibition of ATF6 sensitizes human colonoids to chemotherapy. (A) Patient-derived colonoids were treated with Ceapin-A7 (ATF6 inh., 1 µM, 6 h) prior to the treatment with OxaPt (0–200 µM, 48 h), followed by co-staining with SYTOX and Hoechst. Scale bar = 100 µm. **(B)** SYTOX/Hoechst ratios (each data point represents one organoid) were compared between different treatments. Organoids were isolated from adjacent normal colon tissues of a stage IV CRC patient. OxaPt, oxaliplatin.

effect of the ATF6 inhibition on the resistance to chemotherapy by cytotoxicity assays, based on co-staining with SYTOX, a DNA dye that exclusively penetrates damaged cell membranes, and Hoechst dye, a DNA dye that penetrates membranes of both living and dead cells (**Figure 17**; **Figure 19**). According to the ratio of SYTOX/Hoechst fluorescence intensities, colonoids showed a remarkable increase in the sensitivity to 20 µM OxaPt when treated with Ceapin-A7, as compared to those without inhibitory treatment (**Figure 17B**, $p = 0.0042$). Interestingly, the cytotoxicity observed was on a level with colonoids treated with 200 µM OxaPt, an extremely toxic condition for cells grown in 3D (**Figure 17B**, $p = 0.5613$). Of note, other pharmacological inhibitors targeted to PERK-ATF4 and IRE1-XBP1 signaling branches or activation of ER stress (GSK'157, STF'010 and Tg, respectively) had no observable impact on the resistance of normal-tissue derived colonoids to OxaPt (**Figure 18**), indicating that pharmacological ATF6 inhibition specifically sensitizes colonic epithelial and stem cells to OxaPt therapy.

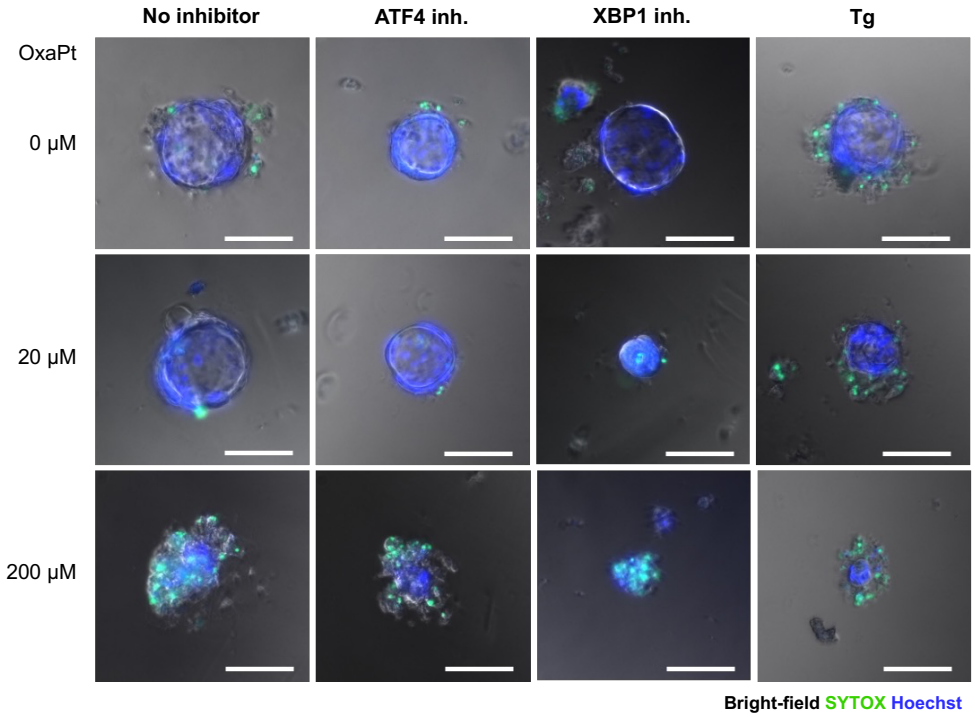

Figure 18: Inhibition of ATF4/XBP1 or activation of ER stress signaling by thapsigargin has no obvious effect on the chemosensitivity of human colonoids. Patient-derived colonoids were treated with GSK'157 (ATF4 inh., 10 µM, 1 h), STF'010 (XBP1 inh., 50 µM, 1 h) or Tg (1 µM, 1 h) prior to the treatment with OxaPt (0–200 µM, 48 h), followed by co-staining with SYTOX and Hoechst. Scale bar = 100 µm. Organoids were isolated from adjacent normal colon tissues of a stage I CRC patient. OxaPt, oxaliplatin; GSK'157, GSK2656157; STF'010, STF-083010; Tg, thapsigargin.

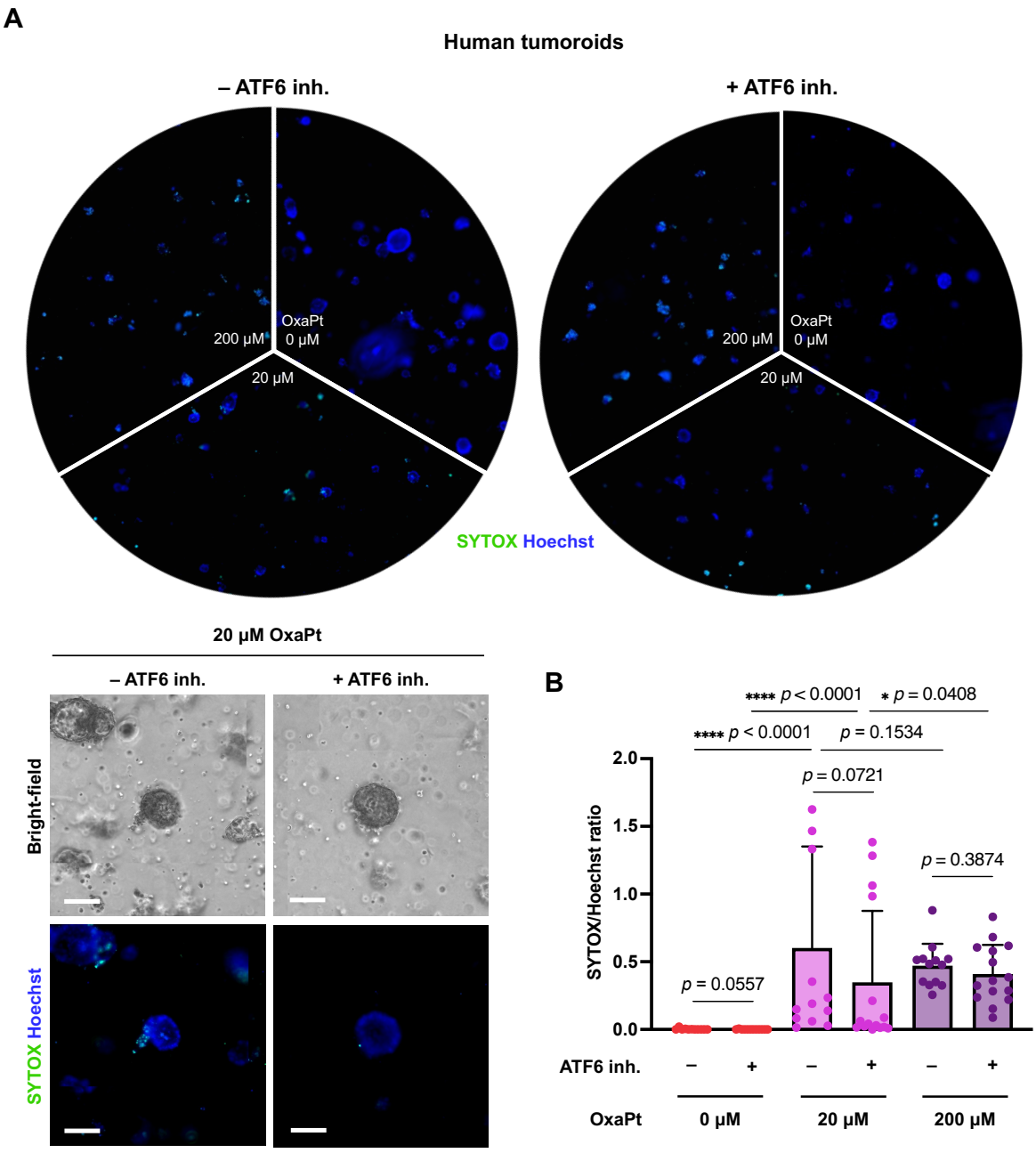

Figure 19: Inhibition of ATF6 in human tumoroids does not affect chemotherapy response. (A) Patient-derived tumoroids were treated with Ceapin-A7 (ATF6 inh., 1 µM, 6 h) prior to the treatment with OxaPt (0–200 µM, 48 h), followed by co-staining with SYTOX and Hoechst. Scale bar = 100 µm. **(B)** SYTOX/Hoechst ratios (each data point represents one organoid) were compared between different treatments. Organoids were isolated from the adenocarcinoma of a stage IV CRC patient. OxaPt, oxaliplatin.

In contrast, tumoroids showed no significant alterations in the sensitivity to 20 µM OxaPt when treated with Ceapin-A7, as compared to those treated with OxaPt alone (**Figure 19B**, *p* = 0.0721). Notably, the sensitivity of tumoroids to OxaPt treatment, regardless of the pharmacological inhibition, was essentially comparable at concentrations of either 20 µM or 200 µM, which was also on a level with normal colonoids treated with 200 µM OxaPt, as described earlier. Thus, it is likely that this value represents the maximum cytotoxic effect of OxaPt that can be measured by this assay.

3.3.4. Chemotherapy induces the ER stress response in non-canonical manner

Kinetics of the ER stress signaling activation in HEK293 cells was analyzed under OxaPt treatment and compared with the "canonical" ER stress responses induced by Tg treatment (**Figure 20**). Immunoblot analysis showed that OxaPt induces cellular responses within a relatively short time scale, which are characterized by cleavage of poly(ADP-ribose) polymerase 1 (PARP1), a typical marker of the DNA damage response (DDR), without detectable upregulation of the ER-mediated chaperone GRP78 on the translational level, unlike the Tg-induced canonical proteostatic responses (**Figure 20A**). The PARP1 cleavage-mediated cellular responses were synchronized with the ATF6 cleavage, while the phosphorylation of eIF2α and induction of ATF4 was found to lag behind these responses by more than 24 h. A PCR-based splicing assay of XBP1 mRNA showed that the upregulation of XBP1 was also delayed by more than 24 h compared to the ATF6 cleavage under the OxaPt-induced ER stress (**Figure 20B**).

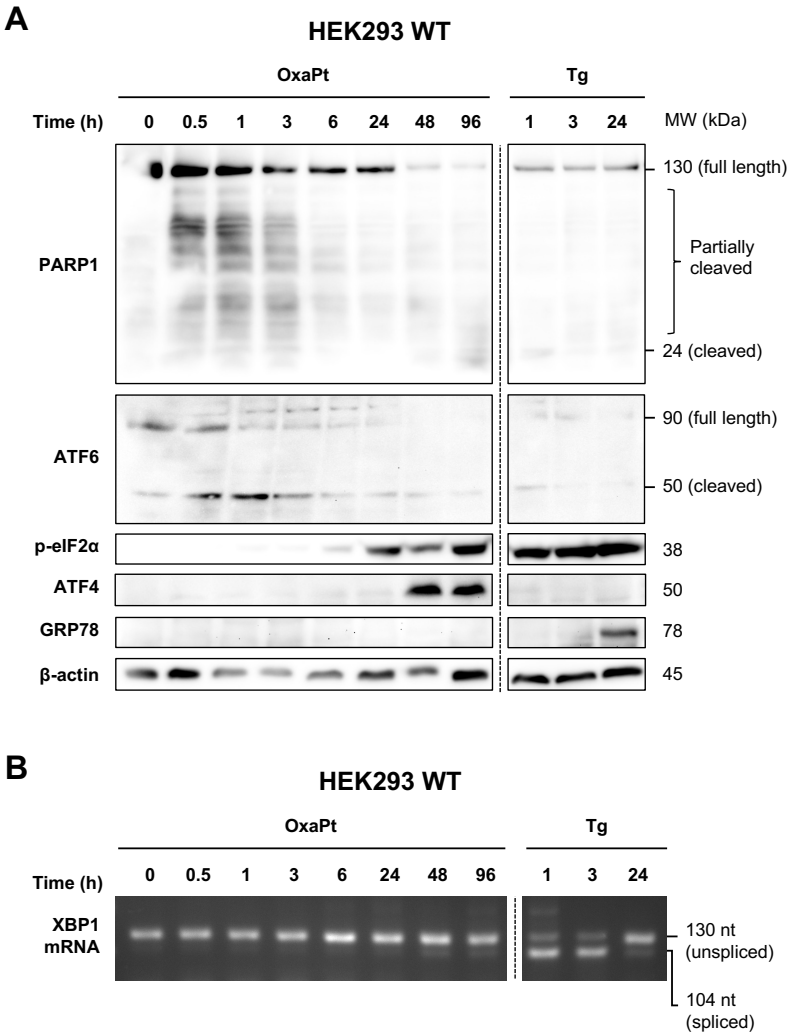

Figure 20: ER stress branches are induced with different time courses depending on chemotherapeutic reagents. (A) Immunoblot analysis of lysates from HEK293 cells treated with OxaPt (20 µM, 0–96 h) or Tg (1 µM, 0–24 h) against poly(ADP-ribose) polymerase 1 (PARP1), ATF6, phosphorylated eIF2α (p-eIF2α), ATF4, GRP78 and β-actin **(B)** PCR-based assay of XBP1 mRNA splicing assay. OxaPt, oxaliplatin; Tg, thapsigargin.

Immunofluorescence microscopy was used to establish a detailed analysis of the subcellular distribution of the reporter protein ATF6-GFP. Based on counterstaining with DNA dyes (DAPI), and a specific marker for the Golgi apparatus (Golgin-97), the fluorescence signal for ATF6-GFP in microscopic images was segmented and quantified in individual cells at defined time points of treatment (**Figure 21**). Taken together, subcellular co-localization analysis of reporter cells showed that ATF6-GFP was rapidly translocated to the Golgi apparatus during the OxaPt treatment compared to a somewhat slower translocation under conditions of the "canonical" ER stress induced by Tg treatment, while no time-dependent changes were observed in H2A-mS control cells during both treatments (**Figure 22A, B**). Of note, morphological changes characterized by altered shape of cellular nuclei (*i.e.*, loss of roundness and shrinkage of nuclear sizes) were observed after treatment with OxaPt for 6 h, but were essentially not observed in Tg treatment (**Figure 22A**).

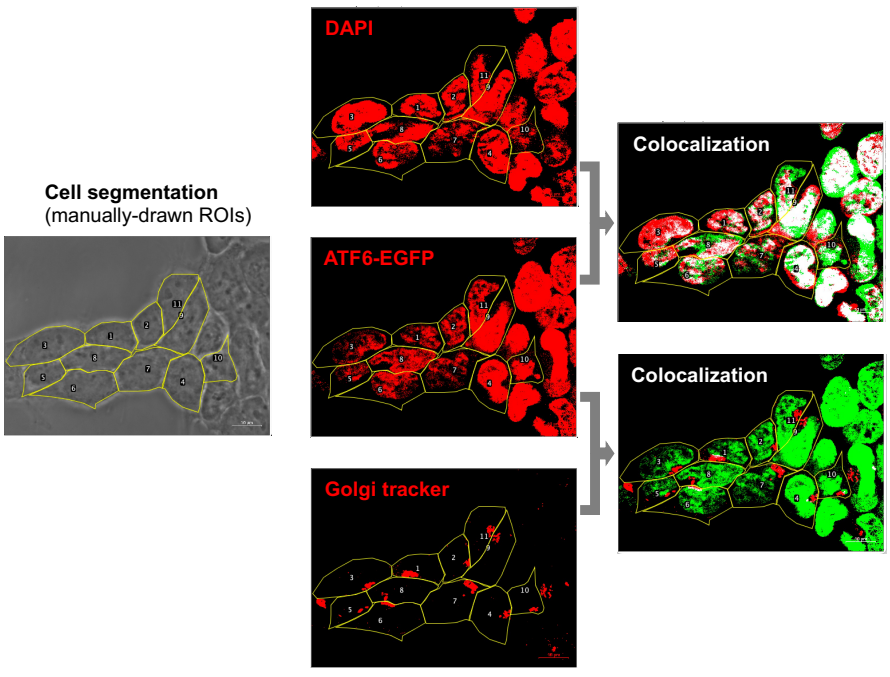

Figure 21: The workflow for analyzing the co-localization of reporter proteins with nucleus and Golgi regions based on optical section images. The ROIs for each cell were manually assigned based on bright-field images, and the co-localization of signals from two reporter channels was quantified.

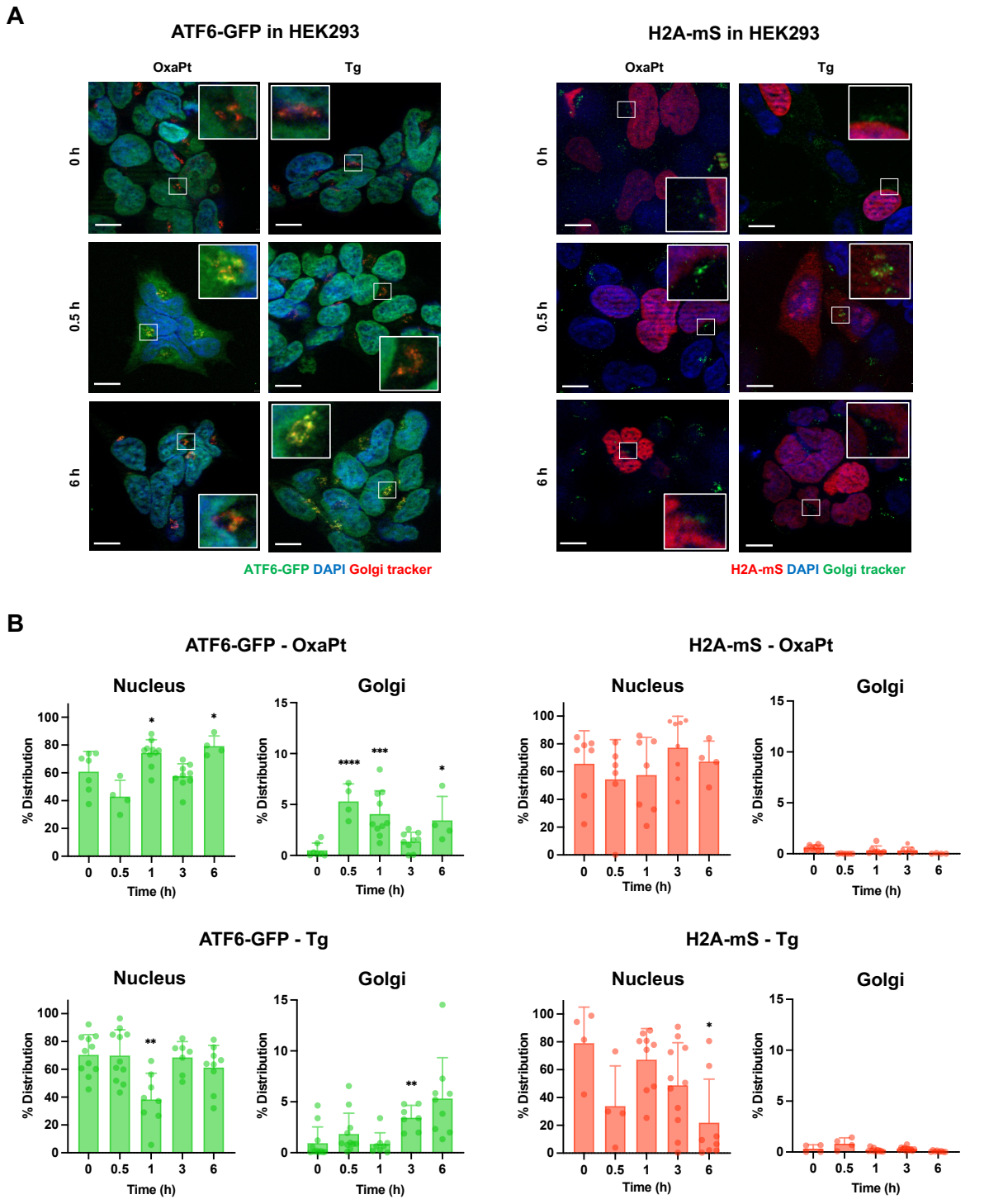

Figure 22: ATF6 rapidly translocates to the Golgi apparatus in response to oxaliplatin treatment. (A) Optical section images of HEK293 ATF6-GFP reporter and H2A-mS control cells after treatment with OxaPt (20 µM, 0–6 h) or Tg (1 µM, 0–6 h). The cells were counterstained with DAPI and anti-Golgin-97 antibody. Scale bar = 10 µm. **(B)** Quantification of ATF6-GFP reporter localization to nucleus or Golgi regions in HEK293 cells was evaluated and compared to that of H2A-mS reporter in respective cells. *$p \leq 0.05$, **$p \leq 0.01$, ***$p \leq 0.001$, ****$p \leq 0.0001$, compared to the 0 h treatment. OxaPt, oxaliplatin; Tg, thapsigargin.

3.3.5. Proteome-wide analysis shows that response to chemotherapy differs between the ER stress signaling branches

To further characterize the effect of the reporter gene expression on the cellular reactions induced by chemotherapy treatment, unbiased proteome-based analysis was carried out of HEK293 wildtype cells, compared to XBP1-mN and ATF6-GFP reporter cells. Mass spectrometry of proteins extracted from wildtype, XBP1-mN or ATF6-GFP cells identified significantly down/upregulated proteins under baseline conditions, as well as upon treatment with OxaPt. For comparison, canonical ER stress was induced by Tg treatment, and canonical programmed cell death (apoptosis) was induced by control staurosporine treatment in wildtype cells. In order to determine the putative shared and unique components of the downstream effects of the treatments, the overlap between the proteomic datasets was assessed (**Figure 23**; **Figure 25A**; **Figure 26A**). Of note, proteins significantly down- or upregulated upon treatment with OxaPt show minor overlap with those for Tg treatment, indicating that canonical unfolded protein response and ER-stress induced by Tg differ substantially from stress conditions by

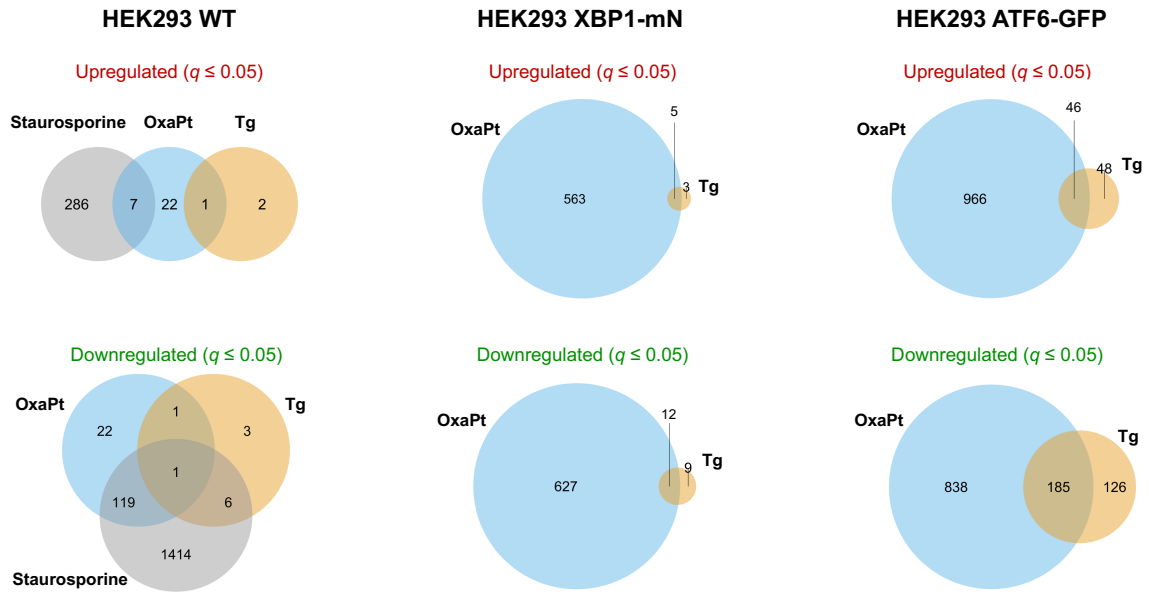

Figure 23: Comparison of proteome between different treatments in HEK293 wildtype, XBP1-mN and ATF6-GFP reporter cells. Venn diagram: the numbers of significantly down/upregulated proteins ($q \leq 0.05$) in HEK293 WT, XBP1-mN and ATF6-GFP reporter cells treated with OxaPt (20 µM, 24 h), Tg (1 µM, 24 h) or Staurosporine (1 µM, 24 h), compared to untreated condition, and overlaps of those for each treatment. OxaPt, oxaliplatin; Tg, thapsigargin.

chemotherapy (**Figure 23**). These observations are in line with the previous findings on immunoblot, showing that the canonical target of activated ATF6, the chaperone GRP78, is not induced by OxaPt (**Figure 20A**). In wildtype cells, proteins significantly down/upregulated upon apoptosis induced by staurosporine were also identified (**Figure 24C**, left). As expected, typical proteins involved in apoptotic pathways, such as the BCL2-associated transcription factor 1 (BCLAF1), were strongly induced. As expected for massive induction of cell death, the number of proteomic chances was highest after staurosporine treatment. On a quantitative basis, OxaPt still induced considerable changes in the cellular proteome of wildtype cells, whereas Tg treatment has only minimal effects. The differential effects associated with the OxaPt- and Tg-related proteomes are shown by Volcano plot analysis (**Figure 24A, B**; **Figure 25B, C**; **Figure 26B, C**, left panels). Since expression of exogenous ER-stress reporter proteins conferred increased resistance against OxaPt, special interest was paid to the altered proteomes in XBP1- and ATF6-reporter cell lines (**Figure 25B, C**, left panels). Several factors involved in ribosome biogenesis (NSA2, RSL1D1, FAM207A (also known as SLX9) and DDX56) were significantly downregulated in both reporter cell lines after treatment with the chemotherapeutic drug, indicating downregulation of ribosomal functionality. In XBP1-reporter cells, which showed the highest resistance against OxaPt, the glucose transporter GLUT3 (or SLC2A3) was highly upregulated, as well as proteins involved in cellular respiration and mitochondrial function (*e.g.*, SDHAF4), indicating rewiring of cellular energy metabolism. Interestingly, the XPB1-reporter line was apparently nonetheless capable of a canonical ER-stress response after Tg treatment, as indicated by significant upregulation of the heat shock protein HSP79 (or HSPA5). In the ATF6-reporter line, and upregulation of ATF3 was noted, a transcription factor from the CREB family, involved in cellular stress response and connected to PERK pathway activation.

The proteome of each cell line treated with OxaPt was further compared by functional enrichment of downregulated or upregulated pathways, revealing differential responses among cell lines: the wildtype cells showed downregulation of the functions for nucleolus, microtubule and ribosomal biogenesis (**Figure 24A**, right), while XBP1-mN reporter cells showed upregulation of lysosome machinery and amino acid metabolism (**Figure 25B**, right). Importantly, ATF6-GFP cells, which were found to have significantly higher resistance against OxaPt treatment, showed a clearly different set of upregulated pathways, including DDR (**Figure 25C**, right). Of note, Tg induced similar proteostatic responses in those cell lines, and wildtype cells did not show apparent changes on the global proteome level even under low

statistical stringency of $q \leq 0.2$ (**Figure 24B**; **Figure 26B, C**, right panels).

In summary, the reporter gene expression positively affected resistance to chemotherapy with OxaPt, among which the XBP1-mN reporter cells showed significantly enhanced resistance to OxaPt compared to the wildtype. In contrast, pharmacological inhibition of the ATF6 pathway sensitized HCT116 cells, while inhibition of the other ER stress signaling branches showed no reduction or reverse effect on the chemotherapy resistance. Of note, the apparent sensitizing effect of pharmacological ATF6 inhibition on the resistance to OxaPt was essentially recapitulated on primary human colonoids by cytotoxicity assays, although tumoroids isolated from human CRC did not respond to the ATF6 inhibition. Kinetics of OxaPt-induced ER stress activation was characterized by immunoblot analysis and immuno-fluorescence microscopy. The results indicated that ATF6 is rapidly activated through translocation to the Golgi apparatus and is closely involved in PARP1 cleavage-mediated cellular responses. Furthermore, mass spectrometric proteome analysis of the ER stress reporter cells displayed substantial differences between the ER branches that mediate ER stress, where the ATF6-dependent modulation appeared to be mainly involved in DNA damage repair, while XBP1 branches are rather multifunctional and involved in ribosomal biogenesis stress.

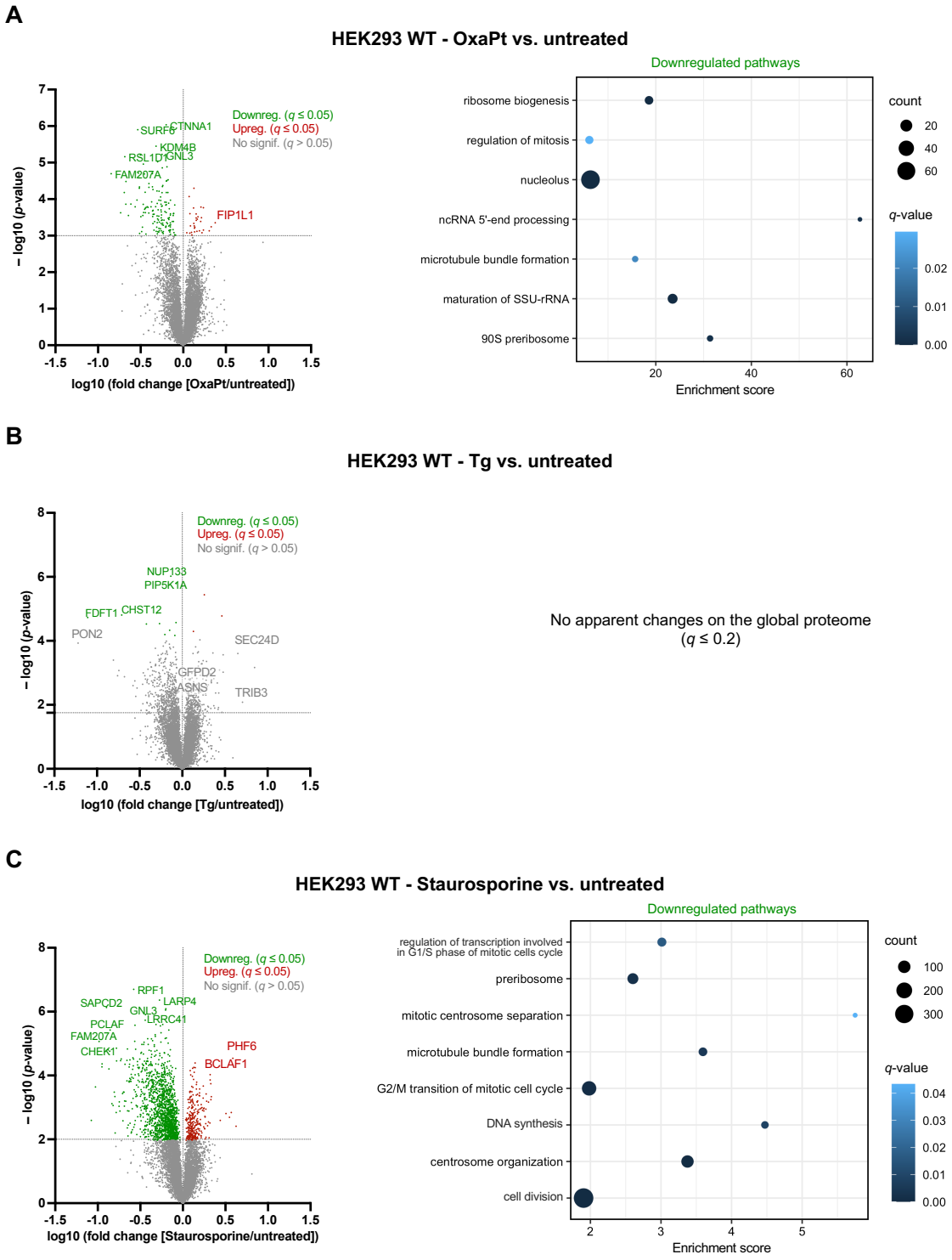

Figure 24: Comparison of proteome between different treatments in HEK293 wildtype cells. (A–C) Volcano plots of down/upregulated proteins (left panels) and enrichment pathway analysis based on gene ontology terms performed for downregulated proteins (right panels, $q \leq 0.05$ or ≤ 0.2) in HEK293 WT cells treated with OxaPt (**A**, 20 µM, 24 h), Tg (**B**, 1 µM, 24 h) or Staurosporine (**C**, 1 µM, 24 h), compared to untreated condition. OxaPt, oxaliplatin; Tg, thapsigargin.

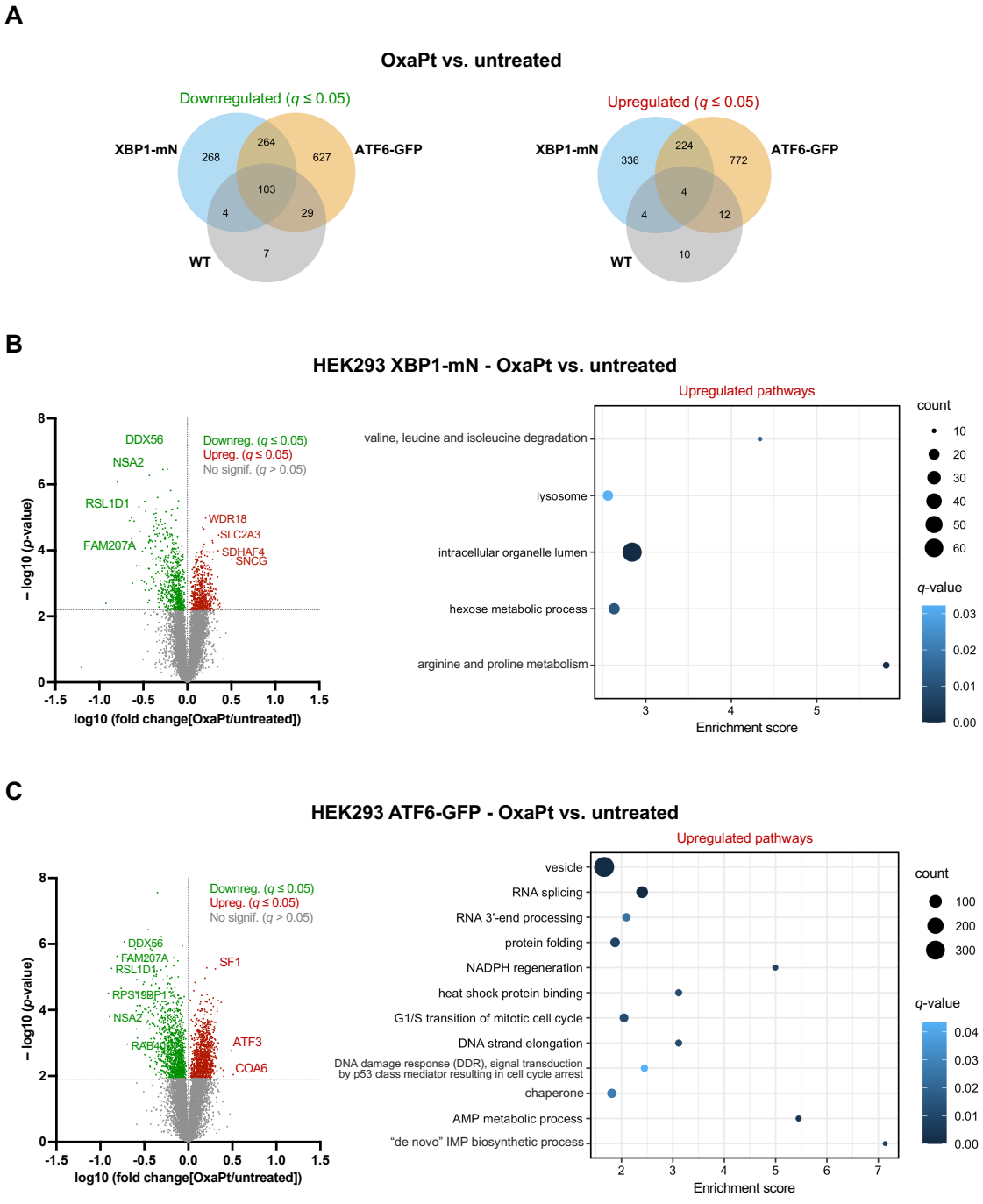

Figure 25: The XBP1- and ATF6-dependent modulation induces different downstream signaling effects on oxaliplatin resistance. (A) Venn diagram: the numbers of significantly down/upregulated proteins ($q \leq 0.05$) in HEK293 WT, XBP1-mN and ATF6-GFP reporter cells treated with OxaPt (20 µM, 24 h), compared to untreated condition. **(B–C)** Volcano plots of down/upregulated proteins in XBP1-mN (**B**) or ATF6-GFP (**C**) cells, compared to untreated conditions (left panels) and enrichment pathway analysis based on gene ontology terms performed for upregulated proteins (right panels, $q \leq 0.05$). OxaPt, oxaliplatin.

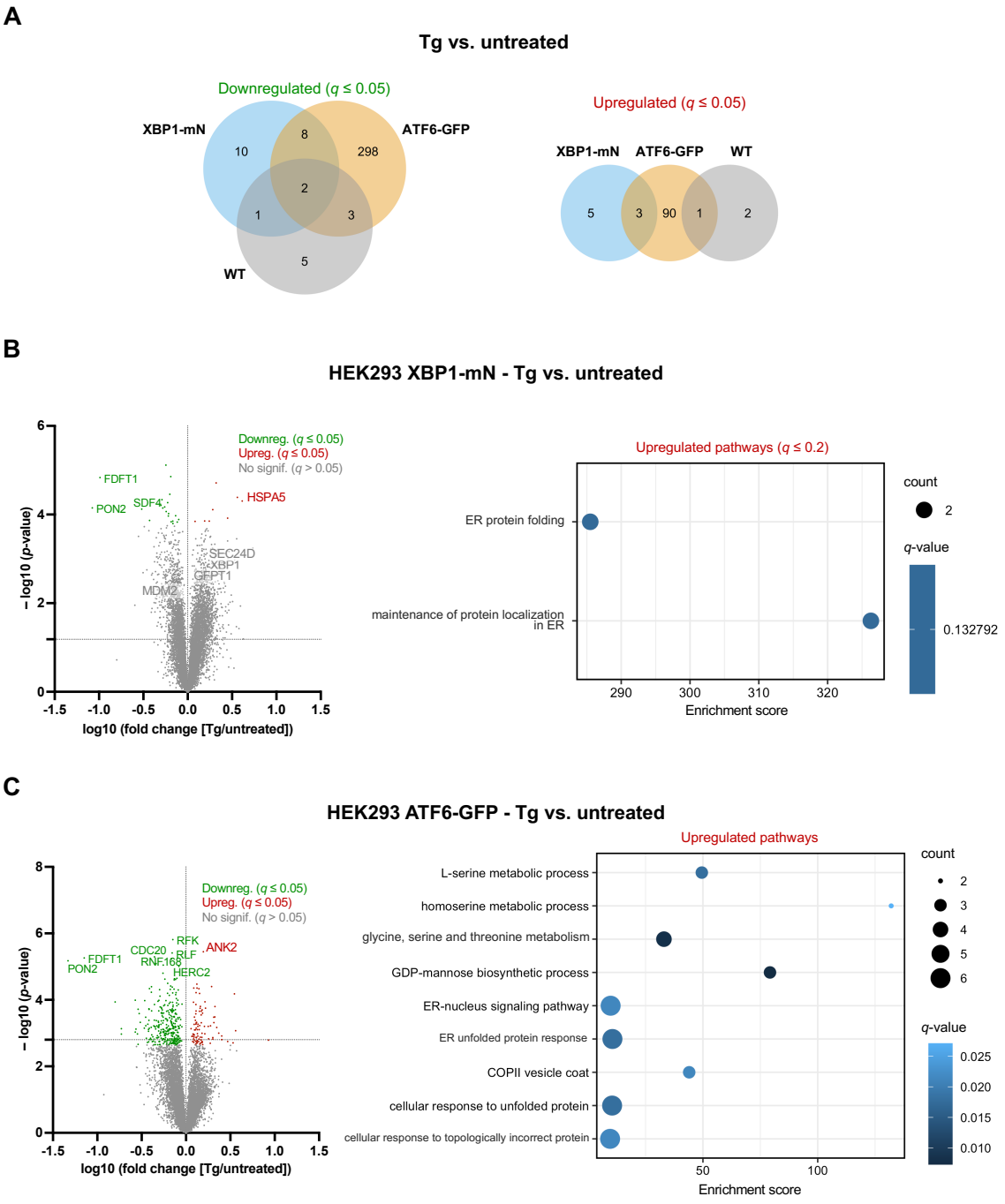

Figure 26: Thapsigargin induces similar proteostatic responses independent of the XBP1- and ATF6-targeted modulation. (A) Venn diagram: the numbers of significantly down/upregulated proteins ($q \leq 0.05$) in HEK293 WT, XBP1-mN and ATF6-GFP reporter cells treated with Tg (1 µM, 24 h), compared to untreated condition. **(B–C)** Volcano plots of down/upregulated proteins in XBP1-mN (**B**) or ATF6-GFP (**C**) cells, compared to untreated conditions (left panels) and enrichment pathway analysis based on gene ontology terms performed for upregulated proteins (right panels, $q \leq 0.05$ or 0.2). Tg, thapsigargin.

3.4. The Role of ER Stress Signaling in Radiotherapy Resistance *in Vitro*

3.4.1. Radiation specifically induces ATF6-reporter expression

The results above collectively suggest that ATF6 may be associated with cellular DNA damage repair after chemotherapy *in vitro*, leading to a hypothesis that ATF6 may confer advantages to cancer cells also with response to other treatments that induce DNA damage. Therefore, the effect of the ER stress reporter expression on the cellular response to radiotherapy was investigated in detail since radiation is known to directly induce DNA damage, such as DNA double-strand breaks (DSB), regarded as the deadliest form of DNA damage to cells (Helleday et al., 2008; Valerie & Povirk, 2003). Control cells and ATF6-reporter cells were treated by irradiation at specific doses (0–8 Gy), and qRT-PCR analysis showed that the total ATF6 expression was relatively high compared to the wildtype, increasing in a time-dependent manner, while the expression of ATF4 and XBP1 were comparable to the wildtype cells and

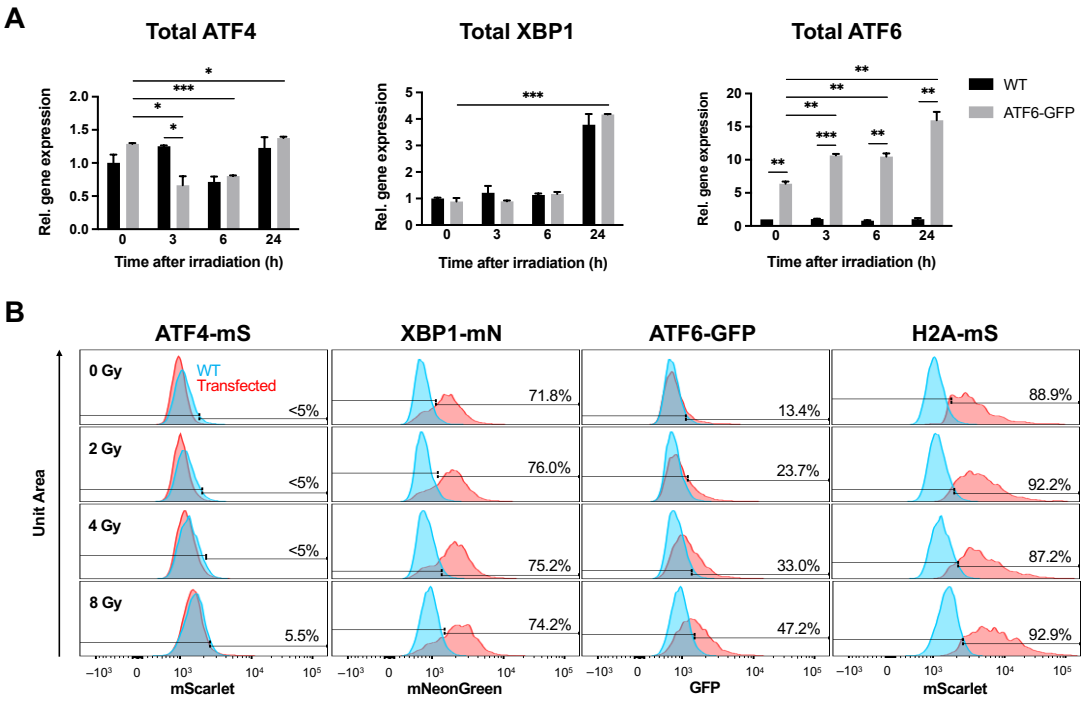

Figure 27: Irradiation specifically induces ATF6-reporter expression. (A) qRT-PCR analysis of the total (endogenous plus exogenous) expression of ATF4, XBP1 and ATF6 in HEK293 reporter cells 24 h after irradiation at 2 Gy. *$p \leq 0.05$, **$p \leq 0.01$, ***$p \leq 0.001$, compared to 0 h after treatment. **(B)** Flow cytometric detection of the reporter gene expression in HEK293 reporter cells 30 h after irradiation at 0–8 Gy.

essentially unresponsive to the radiation treatment (**Figure 27A**). Flow cytometry after X-ray irradiation showed that the ATF6-GFP reporter expression was specifically induced in a dose-dependent manner (**Figure 27B**).

3.4.2. The expression of ATF6 reporter increases radiotherapy resistance

In order to determine the induction of cell death programs more closely, flow cytometric assays based on Annexin and PI staining showed that the irradiation induces apoptosis in a dose-dependent manner (**Figure 28A**). ATF6-GFP cells, as well as H2A-mS control cells, showed significantly more colony formation after irradiation, compared to the wildtype (**Figure 28B**, p = 0.0240 and 0.0173, respectively).

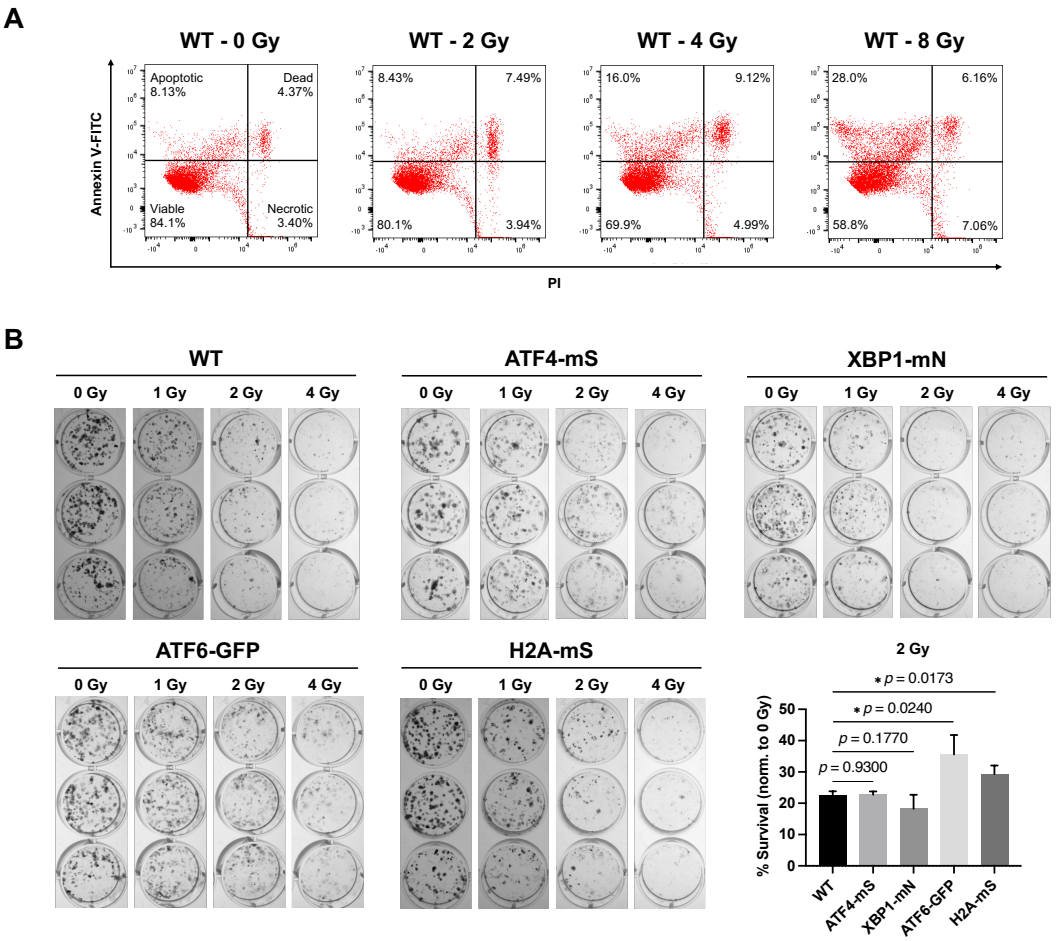

Figure 28: The expression of the ATF6-GFP reporter protein is associated with increased radioresistance. (A) Flow cytometric analysis of apoptosis in HEK293 WT cells 48 h after irradiation at 0–8 Gy. **(B)** Clonogenic assay of HEK293 ATF6-GFP reporter cells irradiated at 0–4 Gy and comparison of the survival rates between the cells irradiated at 2 Gy.

3.5. Excursus: Preliminary Results on Effects of Other Cellular Stress Conditions

The results shown above collectively show that cell-based models can be efficiently used to monitor the effects of chemo-/radiotherapeutic approaches currently used in cancer treatment. Thus, the cellular models and assays were used to carry out preliminary tests on several other potential ER stressors, with the additional aim of establishing further *in vitro* assays for phenotypic analysis.

3.5.1. Natural compounds from gut bacteria and their impact on cell growth

Within a collaboration of the collaborative research center 1371 (funded by the German Research Council, DFG) with Prof. Dr. Tobias Gulder and his group (TU Dresden, Dresden, Germany), natural compounds identified from gut bacteria and purified after recombinant expression in *E. coli* were kindly provided for further characterization of their respective biochemical activity. Specifically, it was found that Bacillamides C and D, which were previously discovered in *Thermoactinomyces* (soil) and *Bacillus sp.* (marine) (Omura et al., 1975; Yu et al., 2009), show an anti-proliferative effect on several human cell lines including HEK293 and HCT116 cells (Hohmann et al., 2024). Bacterial toxins can induce cellular stress pathways in sensitive cells, for example, through ribotoxicity and translational inhibition (Smith et al., 2003), and some compounds have been associated with the ER stress response (Li et al., 2022). Thus, the putative impact of Bacillamide C and D was assessed on non-chemotactic cell migration on a 2D surface based on time-lapse imaging in live-cell microscopy (**Figure 29A**). The tracks that HEK293 wildtype cells traveled during the treatment with Bacillamide C or D showed that the spontaneous cellular migration capacity was drastically decreased in the presence of the tested compounds, as compared to those with no treatment (**Figure 29B**). Furthermore, this method was also applied to analyzing the effect of both compounds on the motility of the ER stress reporter cell lines (introduced earlier) and also compared between each other (**Figure 30**). Interestingly, ATF6-GFP reporter cells showed no significant decrease in cellular motility under the treatment with these compounds (p = 0.3780–0.4778), while the reporter cell line, ATF4-mS, as well as the control line H2A-mS, significantly showed a decrease of motility (**Figure 30A**, $p \leq 0.0001$). Of note, subcellular co-localization analysis based on the immuno-

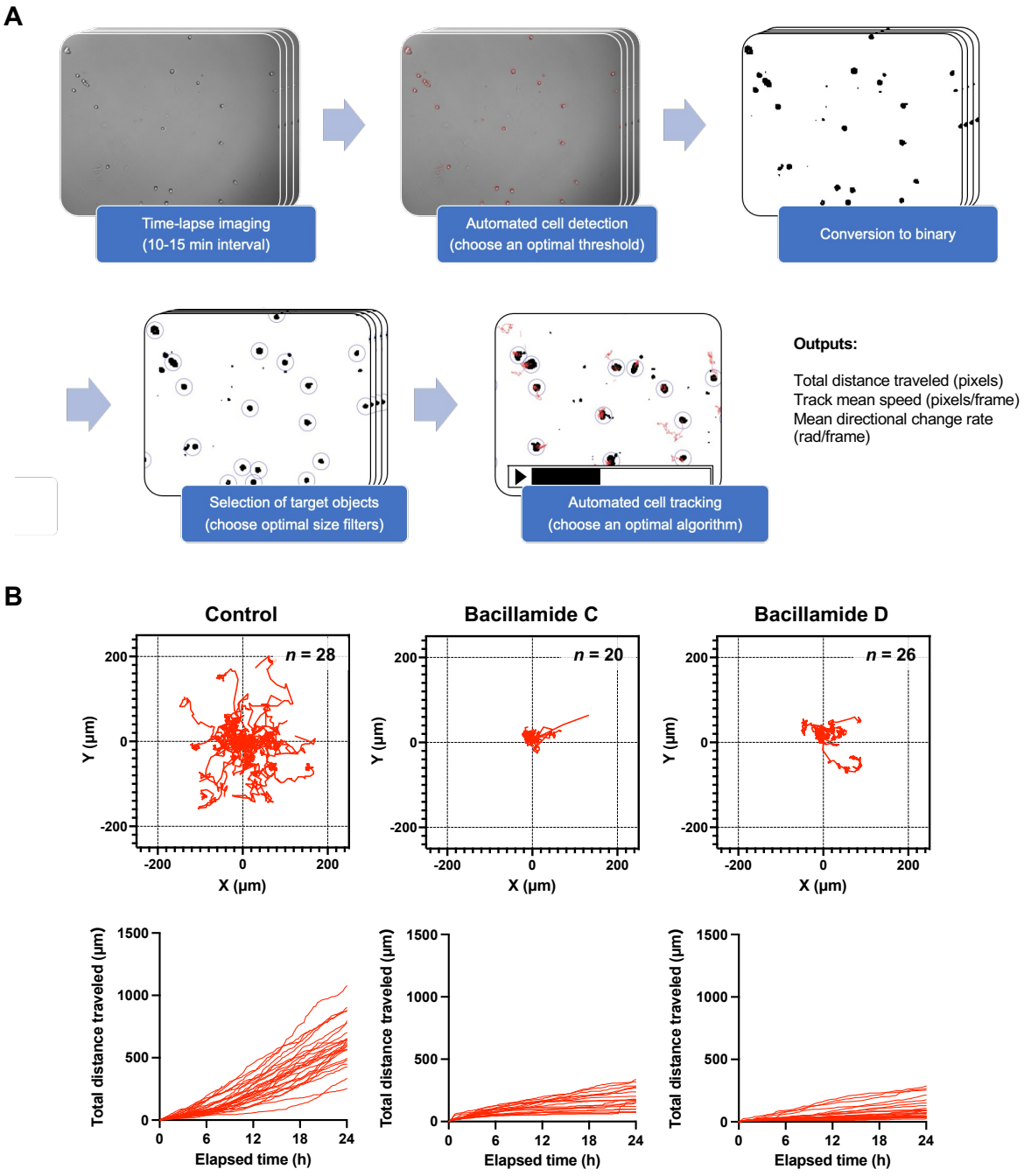

Figure 29: The impact of Bacillamides C and D on 2D cellular migration ability. (A) Workflow for the cell tracking based on time-lapse imaging and semi-automated image analysis. **(B)** Tracks recorded for HEK293 WT cells under the treatment with 250 µM Bacillamide C or D (upper panels) and the total distances traveled during the treatment (bottom panels).

fluorescence microscopy showed a significant increase of the ATF6-GFP reporter protein in the Golgi apparatus of HEK293 cells treated with Bacillamide D, compared to the untreated control (**Figure 30B**).

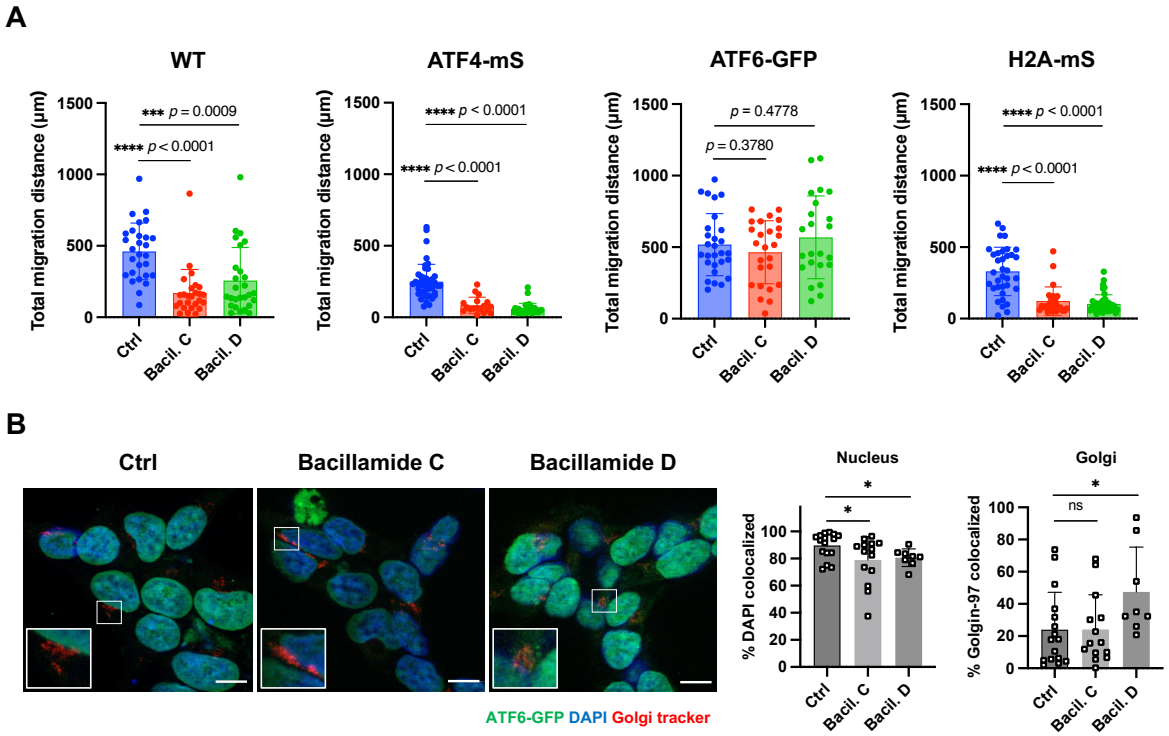

Figure 30: ATF6-GFP reporter is upregulated and specifically associated with less cellular migration ability during the treatment with Bacillamides C and D. (A) Comparison of 2D cellular migration ability between the ER stress reporter cell lines treated with Bacillamides C and D. Total migration distances that HEK293 WT, ATF4-mS, ATF6-GFP or H2A-mS cells traveled during the treatment with 250 µM Bacillamide C or D. **(B)** Optical section images of HEK293 ATF6-GFP reporter cells after treatment with Bacillamide C or D (500 µM, 6 h). The cells were counterstained with DAPI and anti-Golgin-97 antibody. Scale bar = 10 µm. DAPI and Golgin-97 signals colocalized with ATF6-GFP reporter in HEK293 cells were evaluated. *$p \leq 0.05$, compared to the untreated control.

3.5.2. ER stress reporter cells show differences in the reliance on glycolytic metabolism

As described earlier, ER stress signaling has been reported to regulate the glycolytic activity in cancer cells for adaptation to the typically hypoxic environment of solid tumors, which potentiates cancer cells in their resistance against the genotoxic effect of chemo-/radiotherapeutic treatment (Akman et al., 2021). Along that line, the ER stress reporter cells

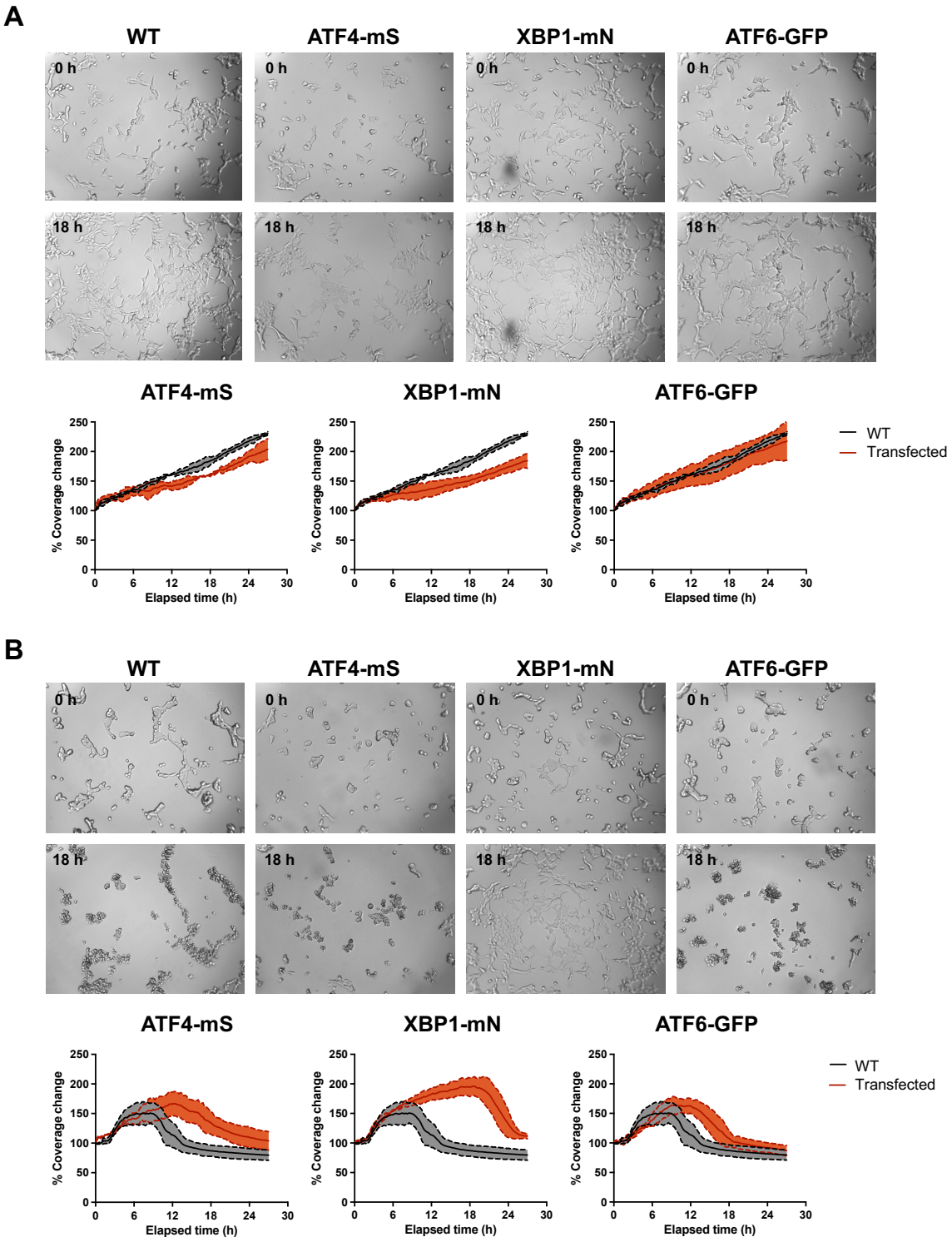

Figure 31: Proliferation activity of the ER stress reporter cells under glucose deprivation. (A, B) HEK293 WT, ATF4-mS, XBP1-mN and ATF6-GFP cells were imaged over time under culture in DMEM containing 7% fetal serum, 2 mM L-glutamine with 25 mM glucose (**A**) or no glucose (**B**). The coverage changes (%) were normalized to the measurement start and given as mean ± standard deviation (*n* = 3).

were compared for their respective proliferative activity under glucose deprivation (**Figure 31**). Unlike the cells growing in a normal medium, cells deprived of glucose stopped proliferation after 12–20 h, and then rapidly lost their viability, visualized as loss of adherence to the culture plate. Of note, the ATF4-mS, XBP1-mN and ATF6-GFP reporter cells showed more prolonged viability than the wildtype (**Figure 31B**). Furthermore, XBP1-mN cells were relatively insensitive to glucose deprivation, maintaining adherence and proliferation ability, whereas ATF6-GFP and ATF4-mS cells appeared more susceptible to this condition. To compare the presumed glycolytic activity, extracellular acidification during the cell culture was evaluated for these cell lines as surrogate readout (**Figure 32**). Compared to the wildtype cells, XBP1-mN and ATF6-GFP cells showed more rapid acidification, suggesting enhanced glycolytic lactate production. In contrast, ATF4-mS cells showed no apparent changes in the acidification

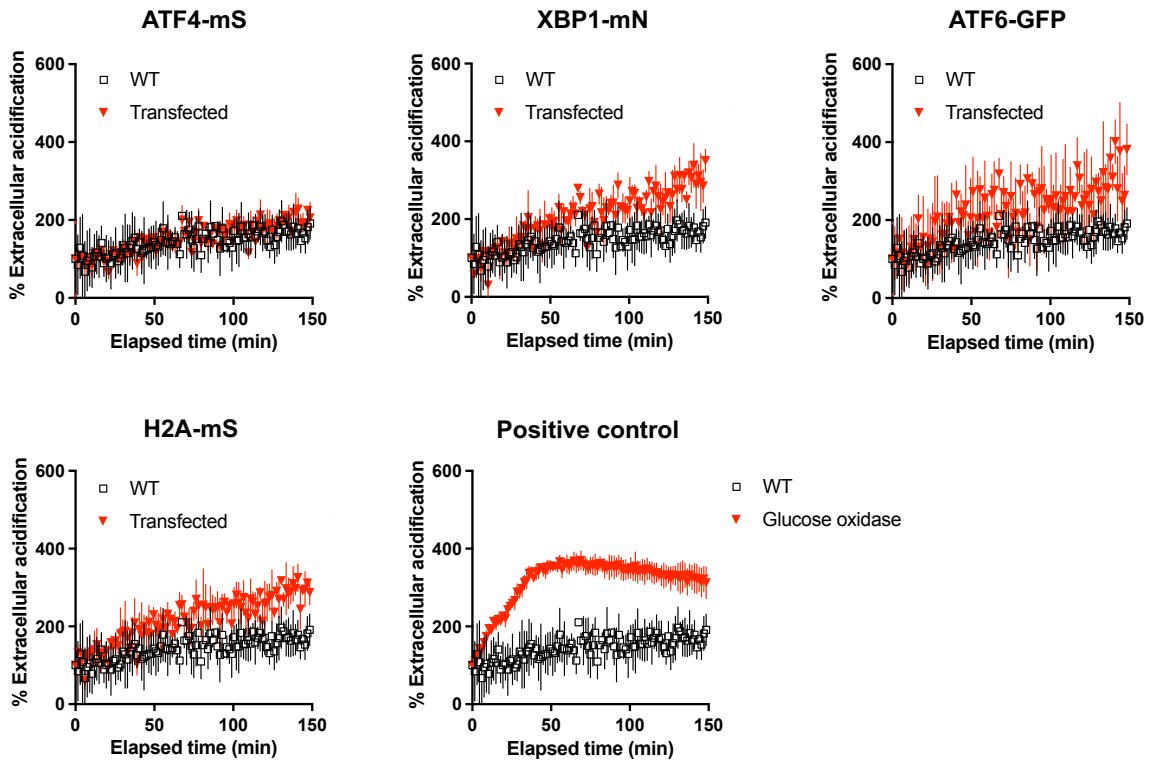

Figure 32: Comparison of the glycolytic activity between the respective ER stress reporter cell lines. The extracellular acidification of HEK293 WT, ATF4-mS, XBP1-mN and ATF6-GFP cells was monitored under culture in a normal conditioned medium using pH-dependent fluorometric analysis. The changes of extracellular acidification (%) were normalized to the start of measurement and given as mean ± standard deviation (*n* = 3). Positive control: addition of 60 µg/ml glucose oxidase.

property. Of note, an increased glycolytic activity was also observed in H2A-mS control cells. Therefore, the observed phenotypic changes should be interpreted with caution and might not be specific to the modification of the ER stress signaling branches.

3.5.3. Modulation of fatty acid desaturation ability and exogenous lipotoxic stress affect the activity of ER stress signaling

Aside from the metabolic switch to glycolytic pathways, alterations in lipid metabolism may also play a vital role in the adaptation of cancer cells. We have previously shown that the lipidome is specifically altered in human CRC and associates with prognosis (Ecker et al., 2021). To meet the high demand for fatty acid supply and increased lipogenesis as a consequence of rapid cell growth and proliferation, tumor cells upregulate lipid-modifying enzymes such as the stearoyl CoA desaturase 1 (SCD1) that is essential for *de novo* synthesis of mono-unsaturated fatty acids from saturated fatty acids (Green et al., 2010). Reportedly, the ER stress signaling pathways are functionally linked to the ER lipid metabolism and can be induced by lipotoxic stress, affecting multiple cellular functions (X. Chen et al., 2016; Tam et al., 2018). Thus, HEK293 wildtype cells and stably transfected HEK293 cells that exogenously overexpress SCD1, SCD1-OE (unpublished results, working group Prof. Janssen) were exposed to lipotoxic stress with the addition of a saturated fatty acid, palmitate (C16:0), and analyzed for the expression and activation of the ER stress proteins (**Figure 33**). In the wildtype cells, the expression and cleavage of ATF6 were increased by the treatment with palmitate in a dose-dependent manner. On the other hand, SCD1-OE cells showed basally high activation of XBP1 and ATF6, producing more amount of sXBP1 and nATF6 as compared to the wildtype, which appeared to be less sensitive to palmitate.

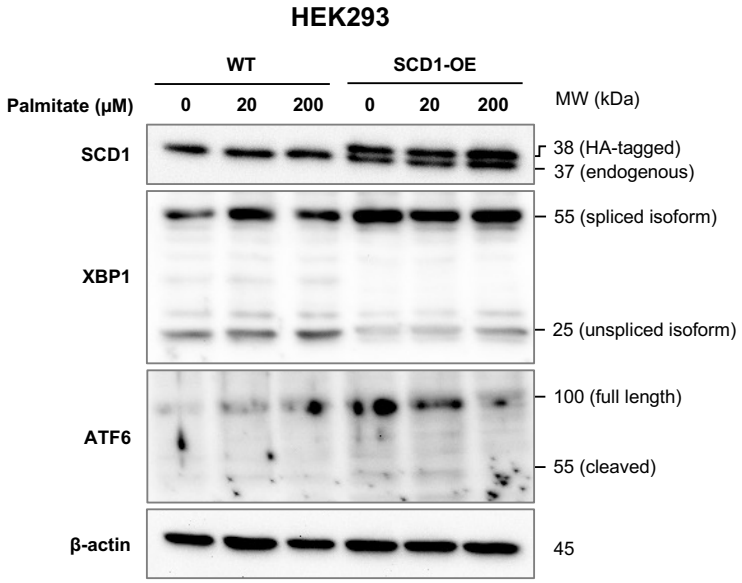

Figure 33: Effect of SCD1 overexpression in HEK293 cells and lipotoxic treatment with a saturated fatty acid on ER stress signaling. HEK293 (wildtype, WT, and SCD1-overexpressing, SCD1-OE) cells were treated with palmitate (0–200 μM, 96 h), and analyzed by Immunoblot against SCD1, XBP1, ATF6 and β-actin.

In summary, the ER stress reporter cell models were also efficiently employed to perform preliminary tests on some bacterial compounds and glucose deprivation. Characterization of 2D migration and proliferation ability of these cells by several methods, mainly based on microscopic image analysis, indicated differences in cellular responses to these potential stress factors dependent on the signaling branches that mediate ER stress. Furthermore, it was shown in HEK293 cells that lipotoxic stress with a saturated fatty acid can induce the ER stress signaling pathways in wildtype cells, while SCD1-overexpressing cells may have basally high activity of the ER stress signaling.

4. DISCUSSION

Cancer is a major public health issue, accounting for nearly 10 million annual deaths, about one in six of all deaths worldwide (Sung et al., 2021). While efforts to promote early detection and prevention are gaining momentum based on many epidemiologic and molecular risk factors proposed to predict and ideally reduce oncogenesis, management of surgical and medical therapies after diagnosis with advanced cancer remains the primary concern for reducing cancer-related deaths. Particularly, colorectal cancer (CRC) is one of the malignancies for which pathogenic mechanisms and progression patterns have been the most elucidated at molecular levels. As described earlier, CRC is known to develop through a complex interplay of abnormalities on (1) chromosomal levels, such as aneuploidy and loss of heterozygosity (LOH); (2) epigenetic levels, including histone modification and methylation of CpG islands in the promoter region; (3) genomic levels by point and frameshift mutations in cancer-related genes such as APC, KRAS, TP53 and BRAF due to defective DNA replication and damage repair (Parmar & Easwaran, 2022; Porter et al., 2021). Based on these mechanistic understandings as well as new findings on additional pathways involved in tumor development, a variety of inherited and acquired molecular features have been associated with the risk of CRC onset and malignant progression (Jaufmann et al., 2021; Maak et al., 2013; Nitsche et al., 2012; Nitsche et al., 2013; Popat & Houlston, 2005; Shibata et al., 1996). However, predicting responses to cancer treatment, such as chemo- and radiotherapy, is still challenging because therapy resistance can also arise due to positive selection of a stress-resistant tumor subpopulation by various therapy-induced adaptive responses, for which molecular mechanisms and clinical impacts are still largely unclear (Holohan et al., 2013).

Endoplasmic reticulum (ER) stress response is a widely studied stress-adaptation program by which cancer cells can survive a hostile microenvironment and intracellular oncogenic changes. It involves three main signaling branches initiated by the ER transmembrane receptor proteins PERK, IRE1 and ATF6, which are individually fine-tuned by transcription factors ATF4, sXBP1 and nATF6, respectively, as well as other unique transcriptional and translational programs. Although it was originally characterized as a mechanism for maintaining ER proteostasis by transiently increasing the protein folding capacity and reducing further protein synthesis (Kaufman, 2002; Mori, 2000), recent studies have suggested a functional connection

between ER stress activation and many other cellular processes such as DNA damage repair and lipid metabolism (Dicks et al., 2015; González-Quiroz et al., 2020). Therefore, the ER stress response constitutes a central hub that integrates various pathways crucial for maintaining cancer hallmark capabilities. Indeed, activation of the ER stress signaling has been observed in many types of human tumors (Wang & Kaufman, 2014) and is also associated with highly proliferative, malignant and aggressive properties in cellular and animal models (Urra et al., 2016), which are closely related to the ability of survival in cytotoxic conditions of cancer therapy. However, there was still a lack of evidence on which signaling branches are important for therapy resistance in a systematic approach, and therefore, the underlying molecular and cellular mechanisms remained poorly understood. Within the present thesis, the individual roles of ER stress signaling branches in chemo- and radiotherapy resistance of CRC were investigated, focusing on the nuclear activity of their key transcription factors ATF4, sXBP1 and nATF6. Two independent approaches with clinical datasets and *in vitro/ex vivo* models highlighted a putative connection between the activation of these transcription factors and cancer therapy responses. First of all, genomic alterations of ATF4, XBP1 and/or ATF6 in human solid tumors were assessed in the publicly available TCGA datasets with respect to prognosis and genomic instability. The observation was verified experimentally in surgically resected CRC patient tumor samples. Of note, we introduced a new method to collect intact cell nuclei from formalin-fixed paraffin-embedded (FFPE) specimens for a flow cytometric analysis of ATF6 positivity in a retrospective human CRC cohort to associate it with their follow-up data. Independent of these clinically relevant results, we established cellular models, including a stable reporter cell-line system to monitor and modulate the activation of ER stress proteins in live cells, with subcellular resolution, and patient-derived organoid models to analyze the therapy-induced expression and activation of ER stress proteins, the downstream effect and cellular responses. Collectively, these results revealed a specific contribution of ER stress signaling branches to cancer therapy resistance, especially focusing on the differential roles of sXBP1 and nATF6 depending on cellular background and therapeutic conditions.

4.1. The Role of ATF6 in Genomic Instability and Response to Cancer Therapy

The analysis of cancer patients in the public TCGA dataset clearly showed that ATF6 is predominantly amplified at a genome level in several of the most prevalent types of solid cancer. In fact, genomic amplifications, especially of ATF6, were much more frequently observed than other genetic alterations reported in TCGA datasets (*e.g.*, point mutations, heterozygous and homozygous genomic losses). The number of patients with ATF6 gene amplification was 36% in all 30 types of cancer together and 23% in CRC alone. In comparison, it has been observed earlier that 7% of CRC cases presented with genetic alterations (mutations, copy number alterations) in ATF6, and around 11% of cases showed increased nATF6 protein expression (Coleman et al., 2018). Of note, genome-level alterations as reported here do not necessarily correspond to changes on the mRNA/protein level or to the activity of a specific factor. Next, the putative association of genome-level alterations of ATF4, XBP1 and ATF6 with post-operative survival was assessed in TCGA dataset, and ATF6 gene amplification was correlated with an increased risk of post-operative disease relapse. Notably, regarding overall survival, ATF4, XBP1 and ATF6 all significantly correlated to poor prognosis, indicating a clear involvement of ER stress in cancer. If one assumes that “disease relapse” is more strongly influenced by therapeutic interventions than the somewhat more generic parameter “overall survival”, ATF6 can be assumed to be specifically involved in the context of therapy response.

Moreover, on the protein level, a high positivity of ATF6 was specifically associated with microsatellite instability (MSI) in a small cohort of surgically resected human CRC. As described earlier, MSI is a molecular fingerprint that reflects defects in the DNA mismatch repair system that normally control mono- and dinucleotide DNA repeats in the genome. It is translated into an accumulation of DNA replication errors and a high frequency of frameshift mutations, causing cell-intrinsic genotoxic stresses (Jiricny, 2006). Reportedly, 10–25% of colon cancer patients are diagnosed with MSI, of which 3% are hereditary (Cherri et al., 2022). Clinically, they are categorized into three subsets based on the MSI profile: MSI-high (MSI-H) is defined as the presence of MSI at ≥2 of the 5 specified DNA microsatellite sites, MSI-low (MSI-L) as MSI at one site, and microsatellite stable (MSS) when no MSI is detected (Murphy et al., 2006). MSI-H status has been investigated as a predictive marker for poor response to 5-fluorouracil

(5-FU)-based adjuvant chemotherapy in stage II CRC without high-risk clinical features (Battaglin et al., 2018), while MSI-H in high-risk stage II CRC or stage III is instead associated with favorable response to 5-FU plus oxaliplatin (OxaPt) combination therapy compared to 5-FU-based monotherapy or surgery alone (Tomasello et al., 2022; Tougeron et al., 2016). Of course, it needs to be acknowledged that the present analysis is based on a small population of patients only, and results have to be interpreted with caution. Nonetheless, flow cytometric analysis clearly showed that intratumoral ATF6 protein expression levels were specifically associated with the presence of MSI, while ATF6 levels in adjacent normal colon, as well as XBP1 in tumors, were not, supporting the TCGA-based analysis on large public datasets that links genomic ATF6 amplification in solid tumor with response to cancer therapy. Notably, MSI-H cases are known to be more frequent in right-sided CRC tumors such as in coecum and colon ascendens that often develop through the “serrated” or “dysplasia-carcinoma” pathway (**Figure 1**). However, the MSI cases analyzed in this thesis were all found to be left-sided (*n* = 3), indicating that the analysis needs to be repeated on larger and unbiased patient cohorts.

Given the indicated limitations of sample size in the flow cytometric data on freshly resected human CRC, TCGA datasets were further analyzed in association with genomic instability and found that genomic amplification of ATF6 is significantly related to an established aneuploidy score (Taylor et al., 2018) and negatively impact on disease-free survival of CRC patients when concurred with TP53 mutation. As mentioned earlier, loss-of-function mutation in TP53 is closely related to chromosomal instability (CIN), and therefore, this result suggests that the amplified ATF6 in TCGA dataset associates with poor therapy response, particularly in the context of CIN. Of note, we also attempted to associate the ATF6 amplification with the MSI MANTIS Score in TCGA dataset, which is used for the MSI detection in pancreatic cancer (Kautto et al., 2017), in combination with several MSI driver gene mutations, such as mismatch-repair enzymes and DNA polymerases, but did not achieve meaningful results because of limited data points and poor distribution of values. Thus, the data analyzed here allow to conclude that ATF6 is associated with genomic instability but do not allow to safely determine whether ATF6 is specifically associated with either MSI or rather CIN in CRC. Rather, it appears that all types of increased genetic instability in cancer cells, either on a chromosomal or microsatellite level, generally favor upregulation and activation of ATF6. So far, activation of ATF6 in the context of human CRC was mainly attributed to inflammatory or microbial changes (Coleman et al., 2018). Taken together, the upregulation of ATF6 may

constitute a selective advantage for cancer cells and facilitate their survival in the presence of stress conditions.

Furthermore, for analysis in a somewhat larger and independent dataset, a method for collecting cell nuclei from human tissue in the form of FFPE specimens was successfully established and applied to the flow cytometric analysis of ATF6 in a retrospective human CRC cohort (n = 26). Although the ATF6 positivity determined in this method tended to be low compared to the conventional flow cytometry using freshly resected samples, the general ratio of staining intensities between different samples appeared to be largely preserved. Of note, several other proteins in nuclear membranes and nucleoplasm that were tested in this study were much less detectable in this method, and therefore, the present method is only applicable to the analysis of ATF6 protein positivity. The positivity of ATF6 determined in the additional human CRC cohort was associated with several clinical characteristics, including clinical follow-up data. Although several findings were in line with earlier findings, such as the presence of MSI (p = 0.0919) and probability of post-operative disease relapse within one year (p = 0.0727), both failed to reach the significance threshold, likely due to the limited sample size. Instead, a statistically significant correlation was observed between high levels of ATF6 and the cumulative risk of disease relapse (p = 0.0206). Collectively, these results modestly support the association of positive ATF6 with increased genomic instability and poor prognosis in CRC.

In addition, the observation in TCGA datasets that ATF6 is dominantly upregulated in the most frequent human cancer types implies that high ATF6 levels mark a pro-tumorigenic milieu or even actively contribute to tumorigenesis. Positive ATF6 protein levels in surgically resected human CRC were also associated with low tumor stages, while ATF6 levels in adjacent normal colon, as well as XBP1 levels in tumors, were not. Positive ATF6 levels in the FFPE cohort also appeared relevant to low lymph node stages and diagnosis at higher ages, albeit not significant. These data have to be interpreted with caution but might also indicate an involvement of ATF6 in tumor initiation and progression.

Due to the high association of amplified ATF6 with increased genomic instability, the following hypothesis can be raised: in tumors with high aneuploidy or unstable DNA microsatellites, which continuously have to cope with DNA alterations and likely also proteotoxic stress, the selective pressure favors the outgrowth of tumor cell clones with amplification of the ATF6 gene locus, which is predicted to provide an advantage for cancer

cells, due to increased cell survival even under high cellular stress conditions. In line with this model, recurrent tumors showed high expression levels of ATF6 (Ginos et al., 2004), and ATF6 levels were shown to correlate with poor prognosis of CRC (Lin et al., 2007). Previous studies have also suggested that activation of the ER stress signaling cross-talks with DNA damage response (DDR) systems and may suppress the onset of genomic instability (Bobrovnikova-Marjon et al., 2010; Henry et al., 2010). For instance, some evidence indicates that XBP1 might directly suppressively affect double-strand break (DSB) repair or p53-driven DDR (Argemí et al., 2017; Tao et al., 2011; Yamamori et al., 2013). However, with respect to the specific role of ATF6, very little is currently known, although ATF6 has recently been reported to sustain the expression levels of the DNA repair protein BRCA1 through the activation of the mammalian target of rapamycin (mTOR) signaling and to protect colon cancer cells from the cytotoxic effect of ER stress-targeting drugs (Benedetti et al., 2022). Therefore, the findings here might represent a novel and clinically relevant connection between the single ATF6 arm and genomic instability.

4.2. Perspectives of the Xnuc-Based Methodology in Cancer Research

FFPE tissues are commonly used in diagnostic histopathology for ongoing patient care but also have been demonstrated as invaluable resources for both basic and translational clinical research (de Gramont et al., 2015; Magdeldin & Yamamoto, 2012; Ostasiewicz et al., 2010). Although the molecular biological application of FFPE archival specimens is basically challenging because of the chemical cross-linking among DNA, RNA and proteins, which needs to be reversed by heating and/or protease digestion (Shi et al., 2011), recent studies have made great progress in the application of FFPE samples to high-throughput profiling of genome, transcriptome, proteome and metabolome with single-cellular or even subcellular resolution by optimal isolation and extraction methods or spatial *in situ* analyses (Ly et al., 2016; Mund et al., 2022; Nwosu et al., 2022; Wang et al., 2023; Xu et al., 2023; Zhao et al., 2021).

In the present study, a flow cytometric method was introduced for evaluating the ATF6 positivity in nuclei collected from FFPE tissue specimens (“Xnuc-based” system (Sato et al., 2019; Sato & Nakatsuji, 2023)) and applied to the analysis of a retrospective human CRC cohort

in association with additional follow-up data. The positivity of nuclear proteins determined by this method was generally lower than that in whole cells dissociated from the corresponding freshly resected samples, evaluated by a standard flow cytometric technique. This lower staining efficiency is largely attributable to damage in the antigenic structures and loss of proteins due to enzymatic digestion and physical disruption with a detergent-containing buffer. Of note, as compared to ATF6, other nuclear proteins such as Lamin A/B1/C and Ki67, which reside in the inner nuclear membrane and nucleoplasm, respectively, were much less detectable in this method, highlighting the fact that the sensitivity is highly dependent on the individual protein, and therefore, the conditions for the treatment with enzymes and detergent should be carefully optimized for each protein of interest. Importantly, the relationship and ratios between the magnitudes of the ATF6 levels determined in the FFPE specimens were reflected by those in the parallel (matched) samples of surgically resected human CRC. Further, a positive correlation with MSI and with the risk of disease relapse was observed, even though it did not achieve significance, essentially recapitulating the results from analysis in TCGA dataset and flow cytometry using freshly resected human CRC. Therefore, the present procedure for the nuclear collection from fixed tissue is applicable to the analysis of ATF6 levels but may not be suited without further adaptations to the analysis of other nuclear proteins. For broader application, it is necessary to increase the sensitivity by further optimizing the steps for antigen retrieval, enzymatic treatment, physical disruption and immunostaining.

Despite the dependence on suitable protein markers of interest, the method presented here could be eventually expanded to further multi-parameter setups by combining multicolor staining of different protein markers, analysis of DNA amount for cell-cycle and aneuploidy characterization. Furthermore, the signal amplification of nuclear proteins could be advantageous for characterizing tumor subpopulations, focusing on the transcriptional activity of certain proteins. Of note, to achieve clearer isolation of intact cell nuclei, several other non-ionic detergents, such as Triton X-100, were tested, taking advantage of their ability to strip membrane proteins from the ER while keeping the nuclear membrane intact (Gagnon et al., 2014; Greenberg & Bender, 2007; Michelsen & von Hagen, 2009). However, this further attempt was hampered by a trade-off between the yield of nuclei isolation from fixed tissue and the loss of nuclear protein stainability, probably because of the covalent cross-links between membrane proteins. Therefore, it is more feasible to counterstain an ER protein

marker such as calnexin and exclude ER-containing subpopulation by gating on flow cytometric data, which might allow for the evaluation of nuclear activity of proteins.

4.3. ER Stress Reporter Cell Lines as Models of Therapy-Resistant Cancer

In the present thesis, cellular models were established where the expression and activation of ATF4, XBP1 or ATF6 was achieved by transfection of a respective reporter gene into human embryo kidney 293 (HEK293) cells, which were chosen based on their relatively low basal ER stress activity among the cell lines tested in this study. The plasmids used in this study were originally designed by other groups for tracking the activation of ER stress response pathways through the exogenous expression of fluorescent ATF4, sXBP1 and ATF6 reporter proteins as surrogate markers (Chen et al., 2002; Nougarède et al., 2018). Indeed, stably transfected cells clearly showed specific induction of the ER stress reporter proteins upon canonical proteotoxic stress with thapsigargin (Tg) and significantly increased translocation of nATF6 to the Golgi apparatus and nucleus. More importantly, the data on the reporter cell lines gathered here collectively showed that the endo- and exogenously expressed proteins behave quite similarly in terms of gene/protein expression, subcellular localization and downstream effects, which allows for comparing the kinetics of ER stress induction between different treatments and to screen for the cellular responses specific to certain signaling branches. Reportedly, a fluorescent probe attached to a protein of interest often has no observable effects on the structure, function, and localization of the protein, even though this may vary between individual proteins and their subcellular localization, and photodamage in live cells can occur due to prolonged imaging (Clyne et al., 2003). Of note, the cytomegalovirus-derived (CMV) promoter can, in general, drive a robust, sometimes up to hundreds-fold increase in the amount of a protein (Qin et al., 2010). Certainly, this strong expression might be considered supra-physiological and could even lead to artifacts. However, in the HEK293-based models generated here, the expression levels were stable and, as stated earlier, the exogenous reporter proteins behaved in a very similar way to their endogenous counterparts. Moreover, the endogenous levels of, *e.g.*, activated ATF6, can also be strongly increased in human cancer, a subgroup of CRC patients showed an almost tenfold increase compared to non-diseased

colon mucosa (Coleman et al. 2018).

Therefore, we employed these reporter cell lines as overexpression models for ATF4, XBP1 and ATF6. The reporter gene expression positively affected resistance to OxaPt, among which the (s)XBP1-mN reporter cells showed a significant increase of resistance to OxaPt compared to the wildtype. On the other hand, ATF6-GFP reporter cells showed a significant increase in survival from radiotherapy, which is known to cause the DSB of genomic DNA. Of note, the H2A-mS control cells, which exogenously express histone H2A-mScarlet, chosen because of its apparent independence from ER stress, essentially did not show ER stress-specific effects on chemotherapy resistance. This indicates that exogenous protein (over-)expression and the likely resulting additional proteotoxic stresses are negligible in this experimental system since all reporter proteins, including the H2A-mS controls, were expressed under the control of similar promoters. Therefore, these reporter cell lines work as overexpression models for the ER-stress transcription factors, which revealed that XBP1-dependent modulation actively promoted chemoresistance, while ATF6-dependent modulation increased radiotherapy resistance.

According to the proteome-based analysis of downstream pathway enrichment, the cellular responses to OxaPt were different from the canonical response to proteotoxic stress induced by Tg (Amodio et al., 2011; Földi et al., 2013) and also different between the reporter cell lines: the ATF6-dependent modulation appeared to be involved in DNA damage repair, while XBP1 branches are rather multi-functional and involved in ribosomal biogenesis stress. To the best of our knowledge, this has not been reported so far. However, ATF6 was shown to be actively involved in resistance against chemotherapy, via its downstream target GRP78. This chaperone was shown to directly associate with the multi-drug resistance-associated protein 1 (MRP1), leading to increased efflux of 5-FU in CRC cells (Zhang et al., 2023). Moreover, GRP78 was also demonstrated to be involved in therapeutic resistance in pancreatic and nasopharyngeal cancer cells (Gifford et al., 2016; Huang et al., 2016). However, both the total proteome as well as immunoblot data indicate that GRP78 is not induced by OxaPt treatment in HEK293 cells, at least under the conditions tested here. Therefore, it can be assumed that the cancer cell responses to ER and proteostatic stress induced by chemotherapeutic drugs can be heterogeneous.

These results, as well as our proteome data, correspond to the immunoblot analysis of HEK293 wildtype cells, in which ATF6 is more closely involved in the poly(ADP-ribose)

polymerase 1 (PARP1) cleavage-induced cellular responses than ATF4 and XBP1. PARP1 cleavage is a hallmark of p53-dependent DDR (Amé et al., 2004). Reportedly, while immortalized HEK293 cells constitutively express viral oncoproteins that compromise function of p53-mediated DNA damage repair, conferring insensitivity to structural and numerical CIN (Bester et al., 2011; Komorek et al., 2010), expression of p53-regulated genes in response to DNA-damaging agents has been demonstrated (Jeon et al., 2012; Kishore et al., 2007). Therefore, the immunoblot data supports the proteome-based results that ATF6 can activate a DNA damage repair in response to OxaPt treatment. Of note, the cellular models and assays were also employed to perform preliminary tests on bacterial compounds (Hohmann et al., 2024) and glucose deprivation and indicated differences dependent on the signaling branches that mediate ER stress, which are worth investigating for further mechanistic insight and clinical implication in combination with other experimental systems specifically designed for these stress responses. For example, recent studies suggest that CRC cells rely on the reversed Warburg effect (Chekulayev et al., 2015; Satoh et al., 2017), which might be connected with the result that the ATF6-GFP reporter cells, mimicking ATF6-overexpressed cells frequently observed in CRC tumors, appeared to be less reliant on glycolytic pathways. In contrast, the XBP1-reporter cell line showed an upregulation of the glucose transporter GLUT3 after OxaPt treatment, indicating that the stress adaptive pathways downstream of the major ER stress sensors differ and allow divergent adaptations. Of course, this straightforward model is of a reductionist nature and does not recapitulate interactions with immune or stroma cells. However, collectively, the reporter cell-based system can be efficiently used to monitor the effects of chemo-/radiotherapy approaches currently used in clinical cancer treatment, as well as for a screening tool to identify potential treatments associated with certain ER stress signaling branches.

4.4. Therapy-Dependent Contribution of the ER Stress Pathways

The results above suggest that ATF6 is responsible for early DDRs, while the XBP1 branch is rather multifunctional and involved in ribosomal biogenesis stress during chemotherapeutic treatment with OxaPt. Ribosomal biogenesis is a very tightly regulated process for protein translation, which involves the production of ribosomal proteins and rRNA encoded by RNA polymerases (Pol). The first step of rDNA transcription induced by RNA Pol I leads to the production of the 47S precursor rRNA (pre-rRNA), which will then be cleaved and assembled with ribosomal proteins to form the 40S and 60S subunits. This step, occurring within sub-compartments of the nucleolus, is affected by the intracellular nutrimental conditions and the activity of oncoproteins such as c-MYC and p53, triggering nucleolar stress leading to cell cycle arrest and/or apoptosis (Russo & Russo, 2017). Hyperactivation of rRNA processing and ribosomal biogenesis plasticity are hallmarks of malignant tumor progression that is essential for increased protein synthesis to maintain unremitting cancer cell growth, emerging as novel therapy targets for human CRC (Drygin et al., 2010; Ferreira et al., 2020).

To the best of our knowledge, the roles of the ER stress signaling branches in these processes and the mechanisms for the acquisition of resistance are still poorly explored, except for the PERK-ATF4 axis or its proximal pathways. One study showed that PERK-mediated ER stress signaling promoted a p53-dependent cell cycle arrest by affecting interaction between several ribosomal proteins (Zhang et al., 2006). Another related study is on characterizing the general control nonderepressible 2 (GCN2), a cytosolic kinase that senses a lack of amino acids and converges on the phosphorylation of eIF2α, in which GCN2 was shown to differentially regulate ribosomal biogenesis in colon cancer cells depending on the nutrient availability, and furthermore, pharmacological co-inhibition of GCN2 branches and RNA Pol I activity enhanced the effect of chemotherapy including OxaPt on patient-derived colon tumor organoids (Piecyk et al., 2023). The present work highlighted the roles of XBP1 and ATF6 in the ribosomal biogenesis stress. Through the microscopy of HEK293 cells treated with OxaPt, morphological changes of the cell nuclei were observed that are typical for damages from nucleolar stress (Yang et al., 2018). Moreover, the findings that the XBP1-dependent modulation induced a more pronounced increase in the resistance to OxaPt than the ATF6-dependent modulation also suggest that induction of ribosomal biogenesis stress by OxaPt is more emphasized than the DDRs when treated for a longer time. Therefore, it may be concluded that activation of the

XBP1-dependent signaling pathways is a dominant factor in the resistance to OxaPt. However, pharmacological inhibition of the IRE1-XBP1 signaling pathways displayed no apparent decrease in the chemoresistance or even induced a slight reverse effect. In contrast, inhibition of the ATF6 signaling pathways sensitized CRC cells to OxaPt, independently recapitulated on human colon organoids. However, no conclusions can be made for the effects of inhibition of ATF6 on OxaPt sensitivity in human tumor-derived organoids, and more experiments are necessary. One possible explanation for the apparent discrepancy regarding the IRE1-XBP1 pathway is that XBP1 plays crucial roles in ribosomal biogenesis stress response but converges on multiple shared downstream effector molecules. Therefore, inhibition of XBP1 can be compensated by other signaling pathways, while inhibition of ATF6 has a much more direct impact because it plays non-redundant critical roles in DDR (**Figure 34A**). Of course, unwanted or non-specific side effects by the pharmacological compounds used to inhibit the ER stress branches cannot be fully excluded. Another and more straightforward explanation is based on the assumption of a time lag between the acute DDR and the subsequent ribosomal biogenesis

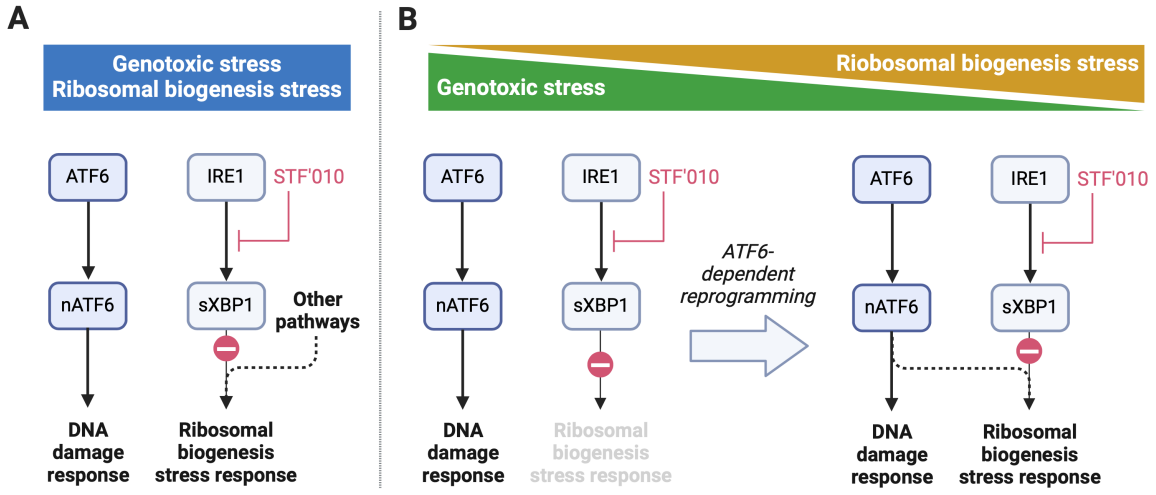

Figure 34: Possible mechanisms that allow cells to evade the effect of IRE1-XBP1 inhibition combined with oxaliplatin treatment. (A) Inhibition of the XBP1-mediated ribosomal biogenesis stress response by STF-083010 (STF'010) can be compensated by other signaling pathways which merge into common downstream pathways. **(B)** In an early phase where genotoxic stress is dominant, cells rely on the ATF6-driven DNA damage response, and inhibition of the XBP1-mediated ribosomal biogenesis stress response by STF'010 does not strongly affect the cell survival. The stress adaptation in an ATF6-dependent manner then reprograms the later ribosomal biogenesis stress response less dependent on the XBP1 function, activating bypass signaling through ATF6. The graphics were created with BioRender.com.

stress responses, which was observed in the immunoblot analysis. Cells first activate DDR for adaptation to the genotoxic aspect of OxaPt, and ribosomal biogenesis stress manifests only later on (**Figure 34B**). Thus, inhibition of the ATF6 branch has an immediate impact on the cytotoxic effect of OxaPt. On the other hand, inhibition of IRE1-XBP1 does not strongly affect the OxaPt-induced ribosomal biogenesis stress responses. This might be expected because adaptation to the initial genotoxic stress in an ATF6-dependent manner renders the cells less dependent on the XBP1 function, activating compensatory pathways through ATF6. For example, a recent study showed that ATF6 is important in regulating DNA repair through the activation of the mTOR signaling in colon cancer cells (Benedetti et al., 2022). On the other hand, the mTOR pathway also reciprocally controls the RNA Pol I activity (H. Chen et al., 2016). Such an indirect connection between ATF6 and ribosomal biogenesis implicates the existence of compensatory pathways for ribosomal biogenesis stress adaptation independent of XBP1 branches. Of note, the activity of IRE1 inhibitor has been validated on several other human cell lines in previous research, with essentially similar concentrations and time scales used in the present study (*e.g.*, 60 µM, 18 h (Papandreou et al., 2011)). Therefore, it is unlikely that the inhibitor loses its activity before the ribosomal biogenesis stress arises. In a context in which genotoxic stress induction is more dominant, such as DSB induced by radiotherapy, the roles of ATF6 in DDR could be more pronounced. Collectively, the contribution of individual ER stress signaling branches is highly dependent on the actual cancer therapies, due to potentially dominant and divergent mechanisms for each specific treatment (**Figure 35**).

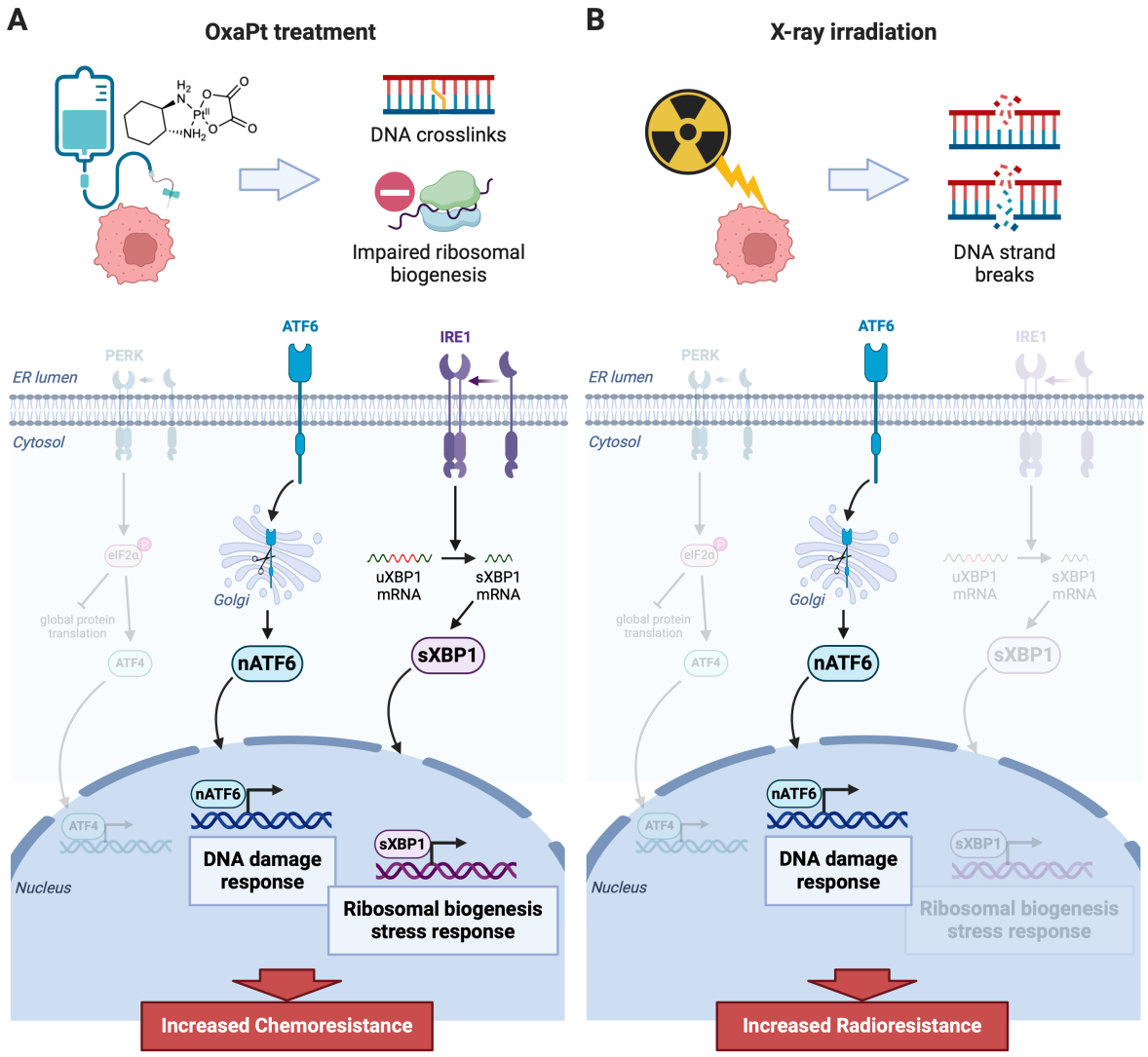

Figure 35: Therapy-dependent contribution of the ER stress pathways. (A) Treatment of cells with oxaliplatin (OxaPt) induces genotoxic and proteotoxic stresses due to DNA cross-link formation and impaired ribosomal biogenesis. To counteract these perturbations, the cells activate DNA damage response and ribosomal biogenesis stress response programs in ATF6- and XBP1-dependent manners, respectively, thereby leading to increased chemotherapy resistance. **(B)** X-ray irradiation of cells causes DNA strand breaks. In such a context where genotoxic stress induction is more dominant, the role of ATF6 in the DNA damage response could be emphasized, resulting in increased radiotherapy resistance. The graphics were created with BioRender.com.

4.5. The Potential of ER Stress Signaling as a Predictive Biomarker and Putative Therapeutic Target

As discussed above, OxaPt has a broad spectrum of impact on cellular adaptive signaling, including DDR and ribosomal biogenesis stress responses. In association with that, OxaPt-based chemo(radio)therapy harbors a risk for developing a multi-drug resistance, which shows cross-resistance to many other chemically and functionally related drugs and inadvertently reduces the options for curative and palliative treatment (Hsu et al., 2018). Therefore, it might be beneficial to stratify cancer patients who potentially show poor response to OxaPt and can eventually develop resistance, ideally before treatment or at early time points of chemotherapy administration. Thus, other therapeutic strategies could be considered, such as targeted interventions already established in the clinics, like tyrosine kinase inhibitors or anti-angiogenic therapeutic antibodies. More specifically, targeting ribosomal biogenesis in cancer cells has gained considerable attention as a novel approach in the treatment of human CRC. For example, CX-5461 and CX-3543, new drugs that selectively bind to rDNA-enriched G-quadruplex, have shown more cytotoxicity in particular cancer cells that have high activity of ribosomal biogenesis, compared to existing chemotherapy such as OxaPt that can also affect rRNA processing in an unselective manner (Drygin et al., 2010; Ferreira et al., 2020). CX-5461 is in phase I/II clinical trials for hematological cancers (Khot et al., 2019), but further mechanistic studies are necessary because it has been shown *in vitro*/*vivo* that cytotoxicity of CX-5461/3543 is mediated by the activation of a robust DDR (Xu et al., 2017). This indicates an interesting cross-talk between ribosomal biogenesis inhibition and DDR activation.

The present thesis proposes and discusses the active involvement of the ER stress signaling pathways of cancer cells in the acquisition of resistance to cancer therapy. Moreover, the potential of ER-stress mediators as predictive biomarkers and therapeutic targets to enhance OxaPt-induced cytotoxicity was specifically investigated and compared with radiotherapy responses. Two hypothetical models were thus raised, based on the clinical and CRC cell-based analysis: (1) tumors that harbor genomic instability can drive selective pressure towards amplification of the ATF6 gene locus, thereby promoting cell survival in highly stressful conditions; (2) cellular responses to the initial genotoxic stress of OxaPt occurs in an ATF6-dependent manner, and it reprograms the adaptive signaling pathways for the subsequent ribosomal biogenesis stress into less dependent on XBP1 function. Of note, this effect was

significantly observed in HCT116 cells, whose basal activity of the ER stress signaling is relatively high, but not in HEK293 cells, which showed less basal activation of the ER stress, indicating that ER stress-targeting treatment is more effective for cancer cells which adapted to the ER stress. Those (1) and (2) collectively suggest that tumors which developed genomic instability can show a positive response to OxaPt-induced cytotoxicity in ATF6 inhibition rather than in XBP1 inhibition, and therefore, it will be meaningful to further investigate whether ATF6 inhibition potentiates ribosomal biogenesis-targeting therapy.

Although the benefit of the pharmacological ATF6 inhibition combined with the OxaPt-based chemotherapy, clearly observed in HCT116 cells, was essentially recapitulated on human organoids from non-diseased colon tissue, human organoids from a CRC tumor showed no apparent changes of sensitivity to OxaPt by ATF6 inhibition. The CRC tumor, from which organoids were established, was resected from a patient who was diagnosed at UICC stage IV, poorly responding to adjuvant chemotherapy, and developed new lymph node and liver metastasis after the timepoint of tumor surgery. Of course, no definitive conclusions can be drawn from the analysis of a single case since patient-derived biomaterials like 3D organoids are, by definition, very heterogeneous. However, the patient tested here belonged to the $ATF6^{high}$ group, as defined by flow cytometric analysis. Therefore, the observed poor response to the combination of ATF6 inhibition in a tumor-specific context indicates the existence of other compensatory mechanisms that can bypass the ATF6-dependent adaptive signaling effect. This finding highlights that there may be limitations of targeting the ER stress signaling branches for cancer therapy. Furthermore, colon cancer stem cells (CSCs), suggested to be more resistant to conventional chemotherapy than differentiated cancer cells (Colak & Medema, 2014), are quiescent and generally considered to have lower ribosomal biogenesis rates that may require additional targeting strategies. In summary, the activation status of the ER stress signaling branches in tumor appears to be a cellular effect of the therapy responses in association with genomic instability and, therefore, is promising as a predictive biomarker for the selection of better treatment options for individual patients. Furthermore, pharmacological intervention with ER stress signaling can potentiate the cytotoxicity of OxaPt treatment. Lastly, the mechanistic insight into the OxaPt-induced cytotoxicity opened a strategic window for ATF6 inhibition to combine with ribosomal biogenesis-targeting therapy.

4.6. Conclusion and Perspectives

This thesis aimed to characterize the individual roles of the three ER stress signaling branches in the context of chemo- and radiotherapy resistance of CRC, focusing on the nuclear presence and putative activity of their key transcription factors ATF4, sXBP1 and nATF6. The approaches with clinical datasets and cellular *in vitro* models, as well as primary *ex vivo* organoid models, independently highlighted a putative connection between the activation of ATF6, either in the form of genomic amplification or on the protein level, and cancer therapy responses in a context with genomic instability. Interestingly, the observation was verified experimentally in a small cohort of surgically resected CRC patient tumor samples, showing that positive ATF6 in protein levels was associated with MSI. This finding may indicate that activation of ATF6 might be associated with different forms of genetic instability and warrants further analysis in more extensive and independent patient cohorts. Of note, a new method was introduced for collecting intact cell nuclei from FFPE specimens within the present thesis, followed by flow cytometric analysis, and it preliminarily showed its use in the analysis of a retrospective human CRC cohort. These results together lead to the hypothesis that high genomic instability exerts selective pressure on tumor cells, favoring tumor cell clones with genomically amplified ATF6, which is advantageous for cellular survival under conditions of high cell proliferation and unresolved ER stress due to the production of mutated and misfolded proteins. However, ATF6 may be induced by other mechanisms, independent of its genomic status, such as transcriptional or post-translational mechanisms, or by interference with other factors in the ATF6 branch of ER stress. Environmental factors, such as the gut microbiome or inflammatory cues, are among the likely upstream inducers. The results of the present thesis may actually be of clinical relevance but clearly require further experimental validation in independent cohorts and by orthogonal methods. Importantly, a stable reporter cell-line system was established to monitor and modulate the activation of ER stress proteins in live cells with subcellular resolution. This model revealed that ATF6 is closely related to the DNA damage responses (DDR) induced by oxaliplatin (OxaPt), while the other ER stress branches, particularly sXBP1, are related to subsequent ribosomal biogenesis stress responses. Since cell-type specific differences may determine the experimental outcomes, it is important to stress that these findings were supported independently by other cellular models, as well as primary patient-derived organoid models, allowing to analyze the therapy-induced

expression and activation of ER stress proteins and the downstream effects and cellular responses. The reporter cell-based system was also used as a screening tool to identify potential pharmacological treatment options associated with certain ER stress signaling branches. Although activation of the sXBP1 branch is potentially involved in ribosomal biogenesis stress responses, inhibition of sXBP1 was not found to be an effective strategy to improve the cytotoxicity of OxaPt. Instead, inhibition of ATF6, which blocks the initial DDR induced by the genotoxic stress of OxaPt, proved to be a promising approach for overcoming resistance to OxaPt. Mechanistically, induction of the ATF6-dependent DDR might also reprogram the adaptive signaling pathways for the subsequent ribosomal biogenesis stress into being less dependent on XBP1 function.

While active and therapy-dependent involvement of the ER stress proteins in the adaptive response against chemo- or radiotherapy leading to resistance could be clarified, their causal impact needs to be addressed in further studies. Transient siRNA knockdown or permanent CRISPR-Cas9 knockout of ATF6 and/or XBP1 in cancer cells is one possible approach for analyzing whether their expression is indispensable for acquiring therapy resistance. A transient siRNA transfection approach was tested in this thesis but it failed to show ER stress-specific cellular responses, *e.g.,* changes in proliferation rate (data not shown), probably because of basal activation of ER stress signaling by translational inhibition. On the other hand, gene knockout by the CRISPR/Cas system would be a more robust approach for characterizing cells without a specifically activated ER stress signaling branch. Of note, a long-term loss in function of the ER stress response can be compensated by other adaptive signaling pathways, which can make it hard to identify specific effects by the knockout of ER stress-related genes. Moreover, there have been reported to be several transgenic mouse models where the ER stress signaling branches were selectively modulated, developing spontaneous intestinal adenocarcinomas. For example, nATF6^{IEC} mice with intestinal epithelial cell (IEC)-specific expression of nATF6 showed tumorigenesis through the induction of intestinal dysbiosis and innate immune response in the absence of early inflammation (Coleman et al., 2018). For another example, transgenic mouse models with deficiency of XBP1 expression and chronic DNA damage in IECs were generated by IEC-specific deletion for ribonuclease H2 subunit B (H2B) and XBP1 (H2B/XBP1$^{\Delta IEC}$ (Welz et al., 2022)). The H2B/XBP1$^{\Delta IEC}$ mice spontaneously developed aggressive metastatic carcinoma, and transcriptome analysis of organoids from H2B/XBP1$^{\Delta IEC}$ crypt cells identified an XBP1-dependent program downstream of p53 that

coordinates DDR via mTOR signaling. Of interest, the latter carcinogenic model suggests that XBP1 is also be involved in the development of cancer malignancy related to genomic instability. On the other hand, the data described in this thesis mainly highlighted a specific role of ATF6 in the DDR-dependent resistance to chemo-/radiotherapy, but also the existence of compensatory mechanisms involved with the XBP1 branch and other uncharacterized adaptive pathways, which most likely is attributable to the failure in overcoming therapy resistance simply by targeting ER stress proteins alone. Therefore, further research should focus on downstream pathways of these ER stress proteins, in combination with *in/ex vivo* models, to identify the exact molecular targets that are efficiently druggable.

The flow cytometric data described in this thesis that suggested the involvement of ATF6 in poor therapy response of human CRC would also provide valuable input for future research on diagnostic and prognostic biomarkers, although they should be further investigated with larger and independent patient cohorts in statistically designed clinical trials with carefully controlled chemo-/radiotherapeutic treatments. Of note, the Xnuc-based approach has the potential for future expansion into the multi-parameter characterization of specific tumor subpopulations within human CRC. Following the current research trend of high-throughput and single-cell-directed approaches, but also with the applicability to histological specimens routinely stored in hospitals, the Xnuc-based methodology would be promising as a future platform for cancer diagnosis.

APPENDIX

Abbreviations

5-FU	5-Fluorouracil
AJCC	American Joint Committee on Cancer
APC	Adenomatous Polyposis Coli
ATCC	American Type Culture Collection
ATF3/4/6	Activating Transcription Factor 3/4/6
b-ZIP	Basic Leucine Zipper
BCA	Bicinchoninic Acid
BCL2	B-Cell Lymphoma 2
BCLAF1	BCL2-Associated Transcription Factor 1
BCR	B-Cell Antigen Receptor
BiP	Binding Immunoglobulin Protein
BRAF	B-Raf Proto-Oncogene
BRCA1	Breast Cancer 1
BSA	Bovine Serum Albumin
c-MYC	Cellular Myelocytomatosis
CBF	CCAAT-Binding Factor
cDNA	Complementary DNA
CDX2	Caudal-Type Homeobox Transcription Factor 2
CHOP	CCAAT-Enhancer-Binding Protein Homologous Protein
CIMP	CpG Island Methylator Phenotype
CIN	Chromosomal Instability
CMV	Cytomegalovirus-Derived
CRC	Colorectal Cancer
CRE	Cyclic AMP Response Element
CRKL	v-Crk Avian Sarcoma Virus CT10 Oncogene Homolog-like
CSC	Cancer Stem Cell
C_t	Threshold Cycle
Cy3	Cyanine 3
DACH	Diaminocyclohexane
DDR	DNA Damage Response

DDX56	DEAD-Box RNA Helicase 56
DFS	Disease-Free Survival
dia-PASEF	Data-Independent Mode with Parallel Accumulation Followed by Serial Fragmentation
DMEM	Dulbecco's Modified Eagle Medium
DSB	DNA Double-Strand Break
ECM	Extracellular Matrix
EGF(R)	Epidermal Growth Factor (Receptor)
eIF2α	Eukaryotic Translation Initiation Factor 2α
EMT	Epithelial-to-Mesenchymal Transition
ER	Endoplasmic Reticulum
ERAD	ER-Associated Degradation
ERSE	ER Stress Element
FACS	Fluorescence-Activated Cell Sorting
FAM207A	Family with Sequence Similarity 207 Member A
FAP	Familial Adenomatosis Polyposis
FASN	Fatty Acid Synthase
FCS	Fetal Calf Serum
FDA	Food and Drug Administration
FDR	False Discovery Rate
FFPE	Formalin-Fixed Paraffin-Embedded
FITC	Fluorescein Isothiocyanate
FOLFOX	5-Fluorouracil/Folinic Acid/Oxaliplatin
FSC	Forward Light Scatter Pulse
GADD34	Growth Arrest and DNA Damage-Inducible Protein 34
(γ)H2AX	(Phosphorylated) Histone H2AX
GCN2	General Control Nonderepressible 2
GFP	Green Fluorescent Protein
GLUT1/3	Glucose Transporter 1/3
GO	Gene Ontology
GRP78	Glucose-Regulated Protein 78
H2B	Ribonuclease H2 Subunit B
HBP	Hexosamine Biosynthetic Pathway
HDI	Human Development Index
HEK	Human Embryonic Kidney
HER2	Human Epidermal Growth Factor Receptor 2
HIFα	Hypoxia Inducible Factor 1α

HPRT	Hypoxanthine Phosphoribosyltransferase
HRI	Heme Regulated Inhibitor
HRP	Horseradish Peroxidase
HSP79/A5	Heat Shock Protein 79/Family A Member 5
IC_{50}	Half-Maximal Inhibitory Concentration
IP3	Inositol Triphosphate
IRB/IEC	Institutional Review Board/Independent Ethics Committee
IRE1	Inositol-Requiring Gene 1
IROX	Irinotecan/Oxaliplatin
ISR	Integrated Stress Response
JNK	c-Jun N-Terminal Kinase
KRAS	Kirsten Rat Sarcoma Proto-Oncogene
LAMP3	Lysosome-Associated Membrane Protein 3
LC	Liquid Chromatography
LDHA	Lactate Dehydrogenase A
LOH 18q	Loss of Heterozygosity at Chromosome 18q
MAPK	Mitogen-Activated Protein Kinase
MGMT	O^6-Methylguanine-DNA Methyltransferase
MLH1	MutL Homolog 1
MRP1	Multi-Drug Resistance-Associated Protein 1
MS	Mass Spectrometry
MSI	Microsatellite Instable/Instability
MSS	Microsatellite Stable/Stability
mTOR	Mammalian Target of Rapamycin
nATF6	N-Terminal Fragment of ATF6
NF-Y	Nuclear Factor Y
NLS	Nuclear Localization Sequence
NOTCH1	Neurogenic Locus Notch Homolog Protein 1
NRF2	Nuclear Factor Erythroid 2-Related Factor 2
NSA2	Nop Seven-Associated 2
OS	Overall Survival
OxaPt	Oxaliplatin
OxM	Oxidized Methionine
PAGE	Polyacrylamide Gel Electrophoresis
PARP1	Poly(ADP-Ribose) Polymerase 1
PCR	Polymerase Chain Reaction

PD1	Programmed Cell Death 1
PDI	Protein Disulfide Isomerase
PERK	Protein Kinase RNA-Like ER Kinase
PI3K	Phosphoinositide-3-Kinase
PKR	dsRNA-Dependent Protein Kinase
PLCγ	Phospholipase Cγ
PTEN	Phosphatase and Tensin Homolog
pTNM	Pathological Tumor-Node-Metastasis Stages
RAD51	Rad51 Recombinase
RAS	Rat Sarcoma
rDNA, rRNA	Ribosomal DNA/RNA
RIDD	Regulated IRE1-Dependent Decay
RIPA	Radioimmunoprecipitation Assay
ROI	Region of Interest
ROS	Reactive Oxygen Species
RSL1D1	Ribosomal L1 Domain-Containing Protein 1
RT	Room Temperature
S1P, S2P	Site-1 and Site-2 Protease
SASH1	SAM and SH3 Domain Containing 1
SCCA1	Squamous Cell Carcinoma Antigen 1
SCD1	Stearoyl-CoA-Desaturase 1
SDB-RPS	Styrene Divinylbenzene-Reverse Phase Sulfonate
SDHAF4	Succinate Dehydrogenase Complex Assembly Factor 4
SLC2A3	Solute Carrier Family 2 Member 3
SLUG	Snail Homolog 2
SLX9	Ribosome Biogenesis Protein Slx9 Homolog
SMAD4	Mothers against Decapentaplegic Homolog 4
SNAIL	Snail Homolog 1
SSC	Side Light Scatter Pulse
s/uXBP1	Spliced/Unspliced Isoform of XBP1
TCGA	The Cancer Genome Atlas
Tg	Thapsigargin
TGF	Transforming Growth Factor
TNBC	Triple-Negative Breast Cancer
TP53	Tumor Protein p53
TRAF	Tumor Necrosis Factor Receptor-Associated Factor

TSC1/2	Tuberous Sclerosis Complex 1/2
TWIST1	Twist-Related Protein 1
UICC	Union Internationale Contre le Cancer
UPL	Universal ProbeLibrary
UPRE	Unfolded Protein Response Element
VEGF	Vascular Endothelial Growth Factor
WEM	William's E Medium
WNT	Wingless-Related Integration Site
WRN	WNT, R-Spondin and Noggin
WT	Wildtype
XBP1	X-Box Binding Protein 1
XELOX	Xeloda/Oxaliplatin
XRCC1	X-Ray Repair Cross-Complementing Protein 1
ZEB1	Zinc Finger E-Box Binding Homeobox 1

Materials

Buffer compositions

BES buffer (2 ×)	50 mM BES (N,N-Bis-(2-hydroxyethyl)-2-aminoethane sulfonic acid), 410 mM NaCl, 1.5 mM Na_2HPO_4, pH 6.96
Laemmli buffer (5 ×)	150 mM Tris-HCl, 10% (w/v) SDS, 50% (v/v) glycerol, 500 mM DTT, 0.01% (w/v) bromophenol blue, pH 6.8
PBS(T)	10 mM Na_2HPO_4, 2 mM KH_2PO_4, 137 mM NaCl, 2.7 mM KCl (+ 0.1% (v/v) Tween 20)
RIPA buffer	50 mM Tris-HCl, 150 mM NaCl, 1 mM EDTA, 1% (v/v) NP-40, 0.25% (w/v) sodium deoxycholate, 0.1% (w/v) SDS, pH 7.4
Running buffer (5 ×)	30 g/l Tris, 144 g/l glycine, 5 g/l SDS
TAE (50 ×)	2 M Tris, 1 M glacial acetic acid, 50 mM EDTA
TBS	50 mM Tris-HCl, 150 mM NaCl, pH 7.4
Transblot buffer (10 ×)	480 mM Tris, 390 mM glycine
Transblot buffer (1 ×)	10% (v/v) 10 × Transblot buffer, 20% (v/v) methanol

PCR primers

#1	Human ATF4 - forward	TCTCCAGCGACAAGGCTAA
#2	Human ATF4 - reverse	CCAATCTGTCCCGGAGAA
#3	Human ATF6 - forward	AATACTGAACTATGGACCTATGAGCA
#4	Human ATF6 - reverse	TTGCAGGGCTCACACTAGG
#5	Human HPRT - forward	GACCAGTCAACAGGGGACAT
#6	Human HPRT - reverse	GTGTCAATTATATCTTCCACAATCAAG
#7	Human XBP1 - forward	CCCTGGTTGCTGAAGAGG
#8	Human XBP1 - reverse	TGGAGGGGTGACAACTGG
#9a	Human sXBP1 - forward	GCTGAGTCCGCAGCAGGT
#9b	Human uXBP1 - forward	CAGACTACGTGCACCTCTGC
#10	Human s/uXBP1 - reverse	CTGGGTCCAAGTTGTCCAGAAT
#11	Mycoplasma target 1 - forward	GGCGAATGGGTGAGTAACACG
#12	Mycoplasma target 1 - reverse	CGGATAACGCTTGCGACCTATG
#13	Mycoplasma target 2 - forward	GGGAGCAAACAGGATTAGATACCCT
#14	Mycoplasma target 2 - reverse	TGCACCATCTGTCACTCTGTTAACCTC

Primary antibodies

Mouse Anti-Golgin-97 (CDF4)	Thermo Fisher Scientific, A-21270
Mouse Anti-Ki67 (MIB-1)	Dako, M7240
Mouse Anti-Lamin A/C (Clone 14)	BD Biosciences, 612163
Mouse Anti-PARP1 (B-10)	SCBT, sc74470
Mouse Anti-α-Tubulin (DM1A)	Sigma-Aldrich, CP06
Mouse Anti-β-Actin (8H10D10)	CST, #3700
Mouse IgG Isotype Control	Abcam, ab37355
Rabbit Anti-ATF4 (EPR24346-182)	Abcam, ab270980
Rabbit Anti-ATF6	Abcam, ab203119
Rabbit Anti-GRP78 (C50B12)	CST, #3177
Rabbit Anti-Lamin A/B1/C (EPR4068)	Abcam, ab108922
Rabbit Anti-Phospho-eIF2α	CST, #9721
Rabbit Anti-XBP1	Abcam, ab37152

Rabbit Anti-α-Calnexin	Enzo, ADI-SPA-860
Rabbit IgG Isotype Control	Abcam, ab37415

Secondary antibodies

Cy3 AffiniPure Goat Anti-Mouse IgG (H+L)	Jackson, 115-165-003
Goat Anti-Mouse IgG (H+L) Alexa Fluor 488	Thermo Fisher Scientific, A32723
Goat Anti-Rabbit IgG (H+L) Alexa Fluor 488	Thermo Fisher Scientific, A11008
Peroxidase-AffiniPure Goat Anti-Mouse IgG (H+L)	Jackson, 115-035-003
Peroxidase-AffiniPure Goat Anti-Rabbit IgG (H+L)	Jackson, 111-035-144

Chemicals

2-(4-Carbamimidoylphenyl)-1H-indole-6-carboximidamide (DAPI)	Thermo Fisher Scientific, Waltham, USA
A83-01 (ALK5 inhibitor)	Tocris Bioscience, Bristol, UK
Acetonitrile, LC-MS grade	Merck, Darmstadt, Germany
Acrylamide (30%)/bis-acrylamide (0.8%) solution	Carl Roth, Karlsruhe, Germany
Advanced DMEM/F-12	Gibco, Billings, USA
Agarose	Sigma-Aldrich, St. Louis, USA
Ammonium chloride (NH_4Cl)	Merck, Darmstadt, Germany
Ammonium hydroxide (NH_4OH)	Merck, Darmstadt, Germany
Ammonium persulfate (APS)	Sigma-Aldrich, St. Louis, USA
Ampicillin	Sigma-Aldrich, St. Louis, USA
Antibiotic-Antimycotic	Gibco, Billings, USA
B-27 supplement	Gibco, Billings, USA
Benzamidine	Sigma-Aldrich, St. Louis, USA
Blotting grade milk powder	Carl Roth, Karlsruhe, Germany
Bovine serum albumin (BSA)	Sigma-Aldrich, St. Louis, USA
Bovine serum albumin (BSA), fatty acid-free	Sigma-Aldrich, St. Louis, USA
Bromophenol blue	Merck, Darmstadt, Germany
Calcium chloride ($CaCl_2$)	Carl Roth, Karlsruhe, Germany
Ceapin-A7 (ATF6 inhibitor)	Merck, Darmstadt, Germany
Collagenase IV	Sigma-Aldrich, St. Louis, USA
Crystal violet (1%) solution	Sigma-Aldrich, St. Louis, USA
Deoxynucleotide triphosphates (dNTPs)	Fermentas, St. Leon-Rot, Germany
Dimethyl sulfoxide (DMSO)	Merck, Darmstadt, Germany
Dispase II	Sigma-Aldrich, St. Louis, USA
Dithiothreitol (DTT)	Fermentas, St. Leon-Rot, Germany
Dulbecco's Modified Eagle Medium (DMEM)	Thermo Fisher Scientific, Waltham, USA
Dulbecco's Phosphate Buffered Saline (PBS)	Thermo Fisher Scientific, Waltham, USA
ECL Western Blotting Substrate	Pierce, Born, Germany
Endopeptidase Lys-C	Promega, Madison, USA
EnVision FLEX Target Retrieval Solution Low pH	Agilent, Santa Clara, USA
Epidermal Growth Factor (EGF)	PeproTech, Rocky Hill, USA
Ethanol	VWR, Radnor, USA
Ethanol, molecular biology grade	Sigma-Aldrich, St. Louis, USA
Ethidium bromide	Carl Roth, Karlsruhe, Germany
Ethylenediaminetetraacetic acid disodium salt dihydrate (EDTA 2Na $2H_2O$)	Carl Roth, Karlsruhe, Germany
FastDigest restriction enzymes	Thermo Fisher Scientific, Waltham, USA
Fetal calf serum (FCS)	Biochrom, Cambridge, UK

Formaldehyde (3.5–3.7%) neutral solution	Otto Fischar, Saarbrücken, Germany
Formic acid	Merck, Darmstadt, Germany
FuGENE HD	Promega, Madison, USA
G418 sulfate (Neomycin)	Merck, Darmstadt, Germany
Gelatin	Carl Roth, Karlsruhe, Germany
GeneRuler 1 kb DNA ladder	Fermentas, St. Leon-Rot, Germany
GeneRuler 100 b DNA ladder	Fermentas, St. Leon-Rot, Germany
Glacial acetic acid	Merck, Darmstadt, Germany
Glycerol	Carl Roth, Karlsruhe, Germany
Glycerol gelatin	Sigma-Aldrich, St. Louis, USA
Glycine	Carl Roth, Karlsruhe, Germany
GSK-2656157 (PERK inhibitor)	Merck, Darmstadt, Germany
Hoechst-33342, trihydrochloride	Invitrogen, Carlsbad, USA
Human insulin	Sanofi, Paris, France
Hydrocortisone hemisuccinate	Sigma-Aldrich, St. Louis, USA
Hygromycin B	Invitrogen, Carlsbad, USA
Immersion Oil	Carl Zeiss, Jena, Germany
Isopropanol	Carl Roth, Karlsruhe, Germany
Kanamycin	Sigma-Aldrich, St. Louis, USA
L-Alanyl-L-glutamine (GlutaMAX)	Thermo Fisher Scientific, Waltham, USA
L-Glutamine	Biochrom, Cambridge, UK
Lysogeny Broth (LB) agar plate	Institute for Medical Microbiology, Immunology and Hygiene, TUM, Munich, Germany
LB medium	Institute for Medical Microbiology, Immunology and Hygiene, TUM, Munich, Germany
Magnesium chloride hexahydrate ($MgCl_2$ $6H_2O$)	Carl Roth, Karlsruhe, Germany
Matrigel	Corning, Corning, USA
Methanol	VWR, Radnor, USA
Mycoplasma Removal Agent	Bio-Rad, Hercules, USA
N-2-Hydroxyethylpiperazine-N-2-ethane sulfonic acid (HEPES) buffer (1 M)	Gibco, Billings, USA
N-Acetylcysteine	Carl Roth, Karlsruhe, Germany
N,N-Bis-(2-hydroxyethyl)-2-aminoethane sulfonic acid (BES)	Sigma-Aldrich, St. Louis, USA
N,N,N',N'-Tetramethyl ethylenediamine (TEMED)	Bio-Rad, Hercules, USA
Nicotinamide	Sigma-Aldrich, St. Louis, USA
Nonyl phenocypolyethoxylethanol-40 (NP-40)	Thermo Fisher Scientific, Waltham, USA
Normal Goat Serum (NGS)	Thermo Fisher Scientific, Waltham, USA
Normocin	Invitrogen, Karlsruhe, Germany
Oligo$(dT)_{18}$ Primer	Fermentas, St. Leon-Rot, Germany
Opti-MEM	Thermo Fisher Scientific, Waltham, USA
Oxaliplatin (OxaPt)	Pharmacy, MRI, TUM, Munich, Germany
PageRuler Prestained Protein Ladder	Thermo Fisher Scientific, Waltham, USA
Palmitate (C16:0)	Sigma-Aldrich, St. Louis, USA
Paraformaldehyde (PFA)	Sigma-Aldrich, St. Louis, USA
Pefabloc	Roche Diagnostics, Basel, Switzerland
Penicillin/Streptomycin	Biochrom, Cambridge, UK
Pepstatin A	Invitrogen, Carlsbad, USA
Phenylmethanesulfonyl fluoride (PMSF)	Sigma-Aldrich, St. Louis, USA
Potassium chloride (KCl)	Carl Roth, Karlsruhe, Germany
Potassium dihydrogen phosphate (KH_2PO_4)	Carl Roth, Karlsruhe, Germany

Prostaglandin E2 (PGE2)	Sigma-Aldrich, St. Louis, USA
Protease Inhibitor Cocktail (PIC)	Roche Diagnostics, Basel, Switzerland
Random Hexamer Primer	Fermentas, St. Leon-Rot, Germany
Recombinant human noggin	PeproTech, Rocky Hill, USA
RevertAid H Minus Reverse Transcriptase	Thermo Fisher Scientific, Waltham, USA
RiboLock RNase Inhibitor	Thermo Fisher Scientific, Waltham, USA
RNase-Free Water	Qiagen, Hilden, Germany
SB-202190 (p38 pathway inhibitor)	Sigma-Aldrich, St. Louis, USA
Sodium chloride (NaCl)	Carl Roth, Karlsruhe, Germany
Sodium deoxycholate	Sigma-Aldrich, St. Louis, USA
Sodium dodecyl sulfate (SDS)	Carl Roth, Karlsruhe, Germany
Sodium fluoride (NaF)	Sigma-Aldrich, St. Louis, USA
Sodium monohydrogen phosphate dehydrate ($Na_2HPO_4\ 2H_2O$)	Carl Roth, Karlsruhe, Germany
Sodium orthovanadate (Na_3VO_4)	Sigma-Aldrich, St. Louis, USA
STF-083010 (IRE1 inhibitor)	Sigma-Aldrich, St. Louis, USA
SYTOX-Green	Thermo Fisher Scientific, Waltham, USA
Taq DNA polymerase	Roche Diagnostics, Basel, Switzerland
Thapsigargin (Tg)	Sigma-Aldrich, St. Louis, USA
Thrombin	GE Healthcare, Milwaukee, USA
Trifluoroacetic acid (TFA)	Merck, Darmstadt, Germany
Tris(hydroxymethyl)aminomethane (Tris)	Sigma-Aldrich, St. Louis, USA
Triton X-100	Carl Roth, Karlsruhe, Germany
TriTrack DNA Loading Dye (6 ×)	Thermo Fisher Scientific, Waltham, USA
Trypan blue	Biochrom, Cambridge, UK
Trypsin-EDTA solution	Sigma-Aldrich, St. Louis, USA
Tween 20	Merck, Darmstadt, Germany
Water, LC-MS grade	Merck, Darmstadt, Germany
Xylene	Merck, Darmstadt, Germany
Y-27632 dihydrochloride (ROCK inhibitor)	Sigma-Aldrich, St. Louis, USA
β-Glycerophosphate	Sigma-Aldrich, St. Louis, USA
β-Mercaptoethanol	Merck, Darmstadt, Germany

Consumables

(Safe lock) Reaction tubes (0.5, 1.5, 2 ml)	Eppendorf, Hamburg, Germany
6-/12-/24-/96-well tissue culture plate	Corning, Corning, USA
Cell culture plates	Corning, Corning, USA
Cell scraper	Sarstedt, Newton, USA
Centrifuge tubes (15ml, 50ml)	Greiner Bio-One, Kremsmünster, Austria
EASYstrainer (40–70 µm)	Greiner Bio-One, Kremsmünster, Austria
FACS tubes (5 ml)	Corning, Corning, USA
Glass slides	Thermo Fisher Scientific, Waltham, USA
Pasteur pipettes	Brand, Wertheim, Germany
PCR 96-Well TW-MT-Platte	Biozym Scientific, Hessisch Oldendorf, Germany
Pipette tips (0.5-10, 20-200, 100-1000 µl)	BD Biosciences, San Jose, USA
ReproSil-Pure-AQ C18 (1.9 µm)	Dr. Maisch, Ammersbach, Germany
SDB-RP StageTips	Merck, Darmstadt, Germany
Silicon Seal Cap Tubes	Starlab, Hamburg, Germany
Whatman Blotting Paper	GE Healthcare, Milwaukee, USA

Commercial kits

Annexin V-FITC Apoptosis Staining/Detection Kit	Abcam, Cambridge, USA
Glycolysis Assay (Extracellular Acidification) Kit	Abcam, Cambridge, USA
LightCycler 480 Probes Master	Roche Diagnostics, Basel, Switzerland
LightCycler 480 SYBR Green I Master	Roche Diagnostics, Basel, Switzerland
MTT Cell Growth Assay Kit II	Sigma-Aldrich, St. Louis, USA
Pierce BCA Protein Assay Kit	Thermo Fisher Scientific, Waltham, USA
Plasmid Mini/Maxi Kit	Qiagen, Hilden, Germany
RevertAid H Minus First Strand cDNA Synthesis Kit	Thermo Fisher Scientific, Waltham, USA
RNeasy Mini Kit	Qiagen, Hilden, Germany
Taq DNA Polymerase Kit	Thermo Fisher Scientific, Waltham, USA
Type-it Microsatellite PCR Kit	Qiagen, Hilden, Germany
Universal ProbeLibrary Set	Sigma-Aldrich, St. Louis, USA
XTT Cell Proliferation Kit II	Roche Diagnostics, Basel, Switzerland

Cell lines

DLD1 (CCL-221)	ATCC, Manassas, USA
HCT116 (CCL-247)	ATCC, Manassas, USA
HEK293 (CRL-1573)	ATCC, Manassas, USA
HepaRG (HPR116080)	Sigma-Aldrich, St. Louis, USA
HT29 (HTB-38)	ATCC, Manassas, USA
SW480 (CCL-228)	ATCC, Manassas, USA
SW620 (CCL-227)	ATCC, Manassas, USA

Technical devices

Biometra Agagel Mini gel system	Analytik Jena, Jena, Germany
Aria III FACS	BD Biosciences, San Jose, USA
AxioObserver Z1 (including ApoTome system)	Carl Zeiss, Jena, Germany
BBD 6220 Cell Culture Incubator	Heraeus, Hanau, Germany
Biometra P25T Standard Power Pack	Analytik Jena, Jena, Germany
Bioruptor Sonicator	Diagenode, Seraing, Belgium
Centrifuge 5424R	Eppendorf, Hamburg, Germany
Centrifuge Megafuge 2.0R	Heraeus, Hanau, Germany
CytoFLEX flow cytometer	Beckmann Coulter, Brea, USA
EG 1160 Paraffin Embedding Center	Leica Microsystems, Wetzlar, Germany
Fastblot semi-dry blotting system	Analytik Jena, Jena, Germany
Fluoroskan Ascent FL microplate fluorometer	Thermo Fisher Scientific, Waltham, USA
HERA Safe Cleanbench	Thermo Fisher Scientific, Waltham, USA
HistoCore PEARL tissue processor	Leica Microsystems, Wetzlar, Germany
HXP 120 C Fluorescence Light Source	Carl Zeiss, Jena, Germany
Hybridization Oven HYBRI 6/12 V	LTF Labortechnik, Wasserburg, Germany
Innova 4230 Refrigerated Benchtop Incubator Shaker	New Brunswick Scientific, Edison, USA
LightCycler 480 II system	Roche Diagnostics, Basel, Switzerland
Mithras LB 940 Microplate Detector	Berthold Technologies, Wildbad, Germany
Motor handpiece MHX/E homogenizer	ZENOX, Overijse, Belgium
MRX Microplate Reader ELISA	Dynatech Laboratories, USA
Multiskan FC microplate photometer	Thermo Fisher Scientific, Waltham, USA
NanoDrop 1000 Spectrophotometer	Thermo Fisher Scientific, Waltham, USA
PerfectBlue gel system	Peqlab, Erlangen, Germany

PureLab Ultra MK II water purification system	ELGA LabWater, Lane End, UK
RS225 X-ray cabinet irradiator	Gulmay Medical, Surrey, UK
Sonoplus SH70G sonicator	Bandelin, Berlin, Germany
SpeedVac vacuum concentrator	Eppendorf, Hamburg, Germany
T10 basic ULTRA TURRAX homogenizer	IKA Instruments, Staufen, Germany
T3 Thermocycler	Analytik Jena, Jena, Germany
timsTOF HT mass spectrometer	Bruker Daltonics, Billerica, USA
UVP ChemStudio imaging system	Analytik Jena, Jena, Germany
UVP GelSolo imaging system	Analytik Jena, Jena, Germany
Vanquish Neo UHPLC system	Thermo Scientific, Waltham, USA
Zeiss Power Supply 232	Carl Zeiss, Jena, Germany
zenCELL owl live cell imager	innoMe, Espelkamp, Germany

Software

DIA-NN (v.1.8.1)	Demichev et al., 2020 (open source)
Fiji/ImageJ (v.2.3.0)	NIH, Bethesda, USA (open source)
FlowJo (v.10.8.1)	BD Biosciences, San Jose, USA
LightCycler 480 (v.1.5)	Roche Diagnostics, Basel, Switzerland
Microsoft office	Microsoft, Washington, USA
Prism (v.9.5.1)	GraphPad, La Jolla, USA
ProbeFinder (v.2.53)	Roche Diagnostics, Basel, Switzerland
R (v.4.2.1)	The R foundation for statistical computing, Vienna, Austria (open source)
ZEN (v.3.0)	Carl Zeiss, Jena, Germany
zenCELL owl (v.2.0)	innoMe, Espelkamp, Germany

Human Cohort

ID	Age	Gender	Diagnosis	Grade	pTNM stage	UICC stage	MS status
#1	47	Female	Cecum CA	G1	pT3, pN1b (3/20), pM0	IIIB	n.a.
#2	67	Female	Sigmoid colon CA	G2	pT3, pN1a (1/7), pM1a (HEP)	IVA	n.a.
#3	45	Male	Hepatic flexure CA	G2	T4a, N2a (4/38), M0	IIIC	n.a.
#4	57	Male	Sigmoid CA	G2	pT2, pN0 (0/14), L0, V0, R0	I	MSS
#5	94	Male	Rectosigmoid CA	G3	pT3, pN1b (2/12), L1, R0	IIIB	n.a.
#6	72	Male	Descending colon CA	G2	pT3, pN0 (0/14), L0, V0, R0	IIA	MSS
#7	70	Male	Ascending colon CA	G2	pT3, pN1a (1/15, ECE+), Pn1, L1, V0, R0	IIIB	MSS
#8	78	Male	Ascending colon CA	G3	pT2, N0 (0/34), L0, V0, Pn0, R0	I	MSS
#9	66	Female	Sigmoid colon CA	G1	pT2, pN1a (1/17), cM0, R0, L1, V0, Pn0	IIIA	MSI
#10	66	Female	Rectum CA	G2	pT2, Pn0(0/17), cM0, Pn0, L0, V0, R0	I	MSI
#11	73	Male	Rectum CA	n.a.	pT3, pN0 (0/24), L0, V0, Pn0, R0	IIA	MSS
#12	66	Female	Ascending colon CA	G3	pT4a, pN2b (23/71), L1, V1, R0, cM0	IIIC	MSS
#13	81	Female	Descending colon CA	G2	pT2, pN0 (0/34), L0, V0, Pn0, R0, cM0	I	MSS
#14	82	Male	Left flexure colon (adeno)CA	G2	pT3, pN2b (11/38), M1c, L1, V0, Pn0, R0	IVC	MSI
#15	80	Female	Ascending colon/coecum CA	G2	pT2, pN1b (2/17), L1, V0, Pn0, R0	IIIA	n.a.
#16	69	Male	Ascending colon CA	G2	pT3, pN2a (6/26, 2.5 cm, ECE+), L1, V0, Pn0, R0	IIIB	MSS
#17	55	Male	Ascending colon CA	G2	pT2, pN0 (0/33), Pn0, V0, R0	I	MSI
#18	79	Male	Ascending colon CA	G2	pT3, pN2b (8/41), V0, L1, Pn0, R0	IIIC	MSI
#19	79	Male	Sigmoid colon CA	G2	pT2, pN0 (0/23), V0, L0, Pn0, R0	I	n.a.
#20	86	Male	Ascending colon CA	G2	pT3, pN1a (1/28, 1.4 cm), L1, V0, pN0, R0	IIIB	MSS
#21	92	Female	Sigmoid colon CA	G2	pT3, pN0 (0/26), L0, V0, Pn0, R0	IIA	MSS
#22	72	Female	Descending colon CA	G2	pT3, pN0(0/23), L0, V0, Pn0, R0	IIA	MSS
#23	68	Female	Ascending colon CA	G2	pT3, pN0 (0/50), L1, V0, Pn0, R0	IIA	MSI
#24	82	Female	Rectosigmoid colon CA	G2	pT3, pN0(0/18), L0, V0, Pn0, R0	IIA	MSS
#25	63	Female	AdenoCA of the Bauhin Valvula	G2	pT3, pN0 (0/31), Pn1, L0, V1, R0	IIA	n.a.
#26	73	Male	Sigmoid colon (adeno)CA	G2	pT4a, pN1c (1/15, Satellite knot), L1, V1, Pn0, R0, cM0	IIIB	MSS
#27	72	Female	Ascending colon CA	n.a.	ypT3, ypN0 (0/46), L0, V0, Pn0, R0, M1 (HEP)	IVA	MSS
#28	53	Female	Descending colon (adeno)CA	n.a.	ypT3, ypN1b (2/34), L1, V1, Pn1, R0, cM1	IVA	MSS
#29	74	Male	Rectum CA	n.a.	cT4a/b, cN2, M+ (HEP, PUL)	IVB	MSS
#30	60	Female	Sigmoid colon CA	n.a.	ypT1, yTis, ypN1a (1/21), Pn0, L1, V0, R0, M+ (HEP)	IVA	MSS
#31	66	Male	Rectum CA	n.a.	pT3, pN1, pM1b	IVB	MSS
#32	66	Male	Sigmoid colon CA	n.a.	pT3, pN0 (0/13), L1, V0, Pn0, low-grade, R0, M0	IIA	MSS

ID	Follow-up data	Processing	Use
#1	n.a.	FFPE	Table 2, Fig. 10
#2	n.a.	FFPE	Table 2, Fig. 10
#3	n.a.	FFPE	Table 2, Fig. 10
#4	No local relapse (≥ 1 yr.)	FFPE	Table 2, Fig. 10
#5	Non-cancer death	FFPE	Table 2, Fig. 10
#6	No local relapse (≥ 1 yr.)	FFPE	Table 2, Fig. 10, S2
#7	No local relapse (≥ 1 yr.)	FFPE	Table 2, Fig. 10
#8	n.a.	Fresh	Table 1, Fig. 6
#9	No local relapse (≥ 1 yr.)	Fresh, FFPE	Table 1, 2, Fig. 6, 10
#10	n.a.	Fresh, organoids	Table 1, Fig. 6, 18
#11	n.a.	Fresh	Table 1, Fig. 6
#12	n.a.	Fresh	Table 1, Fig. 6
#13	n.a.	Fresh, FFPE	Table 1, Fig. 6, 10
#14	n.a.	Fresh	Table 1, Fig. 6
#15	No local relapse (≥ 1 yr.)	FFPE	Table 2, Fig. 10
#16	No local relapse (≥ 1 yr.)	FFPE	Table 2, Fig. 10
#17	No local relapse (≥ 1 yr.)	FFPE	Table 2, Fig. 10
#18	No local relapse (< 1 yr.)	FFPE	Table 2, Fig. 10
#19	Non-cancer death	FFPE	Table 2, Fig. 10
#20	No local relapse (< 1 yr.)	FFPE	Fig. S3
#21	No local relapse (< 1 yr.)	FFPE	Table 2, Fig. 10
#22	Local relapse, new liver metastasis (< 1 yr.)	FFPE	Table 2, Fig. 10
#23	n.a.	FFPE	Table 2, Fig. 10
#24	No local relapse (< 1 yr.)	FFPE	Table 2, Fig. 10
#25	New pulmonary metastasis (< 1 yr.)	FFPE	Table 2, Fig. 10
#26	No local relapse (< 1 yr.)	FFPE	Table 2, Fig. 10
#27	n.a.	Organoids	Fig. 17
#28	New liver/lymph node metastasis (< 1 yr.)	Organoids, FFPE	Table 2, Fig. 10, 19
#29	No local relapse (< 1 yr.)	FFPE	Table 2, Fig. 10
#30	No local relapse (< 1 yr.)	FFPE	Table 2, Fig. 10
#31	New liver metastasis (< 1 yr.)	FFPE	Table 2, Fig. 10
#32	No local relapse (< 1 yr.)	FFPE	Table 2, Fig. 10

List of Figures

List of Tables

Supplemental Figures

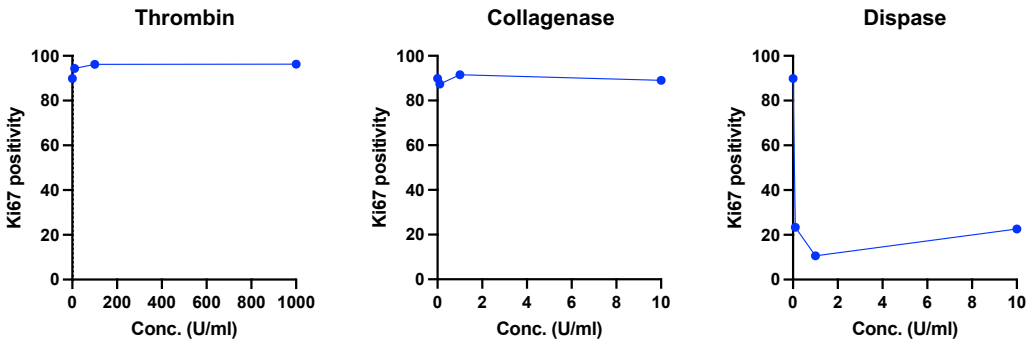

Figure S1: Effect of enzymatic digestion on the Ki67 positivity in the Xnuc-based method. Formalin-fixed HCT116 cells were subjected to antigen retrieval, as described earlier. Then, 0–1000 U/ml thrombin (left), 0–10 U/ml collagenase IV (middle) and 0–10 U/ml dispase II (right) were tested for the optimal conditions by comparing the Ki67 positivity determined by flow cytometry (cut-off levels = upper 95 percentile of the isotype control).

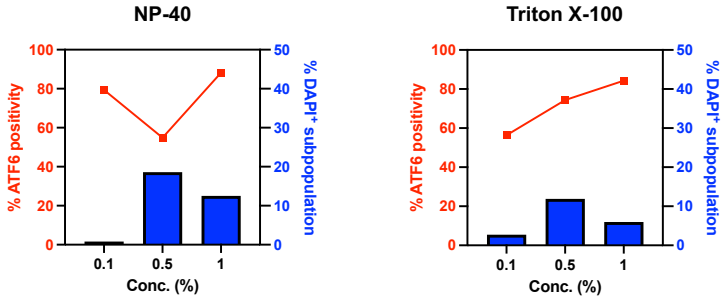

Figure S2: Effect of non-ionic detergents on the ATF6 positivity and recovery rate of intact cell nuclei in the Xnuc-based method. FFPE human colon tumor was subjected to antigen retrieval, thrombin digestion and homogenization, as described before. Then, 0.1–1% NP-40 (left) and Triton X-100 (right) were tested for the optimal condition of the sonication step by comparing the ATF6 positivity determined by flow cytometry (cut-off levels = upper 95 percentile of the isotype control) as well as the recovery rate of DAPI-positive subpopulation.

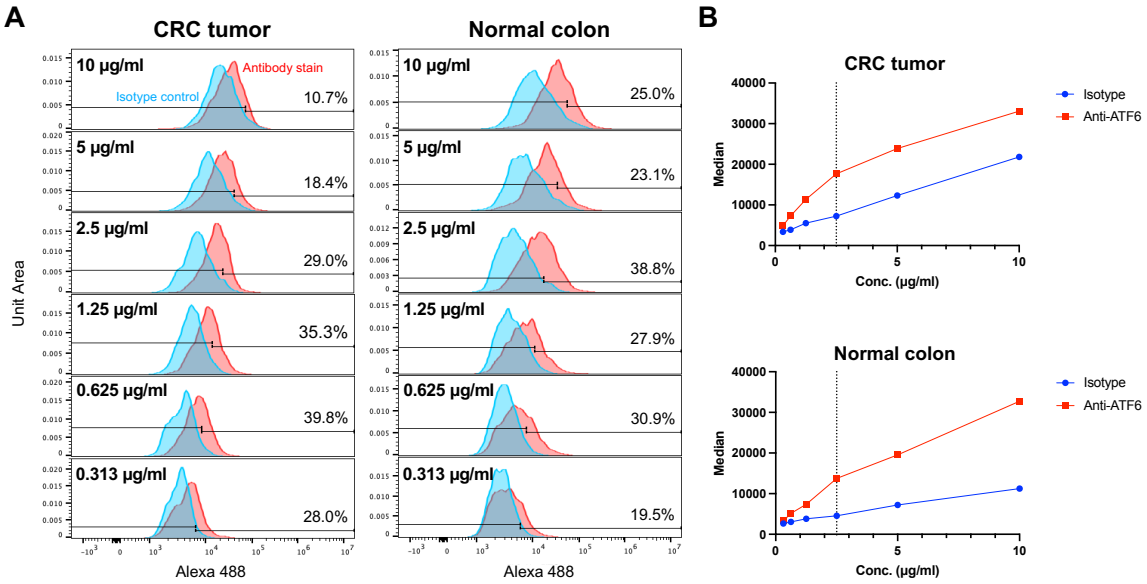

Figure S3: Titration of anti-ATF6 antibody for quantitative evaluation of the ATF6 positivity by the Xnuc-based method. (A) Histograms for isotype control and antibody stain against ATF6 (detection: Alexa488-conjugated secondary antibody) stacked for different concentrations of the primary antibody (0.313–10 µg/ml). Cut-off levels = upper 95 percentile of the isotype control. **(B)** Relationship between the concentration of primary antibody and a median value of fluorescence intensity. The dashed line represents an optimal concentration.

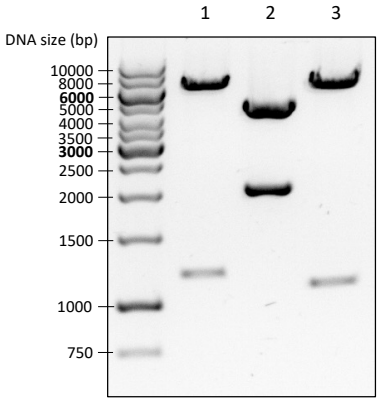

Lane #	1	2	3
Plasmids	pLHCX-ATF4 mScarlet NLS (7973 bp)	pEGFP-ATF6 (6729 bp)	pLHCX-XBP1 mNeonGreen NLS (7868 bp)
Restriction enzymes	ClaI HindIII	SalI HindIII	ClaI HindIII
Expected band sizes (bp)	6800, 1173	4709, 2020	6800, 1068

Figure S4: Validation of the gene inserts along with the vector backbone in plasmids by fragmentation with restriction endonucleases. pLHCX-ATF4 mScarlet NLS, pEGFP-ATF6 and pLHCX-XBP1 mNeonGreen NLS plasmids were digested with specific bacterial restriction endonucleases, and the resulting DNA fragments were analyzed by agarose gel electrophoresis.

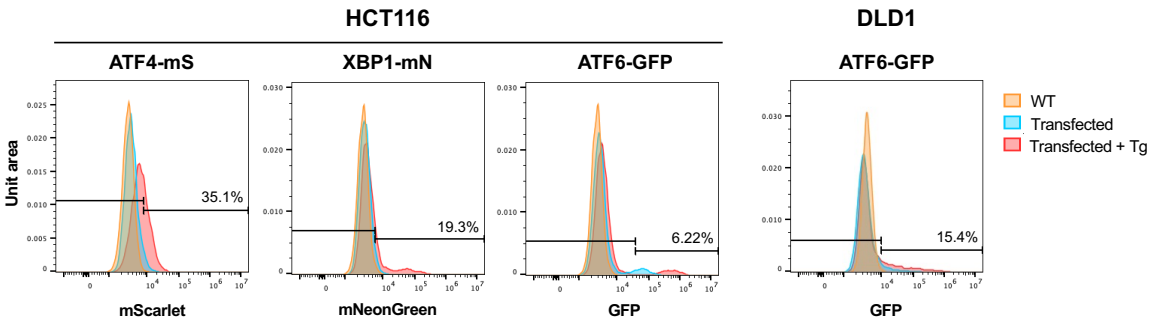

Figure S5: Characterization of HCT116 and DLD1 transfected with ER stress reporter genes. The reporter gene expression in transfected HCT116 and DLD1 cells was analyzed by flow cytometry after treatment with Tg (1 µM, 24 h). Cut-off levels = upper 95 percentile of transfected cells without Tg treatment. Tg, thapsigargin.

References

Acosta-Alvear, D., Zhou, Y., Blais, A., Tsikitis, M., Lents, N. H., Arias, C., Lennon, C. J., Kluger, Y., & Dynlacht, B. D. (2007). XBP1 controls diverse cell type- and condition-specific transcriptional regulatory networks. *Mol Cell*, *27*(1), 53-66.

Akman, M., Belisario, D. C., Salaroglio, I. C., Kopecka, J., Donadelli, M., De Smaele, E., & Riganti, C. (2021). Hypoxia, endoplasmic reticulum stress and chemoresistance: dangerous liaisons. *J Exp Clin Cancer Res*, *40*(1), 28.

Almanza, A., Carlesso, A., Chintha, C., Creedican, S., Doultsinos, D., Leuzzi, B., Luís, A., McCarthy, N., Montibeller, L., More, S., Papaioannou, A., Püschel, F., Sassano, M. L., Skoko, J., Agostinis, P., de Belleroche, J., Eriksson, L. A., Fulda, S., Gorman, A. M., . . . Samali, A. (2019). Endoplasmic reticulum stress signalling – from basic mechanisms to clinical applications. *FEBS J, 286*(2), 241-278.

Amé, J. C., Spenlehauer, C., & de Murcia, G. (2004). The PARP superfamily. *Bioessays*, *26*(8), 882-893.

Amodio, G., Moltedo, O., Monteleone, F., D'Ambrosio, C., Scaloni, A., Remondelli, P., & Zambrano, N. (2011). Proteomic signatures in thapsigargin-treated hepatoma cells. *Chem Res Toxicol*, *24*(8), 1215-1222.

Andruska, N. D., Zheng, X., Yang, X., Mao, C., Cherian, M. M., Mahapatra, L., Helferich, W. G., & Shapiro, D. J. (2015). Estrogen receptor α inhibitor activates the unfolded protein response, blocks protein synthesis, and induces tumor regression. *Proc Natl Acad Sci U S A*, *112*(15), 4737-4742.

Arai, M., Kondoh, N., Imazeki, N., Hada, A., Hatsuse, K., Kimura, F., Matsubara, O., Mori, K., Wakatsuki, T., & Yamamoto, M. (2006). Transformation-associated gene regulation by ATF6α during hepatocarcinogenesis. *FEBS Lett*, *580*(1), 184-190.

Argemí, J., Kress, T. R., Chang, H. C. Y., Ferrero, R., Bértolo, C., Moreno, H., González-Aparicio, M., Uriarte, I., Guembe, L., Segura, V., Hernández-Alcoceba, R., Ávila, M. A., Amati, B., Prieto, J., & Aragón, T. (2017). X-box binding protein 1 regulates unfolded protein, acute-phase, and DNA damage responses during regeneration of mouse liver. *Gastroenterology*, *152*(5), 1203-1216.e1215.

Argilés, G., Tabernero, J., Labianca, R., Hochhauser, D., Salazar, R., Iveson, T., Laurent-Puig, P., Quirke, P., Yoshino, T., Taieb, J., Martinelli, E., & Arnold, D. (2020). Localised colon cancer: ESMO Clinical Practice Guidelines for diagnosis, treatment and follow-up. *Ann Oncol*, *31*(10), 1291-1305.

Arnold, M., Abnet, C. C., Neale, R. E., Vignat, J., Giovannucci, E. L., McGlynn, K. A., & Bray, F. (2020). Global burden of 5 major types of gastrointestinal cancer. *Gastroenterology*, *159*(1), 335-349.e315.

Arnold, M., Sierra, M. S., Laversanne, M., Soerjomataram, I., Jemal, A., & Bray, F. (2017). Global patterns and trends in colorectal cancer incidence and mortality. *Gut*, *66*(4), 683-691.

Atkins, C., Liu, Q., Minthorn, E., Zhang, S. Y., Figueroa, D. J., Moss, K., Stanley, T. B., Sanders, B., Goetz, A., Gaul, N., Choudhry, A. E., Alsaid, H., Jucker, B. M., Axten, J. M., & Kumar, R. (2013). Characterization of a novel PERK kinase inhibitor with antitumor and antiangiogenic activity. *Cancer Res*, *73*(6), 1993-2002.

Auf, G., Jabouille, A., Guérit, S., Pineau, R., Delugin, M., Bouchecareilh, M., Magnin, N., Favereaux, A., Maitre, M.,

Gaiser, T., von Deimling, A., Czabanka, M., Vajkoczy, P., Chevet, E., Bikfalvi, A., & Moenner, M. (2010). Inositol-requiring enzyme 1α is a key regulator of angiogenesis and invasion in malignant glioma. *Proc Natl Acad Sci U S A*, *107*(35), 15553-15558.

Avril, T., Vauléon, E., & Chevet, E. (2017). Endoplasmic reticulum stress signaling and chemotherapy resistance in solid cancers. *Oncogenesis*, *6*(8), e373.

Axten, J. M., Medina, J. R., Feng, Y., Shu, A., Romeril, S. P., Grant, S. W., Li, W. H., Heerding, D. A., Minthorn, E., Mencken, T., Atkins, C., Liu, Q., Rabindran, S., Kumar, R., Hong, X., Goetz, A., Stanley, T., Taylor, J. D., Sigethy, S. D., . . . Gampe, R. T. (2012). Discovery of 7-methyl-5-(1-{[3-(trifluoromethyl)phenyl]acetyl}-2,3-dihydro-1H-indol-5-yl)-7H-pyrrolo[2,3-d]pyrimidin-4-amine (GSK2606414), a potent and selective first-in-class inhibitor of protein kinase R (PKR)-like endoplasmic reticulum kinase (PERK). *J Med Chem*, *55*(16), 7193-7207.

Axten, J. M., Romeril, S. P., Shu, A., Ralph, J., Medina, J. R., Feng, Y., Li, W. H., Grant, S. W., Heerding, D. A., Minthorn, E., Mencken, T., Gaul, N., Goetz, A., Stanley, T., Hassell, A. M., Gampe, R. T., Atkins, C., & Kumar, R. (2013). Discovery of GSK2656157: An optimized PERK inhibitor selected for preclinical development. *ACS Med Chem Lett*, *4*(10), 964-968.

Bahar, E., Kim, J. Y., & Yoon, H. (2019). Chemotherapy resistance explained through endoplasmic reticulum stress-dependent signaling. *Cancers (Basel)*, *11*(3), 338.

Baker, A. M., Cross, W., Curtius, K., Al Bakir, I., Choi, C. R., Davis, H. L., Temko, D., Biswas, S., Martinez, P., Williams, M. J., Lindsay, J. O., Feakins, R., Vega, R., Hayes, S. J., Tomlinson, I. P. M., McDonald, S. A. C., Moorghen, M., Silver, A., East, J. E., . . . Graham, T. A. (2019). Evolutionary history of human colitis-associated colorectal cancer. *Gut*, *68*(6), 985-995.

Barker, N., van Es, J. H., Kuipers, J., Kujala, P., van den Born, M., Cozijnsen, M., Haegebarth, A., Korving, J., Begthel, H., Peters, P. J., & Clevers, H. (2007). Identification of stem cells in small intestine and colon by marker gene Lgr5. *Nature*, *449*(7165), 1003-1007.

Battaglin, F., Naseem, M., Lenz, H. J., & Salem, M. E. (2018). Microsatellite instability in colorectal cancer: overview of its clinical significance and novel perspectives. *Clin Adv Hematol Oncol*, *16*(11), 735-745

Beksac, M., Balli, S., & Akcora Yildiz, D. (2020). Drug targeting of genomic instability in multiple myeloma. *Front Genet*, *11*, 228.

Benedetti, R., Romeo, M. A., Arena, A., Gilardini Montani, M. S., Di Renzo, L., D'Orazi, G., & Cirone, M. (2022). ATF6 prevents DNA damage and cell death in colon cancer cells undergoing ER stress. *Cell Death Discov*, *8*(1), 295.

Bester, A. C., Roniger, M., Oren, Y. S., Im, M. M., Sarni, D., Chaoat, M., Bensimon, A., Zamir, G., Shewach, D. S., & Kerem, B. (2011). Nucleotide deficiency promotes genomic instability in early stages of cancer development. *Cell*, *145*(3), 435-446.

Bindels, D. S., Haarbosch, L., van Weeren, L., Postma, M., Wiese, K. E., Mastop, M., Aumonier, S., Gotthard, G., Royant, A., Hink, M. A., & Gadella, T. W., Jr. (2017). mScarlet: a bright monomeric red fluorescent protein

for cellular imaging. *Nat Methods*, *14*(1), 53-56.

Bobrovnikova-Marjon, E., Grigoriadou, C., Pytel, D., Zhang, F., Ye, J., Koumenis, C., Cavener, D., & Diehl, J. A. (2010). PERK promotes cancer cell proliferation and tumor growth by limiting oxidative DNA damage. *Oncogene*, *29*(27), 3881-3895.

Bolland, H., Ma, T. S., Ramlee, S., Ramadan, K., & Hammond, E. M. (2021). Links between the unfolded protein response and the DNA damage response in hypoxia: a systematic review. *Biochem Soc Trans*, *49*(3), 1251-1263.

Braakman, I., & Bulleid, N. J. (2011). Protein folding and modification in the mammalian endoplasmic reticulum. *Annu Rev Biochem*, *80*, 71-99.

Bruno, P. M., Liu, Y., Park, G. Y., Murai, J., Koch, C. E., Eisen, T. J., Pritchard, J. R., Pommier, Y., Lippard, S. J., & Hemann, M. T. (2017). A subset of platinum-containing chemotherapeutic agents kills cells by inducing ribosome biogenesis stress. *Nat Med*, *23*(4), 461-471.

Byrd, A. E., & Brewer, J. W. (2012). Intricately regulated: a cellular toolbox for fine-tuning XBP1 expression and activity. *Cells*, *1*(4), 738-753.

Calfon, M., Zeng, H., Urano, F., Till, J. H., Hubbard, S. R., Harding, H. P., Clark, S. G., & Ron, D. (2002). IRE1 couples endoplasmic reticulum load to secretory capacity by processing the XBP-1 mRNA. *Nature*, *415*(6867), 92-96.

Carrasco, D. R., Sukhdeo, K., Protopopova, M., Sinha, R., Enos, M., Carrasco, D. E., Zheng, M., Mani, M., Henderson, J., Pinkus, G. S., Munshi, N., Horner, J., Ivanova, E. V., Protopopov, A., Anderson, K. C., Tonon, G., & DePinho, R. A. (2007). The differentiation and stress response factor XBP-1 drives multiple myeloma pathogenesis. *Cancer Cell*, *11*(4), 349-360.

Cassidy, J., Tabernero, J., Twelves, C., Brunet, R., Butts, C., Conroy, T., Debraud, F., Figer, A., Grossmann, J., Sawada, N., Schöffski, P., Sobrero, A., Van Cutsem, E., & Díaz-Rubio, E. (2004). XELOX (capecitabine plus oxaliplatin): active first-line therapy for patients with metastatic colorectal cancer. *J Clin Oncol*, *22*(11), 2084-2091.

Chaney, S. G., & Vaisman, A. (1999). Specificity of platinum-DNA adduct repair. *J Inorg Biochem*, *77*(1-2), 71-81.

Chekulayev, V., Mado, K., Shevchuk, I., Koit, A., Kaldma, A., Klepinin, A., Timohhina, N., Tepp, K., Kandashvili, M., Ounpuu, L., Heck, K., Truu, L., Planken, A., Valvere, V., & Kaambre, T. (2015). Metabolic remodeling in human colorectal cancer and surrounding tissues: alterations in regulation of mitochondrial respiration and metabolic fluxes. *Biochem Biophys Rep*, *4*, 111-125.

Chen, H., Duo, Y., Hu, B., Wang, Z., Zhang, F., Tsai, H., Zhang, J., Zhou, L., Wang, L., Wang, X., & Huang, L. (2016). PICT-1 triggers a pro-death autophagy through inhibiting rRNA transcription and AKT/mTOR/p70S6K signaling pathway. *Oncotarget*, *7*(48), 78747-78763.

Chen, X., Iliopoulos, D., Zhang, Q., Tang, Q., Greenblatt, M. B., Hatziapostolou, M., Lim, E., Tam, W. L., Ni, M., Chen, Y., Mai, J., Shen, H., Hu, D. Z., Adoro, S., Hu, B., Song, M., Tan, C., Landis, M. D., Ferrari, M., . . . Glimcher, L. H. (2014). XBP1 promotes triple-negative breast cancer by controlling the HIF1α pathway. *Nature*,

508(7494), 103-107.

Chen, X., Shen, J., & Prywes, R. (2002). The luminal domain of ATF6 senses endoplasmic reticulum (ER) stress and causes translocation of ATF6 from the ER to the Golgi. *J Biol Chem*, *277*(15), 13045-13052.

Chen, X., Zhang, F., Gong, Q., Cui, A., Zhuo, S., Hu, Z., Han, Y., Gao, J., Sun, Y., Liu, Z., Yang, Z., Le, Y., Gao, X., Dong, L. Q., Gao, X., & Li, Y. (2016). Hepatic ATF6 increases fatty acid oxidation to attenuate hepatic steatosis in mice through peroxisome proliferator-activated receptor α. *Diabetes*, *65*(7), 1904-1915.

Cherri, S., Oneda, E., Noventa, S., Melocchi, L., & Zaniboni, A. (2022). Microsatellite instability and chemosensitivity in solid tumours. *Ther Adv Med Oncol*, *14*, 17588359221099347.

Chevet, E., Hetz, C., & Samali, A. (2015). Endoplasmic reticulum stress-activated cell reprogramming in oncogenesis. *Cancer Discov*, *5*(6), 586-597.

Chou, J. F., Row, D., Gonen, M., Liu, Y. H., Schrag, D., & Weiser, M. R. (2010). Clinical and pathologic factors that predict lymph node yield from surgical specimens in colorectal cancer: a population-based study. *Cancer*, *116*(11), 2560-2570.

Clapham, D. E. (2007). Calcium signaling. *Cell*, *131*(6), 1047-1058.

Clyne, P. J., Brotman, J. S., Sweeney, S. T., & Davis, G. (2003). Green fluorescent protein tagging Drosophila proteins at their native genomic loci with small P elements. *Genetics*, *165*(3), 1433-1441.

Colak, S., & Medema, J. P. (2014). Cancer stem cells – important players in tumor therapy resistance. *FEBS J*, *281*(21), 4779-4791.

Coleman, O. I., Lobner, E. M., Bierwirth, S., Sorbie, A., Waldschmitt, N., Rath, E., Berger, E., Lagkouvardos, I., Clavel, T., McCoy, K. D., Weber, A., Heikenwalder, M., Janssen, K. P., & Haller, D. (2018). Activated ATF6 induces intestinal dysbiosis and innate immune response to promote colorectal tumorigenesis. *Gastroenterology*, *155*(5), 1539-1552.e1512.

Coleman, O. I., Sorbie, A., Bierwith, S., Kövilein, J., von Stern, M., Köhler, N., Wirbel, J., Schmidt, C., Kacprowski, T., & Dunkel, A. (2023). ATF6 activation alters colonic lipid metabolism causing tumor-associated microbial adaptation. *bioRxiv*, 2023.11.03.565267.

Colucci, G., Gebbia, V., Paoletti, G., Giuliani, F., Caruso, M., Gebbia, N., Cartenì, G., Agostara, B., Pezzella, G., Manzione, L., Borsellino, N., Misino, A., Romito, S., Durini, E., Cordio, S., Di Seri, M., Lopez, M., Maiello, E., Montemurro, S., . . . Brunetti, C. (2005). Phase III randomized trial of FOLFIRI versus FOLFOX4 in the treatment of advanced colorectal cancer: a multicenter study of the Gruppo Oncologico Dell'Italia Meridionale. *J Clin Oncol*, *23*(22), 4866-4875.

Compton, C., Fenoglio-Preiser, C. M., Pettigrew, N., & Fielding, L. P. (2000). American Joint Committee on Cancer prognostic factors consensus conference: Colorectal working group. *Cancer*, *88*(7), 1739-1757.

Cox, J. S., Shamu, C. E., & Walter, P. (1993). Transcriptional induction of genes encoding endoplasmic reticulum resident proteins requires a transmembrane protein kinase. *Cell*, *73*(6), 1197-1206.

Croft, A., Tay, K. H., Boyd, S. C., Guo, S. T., Jiang, C. C., Lai, F., Tseng, H. Y., Jin, L., Rizos, H., Hersey, P., & Zhang, X. D. (2014). Oncogenic activation of MEK/ERK primes melanoma cells for adaptation to endoplasmic

reticulum stress. *J Invest Dermatol*, *134*(2), 488-497.

Culy, C. R., Clemett, D., & Wiseman, L. R. (2000). Oxaliplatin. A review of its pharmacological properties and clinical efficacy in metastatic colorectal cancer and its potential in other malignancies. *Drugs*, *60*(4), 895-924.

Cunningham, D., Humblet, Y., Siena, S., Khayat, D., Bleiberg, H., Santoro, A., Bets, D., Mueser, M., Harstrick, A., Verslype, C., Chau, I., & Van Cutsem, E. (2004). Cetuximab monotherapy and cetuximab plus irinotecan in irinotecan-refractory metastatic colorectal cancer. *N Engl J Med*, *351*(4), 337-345.

Dadey, D. Y., Kapoor, V., Khudanyan, A., Urano, F., Kim, A. H., Thotala, D., & Hallahan, D. E. (2016). The ATF6 pathway of the ER stress response contributes to enhanced viability in glioblastoma. *Oncotarget*, *7*(2), 2080-2092.

De Angelis, M. L., Francescangeli, F., La Torre, F., & Zeuner, A. (2019). Stem cell plasticity and dormancy in the development of cancer therapy resistance. *Front Oncol*, *9*, 626.

De Craene, B., & Berx, G. (2013). Regulatory networks defining EMT during cancer initiation and progression. *Nat Rev Cancer*, *13*(2), 97-110.

de Gramont, A., Watson, S., Ellis, L. M., Rodón, J., Tabernero, J., de Gramont, A., & Hamilton, S. R. (2015). Pragmatic issues in biomarker evaluation for targeted therapies in cancer. *Nat Rev Clin Oncol*, *12*(4), 197-212.

de Jong, M. C., Pulitano, C., Ribero, D., Strub, J., Mentha, G., Schulick, R. D., Choti, M. A., Aldrighetti, L., Capussotti, L., & Pawlik, T. M. (2009). Rates and patterns of recurrence following curative intent surgery for colorectal liver metastasis: an international multi-institutional analysis of 1669 patients. *Ann Surg*, *250*(3), 440-448.

Dejeans, N., Pluquet, O., Lhomond, S., Grise, F., Bouchecareilh, M., Juin, A., Meynard-Cadars, M., Bidaud-Meynard, A., Gentil, C., Moreau, V., Saltel, F., & Chevet, E. (2012). Autocrine control of glioma cells adhesion and migration through IRE1α-mediated cleavage of SPARC mRNA. *J Cell Sci*, *125*(Pt 18), 4278-4287.

Denoyelle, C., Abou-Rjaily, G., Bezrookove, V., Verhaegen, M., Johnson, T. M., Fullen, D. R., Pointer, J. N., Gruber, S. B., Su, L. D., Nikiforov, M. A., Kaufman, R. J., Bastian, B. C., & Soengas, M. S. (2006). Anti-oncogenic role of the endoplasmic reticulum differentially activated by mutations in the MAPK pathway. *Nat Cell Biol*, *8*(10), 1053-1063.

Dewhirst, M. W., & Secomb, T. W. (2017). Transport of drugs from blood vessels to tumour tissue. *Nat Rev Cancer*, *17*(12), 738-750.

Dicks, N., Gutierrez, K., Michalak, M., Bordignon, V., & Agellon, L. B. (2015). Endoplasmic reticulum stress, genome damage, and cancer. *Front Oncol*, *5*, 11.

Dilly, A. K., Honick, B. D., Lee, Y. J., Bartlett, D. L., & Choudry, H. A. (2020). Synergistic apoptosis following endoplasmic reticulum stress aggravation in mucinous colon cancer. *Orphanet J Rare Dis*, *15*(1), 211.

Douillard, J. Y., Oliner, K. S., Siena, S., Tabernero, J., Burkes, R., Barugel, M., Humblet, Y., Bodoky, G., Cunningham, D., Jassem, J., Rivera, F., Kocákova, I., Ruff, P., Błasińska-Morawiec, M., Šmakal, M., Canon, J. L., Rother, M., Williams, R., Rong, A., . . . Patterson, S. D. (2013). Panitumumab-FOLFOX4 treatment and RAS

mutations in colorectal cancer. *N Engl J Med*, *369*(11), 1023-1034.

Douillard, J. Y., Siena, S., Cassidy, J., Tabernero, J., Burkes, R., Barugel, M., Humblet, Y., Bodoky, G., Cunningham, D., Jassem, J., Rivera, F., Kocákova, I., Ruff, P., Błasińska-Morawiec, M., Šmakal, M., Canon, J. L., Rother, M., Oliner, K. S., Tian, Y., . . . Sidhu, R. (2014). Final results from PRIME: randomized phase III study of panitumumab with FOLFOX4 for first-line treatment of metastatic colorectal cancer. *Ann Oncol*, *25*(7), 1346-1355.

Drost, J., & Clevers, H. (2018). Organoids in cancer research. *Nat Rev Cancer*, *18*(7), 407-418.

Drygin, D., Rice, W. G., & Grummt, I. (2010). The RNA polymerase I transcription machinery: an emerging target for the treatment of cancer. *Annu Rev Pharmacol Toxicol*, *50*, 131-156.

Dufey, E., Bravo-San Pedro, J. M., Eggers, C., González-Quiroz, M., Urra, H., Sagredo, A. I., Sepulveda, D., Pihán, P., Carreras-Sureda, A., Hazari, Y., Sagredo, E. A., Gutierrez, D., Valls, C., Papaioannou, A., Acosta-Alvear, D., Campos, G., Domingos, P. M., Pedeux, R., Chevet, E., . . . Hetz, C. (2020). Genotoxic stress triggers the activation of IRE1α-dependent RNA decay to modulate the DNA damage response. *Nat Commun*, *11*(1), 2401.

Dunn, T. A., Schmoll, H. J., Grünwald, V., Bokemeyer, C., & Casper, J. (1997). Comparative cytotoxicity of oxaliplatin and cisplatin in non-seminomatous germ cell cancer cell lines. *Invest New Drugs*, *15*(2), 109-114.

Ecker, J., Benedetti, E., Kindt, A. S. D., Höring, M., Perl, M., Machmüller, A. C., Sichler, A., Plagge, J., Wang, Y., Zeissig, S., Shevchenko, A., Burkhardt, R., Krumsiek, J., Liebisch, G., & Janssen, K. P. (2021). The colorectal cancer lipidome: identification of a robust tumor-specific lipid species signature. *Gastroenterology*, *161*(3), 910-923.e919.

Edwards, B. K., Ward, E., Kohler, B. A., Eheman, C., Zauber, A. G., Anderson, R. N., Jemal, A., Schymura, M. J., Lansdorp-Vogelaar, I., Seeff, L. C., van Ballegooijen, M., Goede, S. L., & Ries, L. A. (2010). Annual report to the nation on the status of cancer, 1975-2006, featuring colorectal cancer trends and impact of interventions (risk factors, screening, and treatment) to reduce future rates. *Cancer*, *116*(3), 544-573.

Fagone, P., & Jackowski, S. (2009). Membrane phospholipid synthesis and endoplasmic reticulum function. *J Lipid Res*, *50* Suppl(Suppl), S311-316.

Feng, T., Zhao, R., Zhang, H., Sun, F., Hu, J., Wang, M., Qi, M., Liu, L., Gao, L., Xiao, Y., Zhen, J., Chen, W., Wang, L., & Han, B. (2023). Reciprocal negative feedback regulation of ATF6α and PTEN promotes prostate cancer progression. *Cell Mol Life Sci*, *80*(10), 292.

Feng, Y. X., Sokol, E. S., Del Vecchio, C. A., Sanduja, S., Claessen, J. H., Proia, T. A., Jin, D. X., Reinhardt, F., Ploegh, H. L., Wang, Q., & Gupta, P. B. (2014). Epithelial-to-mesenchymal transition activates PERK-eIF2α and sensitizes cells to endoplasmic reticulum stress. *Cancer Discov*, *4*(6), 702-715.

Ferreira, R., Schneekloth, J. S., Jr., Panov, K. I., Hannan, K. M., & Hannan, R. D. (2020). Targeting the RNA polymerase I transcription for cancer therapy comes of age. *Cells*, *9*(2), 266.

Fink, E. E., Moparthy, S., Bagati, A., Bianchi-Smiraglia, A., Lipchick, B. C., Wolff, D. W., Roll, M. V., Wang, J., Liu, S., Bakin, A. V., Kandel, E. S., Lee, A. H., & Nikiforov, M. A. (2018). XBP1-KLF9 axis acts as a molecular rheostat

to control the transition from adaptive to cytotoxic unfolded protein response. *Cell Rep*, *25*(1), 212-223.e214.

Földi, I., Tóth, A. M., Szabó, Z., Mózes, E., Berkecz, R., Datki, Z. L., Penke, B., & Janáky, T. (2013). Proteome-wide study of endoplasmic reticulum stress induced by thapsigargin in N2a neuroblastoma cells. *Neurochem Int*, *62*(1), 58-69.

Franke, F. C., Müller, J., Abal, M., Medina, E. D., Nitsche, U., Weidmann, H., Chardonnet, S., Ninio, E., & Janssen, K. P. (2019). The tumor suppressor SASH1 interacts with the signal adaptor CRKL to inhibit epithelial-mesenchymal transition and metastasis in colorectal cancer. *Cell Mol Gastroenterol Hepatol*, *7*(1), 33-53.

Franke, F. C., Slusarenko, B. O., Engleitner, T., Johannes, W., Laschinger, M., Rad, R., Nitsche, U., & Janssen, K. P. (2020). Novel role for CRK adaptor proteins as essential components of SRC/FAK signaling for epithelial-mesenchymal transition and colorectal cancer aggressiveness. *Int J Cancer*, *147*(6), 1715-1731.

Fukuda, M., Ohe, Y., Kanzawa, F., Oka, M., Hara, K., & Saijo, N. (1995). Evaluation of novel platinum complexes, inhibitors of topoisomerase I and II in non-small cell lung cancer (NSCLC) sublines resistant to cisplatin. *Anticancer Res*, *15*(2), 393-398.

Gagnon, K. T., Li, L., Chu, Y., Janowski, B. A., & Corey, D. R. (2014). RNAi factors are present and active in human cell nuclei. *Cell Rep*, *6*(1), 211-221.

Gallagher, C. M., Garri, C., Cain, E. L., Ang, K. K., Wilson, C. G., Chen, S., Hearn, B. R., Jaishankar, P., Aranda-Diaz, A., Arkin, M. R., Renslo, A. R., & Walter, P. (2016). Ceapins are a new class of unfolded protein response inhibitors, selectively targeting the ATF6α branch. *Elife*, *5*, e11878.

Ganesh, K., Stadler, Z. K., Cercek, A., Mendelsohn, R. B., Shia, J., Segal, N. H., & Diaz, L. A., Jr. (2019). Immunotherapy in colorectal cancer: rationale, challenges and potential. *Nat Rev Gastroenterol Hepatol*, *16*(6), 361-375.

Garris, C. S., & Pittet, M. J. (2015). ER stress in dendritic cells promotes cancer. *Cell*, *161*(7), 1492-1493.

Gérard, A., Buyse, M., Nordlinger, B., Loygue, J., Pène, F., Kempf, P., Bosset, J. F., Gignoux, M., Arnaud, J. P., Desaive, C., & et al. (1988). Preoperative radiotherapy as adjuvant treatment in rectal cancer. Final results of a randomized study of the European Organization for Research and Treatment of Cancer (EORTC). *Ann Surg*, *208*(5), 606-614.

Ghosh, R., Lipson, K. L., Sargent, K. E., Mercurio, A. M., Hunt, J. S., Ron, D., & Urano, F. (2010). Transcriptional regulation of VEGF-A by the unfolded protein response pathway. *PLoS One*, *5*(3), e9575.

Gifford, J. B., Huang, W., Zeleniak, A. E., Hindoyan, A., Wu, H., Donahue, T. R., & Hill, R. (2016). Expression of GRP78, master regulator of the unfolded protein response, increases chemoresistance in pancreatic ductal adenocarcinoma. *Mol Cancer Ther*, *15*(5), 1043-1052.

Ginos, M. A., Page, G. P., Michalowicz, B. S., Patel, K. J., Volker, S. E., Pambuccian, S. E., Ondrey, F. G., Adams, G. L., & Gaffney, P. M. (2004). Identification of a gene expression signature associated with recurrent disease in squamous cell carcinoma of the head and neck. *Cancer Res*, *64*(1), 55-63.

Glehen, O., Kwiatkowski, F., Sugarbaker, P. H., Elias, D., Levine, E. A., De Simone, M., Barone, R., Yonemura, Y.,

Cavaliere, F., Quenet, F., Gutman, M., Tentes, A. A., Lorimier, G., Bernard, J. L., Bereder, J. M., Porcheron, J., Gomez-Portilla, A., Shen, P., Deraco, M., & Rat, P. (2004). Cytoreductive surgery combined with perioperative intraperitoneal chemotherapy for the management of peritoneal carcinomatosis from colorectal cancer: a multi-institutional study. *J Clin Oncol*, *22*(16), 3284-3292.

Goldberg, P. A., Nicholls, R. J., Porter, N. H., Love, S., & Grimsey, J. E. (1994). Long-term results of a randomised trial of short-course low-dose adjuvant pre-operative radiotherapy for rectal cancer: reduction in local treatment failure. *Eur J Cancer*, *30A*(11), 1602-1606.

Goldberg, R. M., Sargent, D. J., Morton, R. F., Fuchs, C. S., Ramanathan, R. K., Williamson, S. K., Findlay, B. P., Pitot, H. C., & Alberts, S. R. (2004). A randomized controlled trial of fluorouracil plus leucovorin, irinotecan, and oxaliplatin combinations in patients with previously untreated metastatic colorectal cancer. *J Clin Oncol*, *22*(1), 23-30.

González-Quiroz, M., Blondel, A., Sagredo, A., Hetz, C., Chevet, E., & Pedeux, R. (2020). When endoplasmic reticulum proteostasis meets the DNA damage response. *Trends Cell Biol*, *30*(11), 881-891.

Gottesman, M. M. (2002). Mechanisms of cancer drug resistance. *Annu Rev Med*, *53*, 615-627.

Grady, W. M., & Carethers, J. M. (2008). Genomic and epigenetic instability in colorectal cancer pathogenesis. *Gastroenterology*, *135*(4), 1079-1099.

Green, C. D., Ozguden-Akkoc, C. G., Wang, Y., Jump, D. B., & Olson, L. K. (2010). Role of fatty acid elongases in determination of de novo synthesized monounsaturated fatty acid species. *J Lipid Res*, *51*(7), 1871-1877.

Greenberg, M. E., & Bender, T. P. (2007). Identification of newly transcribed RNA. *Curr Protoc Mol Biol*, *Chapter 4*, Unit 4.10.

Greenman, C., Stephens, P., Smith, R., Dalgliesh, G. L., Hunter, C., Bignell, G., Davies, H., Teague, J., Butler, A., Stevens, C., Edkins, S., O'Meara, S., Vastrik, I., Schmidt, E. E., Avis, T., Barthorpe, S., Bhamra, G., Buck, G., Choudhury, B., . . . Stratton, M. R. (2007). Patterns of somatic mutation in human cancer genomes. *Nature*, *446*(7132), 153-158.

Gupta, P. B., Pastushenko, I., Skibinski, A., Blanpain, C., & Kuperwasser, C. (2019). Phenotypic plasticity: driver of cancer initiation, progression, and therapy resistance. *Cell Stem Cell*, *24*(1), 65-78.

Gutiérrez, T., & Simmen, T. (2014). Endoplasmic reticulum chaperones and oxidoreductases: critical regulators of tumor cell survival and immunorecognition. *Front Oncol*, *4*, 291.

Hanahan, D. (2022). Hallmarks of cancer: new dimensions. *Cancer Discov*, *12*(1), 31-46.

Hanahan, D., & Weinberg, R. A. (2011). Hallmarks of cancer: the next generation. *Cell*, 144(5), 646-674.

Harding, H. P., Zhang, Y., & Ron, D. (1999). Protein translation and folding are coupled by an endoplasmic-reticulum-resident kinase. *Nature*, *397*(6716), 271-274.

Harding, H. P., Zhang, Y., Zeng, H., Novoa, I., Lu, P. D., Calfon, M., Sadri, N., Yun, C., Popko, B., Paules, R., Stojdl, D. F., Bell, J. C., Hettmann, T., Leiden, J. M., & Ron, D. (2003). An integrated stress response regulates amino acid metabolism and resistance to oxidative stress. *Mol Cell*, *11*(3), 619-633.

Hayashi, M., Inoue, Y., Komeda, K., Shimizu, T., Asakuma, M., Hirokawa, F., Miyamoto, Y., Okuda, J., Takeshita, A.,

Shibayama, Y., & Tanigawa, N. (2010). Clinicopathological analysis of recurrence patterns and prognostic factors for survival after hepatectomy for colorectal liver metastasis. *BMC Surg*, *10*, 27.

Haze, K., Yoshida, H., Yanagi, H., Yura, T., & Mori, K. (1999). Mammalian transcription factor ATF6 is synthesized as a transmembrane protein and activated by proteolysis in response to endoplasmic reticulum stress. *Mol Biol Cell*, *10*(11), 3787-3799.

Helleday, T., Petermann, E., Lundin, C., Hodgson, B., & Sharma, R. A. (2008). DNA repair pathways as targets for cancer therapy. *Nat Rev Cancer*, *8*(3), 193-204.

Henry, K. A., Blank, H. M., Hoose, S. A., & Polymenis, M. (2010). The unfolded protein response is not necessary for the G1/S transition, but it is required for chromosome maintenance in Saccharomyces cerevisiae. *PLoS One*, *5*(9), e12732.

Hickish, T., Boni, C., Navarro, M., Tabernero, J., Topham, C., Bonetti, A., Clingan, P., Figer, A., Andre, T., & De Gramont, A. (2004). FOLFOX4 as adjuvant treatment for stage II colon cancer (CC): subpopulation data from the MOSAIC trial. *J Clin Oncol*, *22*(14_suppl), 3619-3619.

Hilmi, I., Hartono, J. L., & Goh, K. (2010). Negative perception in those at highest risk - potential challenges in colorectal cancer screening in an urban asian population. *Asian Pac J Cancer Prev*, *11*(3), 815-822.

Hohmann, M., Brunner, V., Johannes, W., Schum, D., Carroll, L. M., Liu, T., Sasaki, D., Clavel, T., Sieber, S. A., Zeller, G., Tschurtschenthaler, M., Janssen, K. P., & Gulder, T. A. M. (2024). Bacillamide D produced by Bacillus cereus from the mouse intestinal bacterial collection (miBC) is a potent cytotoxin in vitro. *Commun Biol, 7*(1), 655.

Hollien, J., Lin, J. H., Li, H., Stevens, N., Walter, P., & Weissman, J. S. (2009). Regulated Ire1-dependent decay of messenger RNAs in mammalian cells. *J Cell Biol*, *186*(3), 323-331.

Holohan, C., Van Schaeybroeck, S., Longley, D. B., & Johnston, P. G. (2013). Cancer drug resistance: an evolving paradigm. *Nat Rev Cancer*, *13*(10), 714-726.

Howarth, D. L., Lindtner, C., Vacaru, A. M., Sachidanandam, R., Tsedensodnom, O., Vasilkova, T., Buettner, C., & Sadler, K. C. (2014). Activating transcription factor 6 is necessary and sufficient for alcoholic fatty liver disease in zebrafish. *PLoS Genet*, *10*(5), e1004335.

Hsu, H. H., Chen, M. C., Baskaran, R., Lin, Y. M., Day, C. H., Lin, Y. J., Tu, C. C., Vijaya Padma, V., Kuo, W. W., & Huang, C. Y. (2018). Oxaliplatin resistance in colorectal cancer cells is mediated via activation of ABCG2 to alleviate ER stress induced apoptosis. *J Cell Physiol*, *233*(7), 5458-5467.

Hu, C. C., Dougan, S. K., McGehee, A. M., Love, J. C., & Ploegh, H. L. (2009). XBP-1 regulates signal transduction, transcription factors and bone marrow colonization in B cells. *EMBO J*, *28*(11), 1624-1636.

Huang, Y. Y., Pu, L. J., Song, L. L., Ma, L. Y., Liu, H., & Jiang, C. C. (2016). Knockdown of GRP78 enhances cell death by cisplatin and radiotherapy in nasopharyngeal cells. *Anticancer Drugs*, *27*(8), 726-733.

Hurwitz, H., Fehrenbacher, L., Novotny, W., Cartwright, T., Hainsworth, J., Heim, W., Berlin, J., Baron, A., Griffing, S., Holmgren, E., Ferrara, N., Fyfe, G., Rogers, B., Ross, R., & Kabbinavar, F. (2004). Bevacizumab plus irinotecan, fluorouracil, and leucovorin for metastatic colorectal cancer. *N Engl J Med*, *350*(23), 2335-

2342.

Iritani, B. M., & Eisenman, R. N. (1999). c-Myc enhances protein synthesis and cell size during B lymphocyte development. *Proc Natl Acad Sci U S A*, *96*(23), 13180-13185.

Ismaili, N. (2011). Treatment of colorectal liver metastases. *World J Surg Oncol*, *9*, 154.

Jagad, R. B., Koshariya, M., Kawamoto, J., Papastratis, P., Kefalourous, H., Patris, V., Tzouma, C., & Lygidakis, N. J. (2008). Management of rectal cancer: strategies and controversies. *Hepatogastroenterology*, *55*(81), 82-92.

Janssen, K. P., Alberici, P., Fsihi, H., Gaspar, C., Breukel, C., Franken, P., Rosty, C., Abal, M., El Marjou, F., Smits, R., Louvard, D., Fodde, R., & Robine, S. (2006). APC and oncogenic KRAS are synergistic in enhancing Wnt signaling in intestinal tumor formation and progression. *Gastroenterology*, *131*(4), 1096-1109.

Janssen, K. P., el-Marjou, F., Pinto, D., Sastre, X., Rouillard, D., Fouquet, C., Soussi, T., Louvard, D., & Robine, S. (2002). Targeted expression of oncogenic K-ras in intestinal epithelium causes spontaneous tumorigenesis in mice. *Gastroenterology*, *123*(2), 492-504.

Jaufmann, J., Franke, F. C., Sperlich, A., Blumendeller, C., Kloos, I., Schneider, B., Sasaki, D., Janssen, K. P., & Beer-Hammer, S. (2021). The emerging and diverse roles of the SLy/SASH1-protein family in health and disease—Overview of three multifunctional proteins. *FASEB J*, *35*(4), e21470.

Jeon, B. N., Kim, M. K., Choi, W. I., Koh, D. I., Hong, S. Y., Kim, K. S., Kim, M., Yun, C. O., Yoon, J., Choi, K. Y., Lee, K. R., Nephew, K. P., & Hur, M. W. (2012). KR-POK interacts with p53 and represses its ability to activate transcription of p21WAF1/CDKN1A. *Cancer Res*, *72*(5), 1137-1148.

Jiang, D., Turner, B., Song, J., Li, R., Diehn, M., Le, Q. T., Khatri, P., & Koong, A. C. (2017). Comprehensive analysis of the unfolded protein response in breast cancer subtypes. *JCO Precis Oncol*, *2017*, PO.16.00073.

Jiao, S., Peters, U., Berndt, S., Brenner, H., Butterbach, K., Caan, B. J., Carlson, C. S., Chan, A. T., Chang-Claude, J., Chanock, S., Curtis, K. R., Duggan, D., Gong, J., Harrison, T. A., Hayes, R. B., Henderson, B. E., Hoffmeister, M., Kolonel, L. N., Le Marchand, L., . . . Hsu, L. (2014). Estimating the heritability of colorectal cancer. *Hum Mol Genet*, *23*(14), 3898-3905.

Jiricny, J. (2006). The multifaceted mismatch-repair system. *Nat Rev Mol Cell Biol*, *7*(5), 335-346.

John, S. K., George, S., Primrose, J. N., & Fozard, J. B. (2011). Symptoms and signs in patients with colorectal cancer. *Colorectal Dis*, *13*(1), 17-25.

Jones, R. P., Jackson, R., Dunne, D. F., Malik, H. Z., Fenwick, S. W., Poston, G. J., & Ghaneh, P. (2012). Systematic review and meta-analysis of follow-up after hepatectomy for colorectal liver metastases. *Br J Surg*, *99*(4), 477-486.

Karali, E., Bellou, S., Stellas, D., Klinakis, A., Murphy, C., & Fotsis, T. (2014). VEGF Signals through ATF6 and PERK to promote endothelial cell survival and angiogenesis in the absence of ER stress. *Mol Cell*, *54*(4), 559-572.

Karapetis, C. S., Khambata-Ford, S., Jonker, D. J., O'Callaghan, C. J., Tu, D., Tebbutt, N. C., Simes, R. J., Chalchal, H., Shapiro, J. D., Robitaille, S., Price, T. J., Shepherd, L., Au, H. J., Langer, C., Moore, M. J., & Zalcberg, J. R.

(2008). K-ras mutations and benefit from cetuximab in advanced colorectal cancer. *N Engl J Med*, *359*(17), 1757-1765.

Kastrinos, F., Samadder, N. J., & Burt, R. W. (2020). Use of family history and genetic testing to determine risk of colorectal cancer. *Gastroenterology*, *158*(2), 389-403.

Kaufman, R. J. (2002). Orchestrating the unfolded protein response in health and disease. *J Clin Invest*, *110*(10), 1389-1398.

Kautto, E. A., Bonneville, R., Miya, J., Yu, L., Krook, M. A., Reeser, J. W., & Roychowdhury, S. (2017). Performance evaluation for rapid detection of pan-cancer microsatellite instability with MANTIS. *Oncotarget*, *8*(5), 7452-7463.

Keum, N., & Giovannucci, E. (2019). Global burden of colorectal cancer: emerging trends, risk factors and prevention strategies. *Nat Rev Gastroenterol Hepatol*, *16*(12), 713-732.

Khot, A., Brajanovski, N., Cameron, D. P., Hein, N., Maclachlan, K. H., Sanij, E., Lim, J., Soong, J., Link, E., Blombery, P., Thompson, E. R., Fellowes, A., Sheppard, K. E., McArthur, G. A., Pearson, R. B., Hannan, R. D., Poortinga, G., & Harrison, S. J. (2019). First-in-human RNA polymerase I transcription inhibitor CX-5461 in patients with advanced hematologic cancers: results of a phase I dose-escalation study. *Cancer Discov*, *9*(8), 1036-1049.

Kidani, Y., Noji, M., & Tashiro, T. (1980). Antitumor activity of platinum(II) complexes of 1,2-diamino-cyclohexane isomers. *Gan*, *71*(5), 637-643.

Kim, J. K., Kang, K. A., Piao, M. J., Ryu, Y. S., Han, X., Fernando, P. M., Oh, M. C., Park, J. E., Shilnikova, K., Boo, S. J., Na, S. Y., Jeong, Y. J., Jeong, S. U., & Hyun, J. W. (2016). Endoplasmic reticulum stress induces 5-fluorouracil resistance in human colon cancer cells. *Environ Toxicol Pharmacol*, *44*, 128-133.

Kim, W., Lee, S., Seo, D., Kim, D., Kim, K., Kim, E., Kang, J., Seong, K. M., Youn, H., & Youn, B. (2019). Cellular stress responses in radiotherapy. *Cells*, *8*(9), 1105.

Kishore, A. H., Batta, K., Das, C., Agarwal, S., & Kundu, T. K. (2007). p53 regulates its own activator: transcriptional co-activator PC4, a new p53-responsive gene. *Biochem J*, *406*(3), 437-444.

Kokame, K., Kato, H., & Miyata, T. (2001). Identification of ERSE-II, a new cis-acting element responsible for the ATF6-dependent mammalian unfolded protein response. *J Biol Chem*, *276*(12), 9199-9205.

Komorek, J., Kuppuswamy, M., Subramanian, T., Vijayalingam, S., Lomonosova, E., Zhao, L. J., Mymryk, J. S., Schmitt, K., & Chinnadurai, G. (2010). Adenovirus type 5 E1A and E6 proteins of low-risk cutaneous beta-human papillomaviruses suppress cell transformation through interaction with FOXK1/K2 transcription factors. *J Virol*, *84*(6), 2719-2731.

Kondo, J., Endo, H., Okuyama, H., Ishikawa, O., Iishi, H., Tsujii, M., Ohue, M., & Inoue, M. (2011). Retaining cell-cell contact enables preparation and culture of spheroids composed of pure primary cancer cells from colorectal cancer. *Proc Natl Acad Sci U S A*, *108*(15), 6235-6240.

Koo, J. H., Leong, R. W., Ching, J., Yeoh, K. G., Wu, D. C., Murdani, A., Cai, Q., Chiu, H. M., Chong, V. H., Rerknimitr, R., Goh, K. L., Hilmi, I., Byeon, J. S., Niaz, S. K., Siddique, A., Wu, K. C., Matsuda, T., Makharia, G., Sollano,

J., . . . Sung, J. J. (2012). Knowledge of, attitudes toward, and barriers to participation of colorectal cancer screening tests in the Asia-Pacific region: a multicenter study. *Gastrointest Endosc*, *76*(1), 126-135.

Koritzinsky, M., Levitin, F., van den Beucken, T., Rumantir, R. A., Harding, N. J., Chu, K. C., Boutros, P. C., Braakman, I., & Wouters, B. G. (2013). Two phases of disulfide bond formation have differing requirements for oxygen. *J Cell Biol*, *203*(4), 615-627.

Krasna, M. J., Flancbaum, L., Cody, R. P., Shneibaum, S., & Ben Ari, G. (1988). Vascular and neural invasion in colorectal carcinoma. Incidence and prognostic significance. *Cancer*, *61*(5), 1018-1023.

Kulak, N. A., Pichler, G., Paron, I., Nagaraj, N., & Mann, M. (2014). Minimal, encapsulated proteomic-sample processing applied to copy-number estimation in eukaryotic cells. *Nat Methods*, *11*(3), 319-324.

Kumar, A., Kennecke, H. F., Renouf, D. J., Lim, H. J., Gill, S., Woods, R., Speers, C., & Cheung, W. Y. (2015). Adjuvant chemotherapy use and outcomes of patients with high-risk versus low-risk stage II colon cancer. *Cancer*, *121*(4), 527-534.

Kurosaki, T., Maeda, A., Ishiai, M., Hashimoto, A., Inabe, K., & Takata, M. (2000). Regulation of the phospholipase C-γ2 pathway in B cells. *Immunol Rev*, *176*, 19-29.

Lamouille, S., Xu, J., & Derynck, R. (2014). Molecular mechanisms of epithelial-mesenchymal transition. *Nat Rev Mol Cell Biol*, *15*(3), 178-196.

Lee, A. H., Iwakoshi, N. N., & Glimcher, L. H. (2003). XBP-1 regulates a subset of endoplasmic reticulum resident chaperone genes in the unfolded protein response. *Mol Cell Biol*, *23*(21), 7448-7459.

Lee, J. J., & Sun, W. (2016). Options for second-line treatment in metastatic colorectal cancer. *Clin Adv Hematol Oncol*, *14*(1), 46-54.

Lee, K., Tirasophon, W., Shen, X., Michalak, M., Prywes, R., Okada, T., Yoshida, H., Mori, K., & Kaufman, R. J. (2002). IRE1-mediated unconventional mRNA splicing and S2P-mediated ATF6 cleavage merge to regulate XBP1 in signaling the unfolded protein response. *Genes Dev*, *16*(4), 452-466.

Leggett, B., & Whitehall, V. (2010). Role of the serrated pathway in colorectal cancer pathogenesis. *Gastroenterology*, *138*(6), 2088-2100.

Leung-Hagesteijn, C., Erdmann, N., Cheung, G., Keats, J. J., Stewart, A. K., Reece, D. E., Chung, K. C., & Tiedemann, R. E. (2013). Xbp1s-negative tumor B cells and pre-plasmablasts mediate therapeutic proteasome inhibitor resistance in multiple myeloma. *Cancer Cell*, *24*(3), 289-304.

Lévi, F., Zidani, R., & Misset, J. L. (1997). Randomised multicentre trial of chronotherapy with oxaliplatin, fluorouracil, and folinic acid in metastatic colorectal cancer. International Organization for Cancer Chronotherapy. *Lancet*, *350*(9079), 681-686.

Lévi, F. A., Zidani, R., Vannetzel, J. M., Perpoint, B., Focan, C., Faggiuolo, R., Chollet, P., Garufi, C., Itzhaki, M., Dogliotti, L., & et al. (1994). Chronomodulated versus fixed-infusion-rate delivery of ambulatory chemotherapy with oxaliplatin, fluorouracil, and folinic acid (leucovorin) in patients with colorectal cancer metastases: a randomized multi-institutional trial. *J Natl Cancer Inst*, *86*(21), 1608-1617.

Leyland-Jones, B., & O'Shaughnessy J, A. (2003). Erythropoietin as a critical component of breast cancer therapy:

survival, synergistic, and cognitive applications. *Semin Oncol*, *30*(5 Suppl 16), 174-184.

Li, C., Liu, X., Wu, J., Ji, X., & Xu, Q. (2022). Research progress in toxicological effects and mechanism of aflatoxin B(1) toxin. *PeerJ*, *10*, e13850.

Li, J., Ma, X., Chakravarti, D., Shalapour, S., & DePinho, R. A. (2021). Genetic and biological hallmarks of colorectal cancer. *Genes Dev*, *35*(11-12), 787-820.

Lin, H. H., Chang, Y. Y., Lin, J. K., Jiang, J. K., Lin, C. C., Lan, Y. T., Yang, S. H., Wang, H. S., Chen, W. S., Lin, T. C., & Chang, S. C. (2014). The role of adjuvant chemotherapy in stage II colorectal cancer patients. *Int J Colorectal Dis*, *29*(10), 1237-1243.

Lin, Y. H., Friederichs, J., Black, M. A., Mages, J., Rosenberg, R., Guilford, P. J., Phillips, V., Thompson-Fawcett, M., Kasabov, N., Toro, T., Merrie, A. E., van Rij, A., Yoon, H. S., McCall, J. L., Siewert, J. R., Holzmann, B., & Reeve, A. E. (2007). Multiple gene expression classifiers from different array platforms predict poor prognosis of colorectal cancer. *Clin Cancer Res*, *13*(2 Pt 1), 498-507.

Ly, A., Buck, A., Balluff, B., Sun, N., Gorzolka, K., Feuchtinger, A., Janssen, K. P., Kuppen, P. J., van de Velde, C. J., Weirich, G., Erlmeier, F., Langer, R., Aubele, M., Zitzelsberger, H., McDonnell, L., Aichler, M., & Walch, A. (2016). High-mass-resolution MALDI mass spectrometry imaging of metabolites from formalin-fixed paraffin-embedded tissue. *Nat Protoc*, *11*(8), 1428-1443.

Maak, M., Simon, I., Nitsche, U., Roepman, P., Snel, M., Glas, A. M., Schuster, T., Keller, G., Zeestraten, E., Goossens, I., Janssen, K. P., Friess, H., & Rosenberg, R. (2013). Independent validation of a prognostic genomic signature (ColoPrint) for patients with stage II colon cancer. *Ann Surg*, *257*(6), 1053-1058.

Magdeldin, S., & Yamamoto, T. (2012). Toward deciphering proteomes of formalin-fixed paraffin-embedded (FFPE) tissues. *Proteomics*, *12*(7), 1045-1058.

Mahadevan, N. R., Anufreichik, V., Rodvold, J. J., Chiu, K. T., Sepulveda, H., & Zanetti, M. (2012). Cell-extrinsic effects of tumor ER stress imprint myeloid dendritic cells and impair $CD8^+$ T cell priming. *PLoS One*, *7*(12), e51845.

Mahadevan, N. R., Rodvold, J., Sepulveda, H., Rossi, S., Drew, A. F., & Zanetti, M. (2011). Transmission of endoplasmic reticulum stress and pro-inflammation from tumor cells to myeloid cells. *Proc Natl Acad Sci U S A*, *108*(16), 6561-6566.

Manfredi, S., Lepage, C., Hatem, C., Coatmeur, O., Faivre, J., & Bouvier, A. M. (2006). Epidemiology and management of liver metastases from colorectal cancer. *Ann Surg*, *244*(2), 254-259.

Marks, G., Mohiuddin, M., & Borenstein, B. D. (1985). Preoperative radiation therapy and sphincter preservation by the combined abdominotranssacral technique for selected rectal cancers. *Dis Colon Rectum*, *28*(8), 565-571.

Martini, G., Troiani, T., Cardone, C., Vitiello, P., Sforza, V., Ciardiello, D., Napolitano, S., Della Corte, C. M., Morgillo, F., Raucci, A., Cuomo, A., Selvaggi, F., Ciardiello, F., & Martinelli, E. (2017). Present and future of metastatic colorectal cancer treatment: A review of new candidate targets. *World J Gastroenterol*, *23*(26), 4675-4688.

Mathé, G., Kidani, Y., Segiguchi, M., Eriguchi, M., Fredj, G., Peytavin, G., Misset, J. L., Brienza, S., de Vassals, F., Chenu, E., & et al. (1989). Oxalato-platinum or 1-OHP, a third-generation platinum complex: an experimental and clinical appraisal and preliminary comparison with cis-platinum and carboplatinum. *Biomed Pharmacother*, *43*(4), 237-250.

Meier, F., Beck, S., Grassl, N., Lubeck, M., Park, M. A., Raether, O., & Mann, M. (2015). Parallel Accumulation-Serial Fragmentation (PASEF): Multiplying Sequencing Speed and Sensitivity by Synchronized Scans in a Trapped Ion Mobility Device. *J Proteome Res*, *14*(12), 5378-5387.

Meusser, B., Hirsch, C., Jarosch, E., & Sommer, T. (2005). ERAD: the long road to destruction. *Nat Cell Biol*, *7*(8), 766-772.

Michelsen, U., & von Hagen, J. (2009). Isolation of subcellular organelles and structures. *Methods Enzymol*, *463*, 305-328.

Minsky, B. D., Cohen, A. M., Enker, W. E., & Paty, P. (1995). Sphincter preservation with preoperative radiation therapy and coloanal anastomosis. *Int J Radiat Oncol Biol Phys*, *31*(3), 553-559.

Moenner, M., Pluquet, O., Bouchecareilh, M., & Chevet, E. (2007). Integrated endoplasmic reticulum stress responses in cancer. *Cancer Res*, *67*(22), 10631-10634.

Moertel, C. G., Fleming, T. R., Macdonald, J. S., Haller, D. G., Laurie, J. A., Tangen, C. M., Ungerleider, J. S., Emerson, W. A., Tormey, D. C., Glick, J. H., & et al. (1995). Intergroup study of fluorouracil plus levamisole as adjuvant therapy for stage II/Dukes' B2 colon cancer. *J Clin Oncol*, *13*(12), 2936-2943.

Morgan, E., Arnold, M., Gini, A., Lorenzoni, V., Cabasag, C., Laversanne, M., Vignat, J., Ferlay, J., Murphy, N., & Bray, F. (2023). Global burden of colorectal cancer in 2020 and 2040: incidence and mortality estimates from GLOBOCAN. *Gut*, *72*(2), 338-344.

Mori, K. (2000). Tripartite management of unfolded proteins in the endoplasmic reticulum. *Cell*, *101*(5), 451-454.

Mujcic, H., Nagelkerke, A., Rouschop, K. M., Chung, S., Chaudary, N., Span, P. N., Clarke, B., Milosevic, M., Sykes, J., Hill, R. P., Koritzinsky, M., & Wouters, B. G. (2013). Hypoxic activation of the PERK/eIF2α arm of the unfolded protein response promotes metastasis through induction of LAMP3. *Clin Cancer Res*, *19*(22), 6126-6137.

Müller-Reif, J. B., Hansen, F. M., Schweizer, L., Treit, P. V., Geyer, P. E., & Mann, M. (2021). A new parallel high-pressure packing system enables rapid multiplexed production of capillary columns. *Mol Cell Proteomics*, *20*, 100082.

Mund, A., Coscia, F., Kriston, A., Hollandi, R., Kovács, F., Brunner, A. D., Migh, E., Schweizer, L., Santos, A., Bzorek, M., Naimy, S., Rahbek-Gjerdrum, L. M., Dyring-Andersen, B., Bulkescher, J., Lukas, C., Eckert, M. A., Lengyel, E., Gnann, C., Lundberg, E., . . . Mann, M. (2022). Deep Visual Proteomics defines single-cell identity and heterogeneity. *Nat Biotechnol*, *40*(8), 1231-1240.

Murphy, K. M., Zhang, S., Geiger, T., Hafez, M. J., Bacher, J., Berg, K. D., & Eshleman, J. R. (2006). Comparison of the microsatellite instability analysis system and the Bethesda panel for the determination of microsatellite instability in colorectal cancers. *J Mol Diagn*, *8*(3), 305-311.

Nagelkerke, A., Bussink, J., Mujcic, H., Wouters, B. G., Lehmann, S., Sweep, F. C., & Span, P. N. (2013). Hypoxia stimulates migration of breast cancer cells via the PERK/ATF4/LAMP3-arm of the unfolded protein response. *Breast Cancer Res*, *15*(1), R2.

Nagy, P., Varga, A., Pircs, K., Hegedűs, K., & Juhász, G. (2013). Myc-driven overgrowth requires unfolded protein response-mediated induction of autophagy and antioxidant responses in Drosophila melanogaster. *PLoS Genet*, *9*(8), e1003664.

Niederreiter, L., Fritz, T. M., Adolph, T. E., Krismer, A. M., Offner, F. A., Tschurtschenthaler, M., Flak, M. B., Hosomi, S., Tomczak, M. F., Kaneider, N. C., Sarcevic, E., Kempster, S. L., Raine, T., Esser, D., Rosenstiel, P., Kohno, K., Iwawaki, T., Tilg, H., Blumberg, R. S., & Kaser, A. (2013). ER stress transcription factor Xbp1 suppresses intestinal tumorigenesis and directs intestinal stem cells. *J Exp Med*, *210*(10), 2041-2056.

Nishizawa, T., & Yahagi, N. (2017). Endoscopic mucosal resection and endoscopic submucosal dissection: technique and new directions. *Curr Opin Gastroenterol*, *33*(5), 315-319.

Nitsche, U., Rosenberg, R., Balmert, A., Schuster, T., Slotta-Huspenina, J., Herrmann, P., Bader, F. G., Friess, H., Schlag, P. M., Stein, U., & Janssen, K. P. (2012). Integrative marker analysis allows risk assessment for metastasis in stage II colon cancer. *Ann Surg*, *256*(5), 763-771; discussion 771.

Nitsche, U., Zimmermann, A., Späth, C., Müller, T., Maak, M., Schuster, T., Slotta-Huspenina, J., Käser, S. A., Michalski, C. W., & Janssen, K.-P. (2013). Mucinous and signet-ring cell colorectal cancers differ from classical adenocarcinomas in tumor biology and prognosis. *Ann Surg*, *258*(5), 775-782; discussion 782-783.

Nougarède, A., Tesnière, C., Ylanko, J., Rimokh, R., Gillet, G., & Andrews, D. W. (2018). Improved IRE1 and PERK pathway sensors for multiplex endoplasmic reticulum stress assay reveal stress response to nuclear dyes used for image segmentation. *Assay Drug Dev Technol*, *16*(6), 350-360.

Nwosu, A. J., Misal, S. A., Truong, T., Carson, R. H., Webber, K. G. I., Axtell, N. B., Liang, Y., Johnston, S. M., Virgin, K. L., Smith, E. G., Thomas, G. V., Morgan, T., Price, J. C., & Kelly, R. T. (2022). In-depth mass spectrometry-based proteomics of formalin-fixed, paraffin-embedded tissues with a spatial resolution of 50–200 µm. *J Proteome Res*, *21*(9), 2237-2245.

O'Sullivan, B., Brierley, J., Byrd, D., Bosman, F., Kehoe, S., Kossary, C., Piñeros, M., Van Eycken, E., Weir, H. K., & Gospodarowicz, M. (2017). The TNM classification of malignant tumours—towards common understanding and reasonable expectations. *Lancet Oncol*, *18*(7), 849-851.

Omura, S., Suzuki, Y., Kitao, C., Takahashi, Y., & Konda, Y. (1975). Isolation of a new sulfur-containing basic substance from a Thermo actinomyces species. *J Antibiot (Tokyo)*, *28*(8), 609-610.

Oromendia, A. B., & Amon, A. (2014). Aneuploidy: implications for protein homeostasis and disease. *Dis Model Mech*, *7*(1), 15-20.

Ostasiewicz, P., Zielinska, D. F., Mann, M., & Wiśniewski, J. R. (2010). Proteome, phosphoproteome, and N-glycoproteome are quantitatively preserved in formalin-fixed paraffin-embedded tissue and analyzable by high-resolution mass spectrometry. *J Proteome Res*, *9*(7), 3688-3700.

Ozcan, U., Ozcan, L., Yilmaz, E., Düvel, K., Sahin, M., Manning, B. D., & Hotamisligil, G. S. (2008). Loss of the tuberous sclerosis complex tumor suppressors triggers the unfolded protein response to regulate insulin signaling and apoptosis. *Mol Cell*, *29*(5), 541-551.

Páez, D., Labonte, M. J., Bohanes, P., Zhang, W., Benhanim, L., Ning, Y., Wakatsuki, T., Loupakis, F., & Lenz, H. J. (2012). Cancer dormancy: a model of early dissemination and late cancer recurrence. *Clin Cancer Res*, *18*(3), 645-653.

Palam, L. R., Baird, T. D., & Wek, R. C. (2011). Phosphorylation of eIF2 facilitates ribosomal bypass of an inhibitory upstream ORF to enhance CHOP translation. *J Biol Chem*, *286*(13), 10939-10949.

Papandreou, I., Denko, N. C., Olson, M., Van Melckebeke, H., Lust, S., Tam, A., Solow-Cordero, D. E., Bouley, D. M., Offner, F., Niwa, M., & Koong, A. C. (2011). Identification of an Ire1alpha endonuclease specific inhibitor with cytotoxic activity against human multiple myeloma. *Blood*, *117*(4), 1311-1314.

Park, S. Y., Lee, S. J., Cho, H. J., Kim, J. T., Yoon, H. R., Lee, K. H., Kim, B. Y., Lee, Y., & Lee, H. G. (2019). Epsilon-globin HBE1 enhances radiotherapy resistance by down-regulating BCL11A in colorectal cancer cells. *Cancers (Basel)*, *11*(4), 498.

Parmar, S., & Easwaran, H. (2022). Genetic and epigenetic dependencies in colorectal cancer development. *Gastroenterol Rep (Oxf)*, *10*, goac035.

Pendyala, L., Kidani, Y., Perez, R., Wilkes, J., Bernacki, R. J., & Creaven, P. J. (1995). Cytotoxicity, cellular accumulation and DNA binding of oxaliplatin isomers. *Cancer Lett*, *97*(2), 177-184.

Pereira, E. R., Liao, N., Neale, G. A., & Hendershot, L. M. (2010). Transcriptional and post-transcriptional regulation of proangiogenic factors by the unfolded protein response. *PLoS One*, *5*(9), e12521.

Pfannschmidt, J., Dienemann, H., & Hoffmann, H. (2007). Surgical resection of pulmonary metastases from colorectal cancer: a systematic review of published series. *Ann Thorac Surg*, *84*(1), 324-338.

Piecyk, M., Triki, M., Laval, P. A., Duret, C., Fauvre, J., Cussonneau, L., Machon, C., Guitton, J., Rama, N., Gibert, B., Ichim, G., Catez, F., Bourdelais, F., Durand, S., Diaz, J. J., Coste, I., Renno, T., Manié, S. N., Aznar, N., . . . Chaveroux, C. (2024). The stress sensor GCN2 differentially controls ribosome biogenesis in colon cancer according to the nutritional context. *Mol Oncol* (Online ahead of print).

Pita-Fernández, S., Alhayek-Aí, M., González-Martín, C., López-Calviño, B., Seoane-Pillado, T., & Pértega-Díaz, S. (2015). Intensive follow-up strategies improve outcomes in nonmetastatic colorectal cancer patients after curative surgery: a systematic review and meta-analysis. *Ann Oncol*, *26*(4), 644-656.

Popat, S., & Houlston, R. S. (2005). A systematic review and meta-analysis of the relationship between chromosome 18q genotype, DCC status and colorectal cancer prognosis. *Eur J Cancer*, *41*(14), 2060-2070.

Porter, R. J., Arends, M. J., Churchhouse, A. M. D., & Din, S. (2021). Inflammatory bowel disease-associated colorectal cancer: translational risks from mechanisms to medicines. *J Crohns Colitis*, *15*(12), 2131-2141.

Qin, J. Y., Zhang, L., Clift, K. L., Hulur, I., Xiang, A. P., Ren, B. Z., & Lahn, B. T. (2010). Systematic comparison of constitutive promoters and the doxycycline-inducible promoter. *PLoS One*, *5*(5), e10611.

Ranganathan, A. C., Zhang, L., Adam, A. P., & Aguirre-Ghiso, J. A. (2006). Functional coupling of p38-induced up-

regulation of BiP and activation of RNA-dependent protein kinase-like endoplasmic reticulum kinase to drug resistance of dormant carcinoma cells. *Cancer Res*, *66*(3), 1702-1711.

Raymond, E., Faivre, S., Chaney, S., Woynarowski, J., & Cvitkovic, E. (2002). Cellular and molecular pharmacology of oxaliplatin. *Mol Cancer Ther*, *1*(3), 227-235.

Raymond, E., Faivre, S., Woynarowski, J. M., & Chaney, S. G. (1998). Oxaliplatin: mechanism of action and antineoplastic activity. *Semin Oncol*, *25*(2 Suppl 5), 4-12.

Replogle, J. M., Zhou, W., Amaro, A. E., McFarland, J. M., Villalobos-Ortiz, M., Ryan, J., Letai, A., Yilmaz, O., Sheltzer, J., Lippard, S. J., Ben-David, U., & Amon, A. (2020). Aneuploidy increases resistance to chemotherapeutics by antagonizing cell division. *Proc Natl Acad Sci U S A*, *117*(48), 30566-30576.

Riddell, I. A. (2018). Cisplatin and oxaliplatin: our current understanding of their actions. *Met Ions Life Sci*, *18*.

Rixe, O., Ortuzar, W., Alvarez, M., Parker, R., Reed, E., Paull, K., & Fojo, T. (1996). Oxaliplatin, tetraplatin, cisplatin, and carboplatin: spectrum of activity in drug-resistant cell lines and in the cell lines of the National Cancer Institute's Anticancer Drug Screen panel. *Biochem Pharmacol*, *52*(12), 1855-1865.

Romero-Ramirez, L., Cao, H., Nelson, D., Hammond, E., Lee, A. H., Yoshida, H., Mori, K., Glimcher, L. H., Denko, N. C., Giaccia, A. J., Le, Q. T., & Koong, A. C. (2004). XBP1 is essential for survival under hypoxic conditions and is required for tumor growth. *Cancer Res*, *64*(17), 5943-5947.

Rose, J., Augestad, K. M., & Cooper, G. S. (2014). Colorectal cancer surveillance: what's new and what's next. *World J Gastroenterol*, *20*(8), 1887-1897.

Rossi, L., Zullo, A., Zoratto, F., Papa, A., Strudel, M., Colonna, M., & Tomao, S. (2012). Chemotherapy and target therapy as neo-adjuvant approach for initially unresectable colorectal liver metastases. *Oncol Rev*, *6*(1), e6.

Roy, B., & Lee, A. S. (1999). The mammalian endoplasmic reticulum stress response element consists of an evolutionarily conserved tripartite structure and interacts with a novel stress-inducible complex. *Nucleic Acids Res*, *27*(6), 1437-1443.

Russo, A., & Russo, G. (2017). Ribosomal proteins control or bypass p53 during nucleolar stress. *Int J Mol Sci*, *18*(1), 140.

Salaroglio, I. C., Panada, E., Moiso, E., Buondonno, I., Provero, P., Rubinstein, M., Kopecka, J., & Riganti, C. (2017). PERK induces resistance to cell death elicited by endoplasmic reticulum stress and chemotherapy. *Mol Cancer*, *16*(1), 91.

Samtleben, S., Jaepel, J., Fecher, C., Andreska, T., Rehberg, M., & Blum, R. (2013). Direct imaging of ER calcium with targeted-esterase induced dye loading (TED). *J Vis Exp (75)*, e50317.

Sato, N., Kuroiwa, M., Nakatsuji, M., & Ishihara, H. (2019). *Method for isolating cell nuclei having enhanced antigenicity from fixed cells or ffpe tissue section, and antigen activator and kit therefor* (WO2019168085A1). W. I. P. Organization.

Sato, N., & Nakatsuji, M. (2023). *Method for enriching cells or cell nuclei* (WO2023053574A1). W. I. P. Organization.

Satoh, K., Yachida, S., Sugimoto, M., Oshima, M., Nakagawa, T., Akamoto, S., Tabata, S., Saitoh, K., Kato, K., Sato,

S., Igarashi, K., Aizawa, Y., Kajino-Sakamoto, R., Kojima, Y., Fujishita, T., Enomoto, A., Hirayama, A., Ishikawa, T., Taketo, M. M., . . . Soga, T. (2017). Global metabolic reprogramming of colorectal cancer occurs at adenoma stage and is induced by MYC. *Proc Natl Acad Sci U S A*, *114*(37), E7697-E7706.

Schewe, D. M., & Aguirre-Ghiso, J. A. (2008). ATF6α-Rheb-mTOR signaling promotes survival of dormant tumor cells in vivo. *Proc Natl Acad Sci U S A*, *105*(30), 10519-10524.

Schreuders, E. H., Ruco, A., Rabeneck, L., Schoen, R. E., Sung, J. J., Young, G. P., & Kuipers, E. J. (2015). Colorectal cancer screening: a global overview of existing programmes. *Gut*, *64*(10), 1637-1649.

Schwarz, D. S., & Blower, M. D. (2016). The endoplasmic reticulum: structure, function and response to cellular signaling. *Cell Mol Life Sci*, *73*(1), 79-94.

Shamu, C. E., & Walter, P. (1996). Oligomerization and phosphorylation of the Ire1p kinase during intracellular signaling from the endoplasmic reticulum to the nucleus. *EMBO J*, *15*(12), 3028-3039.

Shapiro, D. J., Livezey, M., Yu, L., Zheng, X., & Andruska, N. (2016). Anticipatory UPR activation: a protective pathway and target in cancer. *Trends Endocrinol Metab*, *27*(10), 731-741.

Sheshadri, N., Catanzaro, J. M., Bott, A. J., Sun, Y., Ullman, E., Chen, E. I., Pan, J. A., Wu, S., Crawford, H. C., Zhang, J., & Zong, W. X. (2014). SCCA1/SERPINB3 promotes oncogenesis and epithelial-mesenchymal transition via the unfolded protein response and IL6 signaling. *Cancer Res*, *74*(21), 6318-6329.

Shi, S. R., Shi, Y., & Taylor, C. R. (2011). Antigen retrieval immunohistochemistry: review and future prospects in research and diagnosis over two decades. *J Histochem Cytochem*, *59*(1), 13-32.

Shi, Z., Yu, X., Yuan, M., Lv, W., Feng, T., Bai, R., & Zhong, H. (2019). Activation of the PERK-ATF4 pathway promotes chemo-resistance in colon cancer cells. *Sci Rep*, *9*(1), 3210.

Shibata, D., Reale, M. A., Lavin, P., Silverman, M., Fearon, E. R., Steele, G., Jr., Jessup, J. M., Loda, M., & Summerhayes, I. C. (1996). The DCC protein and prognosis in colorectal cancer. *N Engl J Med*, *335*(23), 1727-1732.

Smith, W. E., Kane, A. V., Campbell, S. T., Acheson, D. W., Cochran, B. H., & Thorpe, C. M. (2003). Shiga toxin 1 triggers a ribotoxic stress response leading to p38 and JNK activation and induction of apoptosis in intestinal epithelial cells. *Infect Immun*, *71*(3), 1497-1504.

Song, M., Emilsson, L., Bozorg, S. R., Nguyen, L. H., Joshi, A. D., Staller, K., Nayor, J., Chan, A. T., & Ludvigsson, J. F. (2020). Risk of colorectal cancer incidence and mortality after polypectomy: a Swedish record-linkage study. *Lancet Gastroenterol Hepatol*, *5*(6), 537-547.

Sun, S., Shi, G., Sha, H., Ji, Y., Han, X., Shu, X., Ma, H., Inoue, T., Gao, B., Kim, H., Bu, P., Guber, R. D., Shen, X., Lee, A. H., Iwawaki, T., Paton, A. W., Paton, J. C., Fang, D., Tsai, B., . . . Qi, L. (2015). IRE1α is an endogenous substrate of endoplasmic-reticulum-associated degradation. *Nat Cell Biol*, *17*(12), 1546-1555.

Sung, H., Ferlay, J., Siegel, R. L., Laversanne, M., Soerjomataram, I., Jemal, A., & Bray, F. (2021). Global Cancer Statistics 2020: GLOBOCAN estimates of incidence and mortality worldwide for 36 cancers in 185 countries. *CA Cancer J Clin*, *71*(3), 209-249.

Tam, A. B., Roberts, L. S., Chandra, V., Rivera, I. G., Nomura, D. K., Forbes, D. J., & Niwa, M. (2018). The UPR

activator ATF6 responds to proteotoxic and lipotoxic stress by distinct mechanisms. *Dev Cell*, *46*(3), 327-343.e327.

Tameire, F., Verginadis, II, & Koumenis, C. (2015). Cell intrinsic and extrinsic activators of the unfolded protein response in cancer: Mechanisms and targets for therapy. *Semin Cancer Biol*, *33*, 3-15.

Tao, R., Chen, H., Gao, C., Xue, P., Yang, F., Han, J. D., Zhou, B., & Chen, Y. G. (2011). Xbp1-mediated histone H4 deacetylation contributes to DNA double-strand break repair in yeast. *Cell Res*, *21*(11), 1619-1633.

Tashiro, T., Kawada, Y., Sakurai, Y., & Kidani, Y. (1989). Antitumor activity of a new platinum complex, oxalato (trans-l-1,2-diaminocyclohexane)platinum (II): new experimental data. *Biomed Pharmacother*, *43*(4), 251-260.

Taylor, A. M., Shih, J., Ha, G., Gao, G. F., Zhang, X., Berger, A. C., Schumacher, S. E., Wang, C., Hu, H., Liu, J., Lazar, A. J., Cherniack, A. D., Beroukhim, R., & Meyerson, M. (2018). Genomic and functional approaches to understanding cancer aneuploidy. *Cancer Cell*, *33*(4), 676-689.e673.

Thastrup, O., Cullen, P. J., Drøbak, B. K., Hanley, M. R., & Dawson, A. P. (1990). Thapsigargin, a tumor promoter, discharges intracellular Ca^{2+} stores by specific inhibition of the endoplasmic reticulum Ca^{2+}-ATPase. *Proc Natl Acad Sci U S A*, *87*(7), 2466-2470.

Tian, Y., Kharazmi, E., Sundquist, K., Sundquist, J., Brenner, H., & Fallah, M. (2019). Familial colorectal cancer risk in half siblings and siblings: nationwide cohort study. *BMJ*, *364*, l803.

Tomasello, G., Ghidini, M., Galassi, B., Grossi, F., Luciani, A., & Petrelli, F. (2022). Survival benefit with adjuvant chemotherapy in stage III microsatellite-high/deficient mismatch repair colon cancer: a systematic review and meta-analysis. *Sci Rep*, *12*(1), 1055.

Tougeron, D., Mouillet, G., Trouilloud, I., Lecomte, T., Coriat, R., Aparicio, T., Des Guetz, G., Lécaille, C., Artru, P., Sickersen, G., Cauchin, E., Sefrioui, D., Boussaha, T., Ferru, A., Matysiak-Budnik, T., Silvain, C., Karayan-Tapon, L., Pagès, J. C., Vernerey, D., . . . Zaanan, A. (2016). Efficacy of adjuvant chemotherapy in colon cancer with microsatellite instability: a large multicenter AGEO study. *J Natl Cancer Inst*, *108*(7).

Tung, Y. C., Tsai, M. L., Kuo, F. L., Lai, C. S., Badmaev, V., Ho, C. T., & Pan, M. H. (2015). Se-methyl-L-selenocysteine induces apoptosis via endoplasmic reticulum stress and the death receptor pathway in human colon adenocarcinoma COLO 205 cells. *J Agric Food Chem*, *63*(20), 5008-5016.

UNDP. (2019). Human Development Report 2019: Beyond income, beyond averages, beyond today – Inequalities in human development in the 21st century. In: undp New York.

Urra, H., Dufey, E., Avril, T., Chevet, E., & Hetz, C. (2016). Endoplasmic reticulum stress and the hallmarks of cancer. *Trends Cancer*, *2*(5), 252-262.

Valerie, K., & Povirk, L. F. (2003). Regulation and mechanisms of mammalian double-strand break repair. *Oncogene*, *22*(37), 5792-5812.

van Anken, E., Romijn, E. P., Maggioni, C., Mezghrani, A., Sitia, R., Braakman, I., & Heck, A. J. (2003). Sequential waves of functionally related proteins are expressed when B cells prepare for antibody secretion. *Immunity*, *18*(2), 243-253.

Van Cutsem, E., Cervantes, A., Adam, R., Sobrero, A., Van Krieken, J. H., Aderka, D., Aranda Aguilar, E., Bardelli, A., Benson, A., Bodoky, G., Ciardiello, F., D'Hoore, A., Diaz-Rubio, E., Douillard, J. Y., Ducreux, M., Falcone, A., Grothey, A., Gruenberger, T., Haustermans, K., . . . Arnold, D. (2016). ESMO consensus guidelines for the management of patients with metastatic colorectal cancer. *Ann Oncol*, *27*(8), 1386-1422.

Vattem, K. M., & Wek, R. C. (2004). Reinitiation involving upstream ORFs regulates ATF4 mRNA translation in mammalian cells. *Proc Natl Acad Sci U S A*, *101*(31), 11269-11274.

Verwaal, V. J., van Ruth, S., de Bree, E., van Sloothen, G. W., van Tinteren, H., Boot, H., & Zoetmulder, F. A. (2003). Randomized trial of cytoreduction and hyperthermic intraperitoneal chemotherapy versus systemic chemotherapy and palliative surgery in patients with peritoneal carcinomatosis of colorectal cancer. *J Clin Oncol*, *21*(20), 3737-3743.

Vitale, A., & Denecke, J. (1999). The endoplasmic reticulum-gateway of the secretory pathway. *Plant Cell*, *11*(4), 615-628.

Vogelstein, B., Fearon, E. R., Hamilton, S. R., Kern, S. E., Preisinger, A. C., Leppert, M., Nakamura, Y., White, R., Smits, A. M., & Bos, J. L. (1988). Genetic alterations during colorectal-tumor development. *N Engl J Med*, *319*(9), 525-532.

Walter, F., Schmid, J., Düssmann, H., Concannon, C. G., & Prehn, J. H. (2015). Imaging of single cell responses to ER stress indicates that the relative dynamics of IRE1/XBP1 and PERK/ATF4 signalling rather than a switch between signalling branches determine cell survival. *Cell Death Differ*, *22*(9), 1502-1516.

Wanebo, H. J., Rao, B., Pinsky, C. M., Hoffman, R. G., Stearns, M., Schwartz, M. K., & Oettgen, H. F. (1978). Preoperative carcinoembryonic antigen level as a prognostic indicator in colorectal cancer. *N Engl J Med*, *299*(9), 448-451.

Wang, C., Huang, Z., Du, Y., Cheng, Y., Chen, S., & Guo, F. (2010). ATF4 regulates lipid metabolism and thermogenesis. *Cell Res*, *20*(2), 174-184.

Wang, H., & Mi, K. (2023). Emerging roles of endoplasmic reticulum stress in the cellular plasticity of cancer cells. *Front Oncol*, *13*, 1110881.

Wang, K., Kumar, T., Wang, J., Minussi, D. C., Sei, E., Li, J., Tran, T. M., Thennavan, A., Hu, M., Casasent, A. K., Xiao, Z., Bai, S., Yang, L., King, L. M., Shah, V., Kristel, P., van der Borden, C. L., Marks, J. R., Zhao, Y., . . . Navin, N. E. (2023). Archival single-cell genomics reveals persistent subclones during DCIS progression. *Cell*, *186*(18), 3968-3982.e3915.

Wang, M., & Kaufman, R. J. (2014). The impact of the endoplasmic reticulum protein-folding environment on cancer development. *Nat Rev Cancer*, *14*(9), 581-597.

Wang, Y., Shen, J., Arenzana, N., Tirasophon, W., Kaufman, R. J., & Prywes, R. (2000). Activation of ATF6 and an ATF6 DNA binding site by the endoplasmic reticulum stress response. *J Biol Chem*, *275*(35), 27013-27020.

Wang, Z. V., Deng, Y., Gao, N., Pedrozo, Z., Li, D. L., Morales, C. R., Criollo, A., Luo, X., Tan, W., Jiang, N., Lehrman, M. A., Rothermel, B. A., Lee, A. H., Lavandero, S., Mammen, P. P. A., Ferdous, A., Gillette, T. G., Scherer, P. E., & Hill, J. A. (2014). Spliced X-box binding protein 1 couples the unfolded protein response to

hexosamine biosynthetic pathway. *Cell*, *156*(6), 1179-1192.

Warren, S., & Sommers, S. C. (1949). Pathogenesis of ulcerative colitis. *Am J Pathol*, *25*(4), 657-679

Warwick, R., & Page, R. (2007). Resection of pulmonary metastases from colorectal carcinoma. *Eur J Surg Oncol*, *33 Suppl 2*, S59-63.

Welz, L., Kakavand, N., Hang, X., Laue, G., Ito, G., Silva, M. G., Plattner, C., Mishra, N., Tengen, F., Ogris, C., Jesinghaus, M., Wottawa, F., Arnold, P., Kaikkonen, L., Stengel, S., Tran, F., Das, S., Kaser, A., Trajanoski, Z., . . . Aden, K. (2022). Epithelial X-box binding protein 1 coordinates tumor protein p53-driven DNA damage responses and suppression of intestinal carcinogenesis. *Gastroenterology*, *162*(1), 223-237.e211.

Wolmark, N., Fisher, B., Wieand, H. S., Henry, R. S., Lerner, H., Legault-Poisson, S., Deckers, P. J., Dimitrov, N., Gordon, P. H., Jochimsen, P., & et al. (1984). The prognostic significance of preoperative carcinoembryonic antigen levels in colorectal cancer. Results from NSABP (National Surgical Adjuvant Breast and Bowel Project) clinical trials. *Ann Surg*, *199*(4), 375-382.

Wong, E., & Giandomenico, C. M. (1999). Current status of platinum-based antitumor drugs. *Chem Rev*, *99*(9), 2451-2466.

Wong, R. K., Tandan, V., De Silva, S., & Figueredo, A. (2007). Pre-operative radiotherapy and curative surgery for the management of localized rectal carcinoma. *Cochrane Database Syst Rev (2)*, CD002102.

Wortham, N. C., & Proud, C. G. (2015). eIF2B: recent structural and functional insights into a key regulator of translation. *Biochem Soc Trans*, *43*(6), 1234-1240.

Woynarowski, J. M., Faivre, S., Herzig, M. C., Arnett, B., Chapman, W. G., Trevino, A. V., Raymond, E., Chaney, S. G., Vaisman, A., Varchenko, M., & Juniewicz, P. E. (2000). Oxaliplatin-induced damage of cellular DNA. *Mol Pharmacol*, *58*(5), 920-927.

Wu, R., Zhang, Q. H., Lu, Y. J., Ren, K., & Yi, G. H. (2015). Involvement of the IRE1α-XBP1 pathway and XBP1s-dependent transcriptional reprogramming in metabolic diseases. *DNA Cell Biol*, *34*(1), 6-18.

Wu, X., Xin, Z., Zhang, W., Zheng, S., Wu, J., Chen, K., Wang, H., Zhu, X., Li, Z., Duan, Z., Li, H., & Liu, Y. (2014). A missense polymorphism in ATF6 gene is associated with susceptibility to hepatocellular carcinoma probably by altering ATF6 level. *Int J Cancer*, *135*(1), 61-68.

Xi, Y., & Xu, P. (2021). Global colorectal cancer burden in 2020 and projections to 2040. *Transl Oncol*, *14*(10), 101174.

Xie, Y. H., Chen, Y. X., & Fang, J. Y. (2020). Comprehensive review of targeted therapy for colorectal cancer. *Signal Transduct Target Ther*, *5*(1), 22.

Xu, H., Di Antonio, M., McKinney, S., Mathew, V., Ho, B., O'Neil, N. J., Santos, N. D., Silvester, J., Wei, V., Garcia, J., Kabeer, F., Lai, D., Soriano, P., Banáth, J., Chiu, D. S., Yap, D., Le, D. D., Ye, F. B., Zhang, A., . . . Aparicio, S. (2017). CX-5461 is a DNA G-quadruplex stabilizer with selective lethality in BRCA1/2 deficient tumours. *Nat Commun*, *8*, 14432.

Xu, Z., Zhang, T., Chen, H., Zhu, Y., Lv, Y., Zhang, S., Chen, J., Chen, H., Yang, L., Jiang, W., Ni, S., Lu, F., Wang, Z.,

Yang, H., Dong, L., Chen, F., Zhang, H., Chen, Y., Liu, J., . . . Wang, Y. (2023). High-throughput single nucleus total RNA sequencing of formalin-fixed paraffin-embedded tissues by snRandom-seq. *Nat Commun*, *14*(1), 2734.

Yamamori, T., Meike, S., Nagane, M., Yasui, H., & Inanami, O. (2013). ER stress suppresses DNA double-strand break repair and sensitizes tumor cells to ionizing radiation by stimulating proteasomal degradation of Rad51. *FEBS Lett*, *587*(20), 3348-3353.

Yang, K., Yang, J., & Yi, J. (2018). Nucleolar Stress: hallmarks, sensing mechanism and diseases. *Cell Stress*, *2*(6), 125-140.

Yang, Q., Kim, Y. S., Lin, Y., Lewis, J., Neckers, L., & Liu, Z. G. (2006). Tumour necrosis factor receptor 1 mediates endoplasmic reticulum stress-induced activation of the MAP kinase JNK. *EMBO Rep*, *7*(6), 622-627.

Yoon, S. B., Park, Y. H., Choi, S. A., Yang, H. J., Jeong, P. S., Cha, J. J., Lee, S., Lee, S. H., Lee, J. H., Sim, B. W., Koo, B. S., Park, S. J., Lee, Y., Kim, Y. H., Hong, J. J., Kim, J. S., Jin, Y. B., Huh, J. W., Lee, S. R., . . . Kim, S. U. (2019). Real-time PCR quantification of spliced X-box binding protein 1 (XBP1) using a universal primer method. *PLoS One*, *14*(7), e0219978.

Yoshida, H., Haze, K., Yanagi, H., Yura, T., & Mori, K. (1998). Identification of the cis-acting endoplasmic reticulum stress response element responsible for transcriptional induction of mammalian glucose-regulated proteins. Involvement of basic leucine zipper transcription factors. *J Biol Chem*, *273*(50), 33741-33749.

Yoshida, H., Matsui, T., Hosokawa, N., Kaufman, R. J., Nagata, K., & Mori, K. (2003). A time-dependent phase shift in the mammalian unfolded protein response. *Dev Cell*, *4*(2), 265-271.

Yoshida, H., Okada, T., Haze, K., Yanagi, H., Yura, T., Negishi, M., & Mori, K. (2000). ATF6 activated by proteolysis binds in the presence of NF-Y (CBF) directly to the cis-acting element responsible for the mammalian unfolded protein response. *Mol Cell Biol*, *20*(18), 6755-6767.

Yoshida, H., Okada, T., Haze, K., Yanagi, H., Yura, T., Negishi, M., & Mori, K. (2001). Endoplasmic reticulum stress-induced formation of transcription factor complex ERSF including NF-Y (CBF) and activating transcription factors 6α and 6β that activates the mammalian unfolded protein response. *Mol Cell Biol*, *21*(4), 1239-1248.

Yoshida, H., Oku, M., Suzuki, M., & Mori, K. (2006). pXBP1(U) encoded in XBP1 pre-mRNA negatively regulates unfolded protein response activator pXBP1(S) in mammalian ER stress response. *J Cell Biol*, *172*(4), 565-575.

Yu, J., Li, T., Liu, Y., Wang, X., Zhang, J., Wang, X., Shi, G., Lou, J., Wang, L., Wang, C. C., & Wang, L. (2020). Phosphorylation switches protein disulfide isomerase activity to maintain proteostasis and attenuate ER stress. *EMBO J*, *39*(10), e103841.

Yu, L., Andruska, N., Zheng, X., & Shapiro, D. J. (2016). Anticipatory activation of the unfolded protein response by epidermal growth factor is required for immediate early gene expression and cell proliferation. *Mol Cell Endocrinol*, *422*, 31-41.

Yu, L. L., Li, Z. Y., Peng, C. S., Li, Z.-Y., & Guo, Y.-W. (2009). Neobacillamide A, a novel thiazole-containing alkaloid

from the marine bacterium Bacillus vallismortis C89, associated with South China Sea sponge Dysidea avara. *Helv. Chim. Acta*, *92*, 607-612.

Zaniboni, A., & Meriggi, F. (2005). The emerging role of oxaliplatin in the treatment of gastric cancer. *J Chemother*, *17*(6), 656-662.

Zeng, L., Lu, M., Mori, K., Luo, S., Lee, A. S., Zhu, Y., & Shyy, J. Y. (2004). ATF6 modulates SREBP2-mediated lipogenesis. *EMBO J*, *23*(4), 950-958.

Zhang, F., Hamanaka, R. B., Bobrovnikova-Marjon, E., Gordan, J. D., Dai, M. S., Lu, H., Simon, M. C., & Diehl, J. A. (2006). Ribosomal stress couples the unfolded protein response to p53-dependent cell cycle arrest. *J Biol Chem*, *281*(40), 30036-30045.

Zhang, L., Lu, X., Xu, Y., La, X., Tian, J., Li, A., Li, H., Wu, C., Xi, Y., Song, G., Zhou, Z., Bai, W., An, L., & Li, Z. (2023). Tumor-associated macrophages confer colorectal cancer 5-fluorouracil resistance by promoting MRP1 membrane translocation via an intercellular CXCL17/CXCL22-CCR4-ATF6-GRP78 axis. *Cell Death Dis*, *14*(9), 582.

Zhang, Y., Liu, Y., Zhou, Y., Zheng, Z., Tang, W., Song, M., Wang, J., & Wang, K. (2021). Lentinan inhibited colon cancer growth by inducing endoplasmic reticulum stress-mediated autophagic cell death and apoptosis. *Carbohydr Polym*, *267*, 118154.

Zhao, L., Xing, P., Polavarapu, V. K., Zhao, M., Valero-Martínez, B., Dang, Y., Maturi, N., Mathot, L., Neves, I., Yildirim, I., Swartling, F. J., Sjöblom, T., Uhrbom, L., & Chen, X. (2021). FACT-seq: profiling histone modifications in formalin-fixed paraffin-embedded samples with low cell numbers. *Nucleic Acids Res*, *49*(21), e125.

Zhu, H., Chen, X., Chen, B., Chen, B., Song, W., Sun, D., & Zhao, Y. (2014). Activating transcription factor 4 promotes esophageal squamous cell carcinoma invasion and metastasis in mice and is associated with poor prognosis in human patients. *PLoS One*, *9*(7), e103882.

Acknowledgments

First and foremost, I would like to express my great gratitude to Dr. Klaus-Peter Janßen, who supported me during my doctorate and provided an excellent scientific environment with the freedom to develop and conduct projects independently. Working in his laboratory was an exciting and encouraging experience. Thank you very much for this great opportunity! Thank you, Dr. Hideki Ishihara, Dr. Natsuki Sato and Dr. Masatoshi Nakatsuji, for offering a laboratory space and devices and providing valuable technical advice during my stay in Japan to perform the Xnuc-based analysis. I am especially grateful to Dr. Ishihara for his dedicated efforts to establish our collaboration and for introducing me to the prime opportunity to join it. I would also like to thank Julia Gißibl and Dr. Julius Fischer for their kind cooperation with radiotherapeutic experiments, and thank you, Dr. Dirk Wilhelm and other people in the Dept. of Surgery, for providing CRC patients' samples. Their expertise and technical support have been invaluable to me and have played a crucial role in the success of this thesis. Thank you, Dr. Markus Gerhard and Dr. Raquel Mejias-Luque, for serving on my thesis committee and providing valuable feedback and suggestions. Thank you, Dr. Melanie Laschinger and Dr. Bernhard Holzmann, for your great help and valuable discussions. Furthermore, I want to acknowledge Nitto Boseki Co., Ltd. for their financial support, which allowed me to research this highly interesting topic.

I also want to express my gratitude to all the colleagues in the laboratory and neighbors for the very personal and friendly working atmosphere, as well as to all the fellows in the MLST for their encouraging friendship. We have also spent much time together privately. Thank you for the unforgettable and great time in Bayern! Thank you, Widya, Felicitas, Anja and Gabi, for your indispensable support in the laboratory. A big thank you! Further, I want to thank Max for the collaboration with characterizing natural compounds ("excursus" in the thesis) and Michael for the partnership in establishing co-culture models of organoids and peripheral immune cells (unpublished results), which were exciting parts of my research!

Finally, I want to express my great thankfulness to my family and all my friends for their continuous encouragement and support.